

**Technische Universität München**  
**Lehrstuhl für Entwicklungs-genetik**

## **Genetic alterations in MENX-associated pheochromocytoma**

**Alena Shyla**

Vollständiger Abdruck der von der Fakultät  
Wissenschaftszentrum Weihenstephan für Ernährung, Landnutzung und Umwelt  
der Technischen Universität München zur Erlangung des akademischen  
Grades eines

Doktors der Naturwissenschaften

genehmigten Dissertation.

Vorsitzender: Univ.-Prof. Dr. S. Scherer

Prüfer der Dissertation: 1. apl. Prof. Dr. J. Graw

2. Univ.- Prof. Dr. A. Gierl

3. Univ.- Prof. Dr. M. J. Atkinson

Die Dissertation wurde am 18.02.2008 bei der Technischen Universität München eingereicht und durch die Fakultät Wissenschaftszentrum Weihenstephan für Ernährung, Landnutzung und Umwelt am 15.05.2008 angenommen.

Ich erkläre hiermit an Eides statt, dass ich die vorliegende Arbeit selbständig ohne unzulässige fremde Hilfe angefertigt habe.

Die verwendeten Literaturquellen sind im Literaturverzeichnis vollständig zitiert.

München, den

---

Alena Shyla

## TABLE OF CONTENTS

<b>1. INTRODUCTION</b>	1
<b>1.1. Genetics and biology of pheochromocytoma (PC)</b>	1
<b>1.2. Familial forms of PC and mechanisms of their tumorigenesis</b>	3
1.2.1. Multiple endocrine neoplasia type 2 syndrome (MEN2)	3
1.2.2. Neurofibromatosis type I (NF1)	6
1.2.3. von Hippel-Lindau disease (VHL)	8
1.2.4. PC-PGL syndromes characterized by germline mutations of the succinate dehydrogenase gene (SDH) family	11
1.2.5. Inherited PC susceptibility genes and neuronal developmental apoptosis pathway	14
<b>1.3. Nonsyndromic sporadic PC</b>	16
<b>1.4. Involvement of other genes in PC development</b>	18
1.4.1. Novel PC susceptibility loci	18
1.4.2. Somatic mutations in PC	18
<b>1.5. Comparative genomic hybridization (CGH) and gene expression array analyses of PC</b>	20
<b>1.6. Animal models of PC</b>	22
<b>1.7. The rat model of multiple endocrine neoplasia X (MENX) syndrome</b>	24
<b>1.8. Cyclin-dependent kinase inhibitor <i>CDKN1B</i></b>	26
1.8.1 <i>CDKN1B</i> and its role in human PC and other neuroendocrine tumors formation	28
<b>1.9. Aim of the work</b>	29
<b>2. MATERIALS</b>	31
<b>3. METHODS</b>	36
<b>3.1. Tumor and nontumor tissue samples</b>	36
3.1.1. Preparation of tumor and nontumor tissue for molecular analysis	36
3.1.2. Genotyping on the <i>Cdkn1b</i> gene	36
<b>3.2. Isolation of Nucleic Acids</b>	36
3.2.1. Isolation of genomic DNA from fresh-frozen tissue	36

3.2.2.	Isolation of genomic DNA for CGH array	38
3.2.3.	Isolation of RNA from snap - frozen tissue	38
3.2.4.	Isolation of RNA from microdissected tissue	39
<b>3.3.</b>	<b>Quantification of Nucleic Acids</b>	39
<b>3.4.</b>	<b>LOH analysis</b>	39
3.4.1.	Microsatellite markers	40
3.4.2.	Amplification of DNA microsatellites	41
3.4.3.	Electrophoresis of the DNA extraction products and PCR amplification products	42
3.4.4.	Quantification of the allelic ratio	44
<b>3.5.</b>	<b>Fragment analysis</b>	44
<b>3.6.</b>	<b>TaqMan PCR</b>	45
3.6.1.	Reverse transcription	45
3.6.2.	PCR amplification	46
3.6.3.	Quantification	48
<b>3.7.</b>	<b>Automated fluorescent sequencing</b>	49
3.7.1.	PCR reaction	50
3.7.2.	Purification of PCR products	50
3.7.3.	Sequencing reaction	51
<b>3.8.</b>	<b>Fluorescence in situ hybridization analysis (FISH)</b>	52
3.8.1.	Probe preparation and labelling	53
3.8.2.	Sample preparation	55
3.8.3.	Denaturation of probe and sample	56
3.8.4.	Hybridization of probe to sample (annealing)	57
3.8.5.	Detection	57
3.8.6.	Analysis of the data	59
<b>3.9.</b>	<b>CGH array</b>	59
<b>4.</b>	<b>RESULTS</b>	62
<b>4.1.</b>	<b>The group of experimental animals</b>	62
4.1.1.	Histological analysis of rat adrenal glands with PC	63
<b>4.2.</b>	<b>Microsatellite-based allelotyping of somatic genetic changes in PC (LOH analysis)</b>	63
4.2.1.	Optimization of PCR conditions	65

4.2.2. Allele dilution experiments	67
4.2.3. Genome-wide screening for LOH/AI	68
4.2.4. LOH/AI analysis for genes predisposing to PC development	73
<b>4.3. Quantification of mRNA level of <i>Cdkn2a</i>, <i>Cdkn2c</i>, <i>Sctr</i>, <i>Sdhd</i> and <i>Rassf1</i> gene in MENX-affected rats</b>	77
4.3.1. Validation of standard curves	77
4.3.2. mRNA expression level of <i>Cdkn2a</i> , <i>Cdkn2c</i> , <i>Sctr</i> genes in adrenal glands with PC	79
4.3.3. mRNA expression level of <i>Sdhd</i> , <i>Rassf1</i> genes in adrenal glands with PC	79
<b>4.4. <i>Sdhd</i> and <i>Rassf1</i> sequence analysis</b>	83
<b>4.5. FISH analysis of AI regions on chromosomes 8 and 19</b>	84
4.5.1. Verification and validation of the BAC clones as FISH probes, metaphase FISH analysis	84
4.5.2. Interphase FISH analysis	87
<b>4.6. CGH array studies to identify genomic losses or gains in PC of MENX rats</b>	96
4.6.1. CGH array data analysis	98
4.6.2. Comparative analysis of data received after microsatellite analysis, FISH and CGH array analysis for rat chromosomes 8 and 19	105
<b>5. DISCUSSION</b>	107
<b>5.1. Candidate LOH/AI loci in MENX-PCs</b>	107
5.1.1. LOH/AI loci on rat chromosome 8 and their syntenic regions in the human genome	109
5.1.1.1. Rat chromosomal locus 8q31-q32	109
5.1.1.2. Rat chromosomal loci 8q11-q12 and 8q22-q24	112
5.1.1.3. Rat chromosomal locus 8q24	113
5.1.2. LOH/AI loci on rat chromosome 19 and their syntenic regions in the human genome	113
5.1.2.1. Chromosomal loci 19p14-p12 and 19q12 (37.6-53.9 Mb)	113
5.1.2.2. Rat chromosomal locus 19q11 (24.7-26.3 Mb)	116
5.1.2.3. Rat chromosomal locus 19q12 (53.9-56.9 Mb)	116
5.1.2.4. Rat chromosomal locus 19q11 (26.3-34.4 Mb)	117
<b>5.2. Copy number changes of candidate regions in MENX-PCs</b>	117

<b>5.3. Analysis of rat homologs of genes predisposing to or involved in PC development</b>	119
<b>6. SUMMARY</b>	123
<b>ZUSAMMENFASSUNG</b>	127
<b>7. REFERENCES</b>	131
<b>8. APPENDIX</b>	150

**PRESENTATIONS**

**ACKNOWLEDGEMENTS**

**LEBENS LAUF**

## ABBREVIATIONS

AI	allelic imbalance
BAC clone	bacterial artificial chromosome clone
Bcl-2	apoptosis regulator Bcl-2 protein, encoded by the <i>BCL2</i> gene
Biotin -16-dUTP	biotin-16-2'- deoxyuridine -5'- triphosphate
BMPs	bone morphogenetic proteins
BMP2	bone morphogenetic protein 2, encoded by the <i>BMP2</i> gene
BMP4	bone morphogenetic protein 4, encoded by the <i>BMP4</i> gene
CDK	cyclin dependent kinase
CDKIs	cyclin-dependent kinase inhibitors
Cdkn1a	cyclin-dependent kinase inhibitor 1A ( <i>Rattus norvegicus</i> )
CDKN1B	cyclin-dependent kinase inhibitor 1B
CDKN1C	cyclin-dependent kinase inhibitor 1C
CDKN2B	cyclin-dependent kinase inhibitor 2B
CDKN2A	cyclin-dependent kinase inhibitor 2A
CDKN2C	cyclin-dependent kinase inhibitor 2C
cDNA	complementary DNA
CgA	chromogranin A
CGH	comparative genomic hybridization
CSR	cysteine-rich region of neurofibromin
CT value	threshold cycle value
DAPI	4',6-diamino-2-phenylindole dihydrochloride
dATP	deoxyadenosin-5'-triphosphat
dCTP	deoxycytidine-5'- triphosphate
ddNTP	dideoxyribonucleotide triphosphate
dGTP	deoxyguanosine-5'- triphosphate
Digoxigenin -11- UTP	digoxigenin-11-uridine-5'- triphosphate
dITP	deoxyinosine-5'-triphosphate
DNA	deoxyribonucleic acid
dNTP	deoxynucleotide triphosphate

dTTP	deoxythymidine-5'-triphosphate
dUTP	deoxyuridine-5'-triphosphate
Egln3	egl nine homolog 3 ( <i>C. elegans</i> ), HIF $\alpha$ prolyl hydroxylase
ERBB2	v-erb-b2 erythroblastic leukemia viral oncogene homolog 2
erbB-2	receptor tyrosine-protein kinase erbB-2, encoded by the <i>ERBB2</i> gene
FISH	fluorescence in situ hybridization
FMTC	familial medullary thyroid carcinoma
H&E	hematoxylin/eosin staining
HIF $\alpha$	hypoxia-inducible factor alpha
IP <sub>3</sub>	inositol-1,4,5-triphosphate
JNK	c-Jun N-terminal kinase
LOH	loss of heterozygosity
MEN1	multiple endocrine neoplasia 1
MENX syndrome	rat model of multiple endocrine neoplasia X
MGB probe	minor groove binder probe
mRNA	messenger ribonucleic acid
mut/mut rats	affected rats having two mutated ( <i>mut</i> ) alleles of the <i>Cdkn1b</i> gene and developing MENX syndrome
NEDH	New England Deaconess Hospital rat line
NF1	neurofibromatosis, type 1
NGF	nerve growth factor
PBS	phosphate buffered saline
P53	cellular tumor antigen p53, encoded by the <i>TP53</i> gene
p14(ARF)	cyclin-dependent kinase inhibitor 2A, isoform 4, encoded by the <i>CDKN2A</i> gene
p15(INK4B)	cyclin-dependent kinase 4 inhibitor B, encoded by the <i>CDKN2B</i> gene
p16(INK4A)	cyclin-dependent kinase inhibitor 2A, isoform 1, encoded by the <i>CDKN2A</i> gene
p18(INK4C)	cyclin-dependent kinase 4 inhibitor C, encoded by the <i>CDKN2C</i> gene



p27(KIP1)	cyclin-dependent kinase inhibitor 1B, encoded by the <i>CDKN1B</i> gene
PC	pheochromocytoma
PCR	polymerase chain reaction
PGL	paraganglioma
PI3K	phosphatidylinositol-3-kinase
PKA	protein kinase A
PM <sub>reference</sub>	perfect match signal intensity for the reference sample, labelled with Cy5
PM <sub>test</sub>	perfect match signal intensity for the test sample, labelled with Cy3
PTEN	phosphatase and tensin homolog
PTPRF	protein tyrosine phosphatase, receptor type, F
pVHL	von Hippel-Lindau disease tumor suppressor protein, encoded by the <i>VHL</i> gene
RASSF1	Ras association (RalGDS/AF-6) domain family 1
RB1	retinoblastoma 1
RB	retinoblastoma-associated protein, encoded by the <i>RB1</i> gene
RET	ret proto-oncogene
RNA	ribonucleic acid
RT	reverse transcription reaction
RT-PCR	reverse transcription polymerase chain reaction
SCTR	secretin receptor
SDH	succinate dehydrogenase
SDHB	succinate dehydrogenase complex, subunit B, iron sulfur (Ip) protein
SDHD	succinate dehydrogenase complex, subunit D, integral membrane protein
SD <sup>we</sup>	Sprague Dawley white eye
SSC	standard saline citrate solution
TCA	tricarboxylic-acid cycle
TGFB2	transforming growth factor beta-2 protein, encoded by the <i>TGFB2</i> gene

TGFB3	transforming growth factor beta-3 protein, encoded by the <i>TGFB3</i> gene
TP53	tumor protein p53
UNG	AmpErase uracil-N-glycosylase
VEGF	vascular endothelial growth factor
VHL	von Hippel-Lindau tumor suppressor
Wky	Wistar Kyoto rat strain

# 1. INTRODUCTION

## 1.1. Genetics and biology of pheochromocytoma (PC)

PCs are highly vascularized rare neoplasias of neural crest origin, arising from the chromaffin cells of the adrenal medulla. The histological term “chromaffin” stems from the observation that chromaffin tissue becomes dark after exposure to potassium dichromate. In adults, most chromaffin cells are located in the adrenal medulla, but some are found in other tissues of the sympathetic nervous system, such as the organ of Zuckerkandl, and the abdominal and aorticopulmonary paraganglia. Many of the extra-adrenal chromaffin cells regress postnatally. In rare cases, the extra-adrenal tissues can give rise to PC - related tumors, so-called extra-adrenal PCs or paragangliomas (PGLs) (Koch *et al.*, 2002a; Dannenberg *et al.*, 2003; Manger, 2006). PGLs can originate in either the sympathetic nervous system or parasympathetic ganglia. PGL that arise from the sympathetic nervous system occur most frequently in the retroperitoneum, although they can also occur in the thorax, and are termed extra-adrenal PCs (Maher and Eng *et al.*, 2002; Bryant *et al.*, 2003). PCs and PGLs of sympathetic origin (extra-adrenal PCs) can synthesize, store and secrete large amounts of catecholamines (norepinephrine and epinephrine) plus a variable series of vasoactive peptides (Dluhy, 2002; Ahlman *et al.*, 2006). Owing to inappropriate catecholamine secretion, the majority of PCs give rise to hypertension (Mannelli *et al.*, 1999; Dluhy, 2002; Manger, 2006; Dannenberg *et al.*, 2003). Nonchromaffin PGLs that originate in parasympathetic ganglia (nonchromaffin PGLs or chemodectomas) can be found adjacent to the aortic arch, neck and skull base as local masses and are commonly referred to as head and neck PGLs, glomus tumors or chemodectomas. The site of origin defines the name given to parasympathetic PGLs. In the head and neck, they most commonly occur at the carotid bifurcation, where they are referred to as carotid body tumors. The other common sites of head and neck PGLs are the jugular foramen, along the path of the vagus nerve, and within the middle ear (Rao *et al.*, 1999; Maher and Eng *et al.*, 2002; Bryant *et al.*, 2003). Tumors that arise from the parasympathetic nervous system do not usually secrete catecholamines (Bryant *et al.*, 2003). Although the carotid bodies and other paraganglia in the head and neck are classified as “nonchromaffin”, suggesting that they do not contain any catecholamines, some investigators found dopamine and norepinephrine in carotid bodies. Fewer than 5% of carotid body PGLs have been shown to produce and secrete catecholamines (Rao *et al.*, 1999; Koch *et al.*, 2002a; Manger, 2006).

PCs occur either sporadically or as a part of familial cancer syndromes. Autosomal dominant inherited cancer syndromes that may present with PC include multiple endocrine neoplasia type

2 (MEN2), von Hippel-Lindau syndrome (VHL), neurofibromatosis type 1 (NF1) and the pheochromocytoma-paraganglioma (PC-PGL) syndrome. Familial forms of PC have been associated with germline mutations in *RET*, *VHL*, *NF1*, *SDHB* or *SDHD*, respectively (Table 1.1).

The “rule of 10” is used to describe PCs: a) 10 percent of PCs are extra-adrenal, and of those, 10 percent are extra-abdominal; b) 10 percent are malignant; c) 10 percent are found in patients who do not have hypertension, d) 10 percent are hereditary (Astuti *et al.*, 2001a, b; Dluhy, 2002).

**Table 1.1** Major genetic syndromes associated with pheochromocytoma

Syndrome	Clinical features	Gene	Locus
Multiple endocrine neoplasia type 2A	Medullary thyroid carcinoma Parathyroid hyperplasia Pheochromocytoma	<i>RET</i>	10q11.2
Multiple endocrine neoplasia type 2B	Sympathetic paraganglioma Medullary thyroid carcinoma Pheochromocytoma Ganglioneuromas Marfanoid habitus		
Neurofibromatosis type 1	Neurofibromas Café-au-lait spots Lisch nodules Axillary and inguinal freckling Optic gliomas Sympathetic paraganglioma	<i>NF1</i>	17q11.2
von Hippel-Lindau syndrome	Hemangioblastomas (brain, spine, retina) Clear-cell renal cell cancer Pheochromocytoma Sympathetic paraganglioma	<i>VHL</i>	3p26-25
Pheochromocytoma-paraganglioma syndrome	Pheochromocytoma Sympathetic and parasympathetic paraganglioma	<i>SDHB</i> <i>SDHD</i>	1p35-36 ( <i>PGL4</i> ) 11q23.4 ( <i>PGL1</i> )

Data source: Bryant *et al.*, 2003; Kim and Kaelin, 2004; Bausch *et al.*, 2006b; Mannelli *et al.*, 2007; Jiménez *et al.*, 2006.

It has been recently shown that a germline mutation may be present in 12% to 24% of apparently sporadic PCs (Neumann *et al.*, 2001; Neumann *et al.*, 2002; Amar *et al.*, 2005). In all patients with PC, including those with a known hereditary syndrome or a positive family history, the frequency of germline mutations can approach 30% (Bryant *et al.*, 2003; Gimenez-Roqueplo, 2006; Manger, 2006).

PCs and PGLs both arise from neuroendocrine cells that have differentiated from a common neural crest derived precursor cell (Favier *et al.*, 2005). Furthermore, the tumors share several histopathological features, such that without clinical data on the location and hormone status of the tumor, the discrimination of PC and PGL can be very difficult (Chetty *et al.*, 1998;

McNichol, 2001; Dannenberg *et al.*, 2006; McNichol, 2006). However, there are differences between PCs and head and neck PGLs:

- ✓ it is rare for head and neck PGLs of parasympathetic origin to be secreting tumors (Rao *et al.*, 1999; Koch *et al.*, 2002a; Manger, 2006), whereas PCs and abdominal PGLs are frequently functional
- ✓ most patients with head and neck PGLs develop a slow-growing asymptomatic mass, whereas patients with PCs suffer from hypertensive crises and paroxysmal symptoms (Baysal *et al.*, 2002)
- ✓ the spectrum of mutations in the *SDHB* and *SDHD* genes is different for each tumor type (Baysal *et al.*, 2002; Maher and Eng 2002)

Edsröm *et al.*, (2000b) with a comparative genomic hybridization (CGH) array could not detect any major differences in the pattern of copy number changes between PCs and abdominal PGLs. The authors suggested that PCs and abdominal PGLs (extra-adrenal catecholamine –secreting PGLs) not only share many clinical features, but also have a similar genetic background.

Cascón *et al.* (2005) reported that the CGH alterations of the head and neck parasympathetic PGLs do not correspond to those found in PCs. All these findings indicate that the pathogenesis of PCs and extra-adrenal PGLs of the sympathetic paraganglionic system is different from parasympathetic PGLs.

Currently, the malignant status of PCs/PGLs is established primarily by the presence of metastases at nonchromaffin sites, and although several markers (heat shock protein 90, human telomerase reverse transcriptase, N-cadherin, and others) have been proposed to predict malignancy in those tumors, there is no consensus as to the existence of histological, clinical, or molecular indicators of worse prognosis (Eisenhofer *et al.*, 2004b; Ahlman *et al.*, 2006; McNicol, 2006).

## **1.2. Familial forms of PC and mechanisms of their tumorigenesis**

### **1.2.1. Multiple endocrine neoplasia type 2 syndrome (MEN2)**

MEN2 is an autosomal dominantly inherited cancer syndrome with variable, age-dependent penetrance, occurring in 1 in 300000 live birth. There are three clinically distinct forms of the MEN 2 syndrome: MEN 2A, MEN 2B and familial medullary thyroid carcinoma (FMTC) (Miše *et al.*, 2006). MEN 2A is the most common subtype of MEN2, and almost 50% of patients develop PC. MEN 2A is characterized by medullary thyroid carcinoma in 95% of cases and

hyperplasia of the parathyroid glands in 15-30% of cases as well (Hansford *et al.*, 2000). MEN 2B represents about 5% of all MEN 2 cases (Koch *et al.*, 2002a). MEN 2B patients have medullary thyroid carcinoma in 100 % of cases, PC in 50% of cases, and other features, including marfanoid habitus (tall, thin stature) and multiple mucosal neuromas. MEN 2B is considered to be the most aggressive of the MEN 2 subtypes (Hansford *et al.*, 2000; Santoro *et al.*, 2004). FMTC is characterized only by the appearance of medullary thyroid carcinoma (Hansford *et al.*, 2000; Santoro *et al.*, 2004; Miše *et al.*, 2006).

PCs associated with MEN 2A are most commonly diagnosed between ages of 30 and 40 years. MEN 2A patients are significantly younger at age of PC diagnosis than patients with sporadic PC (Pomares *et al.*, 1998), possibly because MEN2 patients undergo routine medical examination that would detect a PC. Most MEN2A patients develop bilateral PCs, while extra-adrenal PC is extremely uncommon in those patients. Several studies have documented that PCs undergo malignant transformation less frequently in MEN2A patients than in patients with sporadic PCs (Modigliani *et al.*, 1995; Bryant *et al.*, 2003). MEN2-associated PCs are mostly adrenergic, i.e. predominantly epinephrine secreting (Koch *et al.*, 2002b).

The gene responsible for MEN2, the *RET* proto-oncogene, has been localised to chromosome 10q11.2 (Mulligan *et al.*, 1994). The *RET* proto-oncogene encodes a transmembrane receptor of the tyrosine kinase family (Manie *et al.*, 2001; Santoro *et al.*, 2004). It is expressed primarily in neural crest and urogenital precursor cells and is implicated in developmental processes, such as maturation of peripheral nervous system lineages, kidney morphogenesis, spermatogonia differentiation (Miše *et al.*, 2006; Santoro *et al.*, 2004).

In patients with MEN2, germ-line mutations of *RET* are commonly identified and are believed to be activating (Ponder *et al.*, 1999; Hansford *et al.*, 2000; Santoro *et al.*, 2004; Miše *et al.*, 2006). *RET* consists of 21 exons with 6 so-called hot-spot exons (exons 10, 11, 13, 14, 15, 16) in which mutations are identified in 97% of patients with MEN2 (Koch *et al.*, 2002a). Different specific mutations in the *RET* give rise to different clinical types of the MEN2 syndrome (Ponder *et al.*, 1999). Missense mutations affecting cysteine residues in the RET extracellular domain are found in patients with MEN 2A. Approximately 87% of MEN 2A mutations affect codon 634 and the most frequent substitution at this codon is a cysteine to arginine change (C634R), found in more than 50% of cases (Ponder, 1999; Hansford *et al.*, 2000). These cysteine residues are thought to be normally involved in the formation of intramolecular disulfide bonds that determine the tertiary structure of RET. Mutation of a cysteine residue leads to the formation of an aberrant intermolecular bond between two mutated RET monomers and, as a result, to ligand-independent homodimerization and constitutive activation of the RET kinase (Santoro *et al.*, 2004, Miše *et al.*, 2006).

MEN 2B is associated primarily with a single missense mutation of codon 918 (M918T) which is found in more than 90% of all reported cases and mutations of codon 883 in exon 15 (A883F) which is shown to occur in a small number of MEN2B cases. Amino acids 883 and 918 both lie within the substrate binding pocket of the RET tyrosine kinase and mutations of these codons result in RET proteins with altered substrate specificity (Santoro *et al.*, 1995; Hansford *et al.*, 2000; Santoro *et al.*, 2004).

RET can trigger growth, differentiation, or survival responses depending on the cell type or developmental stage in which it is activated (Ponder *et al.*, 1999). RET activates a variety of intracellular signalling pathways, including RAS/ERK, phosphatidylinositol-3-kinase (PI3K/AKT), phospholipase C and c-Jun N-terminal kinase (JNK) pathways (Hansford *et al.*, 2000; Santoro *et al.*, 2004).

Early genetic screening for *RET* mutations is considered the standard care for MEN2. Predictive and diagnostic testing is facilitated by the high incidence of detectable mutations (>95%) and the small number of target codons (Hansford *et al.*, 2000; Bryant *et al.*, 2003).

It remains puzzling why unrelated patients with MEN2 develop PC at different ages, some early in life (for instance, in the first decade), and others as late as in the 7-8<sup>th</sup> decade (Eng *et al.*, 1996; Koch *et al.*, 2002a). This clinical observation suggests that a germline mutation in *RET* is obligatory but perhaps not sufficient to cause tumor formation in MEN2 *in vivo* (Koch *et al.*, 2002b).

In the study of Huang *et al.* (2000) it was demonstrated that PC formation may have been initiated by a *RET* germ-line mutation, followed by duplication of the mutant allele in trisomy 10 or loss of the normal wild-type *RET* allele as a “second activating hit”. Chromaffin cells of the adrenal medulla that contain two mutant *RET* alleles may gain a growth advantage and eventually develop into tumors. Similarly, loss of the wild-type *RET* allele may release a dominant effect of the mutant *RET* allele (Huang *et al.*, 2000). In support of the loss of the wild-type *RET* allele causing PC tumorigenesis, Mulligan *et al.* (1993a) has shown allelic loss on chromosome 10 in MEN2-associated PCs. Interestingly, patients with MEN2 - associated bilateral PC can have a different genetic alteration in each affected adrenal gland: PC of the one organ can have trisomy 10 and the tumor of the second adrenal gland can show loss of the wild-type *RET* allele (Huang *et al.*, 2000). This result suggests that the selection between duplication of the mutant *RET* and loss of the wild-type *RET* allele can be random (Huang *et al.*, 2000).

Somatic genetic alterations of the *VHL* gene may play a role in the tumorigenesis of some MEN2A-related PCs. Koch *et al.* (2002c) analysed four PCs from four unrelated patients with MEN2A having a single germline mutation of *RET* and found loss of heterozygosity (LOH) of the *VHL* gene locus in all tumors and inactivating somatic mutations of *VHL* in three of the four

MEN2A-related PCs. According to the hypothesis suggested by Koch *et al.* (2002c), PC formation in these selected MEN2A-related PCs may occur firstly by a *RET* germline mutation, leading to hyperplasia of chromaffin cells and secondly by a subsequent somatic *VHL* gene deletion and mutation in selected cells, thereby transforming those into PC.

Other allele losses in MEN 2-associated PCs have been reported to occur on 1p, 3p (including the *VHL* gene locus), 3q, 11p, 17p and chromosome 22 (Khosla *et al.*, 1991; Moley *et al.*, 1992; Mulligan *et al.*, 1993a; Benn *et al.*, 2000). The most frequent allele losses (> 50% of tumors) involve chromosomes 1p, 3p, 3q and 22 (Koch *et al.*, 2002a).

Reduced *Nf1* expression was found in 5 of 14 MEN2-related PCs, suggesting a possible role of the *NF1* gene and RAS pathway in tumor formation (Gutmann *et al.*, 1995; Koch *et al.*, 2002b).

### **1.2.2. Neurofibromatosis type I (NF1)**

The neurofibromatoses are autosomal dominant genetic disorders. There are two distinct forms: neurofibromatosis type 1 (NF1) and neurofibromatosis type 2 (NF2). NF1, also known as von Recklinghausen disease, is one of the most common inherited neurological diseases, which affects about one in 3000-4000 individuals. In the UK almost one in every 2500 babies born has NF1. The disorder has almost 100% penetrance but variable expression (Zhu and Parada., 2001; Reynolds *et al.*, 2003). The two major clinical manifestations are the formation of benign tumors along peripheral and optic nerves (neurofibromas and optic gliomas) as well as abnormal distribution of melanocytes (multiple café-au-lait spots). Patients with NF1 also have an increased incidence of other tumor types, including neurofibrosarcoma, PCs, and leukemia, particularly juvenile chronic myelogenous leukaemia. NF1 patients have additional clinical symptoms including hamartomas in the iris (Lisch nodules), macrocephaly, and seizures (Reynolds *et al.*, 2003; Bryant *et al.*, 2003; Trovó-Marqui and Tajara, 2006). PCs are not associated with neurofibromatosis type 2 (NF2) (Reynolds *et al.*, 2003).

PCs occur in 0.1-5.7% of patients with NF1 and in 20-50% of NF1 patients with hypertension (Walther *et al.*, 1999; Reynolds *et al.*, 2003; Bausch *et al.*, 2006a). When NF1 patients are examined at autopsy, the prevalence of PC is higher (3.3 – 13.0 %) (Bryant *et al.*, 2003).

Walther *et al.* (1999) characterized the clinical findings of NF1-associated PC in 148 individuals. The mean patient age at PC was 42 years. Most of the patients (84%) had benign unilateral tumors. Malignant PC was identified in 11% of patients. 10% of patients had bilateral PC, and 6% had extra-adrenal PCs (PGL).



NF1-associated PCs primarily secrete norepinephrine and rarely epinephrine (Walther *et al.*, 1999; Koch *et al.*, 2002b). The course and presentation of PCs in NF1 patients are similar to those in patients with sporadic PCs (Bryant *et al.*, 2003; Bausch *et al.*, 2006b).

NF1 is caused by germline mutations of the neurofibromin 1 (*NFI*) gene that map to chromosome 17q11.2. The gene consists of 61 exons distributed over 350 kilobases (kb) of genomic DNA. Mutation analysis in the *NFI* gene remains a considerable challenge because of the large size of the gene and the presence of 36 pseudogenes (Trovó-Marqui and Tajara, 2006; Bausch *et al.*, 2007). The *NFI* gene encodes neurofibromin; predominantly expressed in neurons, Schwann cells, oligodendrocytes, astrocytes and leucocytes (Trovó-Marqui and Tajara, 2006). Neurofibromin is also expressed in the adrenal gland (Koch *et al.*, 2002a).

Neurofibromin has been found to interact with the RAS-GTPase p21ras proteins (Martin *et al.*, 1990). Neurofibromin, by means of its NF1-RGD domain, increases the GTP hydrolysis rate and reduce the activity of p21ras (Gutmann, 2001; Zhu and Parada, 2001; Trovó-Marqui and Tajara, 2006). It was shown, that the loss of neurofibromin leads to increased levels of activated RAS and augmented cell growth (Gutmann, 2001). Neurofibromin is also involved in a p21ras-independent protein kinase A (PKA)-cAMP pathway and modulates the activity of adenylyl cyclase (the crucial enzyme for the cAMP signalling pathway) (Feng *et al.*, 2004; Trovó-Marqui and Tajara, 2006; Hsuech, 2007).

Molecular genetic analysis of the *NFI* gene in neurofibromatosis associated-PC was done in studies by Bausch *et al.* (2006a, b; 2007). Germline mutations in *NFI* in PC range from nonsense and missense mutations to small and large deletions (Bausch *et al.*, 2006a, b, c). In the study by Bausch *et al.* (2007) 35% of all NF1-associated PC cases had mutations in the cysteine-rich region (CSR) and only 13% in the RAS-GAP (RGD) domain. Bausch *et al.* (2006c) suggests that the CSR of *NFI* could be a prominent mutational target not only in NF1-associated PCs but, perhaps, more universally in all heritable and sporadic PC as well.

*NFI* acts as a tumor-suppressor gene. Tumor-suppressor activity of neurofibromin is thought to depend on its ability to negatively regulate the family of RAS proto-oncogenes (*HRAS*, *KRAS*, and *NRAS*), encoding p21ras proteins which regulate proliferation and differentiation in a variety of cell types (Zhu and Parada, 2001; Gutmann, 2001; Trovó-Marqui and Tajara, 2006). According to Knudson's two hit theory, NF1-related PC development requires biallelic inactivation of a tumor-suppressor gene via mutation, deletion or other mechanisms (Zhu and Parada, 2001, Koch *et al.*, 2002b).

Mice heterozygous for one mutant *Nfi* allele are highly predisposed to the development of PC and myeloid leukaemia (Jaks *et al.*, 1994). The authors demonstrated that approximately 50% of

analysed pheochromocytomas from *Nf1*<sup>+/-</sup> mice have somatic loss of the remaining wild-type *Nf1* allele.

In patients with NF1-associated PC the loss of the remaining wild-type *NF1* allele was shown in three of seven tumors by Xu *et al.* (1992). LOH and biallelic inactivation of both *NF1* alleles also was found in 14 of the 21 NF1-related PCs by Bausch *et al.* (2007). LOH for the *NF1* gene was demonstrated in all six NF1-associated PCs (6/6) by Gutmann *et al.*, (1994). In contrast, no LOH at the *NF1* locus was found in 12 sporadic PCs (Bausch *et al.*, 2007)

Loss of neurofibromin expression can be seen in PCs from patients with and without neurofibromatosis (Xu *et al.*, 1992; Gutmann *et al.* 1994; Gutmann *et al.*, 1995).

Nf1 alterations have not been studied in PGLs, and there are no good indications that NF1 is involved in the genesis of these tumors (Dannenberg *et al.*, 2003).

### **1.2.3. von Hippel-Lindau disease (VHL)**

VHL disease is an autosomal dominantly inherited familial cancer syndrome characterized by susceptibility to haemangioblastomas of the retina and central nervous system, clear-cell renal cell carcinoma, PC, pancreatic islet cell tumors and endolymphatic sac tumors. In addition, renal, pancreatic and epididymal cysts are common (Maher, 2006). VHL disease has an approximate incidence of 1/36 000 live-births (Bryant *et al.*, 2003; Koch *et al.*, 2002b).

A germline mutation in the von Hippel-Lindau tumor-suppressor (*VHL*) gene predisposes carriers to tumors in multiple organs (Hes *et al.*, 2003). The *VHL* gene is a relatively small gene (consists of three exons) located on chromosome 3p25-p26 (Latif *et al.*, 1993; Richards, 2001; Kim and Kaelin, 2004). *VHL* has been shown to act as a tumor suppressor gene according to Knudson's two-hit hypothesis (Kim and Kaelin, 2004). Protein, encoded by the *VHL* gene (pVHL), is widely expressed in normal human tissues and even in organs not a risk for the disease. In human embryos, pVHL is expressed in all three germ layers, with strong expression noted in the central nervous system, kidneys, testes, and lungs. Therefore, the tissue specificity of VHL disease can not be entirely explained by tissue-specific expression during either fetal development or adulthood (Richards, 2001; Hes *et al.*, 2003). pVHL interacts in a tissue-specific manner with many cellular proteins and is involved in the regulation of angiogenesis, fibronectin binding and extracellular matrix assembly, microtubule function, apoptosis, post-transcriptional regulation of target gene expression through mRNA stability effects, regulation of atypical protein kinase C, tyrosine- hydroxylase and plays a role in the cell cycle. pVHL is a ubiquitin ligase for hypoxia-inducible factor alpha (HIF $\alpha$ ) (Clifford *et al.*, 2001; Kim and Kaelin, 2004; Maher, 2006). As a transcription factor HIF activates the expression of genes involved in energy metabolism,

angiogenesis, erythropoiesis, apoptosis, and/or proliferation in response to hypoxia: vascular endothelial growth factor, erythropoietin, glucose transporter-1, platelet-derived growth factor –  $\beta$ , plasminogen activator inhibitor 1, and transforming growth factor-  $\alpha$ . (Richards, 2001; Kim and Kaelin, 2004; Hes *et al.*, 2003; Maher, 2006; King *et al.*, 2006 ).

Germline *VHL* mutations are found in 35-50% of familial or bilateral PC and 2-50% of sporadic cases (Richards, 2001; Bryant *et al.*, 2003; Maher, 2006). The overall frequency of PC in VHL disease is 7-19% (Richards, 2001; Macher and Eng; 2002). On the basis of its clinical expression, VHL disease has been divided in 4 subtypes, with a central role for PC (Table 1.2).

**Table 1.2** Genotype-phenotype correlation for VHL disease and possible pathophysiological mechanisms

VHL disease type	Clinical manifestations			Germline VHL mutations	Molecular defect
	HB	RCC	PC		
Type 1	+	+	-	Microdeletions Large deletions Missense Nonsense Insertions Splice site	Total or partial <i>VHL</i> loss Improper folding of VHL Upregulation of HIF
Type 2A	+	-	+	Missense	
Type 2B	+	+	+	Missense	Upregulation of HIF
Type 2C (familial pheochromocytoma)	-	-	+	Missense	Inability to stabilize microtubules Upregulation of HIF pVHL maintains ability to downregulate HIF Decreased binding to fibronectin Defective fibronectin matrix assembly

Abbreviations: HB, retinal and central nervous system haemangioblastoma; RCC, renal cell carcinoma; PC, pheochromocytoma; VHL, von Hippel-Lindau disease; HIF, hypoxia inducible factor; pVHL, VHL tumor suppressor protein.

Source of data: Richards, 2001; Hes *et al.*, 2003; Bryant *et al.*, 2003; Kim and Kaelin, 2004.

PCs associated with VHL are early-onset, multifocal, may be extra-adrenal, and are associated with a relatively low frequency of malignancy. VHL PCs predominantly secrete norepinephrine. Screening for PC is recommended in all VHL patients starting at age 5 years (Koch *et al.*, 2000b; Bryant *et al.*, 2003).

The nature of the germline *VHL* mutation determines PC risk in VHL disease families as indicated in table 1.2 (Richards, 2001; Clifford *et al.*, 2001; Kim and Kaelin, 2004; Maher, 2006). More than 95% of patients with truncating mutations (frameshift and nonsense mutations) and deletions have VHL type 1. Mutations associated with VHL type 1 disrupt the hydrophobic core of pVHL and are predicted to cause loss of function of pVHL (Table 1.2). Two specific missense mutations are associated with Type 2A VHL: Tyr98His (founder mutation in the Black Forest region in Germany) and Tyr112His (Richards, 2001).

Patients with VHL type 2 have primarily missense mutations (Table 1.2). The missense mutations associated with VHL type 2A and types 2B are within the elongin C binding region ( $\alpha$ -domain) or in the HIF- $\alpha$  subunit binding site ( $\beta$ -domain). This type of missense mutations is predicted to cause only local defects and not to lead to loss of overall structural integrity of VHL. As a result of these mutations, target proteins (e.g. HIF) can not be properly degraded by the proteasome (Maher and Eng, 2002; Bryant *et al.*, 2003, Hes *et al.*, 2003). Codon 167 missense mutations are particularly associated with Type 2B VHL disease with a high incidence of PC within families (Richards, 2001). There are a few hypotheses explaining how missense mutations associated with Type 2 VHL disease may induce tumorigenesis (Hes *et al.*, 2003; Maher, 2006). First of all, the change of one amino acid may lead to a mutated pVHL that bind other proteins compared to a normal pVHL. In other words, pVHL affected by a type 2 missense mutation would exert a gain of function. Alternatively, a missense mutation may display a dominant negative effect: the mutant protein may negatively influence activity of the wild-type protein encoded by the nonmutated allele. A third mechanism of action of VHL type 2 missense mutations is via a gene dosage effect. In this model, different cell types would have individual thresholds for pVHL protein levels that determine cell proliferation, differentiation, and apoptosis. In all these three cases, i.e. gain of function, dominant negative effect, and gene dosage effect, one hit would be enough to induce tumorigenesis of chromaffin cells (Hes *et al.*, 2003; Maher, 2006).

Specific missense mutations have been also observed in families with Type 2C VHL disease (familial PC): Leu188Val, Val84Leu and Ser80Leu. Individuals with these mutations are unlikely to develop haemangioblastomas or renal cell carcinoma (Richards, 2001). Recent data have demonstrated that the missense mutations associated with VHL type 2C (notably in the  $\alpha$ -domain) result in a protein that retains the ability to ubiquitinate HIF-1 $\alpha$  but is defective in the promotion of fibronectin matrix assembly and exhibit decreased fibronectin binding (Hoffman *et al.*, 2001) (Table 1.2). This might suggest that abnormal extracellular matrix formation following pVHL inactivation contributes to the development of PC in the setting of VHL disease (Hoffman *et al.*, 2001; Clifford *et al.*, 2001; Hes *et al.*, 2003).

Altogether, these findings support the hypothesis that deregulation of VHL without complete loss of its functions can drive PC tumorigenesis (Hes *et al.*, 2003; Dannenberg *et al.*, 2003).

But at the same time, PCs from *VHL* germline mutation-positive cases are believed to abide by the Knudson two-hit mechanism of tumorigenesis (Kim and Kaelin, 2004). In accordance with this hypothesis (Knudson, 1986; Lasko, 1991), VHL-related tumors harbour germline inactivating mutation of *VHL* gene (the first hit) and lose the function of the remaining wild-type allele through different genetic alterations at the somatic level – somatic mutation, deletion or

hypermethylation (the second hit) (Richards, 2001; Koch *et al.*, 2002b). Biallelic two-hit *VHL* inactivation was demonstrated in small series of VHL-related PCs (4 different studies encompass a total of only 12 VHL- PCs) with *VHL* germline mutation as the first hit, and 3p25-p26 LOH as the second (Crossey *et al.*, 1994; Khosla *et al.*, 1991; Zeiger *et al.*, 1995; Prowse *et al.*, 1997). There is only one study, based on 36 VHL-associated PCs, demonstrating that indeed a complete biallelic two-hit *VHL* inactivation is a necessary pathogenetic mechanism in VHL-PCs (Bender *et al.*, 2000).

In VHL-associated PCs, LOH and CGH analysis demonstrated frequent allelic losses of chromosome 3p or the whole chromosome 3, chromosome 11p, 11q (Bender *et al.*, 2000; Lui *et al.*, 2002). Lui *et al.* (2002) regards the loss of 11p and/or 11q as VHL-related PC specific genetic alterations.

#### **1.2.4. PC-PGL syndromes characterized by germline mutations of the succinate dehydrogenase gene (SDH) family**

The first locus associated with hereditary PGL was identified on 11q23 (*PGL1*) by genetic linkage analysis (Heutink *et al.*, 1992). Baysal *et al.* (2000) demonstrated that *PGL1* corresponds to the *SDHD* gene in a genetic linkage analysis study of American and Dutch families. Three other loci were identified on 11q13.1 (*PGL2*) (Mariman *et al.*, 1995), 1q21-q23 (*PGL3*) (Niemann *et al.*, 1999), and 1p35-p36 (*PGL4*) (Astuti *et al.*, 2001a). Candidate gene studies showed that *PGL3* and *PGL4* correspond to the *SDHC* and *SDHB* genes, respectively (Astuti *et al.*, 2001a; Niemann and Müller, 2000). The putative *PGL2* locus was shown to be linked to PGLs in a single Dutch family (Mariman *et al.*, 1995), but no susceptibility gene has been identified to date (Maher and Eng, 2002).

*SDHD*, *SDHC*, *SDHB*, *SDHA* encode four subunits of mitochondrial respiratory chain complex II, also known as succinate ubiquinone oxidoreductase or succinate dehydrogenase (SDH). The hydrophilic, catalytic part of the complex consists of a flavoprotein (SDHA) and an iron-sulfur protein (SDHB), which together form the SDH enzyme. The hydrophobic part of the complex includes SDHC and SDHD which anchor the complex to the inner mitochondrial membrane. SDH is a mitochondrial enzyme linking the electron-transport respiratory chain, associated with the inner mitochondrial membrane and Krebs tricarboxylic-acid cycle (TCA). SDH catalyses the conversion of succinate to fumarate (Eng *et al.*, 2003; Gottlieb and Tomlinson, 2005; Favier *et al.*, 2005).

PC occurs in about 5% of head and neck PGL cases (Maher, 2006). Heterozygous germline *SDHD* and *SDHB* mutations were identified in kindreds with familial PC with or without PGL

(Gimm *et al.*, 2000; Astuti *et al.*, 2001a,b). Approximately 40% of patients with familial or bilateral PC and 5-10% of patients with sporadic PC can be carriers of germline *SDHD* or *SDHB* mutations (Astuti *et al.*, 2001a; Gimm *et al.*, 2000; Benn *et al.*, 2003; Maher, 2006). The presence of PGL in a personal or family history increases the likelihood of detecting a *SDHB* or *SDHD* mutation (Neumann *et al.*, 2002; Maher, 2006). Among patients with PC *SDHB* mutations are more frequent than *SDHD* mutations, but the reverse is true for patients with PGL (Gimenez-Roqueplo *et al.*, 2003; Benn *et al.*, 2006; Gimenez-Roqueplo, 2006). Several studies have confirmed that *SDHB* gene mutation is associated with a high risk of malignancy of PC, identifying such mutations as one of the first prognosis factors for PC (Gimenez-Roqueplo *et al.*, 2003; Neumann *et al.*, 2004; Gimenez-Roqueplo, 2006). *SDHB* disease seems to have a lower penetrance than *SDHD* disease (Gimenez-Roqueplo, 2006; Mannelli *et al.*, 2007). Multifocal tumors seem to be more common in patients with *SDHD* mutations (Neuman *et al.*, 2004; Gottlieb and Tomlinson, 2005; Mannelli *et al.*, 2007).

Nonsense and missense mutations, insertions, small and large deletions have been reported in the SDH genes (*SDHD* and *SDHB* genes) of patients with PC and/or PGL (Cascon *et al.*, 2002; Benn *et al.*, 2003; Novosel *et al.*, 2004; Gimenez-Roqueplo, 2006).

Approximately three-quarters of all individuals with PC and germline *SDHD* mutation have mutations in the first three codons of the *SDHD* gene. PC-susceptibility-associated germline *SDHB* mutations have a mutation spectrum throughout exons 2-7 (Maher and Eng, 2002; Eng *et al.*, 2003). Mutations in *SDHD* or *SDHB* that result in truncated proteins cause disassembly of complex II and, therefore, prevent its catalytic and electron-transport functions (Gimenez-Roqueplo *et al.*, 2001; Gimenez-Roqueplo *et al.*, 2002 ). Complete disassembly of complex II causes the predisposition to PC, whereas partial inactivation of its catalytic activity leads to head and neck PGL (Maher and Eng, 2002; Eng *et al.*, 2003).

*SDHC* mutations have only been reported in four families with PGL to date (Nieman *et al.*, 2000; Nieman *et al.*, 2003; Gottlieb and Tomlinson, 2005; Baysal *et al.*, 2004).

No *SDHA* mutation has been identified in patients with PC and/or PGL. Homozygous germline mutations of *SDHA* causes the Leigh syndrome, a rare type of encephalomyopathy in children (Maher and Eng, 2002; Eng *et al.*, 2003; Gottlieb and Tomlinson, 2005). Mutations of *SDHA* only result in a 25-50% decrease of SDH enzymatic activity (Favier *et al.*, 2005).

*SDHD* gene seems to be maternally imprinted with susceptibility to PGL or PC expressed only after paternal transmission (Heutink *et al.*, 1992; Heutink *et al.*, 1994; Badenhop *et al.*, 2001). But so far no conclusive evidence for imprinting and allele specific expression of *SDHD* has been found (Gottlieb and Tomlinson, 2005; Maher, 2006). There is no evidence of imprinting

associated with either *SDHB* or *SDHC* (Baysal *et al.*, 2002; Niemann *et al.*, 2000; Astuti *et al.*, 2001a).

To date, no genotype-phenotype correlations that would explain the variable phenotype of germline mutations in *SDHB* and in *SDHD* are apparent, and genetic or environmental modifiers may be implicated in this process (Astuti *et al.*, 2001a; Benn *et al.* 2003).

The genes encoding SDH are considered as "housekeeping genes" because of their key role in cellular metabolism (Gottlieb and Tomlinson, 2005). But at the same time SDH genes (*SDHD*, *SDHC*, *SDHB*) have been shown to be tumor suppressor genes (Gottlieb and Tomlinson, 2005; Favier *et al.*, 2005; Gimenez-Roqueplo, 2006b). Consistent with Knudson's two-hit hypothesis for tumorigenesis involving a tumor-suppressor gene, a heterozygous germline mutation in an SDH gene is usually associated with somatic loss of the normal allele (LOH), leading to inactivation of the SDH gene (Gottlieb and Tomlinson, 2005). Biallelic inactivation of *SDHB* and *SDHD* genes, resulting in the complete loss of both the catalytic activity of SDH and electron transfer activity, was demonstrated in a set of PCs and PGLs (Gimenez-Roqueplo *et al.*, 2001; Gimenez-Roqueplo *et al.*, 2002).

The molecular and cellular mechanisms linking SDH mutations and tumorigenesis remain unknown and experimental models for the study of these disorders have not yet been developed. Several hypotheses have been put forward. They involve a mitochondrial dysfunction leading to resistance to apoptosis, accumulation of oxygen free radicals and oxidative stress, or pseudo-hypoxia acting as protumoral factor. Metabolic signalling, involving TCA cycle metabolites, such as succinate, as intracellular messengers is also regarded as one of the possible mechanisms which can contribute to PC and/or PGL formation (Eng *et al.*, 2003; Gottlieb and Tomlinson, 2005; Favier, 2005).

Mitochondria can act as an oxygen sensor by increasing the generation of reactive oxygen species, which are required for HIF $\alpha$  DNA-binding activity. The carotid body is the most common site of neck and head PGL. Since the carotid body contains oxygen chemoreceptors, it has been suggested that chronic hypoxic stimulation could account for the high frequency of sporadic occurrence of head and neck PGLs in individuals who live at high altitude (Rodriguez-Cuevas *et al.*, 1998). Chronic hypoxia could also explain the mechanism whereby mutations in SDH proteins (particularly, SDHD protein) lead to hereditary PGLs, and by extrapolation, to PCs (Baysal *et al.*, 2000; Maher and Eng, 2002).

The induction of a pseudo-hypoxic pathway can be a possible link between SDH mutations and tumorigenesis. This pseudo-hypoxia model implies a link between inactivation of SDH and the induction of a hypoxic response under normoxic conditions. This response is mediated by the oxygen-regulated HIF transcription factor (Gottlieb and Tomlinson, 2005; King *et al.*, 2006). In

several reports the levels of HIF1 $\alpha$ , HIF2 $\alpha$  /EPAS1 and /or HIF target genes were shown to be increased in SDHB and SDHD -deficient PCs and PGLs (Gimenez-Roqueplo *et al.*, 2001; Dahia *et al.*, 2005a; Pollard *et al.*, 2005). Moreover, Dahia *et al.* (2005a) found that loss of two genes of succinate dehydrogenase gene family- *SDHB* and *SDHD*- triggers a HIF1 $\alpha$  response. The researchers also discovered that high HIF1 $\alpha$  levels can suppress *SDHB* what suggest a regulatory loop between them that further enhances the "hypoxia" profile of tumors (Dahia *et al.*, 2005a). Comparison of gene expression profiles in VHL-, SDHB- and SDHD-associated PCs demonstrated a shared transcription profile of reduced oxidoreductase and increased angiogenesis / hypoxia target genes (Dahia *et al.*, 2005a). All these findings suggest that *VHL*, *SDHB* and *SDHD* gene inactivation is linked to HIF-dysregulation (Woodward and Macher , 2006; Maher, 2006).

Selak *et al.* (2005) showed that disruption of the mitochondrial complex II results in the accumulation of succinate and consequently in the inhibition of HIF- $\alpha$  prolyl hydroxylases (Egln family members), leading to stabilisation and activation of HIF-1 $\alpha$ , futher implicating HIF dysregulation in PC tumorigenesis. Succinate is not only a substrate for SDH in the mitochondria, but also a product of prolyl hydroxylases. Therefore, the accumulation of succinate by feedback will also inhibit prolyl hydroxylases (Selak *et al.*, 2005; King *et al.*, 2006). These findings confirm the role of the metabolic signalling pathway mediated by succinate in PC and PGL development.

In view of the role of mitochondria in apoptosis inactivation of SDH might lead to failure of apoptosis in neuroendocrine progenitor cells predisposing to the development of PC and PGL (Astuti *et al.*, 2001a,b; Maher and Eng., 2002).

### **1.2.5. Inherited PC susceptibility genes and neuronal developmental apoptosis pathway**

Lee *et al.* (2005) has proposed that all four inherited PC syndromes involving *RET*, *VHL*, *NF1*, succinate dehydrogenase gene family (*SDHB*, *SDHD*) share a common mechanism of tumorigenesis due to impaired developmental culling of sympathetic neuronal precursor cells (Fig.1.1).

They hypothesized that inherited PCs originate from sympathetic neuronal precursor cells that usually undergo c- Jun dependent apoptosis during embryogenesis when growth factors such as nerve growth factor (NGF) become limiting (Estus *et al.*, 1994; Ham *et al.*, 1995; Xia *et al.*, 1995). Jun B is an antagonist of c-Jun such that increased levels of Jun B attenuate c-Jun induced apoptosis in PC cells with NGF withdrawal. Lee *et al.* (2005) found that all pVHL mutants tested (including 2C mutants that retain the ability to degrade HIF) failed to downregulate JunB



following NGF withdrawal, thus promoting cell survival. Furthermore, a similar effect was also demonstrated with activating mutations of *RET*. Straub *et al.* (2003) and Lee *et al.* (2005) showed that EglN3 (HIF $\alpha$  prolyl hydroxylase) is necessary for induction of neuronal apoptosis after NGF withdrawal. It was identified that EglN3 acts downstream of c-Jun and is sensitive to changes in SDH activity such that after *SDH* inactivation, succinate accumulation inhibits the activity of EglN3 thus preventing apoptosis of the neuronal precursor cells.

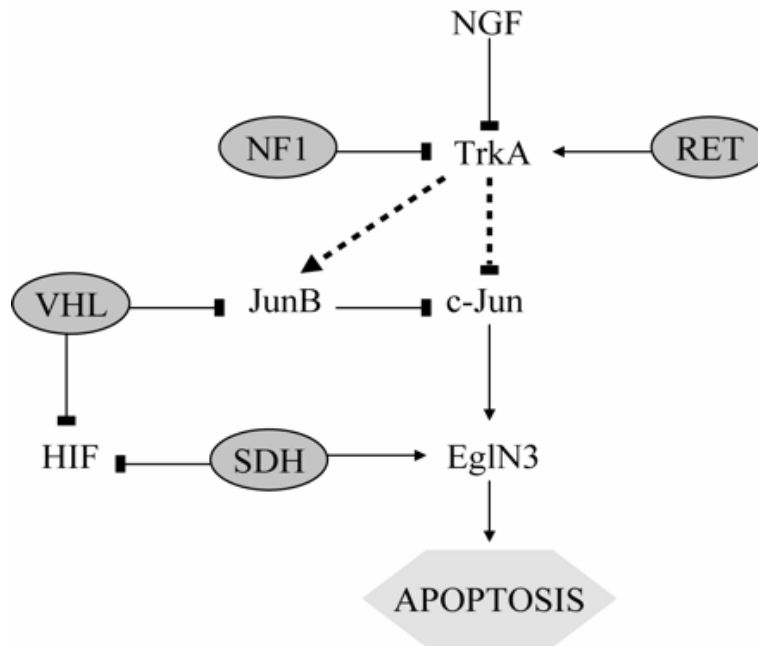


**Fig1.1** Model linking familial PC genes to apoptosis after nerve growth factor (NGF) withdrawal. Germline *NF1*, *RET*, *SDH* (*SDHB*, *SDHD*) and *VHL* mutations allow sympathetic neuronal progenitors to escape from developmental apoptosis and thereby set the stage for their neoplastic transformation. Data source: Lee *et al.*, 2005; Maher, 2006.

Nf1 inhibits downstream signalling by NGF receptor, TrkA, and loss of NF1 promotes NGF-independent survival of embryonic peripheral neurons (Vogel *et al.*, 1995). Activation of RET, like loss of pVHL, has been shown to lead to the induction of Jun B and attenuates apoptosis after NGF withdrawal. SDH inactivation blunts neuronal apoptosis through its effects on EglN3 (Lee *et al.*, 2005).

Thus, all these findings provide a common link between PC development in inherited PC susceptibility syndromes.

### 1.3. Nonsyndromic sporadic PC

When the family history of PC patients is negative for PC, the patient's disease is termed sporadic. However, this designation cannot exclude the possibility of the presence of a de novo germline mutation in one of the PC susceptibility genes (Korpershoek *et al.*, 2006).

Clinical and molecular evaluation of 271 unrelated patients with purported nonsyndromic PC (without a family history of the disease) performed by Neuman *et al.* (2002) revealed that 66 patients (24 %) had deleterious germ-line mutations of one of the known susceptibility genes for PC— *VHL*, *RET*, *SDHD*, and *SDHB*. Of the 271 patients, 241 presented with PC only, whereas 8 presented with both PC and functioning PGLs and 22 with PGL only. Among these 66 patients with germ-line mutations, 45 % had mutations of *VHL*, 20% had mutations of *RET*, and 17 and 18% had mutations of *SDHD* and *SDHB*, respectively. The authors showed that certain subgroups of patients with “sporadic” PC have a higher risk of hereditary disease: those who are relatively young at presentation, those with bilateral or multifocal tumors, and those with extra adrenal PC. It was also demonstrated that multifocal tumors can be gene specific: no patients with mutations of *SDHB* presented with multifocal disease, whereas 40% of those with mutations of *VHL* had multifocal disease. In patients with extra adrenal tumors, no mutations in *RET* were identified while 28% of patients with mutations of *VHL*, *SDHD*, and *SDHB* had extra-adrenal tumors.

Korpershoek *et al.* (2006) investigated 213 cases of apparently sporadic PCs for mutations in *RET* (exons 10, 11, and 16), *VHL*, *SDHD*, and *SDHB*. A total of 7.5% of the apparently sporadic PCs harboured germline mutations in the PC-causing genes (0% *RET*, 4.4% *VHL*, 1.6% *SDHD*, and 1.5% *SDHB*). *VHL* mutations were the most abundant germline mutations discovered in sporadic PCs. Somatic *RET* mutations were found in this study, they include C618Y, C634R, and M918T mutations. No *RET* germline mutations were identified.

Gimenez-Roqueplo *et al.* (2003) carried out a retrospective study of 84 apparently sporadic PC or functional PGL cases collected by the COMETE network and did not find germline *RET* mutations. All patients with syndromic disease or a family history were excluded from the study. Eighty-four patients (57 with a single benign adrenal PC, 6 with extra adrenal PC and 21 with a malignant form of the tumor with an adrenal or extra adrenal primary tumor site) were screened for the PC susceptibility genes – *RET*, *VHL*, *SDHD*, and *SDHB*. In 10 (12%) of the 84 patients germline mutations were identified. 2 (2.4%) patients had mutations in *VHL* gene and 8 (9.5%) had deleterious mutations in *SDHB* gene. LOH at the *SDHB* locus was found in all tumors with *SDHB* mutation. No mutations of *SDHD* were detected. This study demonstrates that the

presence of germline mutations in the *SDHB* gene is strongly associated with extra-adrenal PCs and confers a high risk of recurrence or malignancy of PC.

The study by Amar *et al* (2005) confirmed that *SDHB* mutation is a predictive factor for malignancy of PCs and PGLs and a factor of poor prognosis.

Germline and somatic mutations in *SDHD* gene were identified in apparently sporadic PCs by Gimm *et al.* (2000). Astuti *et al.* (2001a) found germline mutations in *SDHB* gene in familial and sporadic PCs.

RET overexpression is observed in the majority (50-70%) of sporadic PCs that do not harbour somatic mutations, amplifications or rearrangements of *RET*. This indicates that *RET* has a significant role in the tumorigenesis of sporadic PCs, either by autocrine or paracrine stimulation (Matias-Guiu *et al.*, 1995; Takaya *et al.*, 1996; Le Hir *et al.*, 2000; Edsröm *et al.*, 2000a)

RET overexpression is unlikely to occur in extra-adrenal PCs and PGLs. Also, *RET* mutations have not been detected in these tumors (Edsröm *et al.*, 2000a; de Krijger *et al.*, 2000).

In summary, the differences in germline mutation frequencies of *RET*, *VHL*, *SDHD* and *SDHB* genes shown by different studies of hospital-based and population-based series of apparently sporadic PCs can be explained by differences in the investigated populations in different geographical areas (Korpershoek *et al.* , 2006; Jiménez *et al.*, 2007). It is known that the prevalence of VHL syndrome is associated with PC in the Black Forest area of Germany, where there is an estimated VHL prevalence of one in 38.951 (Neuman *et al.*, 1991). Jiménez *et al.* (2007) in his study analyses the question of ascertainment bias and the role of the adequacy of establishing family history in evaluating the true incidence of hereditary PCs in the general population. The question about selection bias in terms of estimation of frequency of *SDHD* mutations in the series of sporadic PCs is discussed in the study by Gimenez-Roqueplo *et al.* (2003).

A partial explanation for the high frequency of hereditary PC without a family history of disease might include spontaneous mutation in one of the susceptibility genes, decreased penetrance, maternal imprinting, although other causes such as gene-gene interactions and gene-environment interactions may be possible (Astuti *et al.*, 2001b; Neuman *et al.*, 2002; Bryant *et al.*, 2003).

Sporadic adrenal PCs may have somatic mutations. Somatic *RET* and *VHL* mutations occur in a low frequency in sporadic PCs: 0 -10% for *RET* gene and < 8% for *VHL* gene (Eng *et al.*, 1995; Hofstra *et al.*, 1996; Brauch *et al.*, 1997; Koch *et al.*, 2002a,b; Korpershoek *et al.*, 2006). Somatic mutations of *SDHB* and *SDHD* genes are also infrequent in cases of sporadic PC (Gimm *et al.*, 2000; Astuti *et al.*, 2001a,b; Aguiar *et al.*, 2001; Astuti *et al.*, 2001a).

Bausch *et al.* (2006c) performed an intragenic mutation scanning of the *NF1* gene in 27 apparently sporadic PCs without germline mutations of *VHL*, *RET*, *SDHB*, and *SDHD*. Of the 27 apparently sporadic cases, one (4%) was found to have a pathogenic germline *NF1* mutation. No somatic or germline *SDHC* mutations were detected in the cases of sporadic PC (Astuti *et al.*, 2001a, Amar *et al.*, 2005).

The concept that germline *NF1*, *RET*, SDH subunit and *VHL* mutations promote PC development by allowing sympathetic neuronal progenitors to escape from developmental apoptosis (Lee *et al.*, 2005) is consistent with the observation that somatic mutations of *SDHB*, *SDHD*, *RET*, *VHL*, and *NF1* are extremely rare in nonhereditary sporadic PC (Maher, 2006; Woodward and Maher, 2006).

## **1.4. Involvement of other genes in PC development**

### **1.4.1. Novel PC susceptibility loci**

At present the susceptibility genes known to predispose to PC formation are the *VHL* (Latif *et al.*, 1993), *RET* (Mulligan *et al.*, 1993b), *NF1* genes (White and O'Connell, 1991; Bausch *et al.*, 2006a,b; Bausch *et al.*, 2007), *SDHB*, *SDHD* (Astuti *et al.*, 2001a,b; Cascon *et al.*, 2002). There are families affected by PC where no germline mutations of these susceptibility genes have been found, thus suggesting that other, still unknown, genes might be involved in the pathogenesis of this tumor (Dannenberg *et al.*, 2000; Cascon *et al.*, 2002; Dahia *et al.*, 2005a; Opocher *et al.*, 2006; Mannelli *et al.*, 2007). Dahia *et al.*, (2005b) reported a novel familial variant of PC consistent with a double recessive digenic inheritance being responsible for the disease phenotype. The authors identified two novel susceptibility loci (Familial PC loci) on chromosomes 2q and 16p13. One of these regions, located on chromosome 2q, appears to involve a tumor-suppressor gene, while the second locus, on chromosome 16p13, coincides with the locus of hereditary neuroblastoma (Dahia *et al.*, 2005b). This finding broadens the spectrum of genetic defects and mode of inheritance of PC.

### **1.4.2. Somatic mutations in PC**

From LOH studies, losses of chromosomal regions 1p (Khosla *et al.*, 1991; Moley *et al.*, 1992; Bender *et al.*, 2000, Benn *et al.*, 2000); 3p (Khosla *et al.*, 1991; Bender *et al.*, 2000), 11p (Tsutsumi *et al.*, 1989; Vargas *et al.*, 1997); 17p (Khosla *et al.*, 1991; Herfarth *et al.*, 1997); and

22q (Bender *et al.*, 2000; Khosla *et al.*, 1991; Tanaka *et al.*, 1992) are known to occur frequently in both sporadic and familial forms of PC.

There are multiple tumor suppressor genes in the region of 1p: *CDKN2C* and *PTPRF* gene. Franklin *et al.* (2000) showed that *Cdkn2c-Cdkn1b* double mutant mice (*Cdkn2c*<sup>-/-</sup> / *Cdkn1b*<sup>-/-</sup>) develop adrenal PC. Subsequent work by Aarts *et al.* (2006) did not detect any mutations in the *CDKN2C* gene, or in the tyrosine kinase domains of the *PTPRF* gene in a panel of 20 PCs. *PTPRF* specifically suppresses the biological activities of RET\_MEN2A mutant proteins by reducing its kinase activity (Qiao *et al.*, 2001). Yang *et al.* (2000) detected altered expression of mRNA and protein level of the *Ptprf* gene in the New England Deaconess Hospital rat line (NEDH) exhibiting spontaneous PC. *Ptprf* mRNA and protein levels were decreased in NEDH adrenal medullary tissue harvested at 2-3 months of age, a period well before early stages of tumors become evident (Yang *et al.*, 2000). PTPRF-deficient PC12 cell clones have decreased levels of PTPRF protein and significantly increased proliferation rates (Tisi *et al.*, 2000).

Allelic loss at 3p is an area harbouring many genes, including *VHL* and *RASSF1*. No mutations in *RASSF1* at 3p21 were found. However, hypermethylation of the CpG island in the promoter region of isoform A of *RASSF1* (*RASSF1A*), was identified in 5 of 23 (20%) sporadic PCs (Astuti *et al.*, 2001c).

Loss of 17p suggests the involvement of *TP53*, which is possibly the most commonly mutated gene in human cancers (Khosla *et al.*, 1991; Dannenberg *et al.*, 2006). Conflicting results exist with regard to the frequency of *TP53* gene alterations in PCs. A high frequency of *TP53* gene mutations has been reported in multiple and malignant PCs (Lin *et al.*, 1994; Yoshimoto *et al.*, 1998), whereas others reported an absence of *TP53* alterations (Dahia *et al.*, 1995; Herfarth *et al.*, 1997).

Overexpression of p53 protein, encoded by the *TP53* gene, was found in PCs and PGLs in the several studies (De Krijger *et al.*, 1999; Gupta *et al.*, 2000; Lam *et al.*, 2001). De Krijger *et al.* (1999) demonstrated that malignant PCs had a higher frequency of p53 and Bcl-2 protein expression than benign ones, suggesting antiapoptotic mechanisms in the pathogenesis of malignant PCs.

In mice, inactivation of both *Pten* and *Cdkn2a* tumor suppressor genes resulted in the development of PC, whereas the classical PC susceptibility genes *Ret*, *Vhl*, and *Nf1* remained intact (You *et al.*, 2002).

Possibly, loss of BMP2 plays a role in PC tumorigenesis by modulating PTEN activity (Aarts *et al.*, 2006). Bone morphogenetic proteins (BMPs) are members of the transforming growth factor- $\beta$  (TGFB) superfamily and have been shown to play a role in cell proliferation and differentiation in bone. However, TGFB2, TGFB3, and BMP4 may also be involved in chromaffin cell

development, since these molecules are highly expressed in the neural crest-derived sympathoadrenal progenitor cells and during migration in embryonic development (Huber *et al.*, 2002; Aarts *et al.*, 2006).

Almost 100% of *Pten* heterozygous mice spontaneously develop bilateral PCs (Podsypanina *et al.*, 1999; Podsypanina *et al.*, 2001; Puc *et al.*, 2006). Moreover, Puc *et al.* (2006) hypothesized that the human *PTEN* gene might be altered in sporadic PC. They analysed 29 human sporadic PCs for mutations within coding sequence of the *PTEN* gene and examined the PTEN protein expression level in a set of human adrenal glands including 8 normal adrenal glands and 11 sporadic PCs. No mutations of the *PTEN* gene were revealed and the level of *PTEN* gene expression was unchanged.

No mutations have been detected in the *CDKN2A* tumor suppressor gene in the series of benign and malignant PCs (Aguiar *et al.*, 1996). But Damman *et al.* (2005) reported inactivation of *CDKN2A* by hypermethylation of its CpG island promoter in 24% of analysed sporadic and MEN2-associated PCs.

Loss of *RBI* gene expression in PCs was found in two studies (Gupta *et al.*, 2000; Lam *et al.*, 2001). Gupta *et al.* (2000) demonstrated that loss of RB protein product was more common in malignant adrenal and extra-adrenal PCs than in benign ones.

The protooncogene *ERBB2* may play a role in PC progression, as indicated by an immunohistochemical study of 34 PCs (27 were sporadic) that revealed a higher intracytoplasmic granular erbB-2 staining in malignant tumors (Castilla-Guerra *et al.*, 1997).

Mutational analysis of the *MEN1* gene was performed on 30 tumors including PCs and abdominal PGLs and did not reveal any mutations of the gene although two polymorphisms were identified (Edström *et al.*, 2000).

In conclusion, in both familial and sporadic PCs, accumulation of mutations and deletions in numerous genes such as *CDKN2C*, *PTPRF*, *RASSF1*, *TP53*, *PTEN*, *CDKN2A*, *RBI*, *MEN1*, may develop during tumor evolution and progression. How these genetic alterations affect biochemical pathways and stimulate tumorigenesis remains to be shown (Koch *et al.*, 2002b).

## **1.5. Comparative genomic hybridization (CGH) and gene expression array analyses of PC**

Modern molecular techniques, such as CGH and gene expression array analyses have been used to elucidate pathogenetic mechanisms of PC development.

There are several studies using CGH arrays to analyze sporadic and familial PCs for chromosomal losses and gains (Dannenberg *et al.*, 2000; Edström *et al.*, 2000b; Lui *et al.*, 2002; Cascón *et al.*, 2005; Aarts *et al.*, 2006). In all studies copy number losses were found more frequently than copy number gains, indicating that the inactivation of tumor suppressor genes plays a critical role in tumorigenesis.

Dannenberg *et al.* (2000) performed CGH analysis on 29 apparently sporadic PCs (19 clinically benign tumors and 10 malignant lesions). 4 of the 29 PCs were extra-adrenal. The most frequently observed changes were losses of chromosomes 1p11-p32 (86%), 3q (52%), 6q (34%), 3p, 17p (31% each), 11q (28%), and gains of chromosomes 9q (38%) and 17q (31%). No difference between adrenal and extra-adrenal tumors was detected. The authors suggest that a high frequency of losses of chromosomes 1p and 3q in the benign tumors indicates that they are important genetic events in early tumorigenesis.

Edström *et al.* (2000b) found similar patterns of CGH alterations in 23 PCs and 11 abdominal PGLs. They studied 4 cases of sporadic malignant tumors, 13 benign sporadic tumors and 6 familial (MEN2A and NF1) PCs. CGH results in PCs revealed frequent losses on chromosomes 1p (83%), 3q (39%), 11p (17%), 3p (17%), 4q (17%), and 11q (13%). Gains were observed predominantly on 16p (15%), 17q (17%), 19q (26%), and 19p (26%). The authors could not detect any major differences in the pattern of copy number changes between PC and abdominal PGL. Loss of 1cen-p13 was detected in the majority of tumors, regardless of subtype and degree of malignancy. It is likely that inactivation of a gene located in this region is an important and early event in the development of these tumor types. Chromosomes 3, 11, 17 and 19 may also be involved in tumor progression.

Lui *et al.* (2002) characterized the genetic profiles of 36 VHL-related and 5 MEN2-associated PCs. The authors found that losses of chromosome 3p or the whole of chromosome 3 was the most common abnormality, detected in 94% of VHL-related PCs. In MEN2-associated tumors either loss of the whole chromosome 3 (80%) or 3q (20%) loss was observed. The loss of chromosome 11p and/or 11q was more common in the group of VHL-related PCs (86%) than in MEN2-associated tumors (40%). Loss of chromosome 1p11-p31 was detected in all MEN2-related PCs, but only in 6 of 36 (17%) VHL-related PCs.

Based on the literature data, sporadic and MEN 2-related PCs appear to have a distinct genetic pathway compare to the VHL-related PCs. In particular, loss of chromosome 1p is important for both MEN2-related and sporadic tumors but not for the VHL-related PCs (Lui *et al.*, 2002; Bender *et al.*, 2000; Aarts *et al.*, 2006). These findings are consistent with a data received by Benn *et al.* (2000), who found loss of 1p in 61% of sporadic PC and 80% of MEN2-related PCs

but none of the two VHL-related PCs. Moreover, the loss of chromosome 11 (loss of 11p and/or 11q) appeared to be specific for VHL-related PCs (Lui *et al.*, 2002).

Cascón *et al.* (2005) showed that the CGH profiles of PCs and head and neck PGLs differ significantly. 72% of the PCs versus only 37.5 % of PGLs showed partial or total loss of chromosome 3. Loss of 1q was found only in PGLs.

In the study by Dahia *et al.*, (2005a) inherited and sporadic PCs and PGLs were segregated into two groups on the basis of gene expression profiling. Cluster 1 comprised all tumors with VHL and SDH mutations, whereas MEN2-related and NF1-associated PCs were included in the cluster 2. The VHL and SDH tumors show high expression of hypoxia-, angiogenesis-, and matrix-related genes, while RET and NF1-PCs are associated with a profile consistent with the activation of the Ras/MAPK pathway. Similar distinctions between gene expression patterns of VHL-related and MEN2-associated PCs were found in the study by Eisenhofer *et al.* (2004a).

To date no reliable clinical or histopathological markers are available to distinguish benign from malignant PCs. Metastases, occurring in approximately 10% of the tumors, are the only convincing sign of malignancy. They may already be present at the time of diagnosis or occur with a latency as long as 25 to 30 years (Eisenhofer *et al.*, 2004b; Ahlman, 2006).

Dannenberg *et al.* (2000) in the series of sporadic PCs demonstrated that progression to malignant tumors was strongly associated with deletion of chromosome 6q and 17p. Underrepresentations of chromosome 17p were observed in metastasizing lesions. Three malignant PCs exhibited simultaneous gains of chromosomes 5p, 7p and 12q, similar to findings for malignant endocrine pancreatic tumors (Dannenberg *et al.*, 2000). There are data which suggest that malignant sporadic PCs may be associated with LOH of 1p (Bender *et al.*, 2000).

In the study by Edström *et al.*, (2000b) it was shown that conversion to a malignant phenotype may be associated with changes on chromosome 11. Loss of 11q22-23, including the *PGL1* locus, was common in malignant PCs.

In the study by Cascón *et al.* (2005) malignant PCs showed a loss of 8p22-23 in association with a gain of 11cen-11q13, indicating that these alterations also could be markers of malignancy.

## **1.6. Animal models of PC**

Adrenal medullary hyperplasia and PCs are rare in most species, but more common in rats (Powers *et al.*, 2000). In addition, adult rat chromaffin cells proliferate in response to a variety of stimuli *in vivo* and *in vitro*. PCs are induced in rats by many non-genotoxic substances, including



drugs that increase sympathetic nervous system activity and food supplements (Tischler *et al.*, 1989; Tischler *et al.*, 1991; Tischler *et al.*, 1993, Tischler *et al.*, 1994; Tischler *et al.*, 1999). Studies by Powers *et al.* (2001, 2005) demonstrated potential utility of the rat model for studying the role of *Ret* in the adrenal medulla and the mechanism of its involvement in MEN2 and other PC syndromes. Upregulation of RET protein expression in rat chromaffin cell cultures by neurturin and glial cell line-derived neurotrophic factor was shown in the study by Powers *et al.* (2001), suggesting a mechanism for potentiation of chromaffin cell mitogenesis. Expression of Ret protein and mRNA was shown to be up-regulated in adult rat adrenal medulla *in vivo* by reserpine (Powers *et al.*, 2005). It is known that long-term administration of reserpine leads to the development of adrenal medullary hyperplasia and PCs in rats (Tischler *et al.*, 1995). A considerable number of transgenic and knockout mouse models have been used for the study of tumorigenic mechanisms of PC development as well (Table 1.3).

**Table 1.3** Mouse models of adrenal medulla hyperplasia and pheochromocytoma

Model	Adrenal medullary hyperplasia / Pheochromocytoma	Frequency (%)	Other neoplasias	Reference
<i>Cdkn1b</i> <sup>-/-</sup>	Hyperplasia of adrenal medulla	100*	multiple organ hyperplasia ( thymus, spleen, testis, ovary, prostate), retinal dysplasia, pituitary tumors	Nakayama <i>et al.</i> , 1996
<i>Cdkn2c</i> <sup>-/-</sup>	Pheochromocytoma	8 (2/24)	tumors of pituitary, thyroid,	Franklin <i>et al.</i> , 2000
<i>Cdkn1b</i> <sup>-/-</sup>	Pheochromocytoma	24 (5/21)	parathyroid glands, pancreas,	Franklin <i>et al.</i> , 2000
<i>Cdkn2c</i> <sup>-/-</sup> <i>Cdkn1b</i> <sup>+/-</sup>	Pheochromocytoma	17 (4/24)	testis, stomach,	Franklin <i>et al.</i> , 2000
<i>Cdkn2c</i> <sup>+/-</sup> <i>Cdkn1b</i> <sup>-/-</sup>	Pheochromocytoma	50 (3/6)	intestine, lungs	Franklin <i>et al.</i> , 2000
<i>Cdkn2c</i> <sup>-/-</sup> <i>Cdkn1b</i> <sup>-/-</sup>	Pheochromocytoma	91 (21/23)		Franklin <i>et al.</i> , 2000
<i>Cdkn2a</i> <sup>+/-</sup> <i>Pten</i> <sup>+/-</sup>	Pheochromocytoma	24 (14/59)	tumors of thyroid gland, breast,	You <i>et al.</i> , 2002
<i>Cdkn2a</i> <sup>+/-</sup> <i>Pten</i> <sup>+/-</sup>	Pheochromocytoma	57 (21/37)	pancreas, colon, lung, endometrium,	You <i>et al.</i> , 2002
<i>Cdkn2a</i> <sup>-/-</sup> <i>Pten</i> <sup>+/-</sup>	Pheochromocytoma	59 (27/46)	testis, hematological neoplasms	You <i>et al.</i> , 2002
<i>Rb1</i> <sup>-/-</sup>	Hyperplasia of adrenal gland	100 (4 <sup>†</sup> )	tumors of eye, the intermediate lobe of the pituitary	Williams <i>et al.</i> , 1994
<i>Rb1</i> <sup>+/-</sup>	Pheochromocytoma	71 (22/31)	tumors of pituitary, parathyroid, thyroid glands, lung	Nikitin <i>et al.</i> , 1999
<i>Nf1</i> <sup>+/-</sup>	Pheochromocytoma	20 (15/75)	not determined <sup>‡</sup>	Powers <i>et al.</i> , 2000
<i>Nf1</i> <sup>+/-</sup>	Pheochromocytoma	19 (8/43)	hematological neoplasms, tumors of lung, liver, fibrous connective tissue	Jacks <i>et al.</i> , 1994
<i>Ret</i> <sup>MEN2B/MEN2B</sup>	Pheochromocytoma	100 (27/27)	hyperplasia of thyroid C-cells, reproductive defect in males	Smith-Hicks <i>et al.</i> , 2000
<i>c-mos</i> transgenic mice	Pheochromocytoma	58 (90/154)	medullary thyroid neoplasms	Schulz <i>et al.</i> , 1992

\*The exact number of analysed animals in the study by Nakayama *et al.*, 1996 is unknown

<sup>†</sup>In the study by Williams *et al.* (1994) adrenal glands of 4 *Rb1*<sup>-/-</sup> mice were histologically examined to prove the presence of hyperplasia.

<sup>‡</sup>Powers *et al.* (2000) used pheochromocytoma cell lines from *Nf1*<sup>+/-</sup> knockout mice (MPC cell line).

Studies performed in mice have shown that neuroendocrine tissues are especially sensitive to defects in cell-cycle regulatory proteins affecting the Rb pathway (Franklin *et al.*, 2000; Pellegata *et al.*, 2007). Franklin *et al.* (2000) characterized two strains of double mutant mice lacking either *Cdkn2c* and *Cdkn1b* or *Cdkn2c* and *Cdkn1a* (Table 1.3) and showed that functional collaborations between different cyclin dependent kinase (CDK) inhibitor genes suppress tumor growth with distinct tissue specificities. While the loss of both *Cdkn2c* and

*Cdkn1b* resulted in spontaneous development of multiple tumors, predominantly in endocrine organs (pituitary, adrenals, thyroid, parathyroid glands, pancreas) by 3 months of age, *Cdkn2c - Cdkn1a* double null mice developed pituitary adenomas, gastric neuroendocrine cell hyperplasia, and lung bronchioalveolar tumors later in life (Franklin *et al.*, 2000). Like *Cdkn2c - Cdkn1b* double mutant mice, *Rb1* heterozygous mice developed neoplastic phenotypes in multiple endocrine tissues, including the pituitary, thyroid, parathyroid, and adrenal glands, providing genetic evidence that *Cdkn2c* and *Cdkn1b* genes function to suppress tumor growth by regulating *Rb1* tumor suppression function (Nikitin *et al.*, 1999). Hyperplasia of the adrenal medulla also develops in mice chimeric for *Rb1*<sup>-/-</sup> (Williams *et al.*, 1994a) (Table 1.3).

You *et al.* (2002) examined functional interactions between *Pten* and *Cdkn2a* genes in the suppression of tumorigenesis in mice and showed that *Cdkn2a* deficiency increase the penetrance and reduce the latency of cancers associated with *Pten* heterozygosity (Table 1.3). The authors showed that all PCs in *Cdkn2a*<sup>+/+</sup>-*Pten*<sup>+/-</sup> mice were diagnosed at 36 weeks of age or older and the majority of them were unilateral. In contrast, *Cdkn2a*<sup>-/-</sup>-*Pten*<sup>+/-</sup> and *Cdkn2a*<sup>+/-</sup>-*Pten*<sup>+/-</sup> mice presented with an earlier onset of PCs, which were often bilateral and larger compare to the size of PCs in *Cdkn2a*<sup>+/+</sup>-*Pten*<sup>+/-</sup> mice. It is interesting to note, that the *CDKN2A* gene encodes two tumor suppressors proteins, p16(INK4A) and p14(ARF) (p19(ARF) in mice), that function as regulators of the RB and p53 pathways, respectively (Rocco *et al.*, 2001).

Mice heterozygous for both *p53* and *Rb1* develop multiple endocrine tumors (with a spectrum similar to those observed in the *Cdkn2c-Cdkn1b*-deficient mice but more aggressive in growth (Williams *et al.*, 1994b).

In summary, all these data support a role of RB pathway, including *Cdkn2c*, *Cdkn1b*, and *Rb1*, in suppressing endocrine tumor initiation and p53 pathway in suppressing tumor progression (Franklin *et al.*, 2000).

## **1.7. The rat model of multiple endocrine neoplasia X (MENX) syndrome**

Fritz *et al.* (2002) has identified a MEN-like syndrome in a Sprague Dawley rat-breeding colony. The MEN-like syndrome was named as MENX syndrome because the spectrum of affected tissues is reminiscent of both MEN type 1 (MEN1) and MEN type 2 (MEN2) syndromes in man (Fritz *et al.*, 2002) (Table 1.4).

Affected animals (indicated as mut/mut) develop bilateral PC and parathyroid adenomas, multifocal thyroid C cell hyperplasia, PGLs, and endocrine pancreas hyperplasia. In addition, affected animals develop bilateral juvenile cataracts in the first few weeks of life (Fritz *et al.*,

2002; Pellegata *et al.*, 2006). In man, the multiple endocrine neoplasia (MEN) syndromes are inherited as autosomal dominant traits and are caused by mutations of either the *MEN1* tumor suppressor gene, encoding the menin protein (MEN1) (Chandrasekharappa *et al.*, 1997; Zarnegar *et al.*, 2002) or the *RET* proto-oncogene (MEN2A, MEN2B) (Mulligan *et al.*, 1993; Hansford and Mulligan, 2000). In contrast to the human syndromes, MENX is inherited recessively (Fritz *et al.*, 2002).

**Table 1.4** Comparison of human MEN phenotypes with the MENX syndrome in rat

Phenotype	MENX	MEN1	MEN2A	MEN2B
Pituitary adenoma	77%	+		
Insulinoma	None	+		
Parathyroid adenoma	65%	+	+	
Pheochromocytoma	95%		+	+
Medullary thyroid hyperplasia	78%		+	+
Paraganglioma	85%		+	
Neuroma	None			+
Causal mutations		MEN 1	RET	

Abbreviations: MENX, multiple endocrine neoplasia X; MEN1, human multiple endocrine neoplasia type 1; MEN2A, human multiple endocrine neoplasia type 2A; MEN2B, human multiple endocrine neoplasia type 2B; + denotes occurrence of the tumor in each disease entity.

Data source: Fritz *et al.*, 2002.

The *MenX* locus was mapped to a 20 megabase (Mb) region of a distal part of rat chromosome 4 (Piotrowska *et al.*, 2003). This linkage analysis excluded the rat homologs of the genes responsible for the MEN syndromes (*RET* and *MEN1*) as well as other genes implicated in cancer syndromes with an endocrine tissue component (namely, *VHL*, *NF1*, and the succinate dehydrogenase subunits B, C, and D genes). In the study by Pellegata *et al.* (2006) the *MenX* locus was placed in a genomic segment of ca. 3Mb on rat chromosome 4, and the *Cdkn1b* gene, which encodes the cyclin-dependent kinase inhibitor p27(Kip1), was identified in this region as the gene responsible for the MENX syndrome development. It was found that affected rats are homozygous for a tandem duplication of 8 nucleotides in exon 2 of *Cdkn1b*. This mutation results in a frameshift after codon 177, predicting a novel C-terminal domain containing forty-two p27(Kip1) unrelated amino-acids residues (Pellegata *et al.*, 2006). Mut/mut rats showed a tissue-specific relative amount of the mutant *Cdkn1b* mRNA. In thymus, spleen, pituitary gland, thyroid, liver, and testis (unaffected tissues) of wild-type and mut/mut rats, there were comparable levels of *Cdkn1b* transcripts, while adrenal glands (affected tissue) of mut/mut animals had a higher level of the mutant *Cdkn1b* transcript than the wt *Cdkn1b* in wt/wt animals. The mutant *Cdkn1b* transcript was expressed at a lower level than the wild-type *Cdkn1b*

transcript in lung and kidney (Pellegata *et al.*, 2006). The authors demonstrated that the rat *Cdkn1b* insertion is responsible for the loss of protein *in vivo*. Immunohistochemical analysis revealed that mut/mut rats have extremely reduced (thyroid, thymus, parathyroid, and brain) or absent (adrenals, pituitary, lung, kidney, liver and testis) p27(Kip1) protein expression (Pellegata *et al.*, 2006).

Noteworthy, PC has complete penetrance in MENX rats: all affected animals develop PC. Adrenal medullary hyperplasia is already evident at 2 months of age and progresses to PC with age (Pellegata *et al.*, 2006).

## **1.8. Cyclin-dependent kinase inhibitor *CDKN1B***

The human *CDKN1B* gene, encoding p27(KIP1), is located on chromosome 12p13 at the junction of 12p12-12p13.1 and belongs to the family of cyclin-dependent kinase inhibitors (CDKIs) Cip/Kip family. This family also includes *CDKN1A* and *CDKN1C*. The Cip/Kip proteins are designated as universal CDKIs because they bind and inhibit complexes containing cyclins A, E, D1, D2, and D3 and their cyclin-dependent kinase (CDK) partners. It is thought that the main target of CIP/KIP inhibitors is cyclin E-CDK2. Overexpression of the Cip/Kip proteins leads to the cell cycle arrest. (Lloyd *et al.*, 1999; Slingerland and Pagano, 2000; Philipp-Staheli *et al.*, 2001; Tessema *et al.*, 2004) (Fig.1.2). p27(KIP1) was first identified as a mediator of TGF $\beta$ -induced G<sub>1</sub> arrest (Koff *et al.*, 1993; Polyak *et al.*, 1994; Slingerland *et al.*, 1994). Cyclin-dependent kinase inhibitor p27(KIP1) acts primarily in G<sub>0</sub> and early G<sub>1</sub>, where it is required for G<sub>1</sub> arrest induced by growth factor deprivation, contact inhibition and loss of adhesion to extracellular matrix (Sherr and Roberts *et al.*, 1999; Slingerland and Pagano, 2000; Philipp-Staheli *et al.*, 2001). p27(KIP1) expression is highest in quiescent cells and declines upon mitogenic stimulation (Sherr and Roberts *et al.*, 1999; Lloyd *et al.*, 1999; Slingerland and Pagano, 2000; Viglietto *et al.*, 2002a). Emerging evidence suggests that p27(KIP1) can regulate cellular functions other than cell-cycle progression, such as cell differentiation, migration and apoptosis (Philipp-Staheli *et al.*, 2001; Blagosklonny, 2002; Collard, 2004; Besson *et al.*, 2004; Baldassarre *et al.*, 2005). The regulation of p27(KIP1) activity is complex. It occurs primarily through the control of its intracellular protein concentration, its distribution among different cyclin-CDK complexes and its sub-cellular localization. Three different mechanisms have been implicated in the regulation of p27(KIP1) expression: transcriptional regulation of the *CDKN1B* promoter, control of mRNA translation, and regulation of the protein degradation rate. It has been shown that the

intracellular level of p27(KIP1) protein is mainly regulated at the post-translational level via proteasome-mediated degradation (Pagano *et al.*, 1995; Viglietto *et al.*, 2002a).

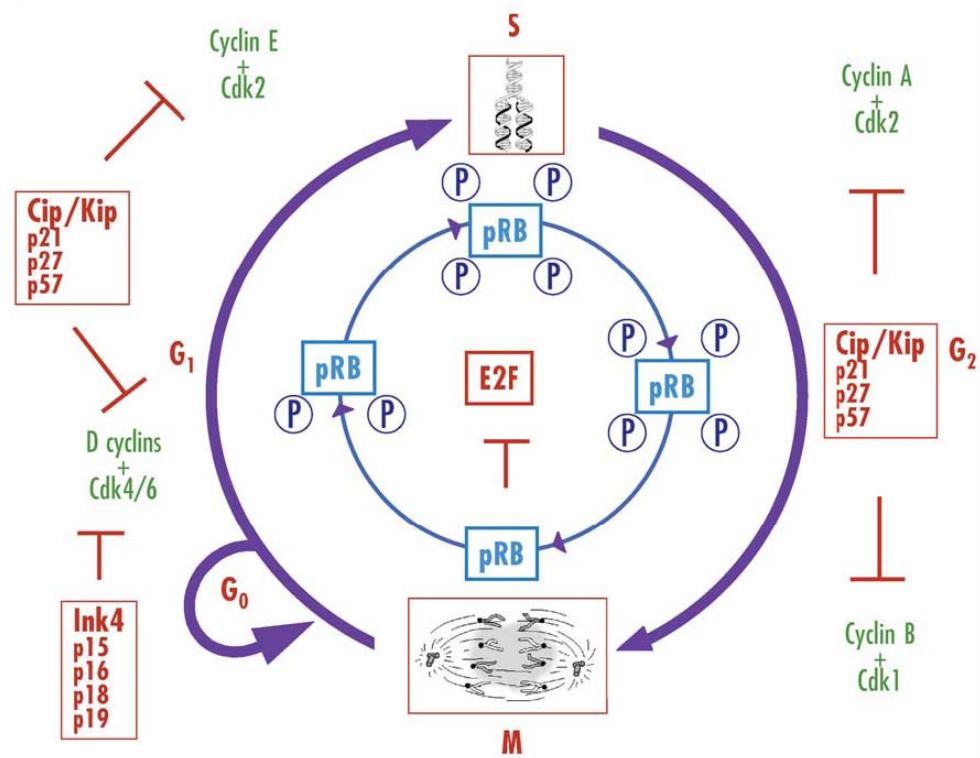


**Fig.1.2** Cell cycle progression is governed by a family of serine-threonine kinases, denoted cyclin-dependent kinases (Cdks), whose activity is regulated by binding of the cyclins, by phosphorylation, and by negative regulators, the Cdk inhibitors p15(INK4B), p16(INK4A), p18(INK4C), p19(INK4D), p21(CIP1), p27(KIP1) and p57(KIP2). The cyclin D and E-dependent kinases contribute sequentially to the phosphorylation of the retinoblastoma gene susceptibility product (pRB), cancelling its ability to repress E2F transcription factor and activating genes for S phase entry.  
Data source: Viglietto *et al.*, 2002a; Slingerland and Pagano, 2000.

In G<sub>0</sub> phase p27(KIP1) is almost exclusively nuclear, whereas in response to mitogenic stimulation a fraction of p27(KIP1) is translocated to the cytoplasm (Rodier *et al.*, 2001; Boehm *et al.*, 2002, Viglietto *et al.*, 2000a). Cytoplasmic relocation due to phosphorylation or sequestration by partner proteins plays an important role in regulating p27(KIP1) functions. It has been proposed that, while p27(KIP1) in the nucleus acts primarily as a tumor-suppressor by modulating cyclin-CDK complexes, cytoplasmic p27(KIP1) has oncogenic properties (Reed, 2002; Blagosklonny, 2002).

Cip/Kip CDK inhibitor *CDKN1B* does not fit the classic tumor suppressor paradigm in humans, because mutations in *CDKN1B* are extremely rare in human cancers. Only a handful of somatic mutations (and no germline mutations) have been reported in the hundreds of human tumor

samples so far analysed (Lloyd *et al.*, 1999; Philipp-Staheli *et al.*, 2001). The presence of hemizygous deletions of *CDKN1B* was shown in hematopoietic malignancies (Sato *et al.*, 1995; Komuro *et al.*, 1995; Pietenpol *et al.*, 1995).

LOH within the *CDKN1B* region is a common feature of some human cancers, including acute myeloid leukaemia, acute lymphoblastic leukaemia, ovarian cancer and prostate cancer (Pietenpol *et al.*, 1995; Takeuchi *et al.*, 1995; Hatta *et al.*, 1997; Kibel *et al.*, 1999).

Inactivation of the *CDKN1B* gene through epigenetic mechanisms was demonstrated only in a small subset of human tumors including lymphoid malignancies and hepatocellular carcinoma (Nakatsuka *et al.*, 2003; Lei *et al.*, 2005). In mouse and rat pituitary cell lines, *Cdkn1b* expression has been shown to be regulated by DNA methylation (Quian *et al.*, 1998).

While loss of one *CDKN1B* allele is frequent in many human cancers, mutation of the remaining allele is rare. This indicates that *CDKN1B* might be haploinsufficient for tumor suppression (Philipp-Staheli *et al.*, 2001). Fero *et al.* (1998) showed that *Cdkn1b* is haploinsufficient in mice heterozygous for a germline deletion of *Cdkn1b* (*Cdkn1b*<sup>+/-</sup> mice). No deletions, point mutations or silencing of the remaining wild-type *Cdkn1b* allele were found in tumor samples of lung, intestine and pituitary from *Cdkn1b*<sup>+/-</sup> mice.

It seems to be that two different mechanisms have been implicated in p27(KIP1) inactivation during the process of human tumorigenesis: downregulation of its expression and exclusion from the nuclear compartment (Viglietto *et al.*, 2002a; Blagosklonny *et al.*, 2002; Reed *et al.*, 2002).

p27(KIP1) expression level is frequently reduced or absent in approximately 50% of human cancer of all types (Slingerland and Pagano, 2000). Reduced p27(KIP1) expression has been associated with the development of human epithelial tumours originating from the majority of human organs, including lung (Esposito *et al.*, 1997), breast (Viglietto *et al.*, 2002a,b; Liang *et al.*, 2002; Shin *et al.*, 2002), colon (Loda *et al.*, 1997; Ciaparrone *et al.*, 1998) ovary (Masculillo *et al.*, 1999), esophagus (Singh *et al.*, 1998), prostate (Tsihlias *et al.*, 1998), thyroid (Baldassarre *et al.*, 1999), and pituitary (Takeuchi *et al.*, 1998; Dahia *et al.*, 1998; Korbonits *et al.*, 2002; Georgitsi *et al.*, 2007). Loss of p27(KIP1) expression is detected also in a subset of malignancies originating from the central nervous system and from lymphoid tissue (Mizumatsu *et al.*, 1999; Piva *et al.*, 1999; Erlanson *et al.*, 1998).

### **1.8.1. *CDKN1B* and its role in human PC and other neuroendocrine tumors formation**

A germline heterozygous nonsense mutation in the human *CDKN1B* gene was identified in a suspected MEN1 patient with no mutations in the *MEN1* gene by Pellegata *et al.* (2006). This mutation predicts premature truncation of the p27(KIP1) protein at codon 76 (CDKN1B\_W76X)

and prevents the truncated p27(KIP1) protein from entering the nucleus. A germline mutation in *CDKN1B* gene was also found in one Dutch patient with suspected MEN1 syndrome in the study by Georgitsi *et al.* (2007). The mutation is heterozygous 19 bp duplication (c.59\_77dup19) in the *CDKN1B* gene leading to a truncated protein product (Georgitsi *et al.*, 2007).

The expression of the cyclin-dependent kinase inhibitor p27(KIP1) was examined in a human panel of 25 PCs, including 23 apparently sporadic PCs and 2 MEN2A-related PCs, and 23 PGLs (Pellegata *et al.*, 2007). A striking decrease/loss of p27(KIP1) expression was observed at a high frequency in PCs (56% cases) but only 18.1% of PGLs showed reduction of p27(KIP1) immunoreactivity. These observations are in agreement with the studies on the MENX rat model system: affected rats develop PC with complete penetrance at young age (< 6 months), while PGLs occur later in the life (> 10 months), and their incidence is only 10% (Pellegata *et al.*, 2007).

Reduced amount of p27(KIP1) protein in corticotroph adenomas and pituitary carcinomas compare to the normal pituitary tissue was observed in the study by Korbonits *et al.* (2002). The authors suggested that the mechanism of p27(KIP1) inactivation is different in the two types of tumor. Corticotroph pituitary adenomas showed a high ratio of phosphorylated to unphosphorylated p27(KIP1), possibly related to increased cyclin E expression. By contrast, malignant pituitary carcinomas showed only very low levels of both phosphorylated and unphosphorylated p27(KIP1) proteins. Absence of p27(KIP1) protein was reported in malignant pituitary tumors suggesting that low or absent p27(KIP1) expression may indicate a more aggressive neoplastic behaviour of tumor (Dahia *et al.*, 1998). Baldassarre *et al.* (1999) found that 80% of p27(KIP1)-expressing thyroid tumors show an uncommon cytoplasmic localization of p27(KIP1) protein, associated with overexpression of cyclin D3.

All these findings establish a causal role between *CDKN1B* alterations and neuroendocrine tumor, particularly PC, formation in humans.

## **1.9. Aim of the work**

As many as 50% of PCs are only discovered post-mortem, mainly because the diagnosis of this neuroendocrine tumor was not considered. Missing the diagnosis almost invariably results in devastating cardiovascular complications or death. PC has earned the title of the “Great Masquerader”, since it can mimic many different conditions, such as anxiety and panic attacks with labile blood pressure, migraine, cardiomyopathy, neuroblastoma, drug-induced

hypertension, Cushing's syndrome, acute infectious disease, hyperthyroidism, menopause, hyperglycemia without diabetes mellitus and many others (Manger, 2006).

The molecular pathogenesis of PC development is not well understood, and the genetic changes identified explain only a fraction of the cases (mainly the hereditary cases).

The MENX rat model provides a unique model for the analysis of the genetic changes associated with PC.

The goals of this study were two-fold:

- ✓ to identify genetic alterations involved in MENX-associated PC development
- ✓ to determine whether the alterations identified in the rat are comparable to published findings in human PCs.

Elucidating the molecular pathogenesis of PC may help in the early diagnosis and in predicting the disease outcome of the affected patients.



## 2. MATERIALS

### 2.1. Equipment

Adhesive Seal applicator	Abgene, UK
Applied Biosystems 3730 DNA Analyzer	Applera GmbH, Darmstadt
Applied Biosystems 7300 Real Time PCR system	Applera GmbH, Darmstadt
Automatic pipette Pipetus ® - akku	Hirschmann equipment, Germany
Balance FISHER	Utting, Germany
Balance Sartorius Universal	Utting, Germany
Biometra ® T personal - 48 PCR machine	Biometra GmbH, Göttingen
Cell incubator	Heraeus instruments, Osterode
Centrifuge Biofuge fresco	Heraeus instruments, Osterode
Centrifuge Biofuge pico	Heraeus instruments, Osterode
Centrifuge EBA 12R	Hettlich Centrifuges, Tuttlingen
Centrifuge Sorvall ® RC-5B Refrigerated Superspeed	Du Pont Instruments, U.S.A
Controlled Environment incubator-shaker	Edison, U.S. A.
Epifluorescence microscope Apotome	Carl Zeiss Vision, Göttingen
Gel documentation machine Bio-Rad	Life Science Group, München
Gene Amp ® PCR System 9700	PE Applied Biosystems, U.S.A.
Horizontal Gel Electrophoreses Chamber	Bio Rad, München
Magnetic Mixer RTC basic	Janke & Kunkel GmbH, Staufen
Microcentrifuge “Butterfly”	ROTH, Karlsruhe
Microtom FRIGOCUT 2800	Reichert-Jung, Nussloch
Microwave LG	LG Electronics, Germany
pH-Meter inoLAB pH level 1	Laboratory Equipment, Wellheim
Semiautomatic single pipettes DISCOVERY	ABIMED, Langenfeld
Shaker REAX top	Heidolph, Germany
Spectrophotometer Nanodrop ND-1000	Kisker products, Steinfurt
Stereomicroscope Wild M5-52765	Heerburg, Switzerland
Thermomixer Comfort	Eppendorf, Hamburg
Thermomixer Thermostat plus	Eppendorf, Hamburg
Thermoplate S	Desaga GmbH, Heidelberg
Thermostat RM6 LAUDA	LAUDA GmbH, Königshofen
Vertical Gel Electrophoreses Chamber	ATTO corporation, Japan
Vortex Genie 2™	Scientific Industries, U.S.A.
Water bath Julabo SW-21C	Julabo GmbH, Seelbach

### 2.2. Consumable materials

Adhesive PCR Foil Seals	Abgene, UK
Bevelled Filter Tips (1-20 µl, 1-100 µl)	STARLAB GMBH, Ahrensburg
Bioloops Kendall (10 µl / 1 µl)	Mansfield, U.S.A.
Cryotubes™ Vials	Apogent™, Denmark

Disposable needles 100 Sterican, 21G x 2"  
Eppendorf tubes (0.5 ml, 1.5 ml, 2 ml)  
Extended Length Filter Tips (0.1-10 µl)  
Falcon® polypropylene round-bottom tubes  
Falcon serological pipette (1ml)  
Falcon tubes (15 ml, 50 ml)  
Filter Tips (101-1000 µl)  
Graduated Filter Tips (1-200 µl)  
Microscope Cover Glasses 12 mm  
Microscope Cover Glasses 24x50 mm  
Microscope Glass Cover Slips 24x60 mm  
Microscope Slides SuperFrost® Plus  
Microscope Slides SuperFrost White  
Optically Clear Adhesive Seal Sheets  
PCR 5-strip tubes  
Pipette Tips DIAMOND (D1000, D200)  
Serological pipettes Cellstar®  
(2 ml, 5 ml, 10 ml, 25 ml)  
Surgical disposable scalpels  
Thermo-Fast® 96 well non-skirted PCR plate (0.2 ml)

Braun Melsungen AG, Melsungen  
Eppendorf, Hamburg  
STARLAB GMBH, Ahrensburg  
Becton Dickinson, France  
Becton Dickinson, France  
Becton Dickinson, France  
STARLAB GMBH, Ahrensburg  
STARLAB GMBH, Ahrensburg  
Assistent, Germany  
Menzel-Glaser, Germany  
Smethwick, Warley, England  
Menzel-Glaser, Germany  
Roth, Karlsruhe  
Abgene, UK  
Eppendorf, Hamburg  
Gilson, France  
Greiner bio-one, Frickenhausen  
  
Aesculap AG, Tuttlingen  
Abgene, UK

### 2.3. Rat strains

F1 (Wky x SD<sup>wc</sup>) hybrid rats  
Sprague Dawley White Eye (SD<sup>wc</sup>/SD<sup>wc</sup>) rats  
Wistar / Kyoto (Wky) female rats

GSF Animal Facility, München  
GSF Animal Facility, München  
Charles River, Germany

### 2.4. Kits

BigDye® Terminator v3.1 Cycle Sequencing Kit  
Nick translation Kit  
2 x TaqMan® Universal PCR Master Mix  
QIAGEN® Large-Construct Kit  
QIAquick® PCR Purification Kit

PE Applied Biosystems,  
Weiterstadt  
Invitrogen GmbH, Karlsruhe  
PE Applied Biosystems,  
Weiterstadt  
Qiagen GmbH, Hilden  
Qiagen GmbH, Hilden

### 2.5. Markers

DNA Molecular weight markers (VIII, IX)  
Gene Ruler™ 1kb DNA ladder  
GeneScan™- 500 LIZ™ Size Standard  
BioTherm™ DNA polymerase

Roche, Mannheim  
Fermentas GmbH, Leon-Rot  
PE Applied Biosystems, UK  
GeneCraft GmbH, Lüdinghausen

### 2.6. Enzymes

Proteinase K, PCR Grade

Roche Diagnostics GmbH,  
Penzberg

Ribonuclease A  
RNaseOUT™ Recombinant Ribonuclease Inhibitor  
Superscript™ II Reverse Transcriptase

Fermentas GmbH, Leon-Rot  
Invitrogen GmbH, Karlsruhe  
Invitrogen, GmbH, Karlsruhe

## 2.7. Nucleotides

dNTP Mix (10mM)  
dNTP set (100mM)

Fermentas GmbH, Leon-Rot  
Fermentas GmbH, Leon-Rot

## 2.8. Chemicals for Electrophoresis Gels

Ammonium persulfat (APS)

Ethidium bromide

ProtoGel™ (30%)

SeaKem® LE Agarose

TEMED

Sigma-Aldrich Chemie GmbH,  
Steinheim

Sigma-Aldrich Chemie GmbH,  
Steinheim

National Diagnostics, England

Biozym, Oldendorf

Sigma-Aldrich Chemie GmbH,  
Steinheim

## 2.9. Compounds for FISH analysis

Albumin bovine serum, Fraction V, ≥ 96%

Anti-Digoxigenin-Rhodamine Fab fragments

Biotin-16-dUTP

Biotinylated antiavidin D antibodies

Citric acid

Dextran sulphate Sodium Salt

4',6-Diamino-2-phenylindole dihydrochloride  
(DAPI)

Digoxigenin-11-UTP

Herrings Sperm DNA (10 mg/ml)

Hoechst 33342, trihydrochloride, trihydrate

Nonidet® P 40 Substitute

Phosphate Buffered Saline (PBS) pH 7.4

Pronase E (from Streptomyces griseus) 4.000.000  
(proteolytic units)/g

Rat Hybloc DNA (1 mg/ml)

Rubber Cement Fixogum

Saline-sodium citrate buffer (SSC) 20x concentrate

Sodium citrate dihydrate

VECTASHIELD® Mounting Medium

ZyMax™ Streptavidin-FITC Conjugate

Sigma- Aldrich Chemie, Steinheim

Roche, Mannheim

Roche, Mannheim

Vector Laboratories, Burlingame

Merck KGaA, Darmstadt

Sigma chemical CO, U.S.A

Sigma- Aldrich Chemie, Steinheim

Roche, Mannheim

Invitrogen GmbH, Karlsruhe

Molecular probes , U.S.A

Sigma- Aldrich Chemie, Steinheim

Sigma- Aldrich Chemie, Steinheim

Merck KGaA, Darmstadt

AGL, Melbourne

Marabu, Tamm

Sigma- Aldrich Chemie, Steinheim

Sigma- Aldrich Chemie, Steinheim

Vector Laboratories, U.S.A

Zymed, U.S.A.

## 2.10. Chemicals for work with BAC clones

Adenosine 5'-triphosphate disodium salt

Chloramphenicol

Sigma- Aldrich Chemie, Steinheim

Roche, Mannheim

Glycerol SigmaUltra

LB Broth Base (Lennox L Broth Base) ®, powder  
Sodium chloride

Sigma-Aldrich Chemie GmbH,  
Steinheim  
Invitrogen GmbH, Karlsruhe  
Merck KGaA, Darmstadt

## 2.11. General chemicals

Absolute ethanol  
Acid phenol:chloroform (5:1 solution) pH 4.5  
Ampuwa®  
Chloroform  
Cresol red  
  
DEPC-treated water  
Formamide, minimum 99% GC  
  
Glycogen (20 mg/ml)  
Isoamyl alcohol GR  
LiChrosolv HPLC water for chromatography  
Phenol:Chloroform: Isoamylalcohol (25:24:1) pH 7.0  
Xylol  
2-Mercaptoethanol  
2-Propanol

Merck KGaA, Darmstadt  
Ambion, Weiterstadt  
Fresenius, Bad Homburg  
Merck KGaA, Darmstadt  
Sigma-Aldrich Chemie GmbH,  
Steinheim  
Invitrogen GmbH, Karlsruhe  
Sigma-Aldrich Chemie GmbH,  
Steinheim  
Roche, Mannheim  
Merck KGaA, Darmstadt  
Merck KGaA, Darmstadt  
Invitrogen GmbH, Karlsruhe  
Merck KGaA, Darmstadt  
Fluka Chemie, Buchs  
Merck KGaA, Darmstadt

## 2.12. Computer software

ABI 7300 Real-time PCR Detection System  
Axiovision Rel 4.6  
Bio Image Intelligent Quantifier  
IDL 6.1

MutationSurveyor 3.10 Validation  
Sequencher 4.1  
SignalMap 1.8

Applied Biosystems, USA  
Carl-Zeis MicroImaging, Germany  
BioQuant, USA  
ITT Visual Information Solutions,  
Austria  
Softgenetics, USA  
Gene Codes, USA  
NimbleGen Systems, Inc., Madison

## 2.13. Buffers

- Lysis buffer for DNA extraction

Reagents	Volume
1 M Tris (pH 8.0)	25 ml
0.5 M EDTA (pH 8.0)	100 ml
5 M NaCl	10 ml
10% SDS	50 ml
distilled water	to 500 ml

- Lysis buffer for RNA extraction

Reagents	Volume
4 M Guanidine thiocyanate in DEPC-water filtered	1 ml
1 M Sodium citrate pH 7.0 in DEPC-water	27 $\mu$ l
2 M Sodium acetate pH 4.7 in DEPC-water	100 $\mu$ l
10% N-Lauroylsarcosine sodium salt (Sarkosyl ) in DEPC-water	53 $\mu$ l
2-Mercaptoethanol (Thioethylene glycol)	7.6 $\mu$ l

- General Purpose PCR Master Mix

Reagents	Volume
Sucrose	3 g
dATP (100 mM)	100 $\mu$ l
dCTP (100 mM)	100 $\mu$ l
dTTP (100 mM)	100 $\mu$ l
dGTP (100 mM)	100 $\mu$ l
Buffer 10X (Bio Therm, no MgCl <sub>2</sub> )	5 ml
MgCl <sub>2</sub> (50 mM)	1.5 ml
Cresol red (100 $\mu$ g/ml)	20 $\mu$ l

As an alternative variant for preparation of PCR Master Mix one can use 5 ml Buffer 10X, including 15 mM MgCl<sub>2</sub>. PCR Master Mix was aliquoted and freezed at -20 °C.

- 5 x TBE buffer

Reagents	Volume
Tris base	54 g
Boric acid	27.5 g
0.5 M EDTA (pH 8.0)	20 ml
distilled water	to 1L

- 6 x Gel loading buffer

Reagents	Volume
Bromophenol blue	0.25%
Xylene cyanol FF	0.25%
Glycerol in water	30%

## **3. METHODS**

### **3.1. Tumor and nontumor tissue samples**

#### **3.1.1. Preparation of tumor and nontumor tissue for molecular analysis**

Adrenal glands with PC dissected from CO<sub>2</sub>-killed rats (Table 4.1) were shock-frozen in liquid nitrogen and stored at -70°C. For all molecular biology methods used in the study only the medulla of the adrenal gland has been used.

Ear tissue samples were collected from the same animals at the age of three- four weeks by punch biopsy, frozen at -70°C.

Adrenal glands of healthy animals were shock-frozen in liquid nitrogen and stored at -70°C. Adrenal glands of one group of healthy animals were microdissected and used for RNA extraction while the remaining glands were fixed in formalin and embedded in paraffin. Paraffin-embedded tissue blocks were used for FISH analysis.

Histopathological hematoxylin/eosin (H&E) evaluation of adrenal glands of affected and healthy animals (control group) has been performed in cooperation with Dr. Calzada-Wack, Dr. Hölzlwimmer (Institute of Pathology, GSF) using established criteria for neoplasia of the rat endocrine system.

#### **3.1.2. Genotyping on the *Cdkn1b* gene**

To identify the group of experimental animals with germ-line *Cdkn1b* mutations genotyping of the *Cdkn1b* gene was performed. Genomic DNA was isolated from ear takes and used for genotyping. DNA isolation was done with phenol-chloroform extraction. DNA was amplified with primers (annealing temperature is 55°C, length of the product is 200 bp) designed for the exon 2 of the *Cdkn1b* gene (Pellegata *et al.*, 2006):

rp27Kip1\_2 forward TCTGTCAGCCATTGTTCTCG

rp27Kip1\_2 reverse GCTAGGGTGTCAGTTTTGTGC.

Polymerase chain reaction (PCR) product was resolved in 10 % polyacrylamide gel.

### **3.2. Isolation of Nucleic Acids**

#### **3.2.1. Isolation of genomic DNA from fresh-frozen tissue**

Isolation of genomic DNA from tumor and non-tumor tissue was performed using the phenol-chloroform extraction method.

## **Phenol-Chloroform Extraction**

10-15 individual microtom sections, each with a thickness of 20  $\mu\text{m}$ , were cut from the medullary part of adrenal glands with PC. The cortical part of the adrenal gland was cut away to avoid contamination of tumor DNA with nontumor tissue. The medullary tissues were pooled in a microcentrifuge tube. H&E staining was done for each tumor sample to verify the presence of PC. 500  $\mu\text{l}$  of Lysis buffer for DNA extraction and Proteinase K (100  $\mu\text{g}/\text{ml}$ ) were added to the tissue. Samples were incubated overnight at 55°C in a Thermomixer with 900 -950 rpm. If needed, lysis was extended until the tissue was completely dissolved. After lysis 500  $\mu\text{l}$  of phenol: chloroform : isoamylalcohol (25:24:1) with pH 7.0 was added to each sample to remove protein contaminants, mixed and centrifuged for 5 min at 6000 x g. The upper phase containing DNA was transferred to a new tube. An equal amount of chloroform was added to the supernatant, mixed and centrifuged for 5 min at 6000 x g. The upper phase was removed and mixed with 2 to 2.5 vol of ice-cold 100% ethanol. Tubes were placed for 30-60 min at -20°C for precipitation and centrifuged for 10 min at 14.000 x g. The DNA pellet was washed with 70% ethanol (300  $\mu\text{l}$ ) to remove salts and small organic molecules and air-dried. DNA was dissolved in 30-50  $\mu\text{l}$  of EB buffer from Qiagen (10 mM Tris-HCl, pH 8.5) and left overnight in the fridge at 4°C. To increase the efficiency of DNA dissolving tubes with DNA were put into the thermomixer for 2 hours at 37°C with gentle agitation. DNA content and integrity was verified by spectrophotometry and electrophoresis (Methods, 3.3 and 3.4.3.).

For DNA extraction from the ear tissues a standard phenol-chloroform extraction protocol was used with appropriate volumes of lysis buffer (100  $\mu\text{l}$ ), phenol:chloroform:isoamylalcohol (100  $\mu\text{l}$ ) and chloroform. (100  $\mu\text{l}$ ). Aliquots of stock solutions of DNA were stored at - 20°C. DNA working solutions of 10 ng/  $\mu\text{l}$  were prepared in water and stored at 4°C.

The quality of DNA was determined by running the extraction products in 1-1.5% agarose gels.

## **Purification and Concentration of DNA from Aqueous Solutions**

The volume of DNA samples was increased with water up to 100-200  $\mu\text{l}$  0.1 vol of 3M sodium acetate (pH 5.3), 2-2.5 vol of ice-cold 100% ethanol and 2  $\mu\text{l}$  of glycogen (20 mg/ml) were added to the sample, carefully mixed by inverting the tube 4-5 times. For precipitation samples were left into the freezer at -20°C for 1-2 hours. Glycogen was added only in cases when the amount of DNA was supposed to be small. After adding glycogen precipitation was done overnight. Washing of DNA pellet after precipitation with following dissolving of DNA was done as for the standard protocol of phenol-chloroform extraction.

### **3.2.2. Isolation of genomic DNA for CGH array**

The isolation of genomic DNA for CGH array was performed using the standard phenol-chloroform extraction method. It was done in two steps. After the first phenol-chloroform purification genomic DNA was dissolved in 200 µl of EB buffer. To generate RNA-free genomic DNA 2 µl of Ribonuclease A (100 µg/ml) was added to the samples. Ribonuclease A is an endoribonuclease that specifically degrades single-stranded RNA at C and U residues. Samples were incubated at 37°C for 1 hour, followed by a second phenol-chloroform extraction for Ribonuclease A inactivation. After the second phenol-chloroform purification precipitation of DNA was performed as above. During genomic DNA extraction all pipette tips used were with wide openings because pipetting genomic DNA through small tip openings causes shearing or nicking. DNA was aliquoted and stored at 4°C.

### **3.2.3. Isolation of RNA from snap - frozen tissue**

10-15 sections with the thickness 20 µm were cut with a microtom from each tumor sample with PC and put in a microcentrifuge tube containing 1 ml of Trizol reagent and incubated for 30 -60 min with periodical vortexing at room temperature. The time of lysis could be extended if tissue debris was visible in the tube. Trizol reagent, a mono-phasic solution of phenol and guanidine isothiocyanate, maintains the integrity of RNA whilst disrupting cells and dissolving cell components. After lysis with Trizol 200 µl of Chloroform : Isoamylalcohol (24:1) per 1 ml of Trizol Reagent was added to the sample. Samples were shortly vortexed, incubated for 2-3 min at room temperature and centrifuged for 10 min at 14.000 x g at 4°C. Addition of chloroform followed by centrifugation separates the solution into an aqueous phase and an organic phase. RNA remains exclusively in the aqueous phase. The volume of the aqueous phase is about 60% of the volume of Trizol Reagent used for homogenization. After transfer of the aqueous phase into the new tube RNA was recovered by precipitation with 2 µl of glycogen (20 mg/ml) and 500 µl of isopropanol per sample. Precipitation was performed at -20°C overnight. After precipitation samples were centrifuged at 20.000 x g for 30 min at 4°C. Supernatant was removed. The RNA pellet was washed with 300 µl of 70% (-20°C) ethanol, centrifuged at 14.000 x g for 5 min at 4°C and air - dried for 5 -10 min. It is important not to let the RNA pellets dry completely as this will greatly decrease its solubility. RNA pellets were dissolved in 30 - 40 µl of DEPC – water, incubated at 40-42°C for 8-9 min and thoroughly resuspended with a pipette. RNA samples were stored at -70°C.



### **3.2.4. Isolation of RNA from microdissected tissue**

Microdissection was performed for normal adrenal glands as described below. To receive sufficient amount of RNA both adrenal glands from an animal were used for microdissection. 20-30  $\mu\text{m}$  tissue sections were made from fresh-frozen tissue. Approximately 4-5 tissue sections were applied per microscope slide SuperFrost which allows stable binding of the tissue to the surface. H&E-staining was done for all samples used for microdissection

Adrenal gland tissue was microdissected freehand under a stereo-microscope Wild M5-52765 using sterile needles. Tissue of the medullary part of each adrenal gland was collected into an eppendorf tube containing 400  $\mu\text{l}$  of lysis buffer for RNA extraction.

Then 400  $\mu\text{l}$  of acid phenol:chloroform (pH 4.5) was added to each sample in lysis buffer. Samples were incubated at room temperature for 30 min. During the time of incubation samples were vortexed 2-3 times for 20 s to increase the efficiency of lysis. After lysis the RNA extraction was performed as described in Methods, 3.2.3.

### **3.3. Quantification of Nucleic Acids**

DNA/RNA yield and purity were determined by spectrophotometric measurement with the Nanodrop device. The ratio  $A_{260}/A_{280}$  was determined. The  $A_{260}/A_{280}$  ratio serves as an estimation of the purity of the RNA and DNA samples from contaminant proteins and aromatic substances (e.g., phenol). Pure DNA has an OD  $A_{260}/A_{280}$  ratio  $\geq 1.8$ . An  $A_{260}/A_{280} < 1.8$  indicates that the DNA sample is contaminated with proteins and aromatic substances. An  $A_{260}/A_{280} > 2$  shows a possible contamination with RNA. For pure RNA samples the value of  $A_{260}/A_{280}$  should be higher or equal to 2.0. If there is a contamination with proteins or phenol, the value of  $A_{260}/A_{280}$  will be less than 2.0.

### **3.4. LOH analysis**

Loss of heterozygosity (LOH) analysis has been used in many types of cancer to localize putative tumor suppressor genes important for carcinogenesis. The principle of the method used here is allelotyping of tumors using polymorphic microsatellite markers distributed throughout the entire genome what allows the analysis of specific allelic losses. This method includes the following steps:

- search and design of microsatellite markers

- amplification of microsatellite markers by PCR
- visualization of PCR products
- data analysis

### **3.4.1. Microsatellite markers**

Microsatellite DNA, also called simple sequence repeats, are small arrays of tandem repeats of a simple sequence (usually less than 100 bp in length) dispersed throughout the genome. The repeated sequence consists of two, three or four nucleotides and can be repeated 10 to 100 times. The number of repeats at a particular locus is hypervariable (highly polymorphic) between individuals of the same species. The hypervariability arises because the repeated simple sequences cause the high frequency of loss or insertion of additional repeats by confusing the DNA replication machinery. Although microsatellite DNA has generally been identified in intergenic DNA or within the introns of genes, a few examples have been recorded within the coding sequences of genes. Maps made using microsatellite markers are very informative.

Microsatellite markers have the advantage of being abundant, dispersed throughout the genome, highly informative and easy to type (Strachan *et al.*, 2004).

### **Rat genome databases used in the work**

Rat genetic maps were taken from the Rat Genome Database ([rgd.mcw.edu/tools/genomescanner](http://rgd.mcw.edu/tools/genomescanner)).

The polymorphic microsatellite markers distinguishing between SD/Rij and WKY/OlaHsd strains were chosen from the Radiation Hybrid map (v.2.1), FHH x ACI genetic map (v.7), SHRSP x BN genetic map (v.7) as being potentially polymorphic between the Sprague Dawley white eye (SD<sup>w<sup>e</sup></sup>) and Wistar Kyoto (Wky) strains. These maps also were used to check the order of microsatellite markers on each chromosome.

### **Primer selection for DNA Microsatellite PCR**

Microsatellite PCR primers were selected from the NCBI database ([www.ncbi.nlm.nih.gov/mapview/map\\_search.cgi?chr=rat.inf](http://www.ncbi.nlm.nih.gov/mapview/map_search.cgi?chr=rat.inf)), and the Ensembl Genome Browser ([www.ensembl.org/Rattus\\_norvegicus/index.html](http://www.ensembl.org/Rattus_norvegicus/index.html)). A group of microsatellite markers was designed using the program [frodo.wi.mit.edu/cgi-bin/primer3/primer3](http://frodo.wi.mit.edu/cgi-bin/primer3/primer3). All primers used in the work were ordered from Metabion. Stock solutions of primers (100 pmol/μl) were diluted in water to give a working concentration of 10 pmol/μl of each primer.

### 3.4.2. Amplification of DNA microsatellites

#### PCR amplification

In the process of PCR a defined fragment of genomic DNA can be selectively amplified using specific oligonucleotides (primers). Primers are short synthetic oligonucleotides (ca 20 bp) complementary to the start (5'-End, Left or Forward Primer) and the end (3'-End, Right, or Reverse primer) of the sequence which has been chosen for amplification. Starting material, double-stranded DNA, is denatured in the first denaturation step of 94-95°C. Then PCR primers bind (anneal) to the complementary single-stranded DNA. The annealing temperature (50-65°C) depends on the length of the primers and guanine /cytosine ratio. In the next step primers are extended in 5'-3'- direction by thermostable Taq DNA-polymerase (from *Thermophilus aquaticus*) in the presence of dNTPs at the optimal enzyme temperature of 72°C. Repetition of the denaturation, annealing and extension reactions during 30-40 cycles increases exponentially the amount of amplicon for molecular analysis. Negative (PCR without DNA template) and positive controls (PCR with known DNA template) are used to make sure there is no contamination of the enzymes and buffers with the template. For amplification of microsatellite markers general purpose master mix was used.

PCR reaction was set up as follows:

#### Mixture for PCR reaction (pro 1 sample)

Reagents	Volume
PCR Master Mix	15 µl
Forward primer (10 pmol/µl)	1 µl
Reverse primer (10 pmol/µl)	1 µl
Taq polymerase (5000 U)	0.2 µl
DNA template (10 ng/µl)	2.5 µl
<b>Final Volume</b>	<b>19.7 µl</b>

PCR Master Mix, a set of primers (forward + reverse), Taq Polymerase were mixed in amounts needed for whole PCR set and pipetted into PCR tubes, then DNA template was added.

The PCR cycle conditions used for PCR amplification as follows:

Programm	Temperature/Time
Initial Denaturation	94°C / 5 min
<b>3-step cycling</b>	
Denaturation	94°C / 30 s
*Annealing	52 -60°C / 40 s
Extension	72°C / 40 s
<b>Number of cycles : 28</b>	
Final Extension	72°C / 10 min

\*annealing temperature was adjusted for each set of primers

Reactions were stopped by cooling to 4°C and the products were resolved by electrophoresis. Negative and positive controls for amplification of microsatellites were set up in parallel. Negative controls contained no template. Positive controls were performed using parental DNA of F2 hybrid animals bred by crossing SD<sup>we</sup>/SD<sup>we</sup> male rats with F1 (Wky x SD<sup>we</sup>) females.

### 3.4.3. Electrophoresis of the DNA extraction products and PCR amplification products

PCR reaction products were separated by agarose (2-3%) or polyacrylamide (10%) gel electrophoresis. To check the quality of DNA extraction products 1-1.5% agarose gel was used. For preparation of agarose gel 1.0-3.0 g agarose powder was dissolved in 100 ml of 1×TBE buffer prepared from 5×TBE buffer stock by boiling for 2-3 min in the microwave. After slight cooling 10 µl of etidium bromide (10 mg/ml) per 100 ml of 1×TBE buffer was added to the gel to enable fluorescent visualisation of the DNA fragments in UV light. The warm mixture was poured into a gel tray and a well-forming comb was applied. The gel was allowed to solidify for at least 30 min, the comb was taken out, and the gel placed in an electrophoresis chamber and covered with 1 × TBE buffer.

The sample was mixed with 6 × loading buffer in a ratio 5:2 and loaded into a gel well. The loading buffer prevents escape of the mixture from the slot and serves as a visible co-migrating marker. DNA molecular weight marker mixed in the same ratio as a DNA sample was loaded in the vacant lane in the gel to allow size determination of the fragments. For resolution of PCR amplification products DNA molecular weight markers VIII and IX were used. Gene Ruler™ 1kb DNA ladder was used to estimate the quality of DNA extraction products. Electrophoresis was run for 60 -120 min at a constant voltage 50-90 V. In the electrical field negative nucleic acids migrate to the anode. Separation depends on the size of molecule, as the speed of migration

through the gel pores is proportional to the inverse logarithm of the molecular weight. Visualization of the DNA molecules in the gel was performed by staining with ethidium bromide under the UV light, thereby allowing estimation of the size and quantity.

### **Polyacrylamide gel electrophoresis**

Microsatellite alleles which differ in length by less than 10% were separated using 10% nondenaturing polyacrylamide gels, which give much higher resolution than agarose:

#### **10% polyacrylamide gel**

<b>Reagents</b>	<b>Volume</b>
30% acrylamide /bisacrylamide	6.66 ml
5 × TBE	4 ml
10% APS	140 µl
distilled water	9.2 ml
TEMED	7 µl

Components for polyacrylamide gel were thoroughly mixed and the mixture was poured between two sealed glass plates and a 20-well-forming comb was applied. The gel was left for 30 -40 min to polymerize, the comb and spacers for sealing were removed and the assembly was placed in a vertical electrophoresis chamber filled with 1 ×TBE buffer. PCR products were mixed with 6 × loading buffer in the ratio 10:2 for loading. 5 µl of DNA molecular weight marker was mixed with 1 µl of 6 × loading buffer and 1 µl of the water and loaded at the same time with samples into the gel. Electrophoresis was performed for 2-3 hours at a constant voltage of 150-200 V, according to product size. After the completion of electrophoresis the glass plates were separated and the polyacrylamide gel was transferred by hand into a dish containing 10 µl of ethidium bromide (10 mg/ml) in 200 ml of 1× TBE buffer for 5 min for DNA staining.

### **Documentation of microsatellite gel images**

PCR products on agarose and polyacrylamide gels were visualised by ethidium bromide fluorescence under the UV-light, photographed using the gel documentation machine Bio-Rad and digitally recorded for quantification of the allelic ratio.

### 3.4.4. Quantification of the allelic ratio

Loss of heterozygosity /Allelic imbalance (LOH/AI) was initially scored by eye by comparing the intensity of the PCR products from the two alleles in normal tissue with those in PC in the gel photographs. Digital gel images were prepared and quantified using automated densitometry (Bio Image Intelligent Quantifier) which expresses each DNA band as a percent of the integrated intensity (% I.I).

Changes in the allelic ratio in PC samples compared to normal tissue were defined by the following ratio and expressed as a percentage:

$$\text{Allelic Ratio (PC)} = (\text{Allele1}^{\text{N}} : \text{Allele2}^{\text{N}}) : (\text{Allele1}^{\text{PC}} : \text{Allele2}^{\text{PC}}),$$

where N – DNA, extracted from normal tissue

T – DNA, extracted from tumor tissue (PC)

Samples were considered as having AI or LOH when the ratio was more than 50% (Ritland *et al.*, 1997; Stern *et al.*, 2000; Försti *et al.*, 2001; Kuosaitė, 2001; Zhang *et al.*, 2001).

### 3.5. Fragment analysis

For markers having allelic imbalance microsatellite analysis was repeated with fluorescently labelled primers. This method was also used in cases when it was not possible to resolve PCR products in 3% agarose gel or in the 10% polyacrylamide gel.

All 5'-FAM (6-FAM) modified primers were ordered from Metabion. The PCR reaction was set up according to the protocol:

#### Mixture for PCR reaction (pro 1 sample)

Reagents	Volume
Buffer 10X containing 15 mM MgCl <sub>2</sub>	2.5 µl
dNTP mix ( 10 mM)	0.5 µl
5'-FAM Forward primer (10 pmol/µl)	1 µl
Reverse primer (10 pmol/µl)	1 µl
Gene Craft Tag polymerase (5000 U)	0.25 µl
Water	17.25 µl
DNA template	2.5 µl
<b>Final Volume</b>	<b>22.5 µl</b>

The PCR cycle conditions were the same as those used for amplification of DNA microsatellite markers. PCR product was loaded into the 2% agarose gel to check the quality of PCR reaction. Samples were diluted with a Hi-Di™ formamide in the ratio 1:100. The dilution of the PCR product depends on the efficiency of the PCR reaction. 12 µl of diluted PCR product was loaded in 96-well PCR plate and mixed with 1 µl of GeneScan™-500 LIZ® Size standard. The plate with samples was denatured at 95 °C for 2 min and immediately chilled on ice for 5 min. Samples were loaded in an Applied Biosystems 3730 DNA Analyzer capillary machine for electrophoresis.

### **GeneScan™-500 LIZ® Size standard**

GeneScan™-500 LIZ® Size standard is a set of fluorescent-labelled DNA fragments of known sizes used for determining the size of unknown DNA fragments run on ABI PRISM® DNA sequencer. This marker is designed for sizing DNA fragments in the 35-500 bp range. It has an internal lane size standard which runs in the same lane or capillary injection as the samples, and which contains fragments of unknown sizes labelled with the LIZ® fluorophore. GeneScan® Analysis Software automatically calculates the size of the unknown DNA sample fragments by generating a calibration or sizing curve based upon the migration times of the known fragments in the standard. The unknown fragments are mapped onto the curve and the sample data is converted from migration times to fragment sizes. For the fragment analysis GeneScan™-500 LIZ® Size standard should be diluted in Hi-Di™ formamide (1:100).

### **LOH/AI analysis**

Allele size, height and area of alleles of normal/tumor pairs were determined by Genemapper 3.5 software. AI/LOH was analyzed by determining the height of each allele and calculating the allelic ratio (Methods, 3.4.4.). A sample was scored as showing AI/LOH if the allelic ratio was more than 50 %.

## **3.6. TaqMan PCR**

TaqMan PCR involves two steps: reverse transcription reaction (RT) and PCR amplification.

### **3.6.1. Reverse transcription**

Reverse transcription-polymerase chain reaction (RT-PCR) is a sensitive method for the detection of mRNA expression levels. The isolated RNA was reverse transcribed to produce

cDNA templates required for PCR amplification. Random primers were used for first-strand cDNA synthesis with a final concentration 1  $\mu\text{g}/\mu\text{l}$ . The primers are random hexadeoxynucleotides. 1  $\mu\text{g}$  of the total RNA was diluted with DEPC-treated water to a total volume of 10  $\mu\text{l}$ . After addition of 2  $\mu\text{l}$  of random primers samples were incubated for 10 min at room temperature. Then for RT to each sample was added 9  $\mu\text{l}$  of following mixture:

**Mixture for reverse transcription (pro 1 sample)**

Reagents	Volume
5 X First-Strand buffer	4 $\mu\text{l}$
0.1 M DTT	2 $\mu\text{l}$
dNTP mix (10 mM each)	1 $\mu\text{l}$
RNaseOUT™ Recombinant Ribonuclease Inhibitor	1 $\mu\text{l}$
SuperScript™ II Reverse Transcriptase (10000 U)	1 $\mu\text{l}$

Samples were incubated for 1 hour at 42°C. The reaction was inactivated by heating at 95°C for 5 min. Samples were stored at – 20°C.

**3.6.2. PCR amplification**

For TaqMan the PCR TaqMan gene expression assays (Table 3.1) were used from Applied Biosystems.

**Table 3.1 Assays on demands (Applied Biosystems)**

Genes	Availability	Assay on demand ID
<i>Sdhd</i>	Pre-made	Rn 01644331_g1
<i>Rassf1</i>	Pre-made	Rn 01445298_m1
<i>Cdkn2a</i>	Made to Order	Rn 01433231_m1
<i>Cdkn2c</i>	Inventoried	Rn 00590868_m1
<i>Sctr</i>	Inventoried	Rn 00579585_m1
$\beta$ -2 microglobulin	Inventoried	Rn 00560865_m1

- *m* for assays over an exon-exon boundary
- *g* for assays that are over an exon-exon boundary but that may still detect genomic DNA:

Each assay consists of two unlabelled PCR primers and a minor groove binder (MGB) probe for detecting the sequence of interest. The TaqMan MGB probe contain a reporter dye (6-FAM) linked to the 5' end of the probe and a nonfluorescent quencher at the 3' end of the probe. MGBs



increase the melting temperature without increasing probe length; they also allow the design of shorter probes.

During PCR, the TaqMan MGB probe anneals specifically to a complementary sequence between the forward and reverse primer sites. When the probe is intact, the proximity of the reporter dye to the quencher dye results in suppression of the reporter fluorescence primarily by Förster –type, or fluorescent resonance energy transfer (FRET). In other words, as long as both fluorochromes are retained on the probe the quencher molecule absorbs all fluorescence from the reporter. The Taq polymerase cleaves only probes that are hybridized to the target. Cleavage separates the reporter dye from the quencher dye, resulting in increased fluorescence by the reporter. The increase in fluorescence signal occurs only if the target sequence is complementary to the probe and is amplified during PCR. Because of these requirements, any non-specific amplification is not detected. Polymerization of the strand continues, but the 3' end of the probe is blocked to prevent extension of the probe during PCR. The amount of fluorescence released during each amplification cycle is proportional to the amount of product generated in each cycle. Applied Biosystems 7300 Real-Time PCR System allows quantification of PCR reaction products and quantifies the fluorescence during each cycle with calculation of the threshold cycle (CT) value for each sample used for TaqMan PCR.

This system estimate relative expression of genes. For quantification of the expression level of genes of the interest, a house-keeping gene,  $\beta$ -2 microglobulin, was used as an endogenous control. Genes present at a consistent expression level in all experimental samples can be used as endogenous control. Using an endogenous control as a reference allows to normalize quantification of a cDNA target for differences in the amount of added cDNA.

Relative quantification was performed using the standard curve method by Applied Biosystems 7300 Real-Time PCR Detection System. Standard curves were plotted for both the target (the genetic sequence of interest) and the endogenous reference.

In the RT step, cDNA was reverse transcribed from total RNA samples using random primers.

TaqMan PCR was performed according to the following scheme:

**Mixture for TaqMan PCR (pro 1 sample):**

Reagents	Volume
2X TaqMan Master Mix (AmpErase UNG)	10 $\mu$ l
Assay on demand	1 $\mu$ l
DEPC-treated water	5 $\mu$ l

AmpErase uracil-N-glycosylase (UNG) is a pure, nuclease-free, 26-kDa recombinant enzyme encoded by the *Escherichia coli* uracil-N-glycosylase gene. UNG acts on single- and double-stranded dU-containing DNA creating an alkali sensitive apyrimidic site in the DNA. Apyrimidinic sites block replication by DNA polymerases. The enzyme has no activity on RNA or dT-containing DNA (Longo *et al.*, 1990).

2 x TaqMan Master mix contains 10x Taqman PCR buffer, 25 mM MgCl<sub>2</sub>, 200 µl dATP, 200 µl dCTP, 200 µl dGTP, 400 µl dUTP, 1.25 U AmpliTaq Gold.

In the PCR step, 16 µl mixture of TaqMan PCR was aliquoted in 96-well PCR plate. 4 µl of diluted RT product was added to each well. All samples were pipetted in duplicates. Negative control samples and calibrator RT product were loaded in parallel. RT product was diluted with DEPC-treated water for the same number of genes in all TaqMan PCR runs. cDNA of rat brain (calibrator) was used for plotting standard curves for genes of the interest and the endogenous control by five-fold serial dilutions for 8 points.

The thermal cycling conditions for the 7300 Real-Time PCR System were set up as follows:

<b>AmpErase UNG activation</b>	
50°C	2 min
<b>Activation of Ampli Taq Gold enzyme</b>	
95°C	10 min
<b>PCR (40 cycles)</b>	
94°C	15 s
60°C	1 min
<b>4°C to stop reaction</b>	

### 3.6.3. Quantification

After performing the PCR amplification the plots for an entire plate were analysed with the 7300 Sequence Detection System. The default baseline was adjusted to the fluorescence of the earliest amplification plot and a threshold equal to 0.1 was used.

For quantitative analysis data were exported to an Excel format, and standard curves (log input amount against the CT value for *Cdkn2a*, *Cdkn2c*, *Sctr*, *Sdhd*, *Rassf1* genes and for the endogenous reference  $\beta$ -2 microglobulin) were plotted. Linear regression analysis was used to calculate the relative amount of mRNA for unknown samples. The relative mRNA expression level of genes of the interest was normalized for input RNA against rat  $\beta$ -2 microglobulin gene expression in the sample.

The relative mRNA expression level of genes was calculated using following formulas (Dr. Rosemann, Institute of Radiation Biology, GSF; Calzada-Wack *et al.*, 2002):

$$A = 10^{B-C} \text{ or } \log_{10} = B-C,$$

where A = the relative amount of mRNA of the sample

$$B = \text{Mean CT}_{\text{sample}} - \text{CT dif.}_{\text{sample}} / \text{lin.coef.}_{\text{sample}}$$

$$C = \text{Mean CT}_{\beta 2m} - \text{CT dif.}_{\beta 2m} / \text{lin.coef.}_{\beta 2m}$$

$$\text{CT dif.}_{\text{sample}} = \text{Mean CT}_{\text{calibrator of the sample}} ((\text{lin.coef.}_{\text{sample}} \times \log_{10}(5)) + \text{abs.coef.}_{\text{sample}})$$

$$\text{CT dif.}_{\beta 2m} = \text{Mean CT}_{\text{calibrator of } \beta 2m} ((\text{lin.coef.}_{\beta 2m} \times \log_{10}(5)) + \text{abs.coef.}_{\beta 2m})$$

$\beta 2m$  -  $\beta$ -2 microglobulin

Values of linear and absolute coefficients are taken from regression formulars received basing on standard curves for genes of the interest and  $\beta 2$ -microglobulin: (Results, 4.3.1).

$$\text{CT} = \text{lin. coef.} \times \text{conc} + \text{abs. coef.}$$

### Statistical analysis

To estimate the difference between relative amount of mRNA of tumor samples and mRNA level of control group of samples standard double-sided t-test was used. P values less than 0.05 were considered to indicate a statistically significant difference in mRNA level.

### 3.7. Automated fluorescent sequencing

For automated fluorescent DNA sequencing fluorescent dyes are incorporated into DNA extension products using 3'- dye labelled dideoxynucleotide triphosphates. Four different dyes are used to identify the G, C, A, and T nucleotides, each of which emits light at a different wavelength when excited by an argon ion laser. Therefore, all four bases can be detected and distinguished using one reaction tube. For cycle sequencing reaction Biometra® T personal - 48 PCR machine was used. Thermal cycling of denaturation, annealing, and extension using a single sequencing primer (unlabeled 5' -Primer) resulted in a linear amplification of the extension products. Addition of all four fluorescent dyes 3' -dye labelled dideoxynucleotides (ddNTPs, 3'-dye labelled terminators) simultaneously terminated and labelled the extension products. Products of the sequencing reaction, labelled with four different fluorescent dyes, were separated according to their size in a 48 capillary machine Applied Biosystems 3730 DNA Analyzer (Genome Analysis Center, GSF).

Process of sequencing includes following steps:

- PCR reaction
- Purification of PCR product
- Sequencing reaction

### 3.7.1. PCR reaction

For sequencing reaction PCR was set up according to the following scheme:

#### Mixture for PCR reaction (pro 1 sample)

Reagents	Volume
Buffer 10X containing 15 mM MgCl <sub>2</sub>	2.5 µl
dNTP mix (10 mM)	0.5 µl
Forward primer (10 pmol/µl)	1 µl
Reverse primer (10 pmol/µl)	1 µl
Gene Craft Tag polymerase (5000 U)	0.25 µl
Water	17.25 µl
DNA template	2.5 µl
<b>Final Volume</b>	<b>22.5 µl</b>

The PCR cycle conditions were the same as for microsatellite analysis. PCR was performed for 30 cycles. To estimate the quality of PCR reaction PCR products were loaded into the 2% agarose gel.

### 3.7.2. Purification of PCR products

Purification of PCR products was performed by using QIAquick PCR purification kit. The QIAquick system combines spin-column technology with selective binding properties of silica-gel membrane and allow to purify fragments ranging from 100 bp to 10 kb from primers, nucleotides, polymerases and salts. DNA adsorbs to the silica – membrane in the presence of high salt while contaminants pass through the column.

1 volume of PCR product was mixed with 5 volumes of Buffer PB. To bind DNA, samples were applied to the QIAquick column and centrifuged for 30-60 s at 13000 rpm. During the DNA adsorption step, unwanted primers and impurities, such as salts, enzymes, unincorporated nucleotides do not bind to the silica membrane, but flow through the column. For washing 0.75 ml ethanol containing Buffer PE was added to the QIAquick columns. Samples were centrifuged for 1 min at 20.000 x g twice to completely remove ethanol from buffer PE. Salts are quantitatively washed away by PE buffer. Elution of DNA was performed with 50 µl Buffer EB (10 mM Tris-HCl, pH 8.5) added to the center of the QIAquick membrane. For optimal DNA

yield the columns were incubated in elution buffer for 1 min at room temperature and centrifuged for 1 min at 20.000 x g.

The concentration of purified PCR product was measured with the Nanodrop. Amount of DNA used for sequencing reaction was adjusted to have 20 -30 ng of DNA per reaction (recommendation of Genome Analysis Center, GSF)

### 3.7.3. Sequencing reaction

The BigDye Terminator Cycle Sequencing Kit was used for sequencing reaction. This Kit contains AmpliTaq DNA polymerase, the BigDye terminators (A-dye terminator labelled with dichloro (R6G), C-dye terminator labelled with dichloro (ROX), G-dye terminator labelled with dichloro (R110), and T-dye terminator labelled with dichloro (TAMRA)), all four deoxynucleoside triphosphates (dATP, dCTP, dTTP, dUTP), MgCl<sub>2</sub> and Tris- HCl buffer, pH 9.0. The dNTP mix includes dTTP in place of dGTP to minimize band compressions. The dNTP mix also uses dUTP in place of dTTP. dUTP improves the incorporation of the T terminator and results in a better T pattern.

Sequencing reactions were performed in 96 - well PCR plates as follows :

#### Mixture for sequencing reaction (pro 1 sample)

Reagents	Volume
Big Dye terminator mix v. 3.1	2 µl
5X Buffer	0.94 µl
DMSO	0.3 µl
primer (either forward or reverse) 10 pmol/µl	1 µl
Template	20-30 ng
HPLC water	to 10 µl

For the PCR reaction the following conditions were chosen:

Programm	Temperature/Time
Initial Denaturation	96 °C / 1 min
<b>3-step cycling</b>	
Denaturation	96 °C / 100 s
Annealing	50 °C / 5 s
Extension	60°C / 4 min
<b>Number of cycles : 35</b>	
hold at 4°C until ready to purify	

## **Ethanol precipitation**

Ethanol precipitation was chosen as the method for purification of cycle sequencing products.

5 µl of PCR products were pipetted in 96-well PCR plate. 15 µl of 100% Ethanol was added to each well containing PCR product. Plate was sealed with aluminium folia, incubated at room temperature for 15 min in the dark and centrifuged for 30 min at 4°C at 6000 x g. After discarding the supernatant 15 µl of 70% ethanol was added to the plate. The plate was spun at 4°C for 30 min at 6000 x g.

The supernatant was discarded by spinning the inverted plate in the centrifuge at very low speed for a few seconds. The plate was dried up-side-down at room temperature in the dark for 30-60 min. Pellets were resuspended in 50 µl of HPLC water.

After the sequencing reaction and ethanol precipitation PCR extension products containing the mixture of strands, all of different length and all ending with a fluorescently-labelled ddNTP, underwent sequence analysis by the Genome Analysis Center core facility.

Sequencing data (electropherograms of samples and sequence text files) were analyzed by using the Sequencher 4.1 and MutationSurveyor 3.10 Validation programs.

## **3.8. Fluorescence in situ hybridization analysis (FISH)**

FISH allows direct visualization of large genetic alterations in a cell by cell manner. The aim of the technique is to demonstrate either imbalances, in the form of gains or losses of segments of chromosome materials, or to show specific breakpoints with or without imbalance (Beatty *et al.*, 2002). FISH can be performed on tissue (fresh, frozen, or formalin-fixed paraffin-embedded), touch preps, cytopins, or cell cultures (Beatty *et al.*, 2002).

The basic requirements of the FISH technique are therefore (Rautenstraß *et al.*, 2002):

- ✓ a probe that is specific for the sequence of interest
- ✓ fluorescent or nonfluorescent labelling of this probe to allow appropriate detection
- ✓ a biological specimen with preservation of sufficient morphological detail to determine the localization of the labelled probe after hybridization.

The standard FISH protocol includes the following steps:

- Probe preparation and labelling
- Sample preparation
- Denaturation of probe and sample
- Hybridization of probe to sample (annealing)
- Post-hybridization washing

- Detection

### **3.8.1. Probe preparation and labelling**

#### **Isolation of genomic DNA from BAC clones**

FISH analysis was performed for rat chromosomes 8 and 19. Genomic DNA extracted from bacterial artificial chromosome (BAC) clones was used as a probe. The BAC clones were ordered from Children's Hospital and Research Center at Oakland, California; BACPAC Resources (CHORI center) (Table 4.29).

BAC clones were received as bacterial LB agar stab culture. The DH10 E.coli host cells with plasmids containing the DNA insert of interest were placed onto LB agar containing 12.5 µg/ml chloramphenicol. This culture was streaked to produce single colonies. Genomic DNA from the BAC clones was extracted by using the Qiagen Large-Construct Kit. A single colony from a freshly streaked plate was isolated and inoculated in 2-5 ml LB medium containing 12.5 µg/ml chloramphenicol. Cells were incubated for 8 hours at 37°C with vigorous shaking. This initial culture was added to 500 ml LB medium (1/500 to 1/1000 dilution) and grown at 37°C for 12 - 16 h with intensive shaking (~ 300rpm). Glycerol stock of the clones were prepared and stored at - 70°C. Lennox L Broth Base powder was used for preparation of LB medium. Additionally 5 g NaCl was added to the medium to obtain the highest yield of large-construct DNA. The bacterial cells were harvested by centrifugation at 6000 x g for 15 min at 4°C. Bacterial pellets were weighted and the weight was approximately 3 g/liter of medium. This weight corresponds to cell density of around  $3-4 \times 10^9$  cells/ml. It is an optimal density of cells for efficient use of the Large-Construct Kit. The pellets were sequentially resuspended in 20 ml P1 with Ribonuclease A and 20 ml P2 buffers for alkaline lysis. For precipitation 20 ml of chilled buffer P3 was added. The precipitated material contains genomic DNA, proteins, cell debris, and potassium dodecyl sulphate. Samples were centrifuged at 20000 x g for 30 min at 4 °C. Supernatant was removed and filtered. The filtration step was carried out to avoid precipitation of suspended or precipitated material forming after addition of P3 buffer, which could lead to incomplete exonuclease digestion. DNA was precipitated by adding 36 ml isopropanol and centrifuged at 20000 x g for 30 min at 4°C. The DNA pellet was washed with 5 ml 70% ethanol, and centrifuge at 20000 x g for 15 min. The 70% ethanol removes precipitated salt and replaces isopropanol with the more volatile ethanol, making the DNA easier to redissolve. The DNA pellet was air-dried and redissolved in 9.5 ml buffer EX. The ATP-Dependent Exonuclease digestion step ensures selective removal of contaminating broken strands of genomic DNA as well as nicked or damaged large-construct DNA. 200 µl ATP-Dependent Exonuclease and 300 µl ATP solution were added to the dissolved DNA. Samples were incubated in a water bath at 37°C for 60 min,

mixed with 10 ml Buffer QS and applied to equilibrated QIAGEN- tips. Large-construct DNA is bound to QIAGEN Resin under appropriate low-salt and pH conditions. The QIAGEN- tips were washed with 2 × 30 ml Buffer QC (medium-salt wash). This washing allows to remove RNA, proteins, dyes, and low-molecular - weight impurities. Large-construct DNA was eluted with 15 ml high-salt Buffer QF, prewarmed to 65°C, precipitated with 10.5 ml room-temperature isopropanol and washed with 5 ml room-temperature 70% ethanol. DNA was air-dried and redissolved in a suitable volume of EB buffer. DNA concentration was determined with the Nanodrop.

To check BAC clones PCR was performed with primers designed to detect introns of genes mapping to the regions of each BAC clone (Fig. 4.16). PCR was done at the same conditions as above (Methods, 3.4.2). A single colony was used as the template for PCR.

### **Probe labelling**

DNA probes were labelled with biotin or digoxigenin dUTP by nick translation. Nick translation uses the simultaneous activity of two enzymes: DNaseI, which creates random nicks in the template and E.coli DNA polymerase I, which through its 5'- 3' exonuclease activity removes nucleotides, while the 5'- 3' polymerase activity adds nucleotides to all the available 3'-ends created by the DNase. Thus this approach allows the introduction of labelled nucleotides into the probe molecules. Purity of the probe and size of labelled fragments (100-400 bp) are critical in producing the best signal-to-background ratios. Nick translation was performed according to the following scheme:

#### **Mixture for nick translation (pro 1 sample)**

<b>Reagents</b>	<b>Volume</b>
dNTP Mix (minus dTTP)	5 µl
Pol I/DNase I Mix	5 µl
Biotin-16-dUTP or Digoxigenin-11-dUTP	2.5 µl
DNA from BAC clone (1µg)	x µl
Water	x µl
<b>Total volume</b>	<b>50 µl</b>

Samples were incubated for 70 min at 16°C. Incubation was performed for 70 min, 90 min, and 120 min at 16°C but the best results after FISH analysis were received only with time of incubation 70 min. That is why 70 min of incubation was chosen as an optimal time for nick translation. To stop the reaction 5 µl of Stop buffer (0.5 M EDTA, pH 8.0) was added to the



samples. Samples were incubated for 5 min at 70 °C. Then samples were thoroughly mixed with 5 µl Herrings Sperm DNA (10 mg/ml), 20 µl Rat Hybloc DNA (1mg/ml), or Cot-1 DNA. For precipitation 1/10 volume of 3M sodium-acetate (pH 5.3) and 2-2.5 volume of ice-cold 100% ethanol were added to the samples. Precipitation was performed overnight at -20°C. Ethanol precipitation of probes in the presence of excess Cot-1 DNA and Herrings Sperm DNA reduces non-specific binding during hybridization of the probe to the sample. Samples were centrifuged at 20.000 x g for 30-40 min at 4°C. DNA pellet was washed with 500 µl of ice-cold 70% ethanol with following centrifugation at 20.000 x g for 5min at 4°C. Pellets were dried for 15 min at 65°C and mixed with 25 µl Mastermix and 25 µl formamide. Mastermix and formamide were prewarmed to 37°C. Mastermix contains 4 parts 50% dextransulfate in water, 4 parts water and 2 parts 20 ×SSC. The formamide should be of high quality and be deionized to pH 7.0. Labelled probes were stored at – 20°C.

### **Nonspecific nucleic acids competitors**

Many copies of disperse repeats are expected to be present in almost all BAC clones that are used as probes for FISH analysis. To avoid cross hybridization to other chromosomal regions containing these repeated sequences excess unlabelled Cot-1 DNA and Herrings Sperm DNA were added to the probe mixture prior to hybridization. Nonspecific nucleic acids competitors bind to the probes repeat sequences which in turn can not hybridize to the chromosomal repetitive DNA leaving the unique sequences in the probe single-stranded and free to hybridize to the chromosomal DNA. Cot-1 DNA repetitive sequences are species specific. Thus the Cot-1 DNA used for hybridization should be derived from the same species as the sample used for FISH analysis.

### **3.8.2. Sample preparation**

For FISH analysis two kinds of slides were used: slides preprepared with rat metaphases and slides with tissue sections from paraffin-embedded tissue.

The specificity of labelled probes was checked by using slides with preprepared rat metaphases. These slides were provided by Dr. Chevillard and Dr. Guilly, CEA, France. Cytogenetic analysis of the slides after FISH analysis on rat metaphases was done by Dr. Guilly.

Tumor samples with PC were fixed in formalin and embedded in paraffin. Tissue sections with thickness 10 µm were cut and placed on SuperFrost slides. H& E staining was performed for one slide for each tumor sample. H & E stained slides were used as reference for FISH data analysis.

Deparaffinization was performed at room temperature as follows:

Steps	Reagents	Time
1	Xylool	2 x 20 min
2	Isopropanol	5 min
3	100% Ethanol	5 min
4	90% Ethanol	5 min
5	70% Ethanol	5 min
6	PBS (pH 7.0)	5 min

After deparaffinization pre-treatment of the slides with tissue sections was performed to make nucleic acids contained within samples available to the probe (unmasking). Pretreatment was done using following scheme:

Steps	Reagents	Time / Temperature
1	Citrate buffer	20 min in microwave (350 W)
2	PBS (pH 7.0)	5 min, room temperature
3	0.05 % Pronase E ( 50 µg Pronase E / 100 ml PBS)	5 min, 37°C
4	PBS (pH 7.0)	2 × 5 min, room temperature

The samples were dehydrated with ice-cold ethanol washes (70%, 90%, 100%) for 5 min each and the slides with cover slips or cover glasses of suitable size were dried at 37°C.

Deparaffinization and pretreatment were not performed for slides with rat metaphases. They were directly dehydrated with ethanol as it was described above and dried at 37°C.

### 3.8.3. Denaturation of probe and sample

The DNA probe and the DNA target molecules can either be denatured separately or by co-denaturation. Co-denaturation was used in the current study.

Labelled probes were thoroughly mixed and spinned briefly. Appropriate amount of the probe was added to the pre-warmed at 37°C slides, covered with a cover slip and sealed with the rubber cement “Fixogum”. Slides were denatured for 10 min at 80°C. Heating double-stranded DNA in the presence of formamide destabilizes the DNA and permits strand dissociation to occur at a lower temperature thus maintaining chromosome morphology.

### 3.8.4. Hybridization of probe to sample (annealing)

After denaturation samples were placed in a sealed moist chamber. Hybridization was performed overnight at 37°C. Maintaining a humid environment during hybridization prevents the slides from drying out and compromising hybridization efficiency. The time required for hybridization depends on the target sequence, i.e. highly repetitive DNA requires a short hybridization (2-4 h) while low or single copy targets require overnight hybridization, and the purity of the DNA probe.

### Post-hybridization washing

After hybridization unbound probe was removed. This was carried out by washing the slide in standard saline citrate solution (SSC) where probe-target hybrids are stable. The specificity of the washing can be regulated by altering the salt concentration of the washing solutions, formamide concentration and temperature. Rubber cement was removed with forceps and coverslips were detached from the slides by placing the slides in the solution 50 % Formamide in 2 x SSC for 30 - 60 s. Post-hybridization washing was performed, as follows:

Steps	Reagents	Time / Temperature
1	50% Formamide in 2xSSC	3 × 10 min / 43°C
2	2xSSC	3 × 5 min / 43°C
3	2xSSC, 0.1% NP40	1 × 5 min / 60°C

Slides were immersed into the blocking solution and incubated for 30 min at room temperature. Performing a blocking step allows to reduce a high background. Blocking solution includes 4 × SSC, 0.1% NP40, 3% BSA.

### 3.8.5. Detection

After the final washing step the presence and localization of probe-target hybrids was demonstrated by detection of the labelled probe:

### Probe detection scheme

Label	Layer 1	Layer 2	Fluorescence color
one-color FISH			
Bio	Streptavidin-FITC conjugate(1:20)	Biotinylated anti -avidin D antibodies (1:50)	Green
Dig	-	Anti-digoxigenin-rhodamine antibodies (1:200)	Red
two-color FISH			
Bio + Dig	-	Streptavidin-FITC conjugate(1:50) + Anti-digoxigenin-rhodamine antibodies (1:50)	Red and green

Abbreviations: Bio, biotin; Dig, digoxigenin

One-color FISH was performed on rat metaphases spreads to check the specificity of BAC FISH probes for rat chromosomes 8 and 19. Interphase FISH analysis with one locus-specific probe CH230-385B22 (8q22) was performed on paraffin - embedded tissue of PC samples for chromosome 8. Two-color FISH (dual FISH) was used for interphase FISH analysis with locus-specific probes CH230-398H16 (19q11) and CH230-89I12 (19q12) for rat chromosome 19. For two-color FISH overlapping red and green signals can produce a yellow signal.

For visualization of probes labelled with digoxigenin anti-digoxigenin-rhodamine antibodies (1:200) in blocking solution were used. 200 µl antibodies were added to each slide, covered with a coverslip, and incubated for 90 min at 37°C in the moist chamber

For detection of biotin labelled probes Streptavidin-FITC conjugate (1:20) antibodies in blocking solution were used with following incubation of slides in the moist chamber for 60 min at 37°C. In case if the signal from the biotin-labelled probe is weak after the incubation with Streptavidin-FITC conjugate antibodies one can increase the signal intensity by adding biotinylated anti-avidin D antibodies according to the following protocol:

Steps	Reagents	Time / Temperature
1	Biotinylated anti -avidin D antibodies (1:50) in the blocking solution	45 min / 37°C
2	4×SSC, 0,1% NP40	3×2 min / 37°C
3	Streptavidin - FITC conjugate (1:20) in the blocking solution	60 min / 37°C
4	4×SSC, 0,1% NP40	3×2 min / 37°C

The protocol for the enhancement of the signal from biotin-labelled probe was used for FISH analysis on rat metaphases spreads to check the specificity of the biotinylated BAC probe CH230-406J14 for rat chromosome 8.

For dual FISH analysis a mixture of equal amount of biotin-labelled and rhodamin-labelled probes was used for hybridisation to the sample. For detection of both probes a cocktail of antibodies containing Streptavidin-FITC conjugate (1:50) and anti-digoxigenin-rhodamine Fab fragments (1:50) was added to each sample. Samples were incubated for 90 min at 37°C. After incubation with antibodies coverslips were removed and samples were rinsed 3 × 2 min in 4×SSC, 0.1% NP40 solution at room temperature and briefly in PBS. For counterstaining of chromosomes or nuclei the slides were immersed in Hoechst 33342 (15 µg/ml) for 5 min. Instead of Hoechst 33342 DAPI staining was used for counterstaining of slides with rat metaphases after FISH analysis. Slides with rat metaphases were incubated in DAPI solution (0.1 µg/ml in 2 × SSC) for 10 min at room temperature and washed in 2 × SSC for 5 min at room temperature. Then 1-2 drops of VECTASHIELD Mounting Medium (antifade solution) were dispensed onto the slide and covered with the coverslip of the appropriate size. Coverslip was gently pressed to disperse VECTASHIELD over the entire slide and to avoid excessive liquid. After mounting, coverslipped slides will not dry out and can be reviewed for months afterward without sealing.

### **3.8.6. Analysis of the data**

To visualize fluorescently labelled probes epifluorescence microscope Apotome equipped with filter sets for DAPI, FITC, Cy3, Cy5 was used (power field: 63 × DIC, Cond. BF).

For FISH data analysis Z-stack optical sectioning with a thickness 0.625 µm was done for each sample. Z-stacks were analyzed with programs Axiovision Rel. 4.6, LSM Image Browser. Overlapping and truncated nuclei, nuclei with diffuse and weak signals, split signals and very stringy signals were not analysed. For each section of PC samples 100 nuclei were count from tumor area (adrenal medulla) and adjacent nontumor area (adrenal cortex). 100 nuclei were analysed from samples of normal adrenal gland (adrenal medulla was examined). The value of cut off was determined by calculation of mean percent of cells of control areas (cortical part of PCs, normal adrenal medulla tissue sections) showing 1 signal for one-color FISH and 1:1 ratio of signals for two-color FISH plus/minus three standard deviations. The cut off value was calculated separately for the BAC probe CH230-385B22 (8q22) and probes CH230-398H16 (19q11) and CH230-89I12 (19q12) used for FISH analysis for rat chromosome 8 and 19, respectively.

### **3.9. CGH array**

Rat whole genome CGH array hybridizations were performed by NimbleGen ([www.nimblegen.com](http://www.nimblegen.com)). This array was designed and constructed based on the RGSC 3.4 Ensembl

July 2005 data. The array has a median probe spacing of 5,303 bp. Probes (oligonucleotides) were synthesized using an isothermal format and vary in length from 45 to 85 bp.

RNA-free genomic DNA for the CGH array was extracted from fresh – frozen tissue of 7 tumor samples with PC using standard phenol-chloroform extraction (Methods, 3.2.1). All PC samples used for the CGH array analysis were mature large tumors with characteristic compression of cortex. Macroscopically the border between medullary and cortical parts of tumors of the adrenal glands was easy to recognize. Before sections were cut from tumors the cortical part was removed. For DNA extraction only the medulla of adrenal gland was used (Methods, 3.2.2.). As a control, pooled genomic DNA from 7 female rats was used. Samples were analyzed for quality and purity with gel electrophoresis using 1% agarose gel. On NimbleGen's recommendation unsonicated genomic DNA samples suitable for CGH analysis should have one strong band at the top of the gel without significant signs of degradation. If there is more than one band or smearing in the unsonicated genomic sample it may be degraded or have a contaminant that can affect the labelling procedure. The concentration of DNA samples used for CGH array was measured with Nanodrop. The samples were concentrated to 250 ng/  $\mu$ l in nuclease - free water. The value of  $A_{260}/A_{280}$  should be at least 1.7. NimbleGen requires 3  $\mu$ g of genomic DNA from each test sample: 1  $\mu$ g of DNA is used per hybridization and 1  $\mu$ g is needed for quality control performed by the company itself.

In this technique the test and reference DNA samples are independently sheared by sonication (sonicated sample should be a smear from ~500-2000 bp) and labeled with dye-modified random primers. NimbleGen uses a 2-color protocol for sample labeling: Cy3 labeled random primers for the test sample and Cy5 labeled random primers for the reference. The random primer reaction uses Klenow DNA polymerase which provides ~50 fold amplification in the labelling step. Labeled test and reference DNA were combined and competitively hybridized to a NimbleGen CGH array. Hybridization of repetitive sequences is blocked by adding Cot-1 DNA. The array is stringently washed, dried, and scanned.

CGH analysis is a multi-step process that begins with TIFF image files and ends with predicted copy number regions called segments (Fig. 2.1). TIFF images are extracted using NimbleScan 2 software, NimbleGen System's image quantification and data analysis package. Grids are placed on each image and the quantification area for each feature is adjusted for optimal placement. Signal intensity information for test and reference samples is saved in PAIR report files provided by NimbleGen. Then the signal intensity information is combined with the genome position data for each probe. This information is supplied by a POS file (NimbleGen data format). After combining the signal intensity information with the genomic coordinate information, the Cy3

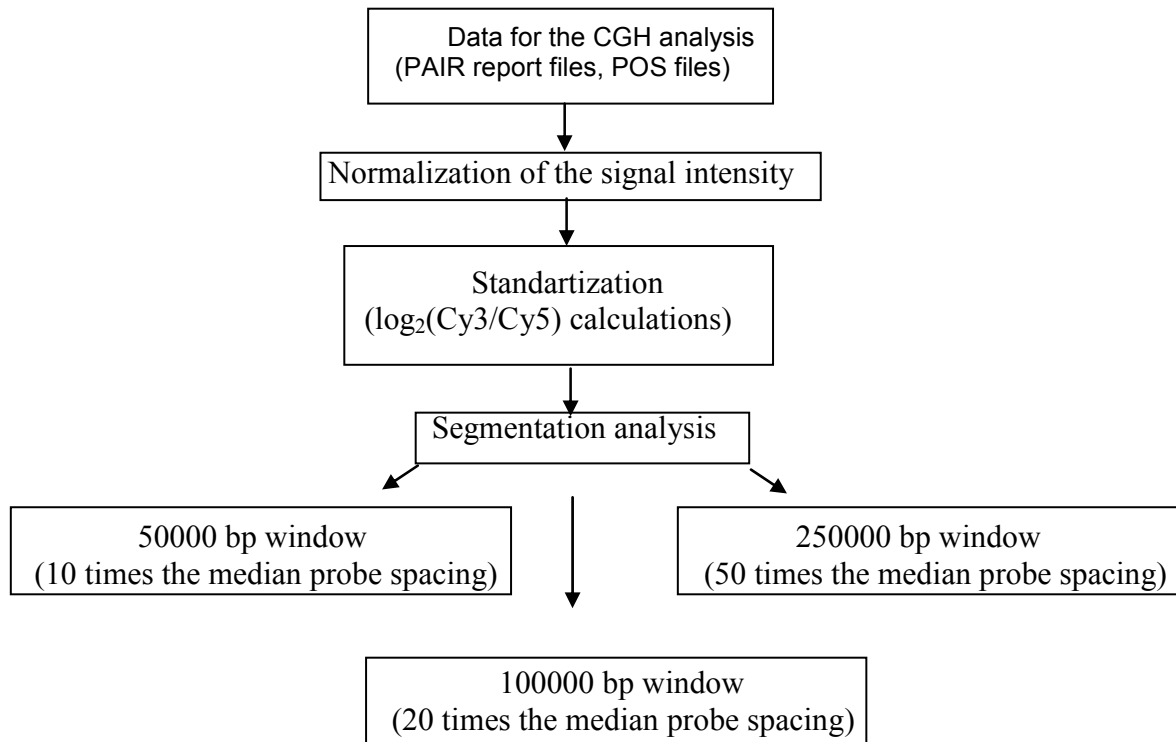


**Fig. 2.1** Sequential steps in array-CGH data analysis.

and Cy5 signal intensities are normalized to one another. Then  $\log_2(Cy3/Cy5)$  ratio calculations are performed (hereafter,  $\log_2(PM_{\text{test}}/PM_{\text{reference}})$ , where  $PM_{\text{test}}$ , the perfect match signal intensity for the test sample, labelled with Cy3;  $PM_{\text{reference}}$ , the perfect match signal intensity for the reference sample, labelled with Cy5). Once the data has been normalized, DNA segmentation analysis is performed. This includes a window averaging step, where the probes that fall into a defined base pair window size are averaged. Rather than using a sliding window approach, adjacent windows are averaged. Averaging reduces the size of the data set and the noise in the data, what allows some segments to be found that might otherwise be missed. NimbleGen uses 3 different window sizes corresponded to 10, 20, and 50 times the median probe spacing on the design. Different window sizes are used, because smaller segments may be missed when the data is averaged using large window size. Large window size (for example, window with the size 50 times median probe spacing) results in less noise, but less sensitivity. Window with averaging size 50000 bp (10 times the median probe spacing) has the highest level of resolution and at the same time the highest level of the noise. Normalization and segmentation of data was also performed by NimbleGen.

## 4. RESULTS

### 4.1. The group of experimental animals

The MENX phenotype was initially identified in a Sprague Dawley (SD) rat colony and maintained as previously reported (Fritz *et al.*, 2002). Animals expressing the mutant phenotype were indicated as SD<sup>we</sup>/SD<sup>we</sup> for Sprague Dawley white eye in reference to the presence of juvenile cataracts. To fine map the MenX gene, *Cdkn1b*, firstly, SD<sup>we</sup>/SD<sup>we</sup> homozygous male rats were crossed with Wistar Kyoto (Wky) female rats. Then F1 (Wistar- Kyoto × SD<sup>we</sup>) females were backcrossed with SD<sup>we</sup>/SD<sup>we</sup> males to generate F2 animals (Piotrowska *et al.*, 2004, Pellegata *et al.*, 2006).

**Table 4.1** F2 animals selected for analysis

Case number	Tissue section number	Ear take number	Sex of animals	Age (months)	Eye phenotype	Histological diagnosis
PC1	04/813	473	male	10	Bds	Bilateral PC
PC2	04/1063	491	male	10	Bds	Bilateral PC
PC3	04/1263	493	male	11	Bds	Bilateral PC
PC4	04/1498	497	male	11	Bds	Bilateral PC
PC5	04/1155	501	female	10	Bds	Bilateral PC
PC6	04/1248	509	male	11	Bds	Bilateral PC
PC7	04/1264	544	male	11	Bds	Bilateral PC
PC8	04/1064	545	male	10	Bds	Bilateral PC
PC9	04/1329	562	male	12	Bds	Bilateral PC
PC10	04/1036	572	female	10	Bds	Bilateral PC
PC11	04/1065	574	female	10	Bds	Bilateral PC
PC12	04/1427	607	female	11	Cat. on left eye	Bilateral PC
PC13	04/1342	608	female	11	Bds	Bilateral PC
PC14	04/1299	614	male	11	Bds	Bilateral PC
PC15	04/1300	617	male	11	Bds	Bilateral PC
PC16	04/1444	625	female	11	Bds	Bilateral PC
PC17	04/1257	626	female	10	Bds	Bilateral PC
PC18	04/1246	631	male	10	Bds	Bilateral PC
PC19	04/504	649	male	8	Bds	Bilateral PC
PC20	04/1302	669	female	10	Bds	Bilateral PC

Abbreviations: F2 animals, animals were obtained from a F1 (Wistar- Kyoto × SD<sup>we</sup>) × SD<sup>we</sup>/SD<sup>we</sup> backcross, where SD<sup>we</sup> (Spaque-Dawley white eye) indicates the MENX affected animals; Bds, cataracts are on both eyes; Cat on left eye, cataract is only on the left eye; Bilateral PC, bilateral pheochromocytoma

Affected animals with the MENX syndrome develop pituitary adenoma, parathyroid adenoma, medullary thyroid hyperplasia, and paraganglioma within the first year of life (Fritz *et al.*, 2002).



In 100% of cases affected animals develop PC. The following criteria have been used for the selection of animals for the current study:

- presence of cataract
- homozygous mutation of the *Cdkn1b* gene
- presence of PC.

Based on these criteria 20 F2 animals were selected for the current study and were designated PC1-PC20 (Table 4.1.). F2 animals were used because need homozygous state for the mutated *Cdkn1b* gene and heterozygous state for other genes to perform LOH/AI study,

#### **4.1.1. Histological analysis of rat adrenal glands with PC**

Adrenal glands with PCs were collected from 20 affected rats with MENX syndrome. H&E staining was performed for each tumor sample. The presence of PC was confirmed by histopathological analysis of H&E stained slides (in cooperation with Dr. Calzada-Wack, Dr.Hözlwimmer, Institute of Pathology, GSF). In all cases there were mature large benign PCs, highly vascularized, with significant compression of cortex (Fig. 4.2G, H). Large lesions were hemorrhagic, necrotic, and cystic (Fig. 4.2D, E). The neoplastic medullary cells are arranged into small nests or alveoli (“zellballen”) by a rich vascular network (Fig. 4.2F). The tumor tissue samples contained > 80% tumor cells.

For molecular analysis fresh frozen tumor tissue from the medullary part of adrenal glands, dissected free from the cortical part, has been used (Fig. 4.2C). DNA was extracted from the tumor tissue. FISH analysis has been performed on paraffin-embedded tissue of PC samples. As a control paraffin-embedded tissue sections of normal adrenal gland were used (Fig. 4.2A). Paraffin embedding allows preserving tissue morphology what it is important for the accurate FISH data analysis. Morphologic detail of the tissue is usually not well preserved in fresh frozen sections (Fig. 4.2C).

#### **4.2. Microsatellite-based allelotyping of somatic genetic changes in PC (LOH analysis)**

LOH/AI studies have been used to identify putative tumor suppressor genes involved in tumorigenesis. This approach can identify chromosomal regions that are consistently lost in tumor but not in normal adjacent tissues. LOH at a polymorphic locus is detectable by loss or reduction of one allele. Various chromosomal mechanisms can account for loss of the allele in a tumor sample compared to normal DNA from the same animal: (a) deletion detected as loss of

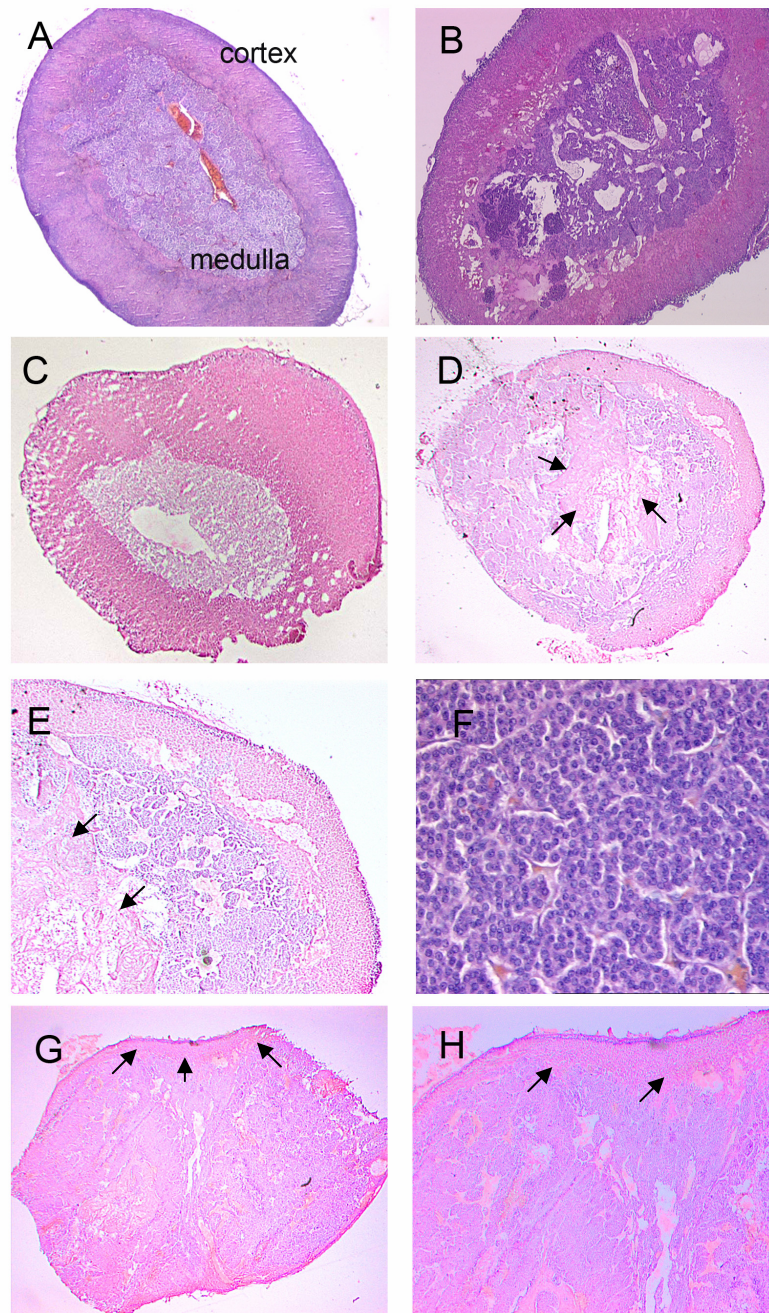


**Fig. 4.2** (A and C) The figures show normal adrenal glands in rats with the medullary part in the center and the distinct adrenal cortex. (A) Paraffin-embedded tissue H&E, original magnification 20x; (C) Fresh frozen tissue, H&E, original magnification 20x. (B, D, E, F, G and H) Benign PC of adrenal medulla in rat. (B) Paraffin-embedded tissue, case PC12 H&E, original magnification 25x. Tumors demonstrate areas of hemorrhage and necrosis (D and E, indicated by the arrows; (D) Fresh frozen tissue, case PC11, H&E, original magnification 25x; (E) At higher magnification of (D), H&E, 125x), and significant compression of cortex (G and H, shown by the arrows; (G) Fresh frozen tissue, case PC14, H&E, original magnification 25x; (H) At higher magnification of (G), H&E 125x). (F) The benign neuroendocrine tumors demonstrate characteristic nests of cells (“Zellballen”) without prominent mitotic activity. Additionally, the cells are characterized by uniformity (similar in shape and size) and overlapping of the nuclei. Paraffin-embedded tissue, case PC275, H&E, original magnification 320x).

one allele without a corresponding increase in the intensity of the signal for the other allele; (b) partial deletion; (c) deletion followed by duplication of remaining allele resulting in two copies of one allele and loss of the other (d) mitotic recombination; (e) localized mechanisms of chromosomal alteration such as point mutations, small deletions, or gene conversions (Lasko *et al.*, 1991).

100% of rats affected by the MENX syndrome develop adrenal medullary hyperplasia that develops into PC with age. To identify putative tumor suppressor genes involved in the transition of adrenal medullary cells from normal to neoplastic phenotype a genome-wide LOH/AI screening was performed comparing tumor and matched normal DNA from the same animals. Twenty adrenal glands with PC have been collected from F2 animals (Table 4.1). DNA was extracted from tumor tissue (medulla of adrenal gland) and normal tissue (ear take). DNA was amplified with primers specific for microsatellite markers. PCR product was resolved either on 3% agarose gel or on 10% polyacrylamide gel (Fig 4.3A) and quantified using Bio Image Intelligent Quantifier (Fig. 4.3B). 50% of allelic imbalance (AI) was taken as the conventional cut-off for LOH/AI definition, as used elsewhere (Ritland *et al.*, 1997; Stern *et al.*, 2000; Försti *et al.*, 2001 Kuosaite, 2001; Zhang *et al.*, 2001). For cases having LOH/AI the microsatellite analysis was repeated. For some markers microsatellite fragment analysis using 5'-FAM labelled primers was performed if it was not possible to resolve PCR product on 10% polyacrylamide gel or when confirmation of the presence of AI was necessary (Fig. 4.3C).

Paired tumor-normal DNA samples were genotyped using a total of 158 microsatellite markers, of which 85 turned out to be informative (heterozygous) in at least half of the cases. The average coverage was of approximately 1 marker every 20-30 Mb. All markers suitable for analysis of LOH/AI are listed in the section Appendix, Table 4.2. Information about the other tested microsatellite markers is given in the section Appendix, Table 4.3.

#### **4.2.1. Optimization of PCR conditions**

For PCR reaction appropriate conditions were determined to allow the PCR products to be in their exponential phase (essential for quantification). The exponential phase of PCR amplification occurs when reaction components are still in excess and the PCR products are accumulating at a constant rate. In late stages of a PCR there is the attenuation in the exponential rate of product accumulation. It is the so-called plateau effect when there is a maximal yield of PCR product. In the plateau phase the signal intensity of PCR product is also maximal and does not allow evaluation of the allelic ratio of the amplified DNA samples and, as a result, AI of analyzed tumor and matched normal samples can not be appreciated.

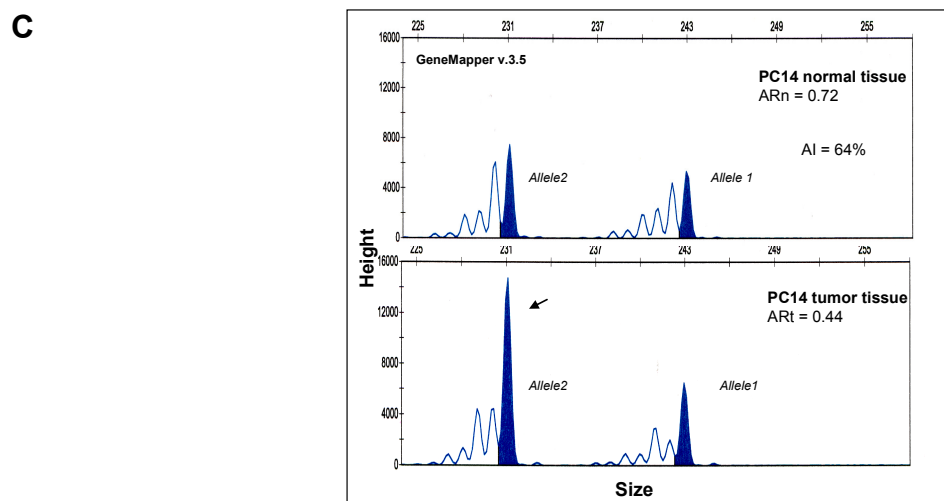
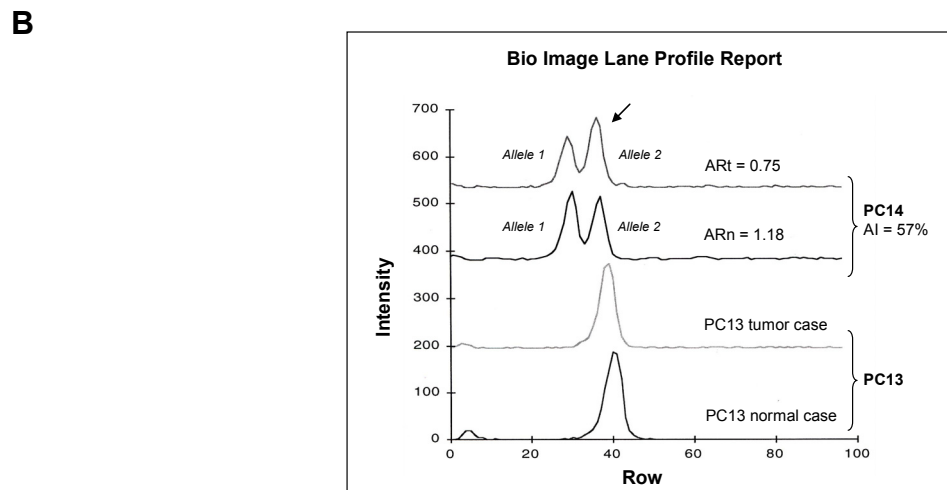
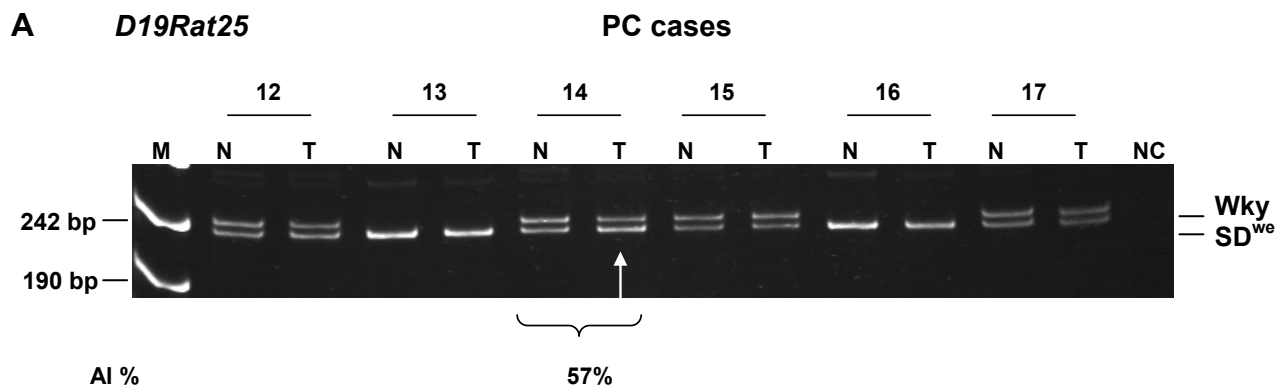


**Fig. 4. 3** LOH/AI analysis of PC samples amplified with microsatellite marker *D19Rat25*.

(A) Paired normal-tumor DNA samples were amplified with the marker *D19Rat25* and PCR product was resolved on 10% polyacrylamide gel. Pictures of ethidium bromide-stained gels were used for band intensity quantification and evaluation of allelic ratio. The case of AI is indicated with an arrow. The value of allelic ratio is shown (in percent). (B) Bands were quantified with Bio Image Intelligent Quantifier. There is an example of Bio Image Lane Profile report for PC13 (noninformative case) and PC14. PC14 case has AI (arrow). The sample from the normal tissue corresponding to PC14 gives 2 peaks of approximately the same intensity. For the tumor sample the intensity of peaks is significantly different what denotes the presence of AI. (C) To confirm AI indicated at the marker *D19Rat25* the same PC14 case was analyzed with microsatellite fragment analysis. AI was estimated with the program GeneMapper v.3.5.

Abbreviations: M, molecular weight marker VIII; NC, negative control; PC cases, pheochromocytoma cases; ARn, allelic ratio for normal sample; ART, allelic ratio for PC sample; AI, allelic imbalance.

To define the optimal number of cycles for the markers, two markers *D1Rat90* and *RND1Lev1* were subjected to PCR at different numbers of cycles (26, 28, 30 and 32) (Fig. 4.4). PCR amplification of samples PC11, PC12 for the marker *RND1Lev1* and PC13, PC17 for the marker *D1Rat90* (Fig.4.4) was performed in replicates. 5 and 10  $\mu$ l aliquots of the PCR product were loaded into the slots of 10% polyacrylamide gel. Ethidium bromide-stained gels were visually evaluated. For both microsatellite markers 28 cycles was found to be the optimal number of cycles. All PCR reactions for LOH/AI screening subsequently were performed at 28 cycles.

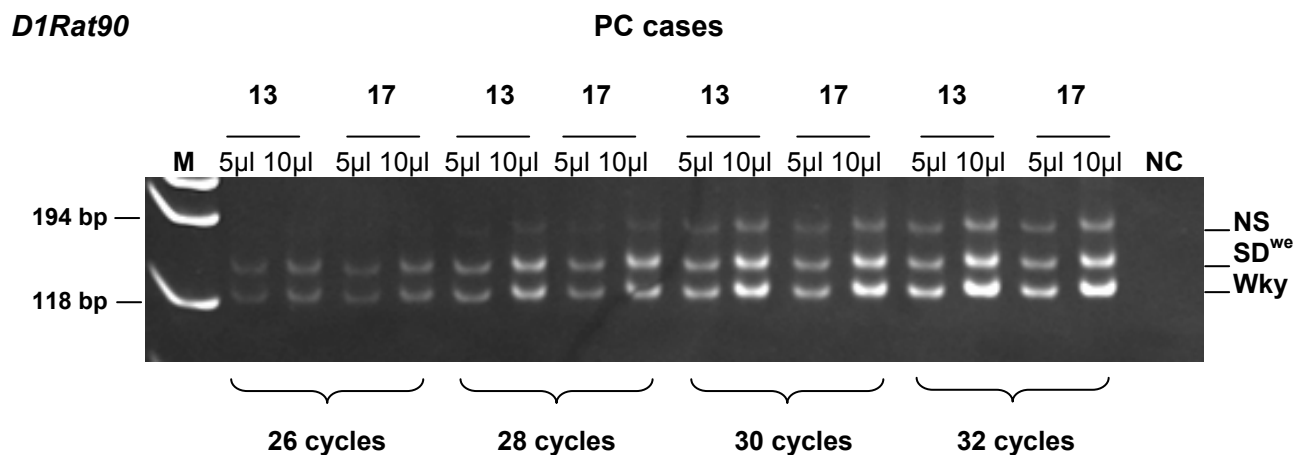


**Fig. 4.4** Semiquantitative determination of the optimal number of cycles. PCR reaction was performed for the marker *D1Rat90* for different number of cycles using samples PC13 and PC17 in replicates. PCR product was resolved on 10% polyacrylamide gel. 28 cycles is an optimal number of cycles which allow PCR product to be in the exponential phase.

Abbreviations: M, molecular weight marker IX; NC, negative control; NS, nonspecific product; PC cases, pheochromocytoma cases.

#### 4.2.2. Allele dilution experiments

To determine the sensitivity of the method, two DNA samples from animals homozygous for a Wky allele and for a  $SD^{we}$  allele, respectively, were mixed in selected ratios (Table 4.25). Mixed DNA samples were amplified in replicates with primers specific for three different microsatellite markers (*D4Rat136*, *D5Rat143*, and *D15Rat16*) and the bands were resolved on 3% agarose gel. Pictures of ethidium bromide-stained gels were used for band intensity quantification and LOH/AI evaluation using Bio Image Intelligent Quantifier (Fig. 4.5). For all tested microsatellite markers the presence of 10%  $SD^{we}$  DNA, mimicking “nontumor” DNA, in mixed DNA samples could be detected. It means that different markers are detected with similar sensitivity. This is consistent with observation made by Liu *et al.*, (1999).

**Table 4.25** DNA mixtures mimicking the mixed heterogeneous cell population expected to occur in tumor tissue

Sample	“Nontumor” DNA contamination represented (%)	Relative content of “tumor” DNA (%) Wky	Relative content of “nontumor” DNA (%) Sd <sup>wc</sup>
1	0	100	0
2	10	90	10
3	20	80	20
4	40	60	40
5	50	50	50
6	60	40	60
7	80	20	80
8	100	0	100

Sample 1 contains only Wky DNA, presenting 100% tumor DNA. Sample 8 is a pure SD<sup>wc</sup> DNA (100%). Samples 2-7 contain different percent of “nontumor” DNA contamination.

#### 4.2.3. Genome-wide screening for LOH/AI

After the genome-wide scan for LOH/AI in PC samples no 100% loss of any single allele was detected. We identified AI for the following chromosomes: 1q, 3p, 3q, 8q, 11q, 19p, 19q. Informative (heterozygous) samples were considered as having LOH/AI if the reduction in allelic intensity of any one of the two alleles was > 50%.

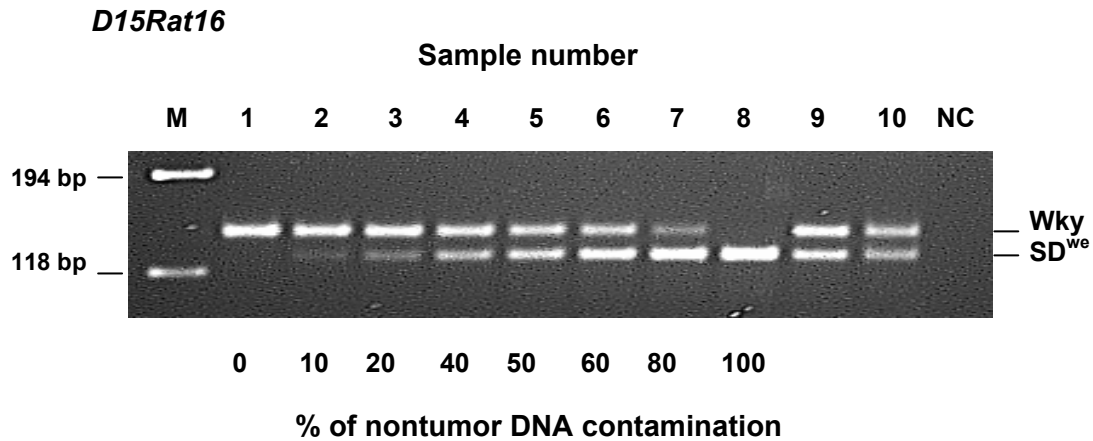
Rat chromosome 1 was analysed in twenty frozen PCs using 8 microsatellite markers with an average spacing 31 Mb (Appendix, Table 4.4). AI was detected at one microsatellite marker *D1Rat90* (1q55) for one case PC14, 13% (1/8 informative cases).

Chromosome 3 was analysed using 5 microsatellite markers with an average spacing 30 Mb (Appendix, Table 4.6). AI was detected at microsatellite marker *D3Rat56* (3p13) for case PC14 and *D3Rat108* (3q23) for case PC5. The mean frequency of LOH/AI on chromosome 3 was 13%.

Rat chromosome 11 was analysed using 4 microsatellite markers with an average spacing 22 Mb (Appendix, Table 4.14). AI was detected at one microsatellite marker *D11Rat46GSF1* (11q23) for case PC16 with the frequency of LOH/AI of 8% (1/13 informative cases).

Two animals out of 20 (PC13 and PC20) showed AI at all 8 informative loci of chromosome 8, suggesting either complete loss of one copy of the chromosome or loss of a large genomic region (Appendix, Table 4.11). The average percent of LOH/AI frequency on chromosome 8 is 14% and varies from a minimum of 7% (1/14 informative cases) at the marker *D8Rat33* to a maximum of 29% (2/7 informative cases) at *D8Rat76* (Fig. 4.6).

**A**



**B**

Samples number	"Nontumor" DNA contamination (%)	% I.I. of Wky allele (mean± SD)	% I.I. of SD <sup>we</sup> allele (mean± SD)	LOH/AI (%) (mean± SD)
1	0	100	0	-
2	10	84.07 ± 0.01	15.93 ± 0.01	79.0 ± 0.01
3	20	76.57 ± 1.89	23.43 ± 1.89	66.5 ± 3.54
4	40	64.01 ± 4.60	35.99 ± 4.60	37.5 ± 6.36
5	50	51.71 ± 2.47	48.29 ± 2.47	7.0 ± 4.24
6	60	44.04 ± 0.30	55.96 ± 0.30	40.0 ± 1.41
7	80	24.41 ± 0.01	75.59 ± 0.01	71.0 ± 0.01
8	100	0	100	-

**Fig. 4.5** Test for sensitivity of allelotyping. Microsatellite marker *D15Rat16*. (A) 3% agarose gel electrophoresis of PCR products of DNA mixed samples with different percent of "nontumor" DNA contamination. Samples homozygous for Wky and SD<sup>we</sup> alleles are mixed in different ratios (Table 4.25). Samples 9-10 are amplified normal DNA from heterozygous Wky/ SD<sup>we</sup> animals. (B) LOH/AI analysis of DNA mixed samples. The percent of I.I. of different alleles was calculated for each sample by Bio Image Intelligent Quantifier. The values of I.I. are the mean of two independent experiments ± SD. LOH/AI of the mixed samples was estimated using a formula for calculation of LOH/AI (Section Materials and Methods, 3.4.4) in comparison with samples 9-10 (A), representing a normal tissue. Allelic ratio for normal samples is equal to 1.1.

Abbreviations: M, molecular weight marker IX; NC, negative control; % I.I., percent of integral intensity of allele, used for evaluation of LOH/AI.

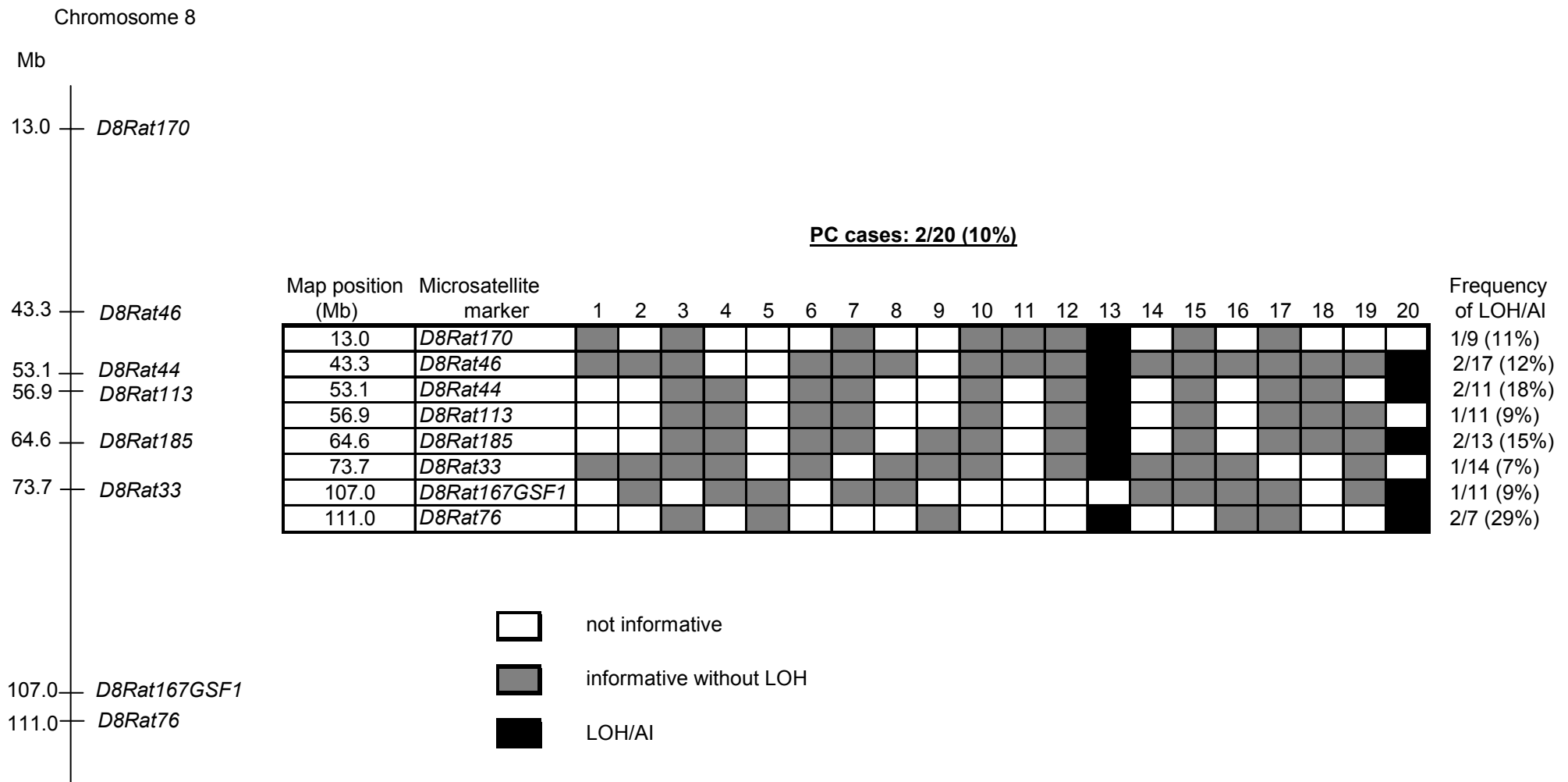


**Figure 4.6** LOH/AI analysis for markers on rat chromosome 8 of 20 MENX-PCs. For every locus, the frequency of LOH/AI positive cases is indicated by number of LOH/AI positive cases/number of informative cases. Allelic imbalance was detected in 2 of 20 cases with PCs. Abbreviations: PC, pheochromocytoma; LOH, loss of heterozygosity; AI, allelic imbalance.



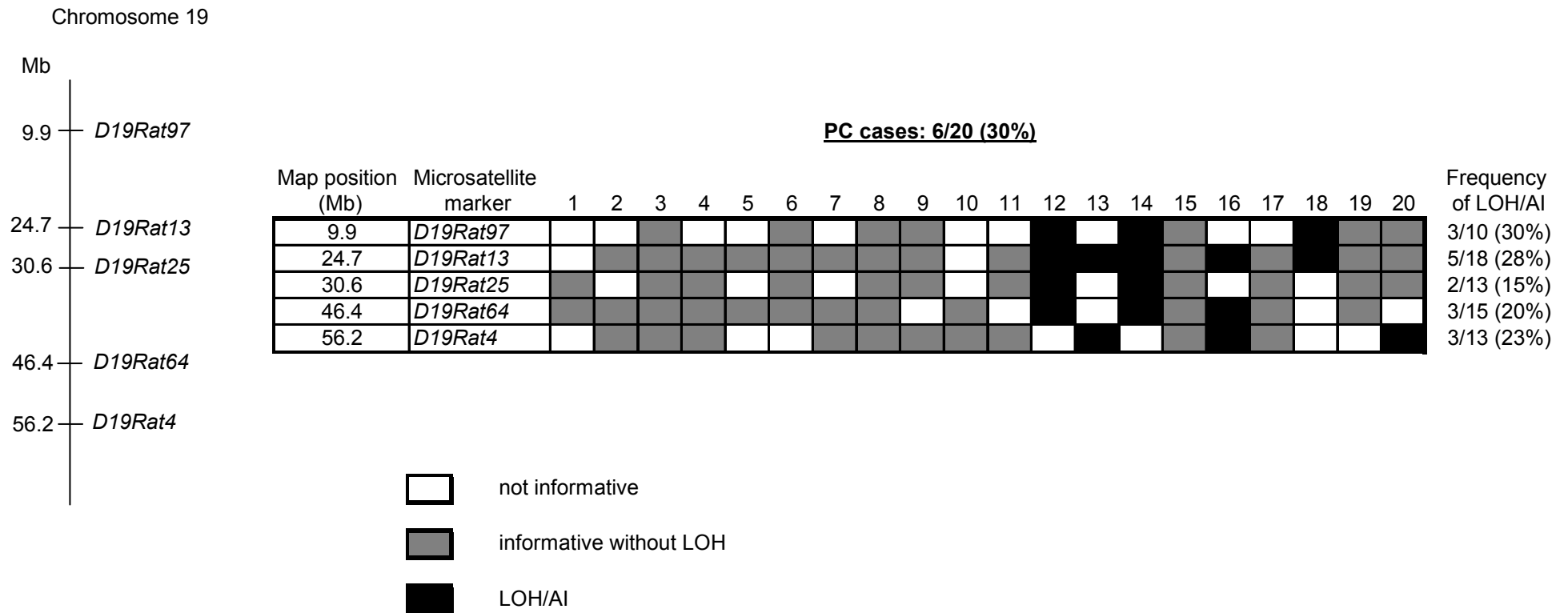


**Figure 4.7** LOH/AI analysis for markers on rat chromosome 19 of 20 MENX-PCs. For every locus, the frequency of LOH/AI positive cases is indicated by number of LOH/AI positive cases/number of informative cases. Allelic imbalance was detected in 6 of 20 cases with PCs. Abbreviations: PC, pheochromocytoma; LOH, loss of heterozygosity; AI, allelic imbalance.

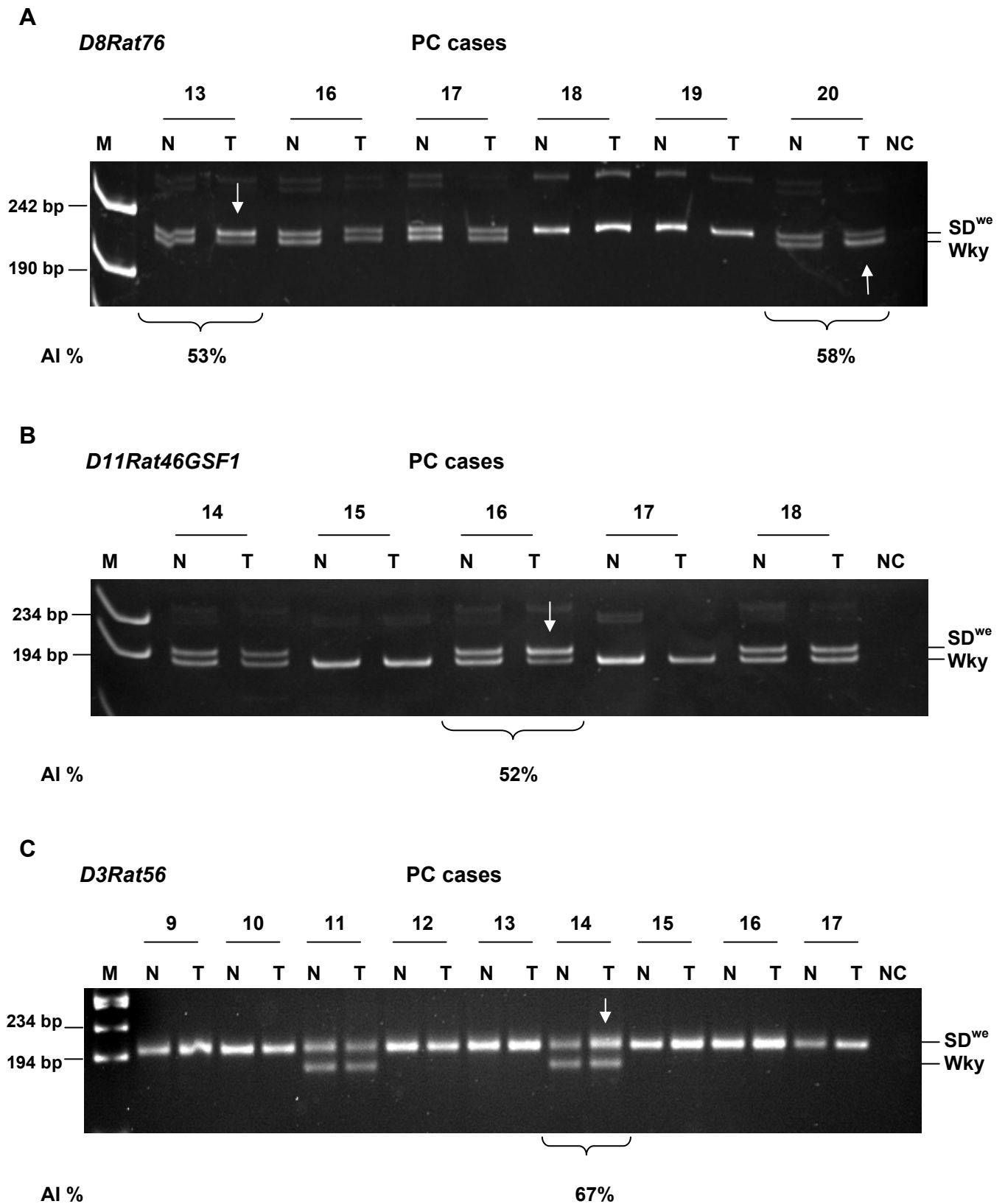


**Fig. 4.8** Amplification of microsatellite markers *D8Rat76*, *D11Rat46GSF1*, *D3Rat56* in a subset of PC samples. PCR products were resolved on 10% polyacrylamide gel (A, B) or on 3% agarose gel (C). Gels were stained with ethidium bromide and band intensities were quantified using Bio Image Intelligent Quantifier. Cases of allelic imbalance are indicated with arrows. For each case of allelic imbalance the value of allelic ratio for paired normal-tumor DNA samples is shown (in percent).

Abbreviations: M, molecular weight marker VIII (A), IX (B, C); NC, negative control; AI, allelic imbalance; N, normal DNA sample; T, tumor DNA sample; PC cases, pheochromocytoma cases.

AI was observed for the whole of chromosome 19 in 5 tumors (PC12, PC13, PC14, PC16, PC18). For PC20 AI was only detected at marker *D19Rat4* on the distal part of the chromosome (Appendix, Table 4.22). The rest of the informative markers show retention of heterozygosity in PC20. The mean frequency of LOH/AI on chromosome 19 was 23%, ranging from a minimum of 15% (2/13 informative cases) at the marker *D19Rat25* to a maximum of 30% (3/10 informative cases) at the most proximal marker *D19Rat97* (Fig. 4.7). The distribution of AI regions on chromosome 19 indicates the presence of a large deletion or loss of one copy of the chromosome for PC12, PC13, PC14, PC16 and PC18 cases. Deletion of the terminal part of the chromosome 19 is indicated for PC20.

Results of genome-wide LOH/AI screening with LOH/AI data at each informative marker for all analysed rat chromosomes are shown in Appendix, Tables 4.4 – 4.24. AI patterns for rat chromosomes 3, 8, 11 are given in Fig. 4.8.

To confirm the presence of AI detected with gel-based microsatellite analysis fragment analysis has been performed for PC cases having AI and for few PC cases without AI. To estimate the degree of correlation of data received after these two methods correlation analysis has been done (Table 4.26). Correlation analysis revealed a strong correlation between the two sets of data (R= 0.98).

#### **4.2.4. LOH/AI analysis for genes predisposing to PC development**

The rat homologs of human genes predisposing to PC development (*Ret*, *Vhl*, *Nf1*, *Sdhd*, *Sdhb\_predicted*) and some known tumor suppressor genes (*Men1*, *Cdkn2b*, *Cdkn2a*, *Cdkn2c*, *Tp53*, *Rb1*) were analyzed for the presence of LOH/AI. The list of genes used for LOH/AI is shown in the table 4.27. For the *Pten* gene the intragenic marker *RND1Lev1* was used and neither LOH nor AI was detected. Flanking microsatellite markers have been used for genes *Men1*, *Cdkn2b*, *Cdkn2a*, *Cdkn2c*, *Ptprf*, *Sdhb\_predicted*, *Tp53*, *Nf1*, *Rb1* and no LOH/AI was identified either in upstream or downstream of these genes. The genes *Sdhd* and *Rassf1* are located within a region of AI on rat chromosome 8.

The schematic representation of the results of LOH/AI for microsatellite markers and candidate genes is illustrated in Fig. 4.9.

**Table 4.26** Correlation between microsatellite analysis and microsatellite fragment analysis

Marker name	Sample number	LOH/AI (%)	
		Microsatellite analysis	Fragment analysis
<i>chromosome 8</i>			
<i>D8Rat44</i>	<b>PC13</b>	61	51
	PC15	12	12
	PC18	7	7
<i>D8Rat185</i>	<b>PC20</b>	49	54
	<b>PC13</b>	50	53
	PC15	14	9
	PC18	20	8
<i>D8Rat46</i>	<b>PC20</b>	54	54
	<b>PC13</b>	52	49
	PC15	2	7
	PC18	1	1
<i>D8Rat76</i>	<b>PC20</b>	64	51
	<b>PC13</b>	53	61
	PC16	3	2
	PC17	5	2
	<b>PC20</b>	58	46
<i>chromosome 19</i>			
<i>D19Rat25</i>	PC8	9	1
	PC9	2	10
	PC11	43	47
	<b>PC12</b>	35	48
	<b>PC14</b>	57	64
<i>D19Rat64</i>	PC3	4	4
	<b>PC12</b>	54	54
	<b>PC14</b>	51	50
	<b>PC16</b>	46	50
<i>D19Rat97</i>	PC9	6	0
	<b>PC12</b>	61	61
	<b>PC14</b>	50	50
	<b>PC18</b>	53	58
<i>D19Rat4</i>	PC8	0	4
	PC9	2	20
	PC10	37	41
	PC11	38	39
	<b>PC13</b>	60	53
	<b>PC16</b>	50	50
	<b>PC20</b>	56	57

Cases in bold show an allelic imbalance. For all PC cases microsatellite analysis and fragment analysis has been performed using the same set of primers specific for tested microsatellite markers. In case of fragment analysis 5'-FAM modified Fw primers were used while Rev primers were unlabelled. The coefficient of correlation  $R = 0.98$  what indicates a strong correlation between data received with these two methods.

**Table 4.27** Rat homologs of genes predisposing to PC development.

Gene name (RGD symbol)	Gene description (Ensembl, RGD)	Genomic location	Microsatellite markers	Marker name
<i>Men1</i> *	multiple endocrine neoplasia 1	1q43	flanking	<i>D1Rat112</i> , <i>D1Rat74</i>
<i>Pten</i> <sup>†</sup>	phosphatase and tensin homolog	1q52	intragenic	<i>RND1Lev1</i>
<i>Vhl</i>	von Hippel-Lindau syndrome homolog	4q41.3 - 4q42.1	not suitable	–
<i>Ret</i>	ret proto-oncogene	4q42	not suitable	–
<i>Cdkn1b</i> ( <i>p27</i> )	cyclin-dependent kinase inhibitor 1B	4q43	not suitable	–
<i>Cdkn2b</i> ( <i>p15</i> )*	cyclin-dependent kinase inhibitor 2B	5q32	flanking	<i>D5Rat152</i> , <i>D5Rat71</i>
<i>Cdkn2a</i> ( <i>p16</i> )*	cyclin-dependent kinase inhibitor 2A	5q32	flanking	<i>D5Rat152</i> , <i>D5Rat71</i>
<i>Cdkn2c</i> ( <i>p18</i> )*	cyclin-dependent kinase inhibitor 2C	5q35	flanking	<i>D5Rat95</i> , <i>D5Rat79</i>
<i>Ptprf</i> *	protein tyrosine phosphatase, receptor type, F	5q36	flanking	<i>D5Rat95</i> , <i>D5Rat79</i>
<i>Sdhd</i> _predicted*	succinate dehydrogenase complex, subunit B, iron sulfur (lp) (predicted)	5q36	flanking	<i>D5Rat79</i> , <i>D5Rat47</i>
<i>Sdhd</i> <sup>‡</sup>	succinate dehydrogenase complex, subunit D, integral membrane protein	8q23	flanking	<i>D8Rat44</i> , <i>D8Rat113</i>
<i>Rassf1</i> ( <i>Rassf1a</i> ) <sup>‡</sup>	Ras association (RalGDS/AF-6) domain family 1	8q32	flanking	<i>D8Rat76</i>
<i>Tp53</i> *	tumor protein p53	10q24	flanking	<i>D10Rat116</i> , <i>D10Mit2</i>
<i>Nf1</i> *	neurofibromatosis 1	10q25	flanking	<i>D10Mit2</i> , <i>D10Arb27</i>
<i>Rb1</i> *	retinoblastoma 1	15q12	flanking	<i>D15Rat16</i> , <i>D15Rat133</i>

\*Genes have been analyzed using flanking microsatellite markers and neither allelic imbalance nor LOH were detected in the upstream and downstream regions of analysed genes.

<sup>†</sup>For the *Pten* gene the intragenic marker *RND1Lev1* has been used and LOH/AI was not identified.

<sup>‡</sup>*Sdhd* and *Rassf1* genes are in regions of allelic imbalance.

For genes without any symbol there is no information about the presence of LOH/AI on few reasons: a) most of the tested microsatellite markers were not informative (homozygous); b) informative microsatellite markers were not used for LOH/AI study because of a low heterozygous rate (only 1-3 animals out of 20 MENX-affected rats were informative (heterozygous) for these markers).

For gene information Ensembl Genome Browser ([http://www.ensembl.org/Rattus\\_norvegicus/geneview](http://www.ensembl.org/Rattus_norvegicus/geneview)) and RGD (Rat Genome Database) ([http://rgd.mcw.edu/tools/genes/genes\\_view.cgi](http://rgd.mcw.edu/tools/genes/genes_view.cgi)) were used.

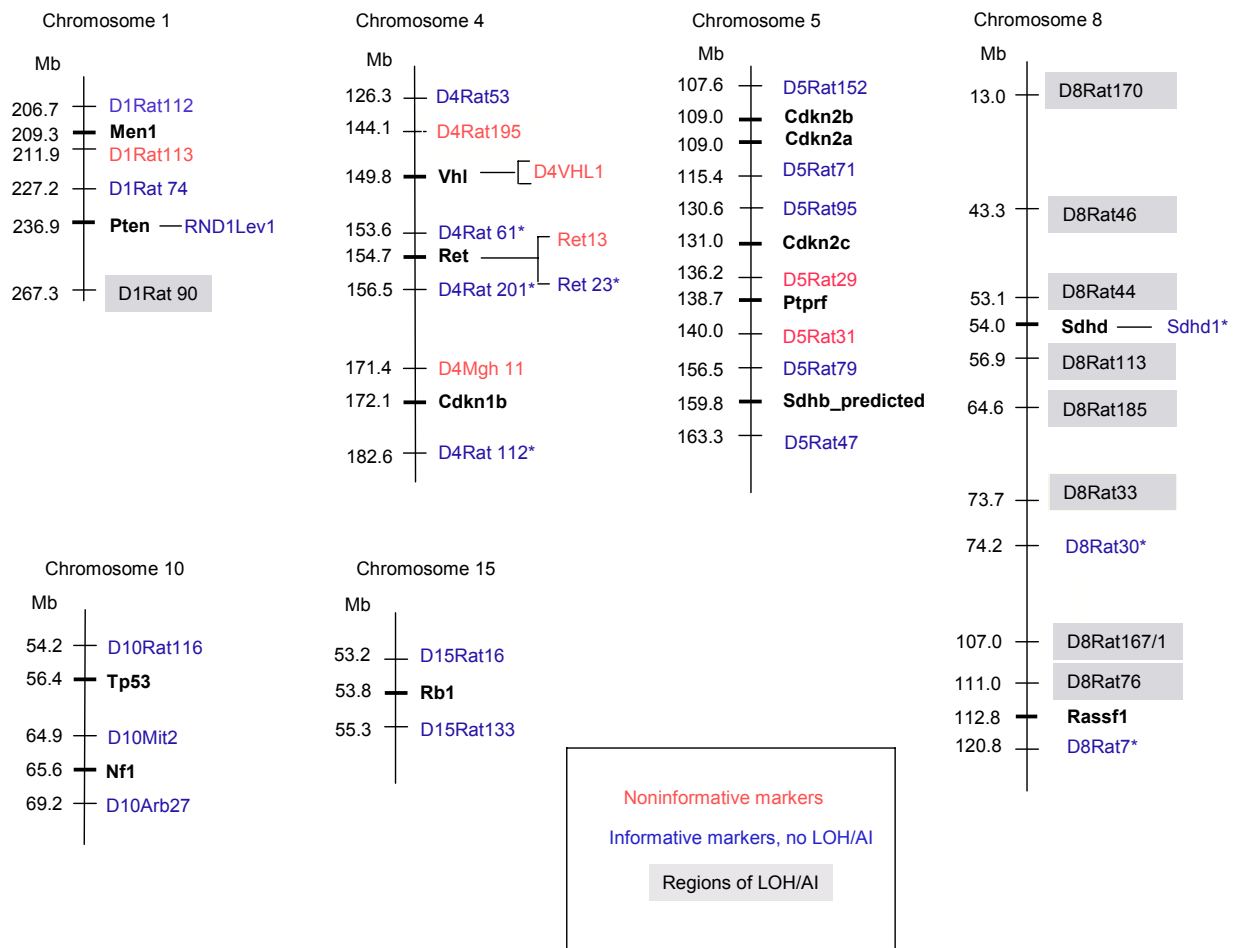


**Fig. 4.9** Schematic presentation of LOH/AI analysis of rat homologs of human genes predisposing to PC development and some tumor suppressor genes. Only fragments of the rat relevant chromosomes, containing genes of interest, are illustrated, except for Chr 8 where all markers are depicted.

\*Microsatellite markers were not used for LOH/AI analysis because of the low frequency of heterozygosity at this site (Appendix, Table 4.3)

Abbreviations: LOH, loss of heterozygosity; AI, allelic imbalance.

### 4.3. Quantification of mRNA level of *Cdkn2a*, *Cdkn2c*, *Sctr*, *Sdhd* and *Rassf1* genes in MENX-affected rats.

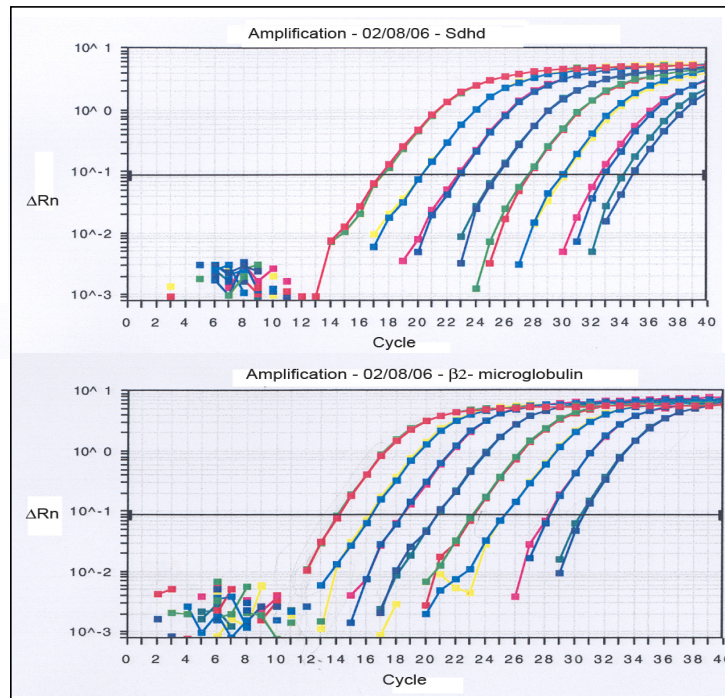
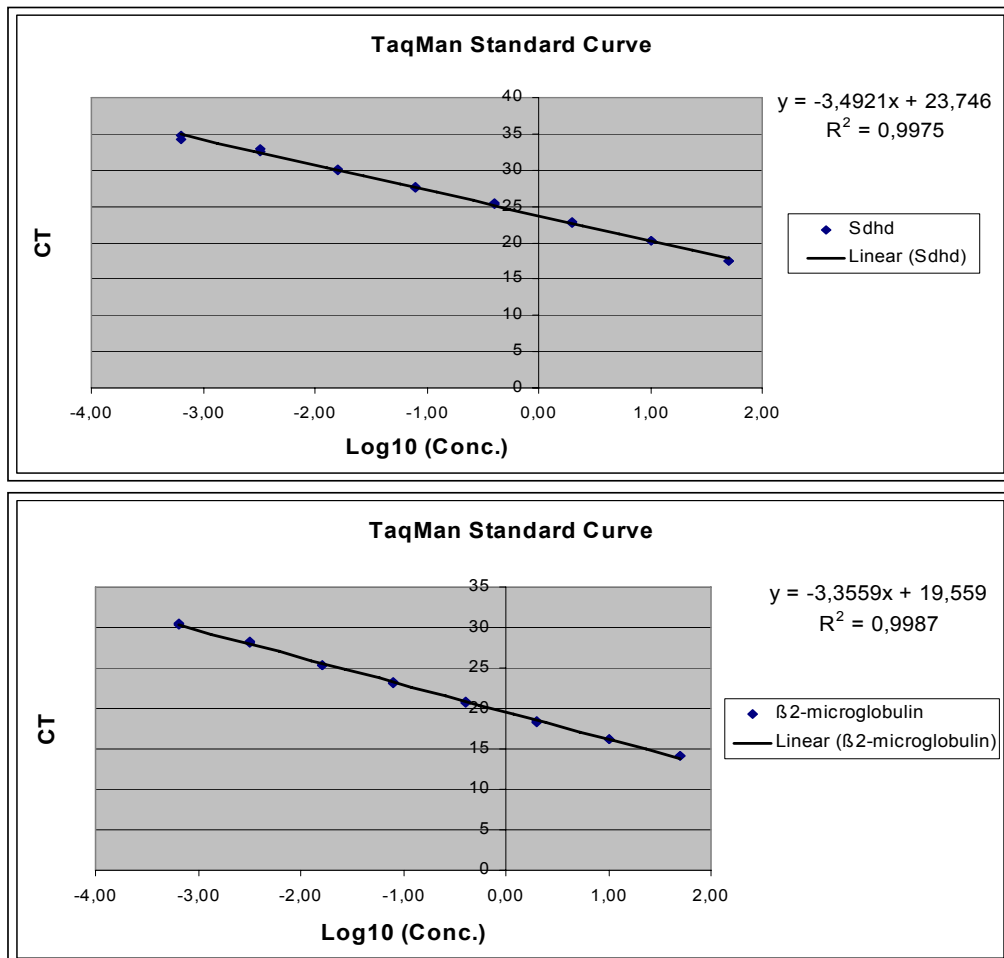
Dr. Pellegata (Institute of Pathology, GSF) has analyzed a few cases of adrenal gland medullary hyperplasia from MENX-affected animals with microarray expression analysis chips from Affymetrix and found significant upregulation of *Cdkn2a*, *Cdkn2c*, *Sctr* genes in samples with hyperplasia compared to normal adrenal medulla samples (unpublished observation).

LOH/AI screening of the rat genome has revealed AI regions on the rat chromosome 8: 2 out of 20 analysed MENX-rats (10%) show an AI at all informative microsatellite markers distributed over the chromosome 8, suggesting the presence of a large deletion (Fig. 4.6). *Sdhd* is located on the long arm of chromosome 8 (8q23 locus). The *Rassf1* gene is located in the chromosomal segment of 8q32.

Basing on these data we conducted an analysis of the mRNA level of *Cdkn2a*, *Cdkn2c*, *Sctr*, *Sdhd* and *Rassf1* genes in PCs using quantitative Real-Time (TaqMan) PCR assay.

#### 4.3.1. Validation of standard curves

Real-time PCR-based standard curves for *Cdkn2a*, *Cdkn2c*, *Sctr*, *Sdhd* and *Rassf1* target genes and for the endogenous control gene  $\beta$ 2-microglobulin (housekeeping gene) were constructed using calibrator RNA extracted from normal rat brain and serially diluted five-fold (50, 10, 2, 0.4, 0.08, 0.016, 0.0032, 0.00064 ng of rat brain genomic RNA). Figure 4.10A shows amplification plots for *Sdhd* and  $\beta$ 2-microglobulin genes. For each reaction, the value of the fluorescence emission intensity of the reporter dye (FAM) is divided by the value of the fluorescence emission intensity of the passive reference dye (ROX) to obtain a ratio defined as the normalised reporter signal ( $R_n$ ).  $\Delta R_n$  represents the  $R_n$  minus the baseline signal. In figure 4.10A cycle number reported on the X-axis is plotted versus the logarithm of change in the normalised reporter signal ( $\Delta R_n$ ). Standard curves for the *Sdhd* and  $\beta$ 2-microglobulin genes were generated by plotting the CT value for each calibration point against the logarithm base 10 of calibrator DNA concentration ( $\log_{10}(\text{Conc.})$ ) (Fig. 4.10B). The threshold cycle (CT) represents the fractional cycle number at which a significant increase in  $R_n$  above a selected threshold (horizontal black line on the amplification plot (Fig. 4.10A)) can be first detected. Data for standard curves were obtained from two replicates for each dilution. For quantification of relative amount of mRNA level of the target genes values of linear and absolute coefficients have been used (Methods, 3.6.2). The linear coefficient is equal to the mean slope of the standard curve. The mean slopes of the standard curves for the two genes are  $-3.4921$  for the *Sdhd* gene

**A****B**

**Fig. 4.10** Amplification plots of Real-Time detection of the *Sdh* gene and the β2-microglobulin gene by TaqMan reaction with a variable starting DNA amount (A) and the calibration curves for *Sdh* and β2-microglobulin (B). (A) Amplification plots with a starting concentration of 50, 10, 2, 0.4, 0.08, 0.016, 0.0032, 0.00064 ng of rat brain genomic DNA (calibrator) for each gene. (B) The standard (calibration) curves for each gene were generated by plotting the value CT vs. the logarithm base 10 of calibrator concentration (log<sub>10</sub> (Conc)).



and -3.3559 for the  $\beta$ 2-microglobulin gene. The absolute coefficients are 23.746 for *Sdhd* and 19.559 for  $\beta$ 2-microglobulin. The correlation coefficients of curve fitting were  $R^2 = 0.9975$  and  $R^2 = 0.9987$ , respectively.

#### **4.3.2. mRNA expression level of *Cdkn2a*, *Cdkn2c*, *Sctr* genes in adrenal glands with PC**

Total RNA was extracted from the 13 frozen PCs: PC3, PC4, PC6, PC7, PC12, PC13, PC14, PC15, PC16, PC17, PC18, PC19, and PC20. For adrenal glands of unaffected animals (control group) microdissection was performed to specifically select adrenal medullary cells and eliminate the adrenal cortical cells, not involved in PC development. Three littermates having two normal *Cdkn1b* alleles were selected as the control group. TaqMan assays have been done according to the standard protocol (Methods, 3.6). Real-Time RT-PCR results showed a significant increase of the mRNA level of *Cdkn2a*, *Cdkn2c*, and *Sctr* in the analysed PC samples compared to the control group of wild-type animals (Fig. 4.11, 4.12 and 4.13, respectively). *Sctr* and *Cdkn2a* mRNA levels in tumor samples are dramatically increased relative to the controls, being 29 and 44- fold higher (MENX-PCs values) than in normal adrenal medulla samples, respectively. In PCs there was significantly more *Cdkn2c* mRNA than in wild-type animals: the mean expression of *Cdkn2c* in MENX-associated PCs (MENX-PCs value) was 3 times higher than in adrenal medullary tissue from normal rats. For comparison of mRNA level between the control group and the PC samples the two-sided t-test was used.

#### **4.3.3. mRNA expression level of *Sdhd*, *Rassf1* genes in adrenal glands with PC**

RNA was extracted from 15 tumor samples: PC3, PC4, PC6, PC7, PC9, PC11, PC12, PC13, PC14, PC15, PC16, PC17, PC18, PC19, and PC20. Adrenal glands of wild-type animals without mutation in the *Cdkn1b* gene have been microdissected to extract RNA only from the medullary part of adrenal gland (control). Control group consisted of 4 unaffected animals. At the mRNA level *Sdhd* and *Rassf1* were expressed at comparable level in tumor and normal adrenal tissues (Fig. 4.14 and 4.15). AI observed in PC13 and PC20 cases for all informative microsatellite markers (Fig.4.6) has no effect on mRNA level of *Sdhd*, *Rassf1* genes.

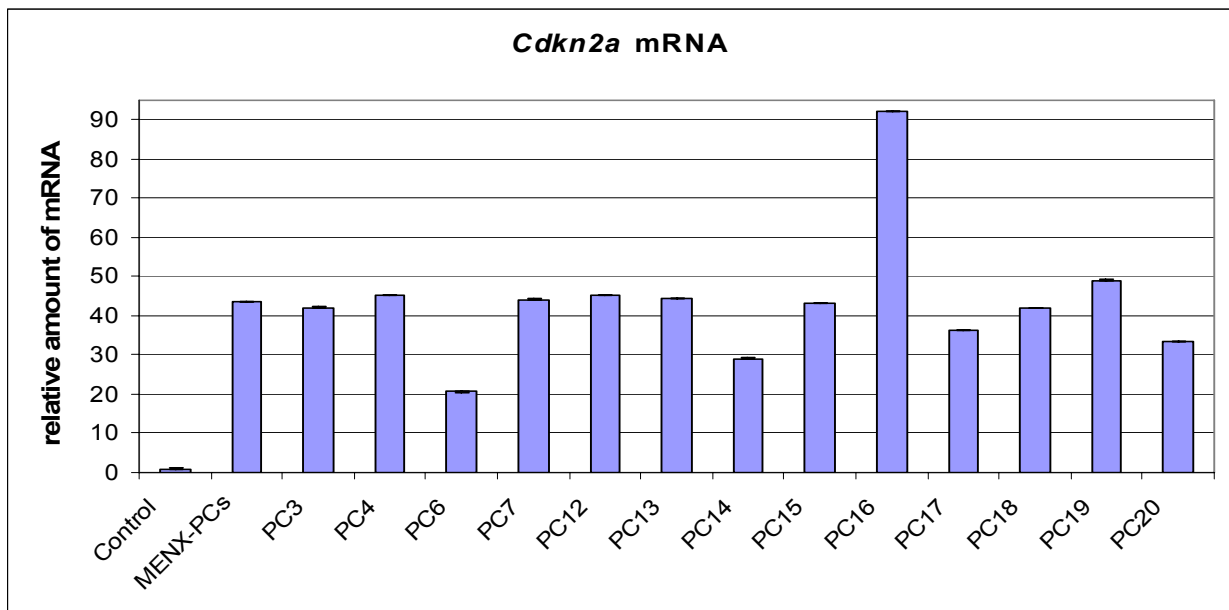


**Fig. 4.11** Real-time RT-PCR to determine the level of expression of *Cdkn2a* in adrenal glands of MENX-affected and control rats. The average level of *Cdkn2a* mRNA in normal medullary tissue of adrenal glands of wild-type animals (n = 3) is arbitrarily set at 1 (control). The level of *Cdkn2a* mRNA in PC samples is normalized against the averaged value of relative amount of *Cdkn2a* mRNA in normal adrenal medulla samples. Values are the mean of two experiments  $\pm$  standard deviation. Standard deviation of MENX-PCs, PC4, PC12, PC13, PC15, PC16, PC17, PC18, PC20 samples is  $\leq 0.04$  and not visible. The value of MENX-PCs corresponds to the mean value of *Cdkn2a* mRNA level in all analysed PC samples. There is significantly more *Cdkn2a* mRNA in PCs than in normal adrenal medulla tissues (P = 0.001; P<0.05; two-sided t-test).

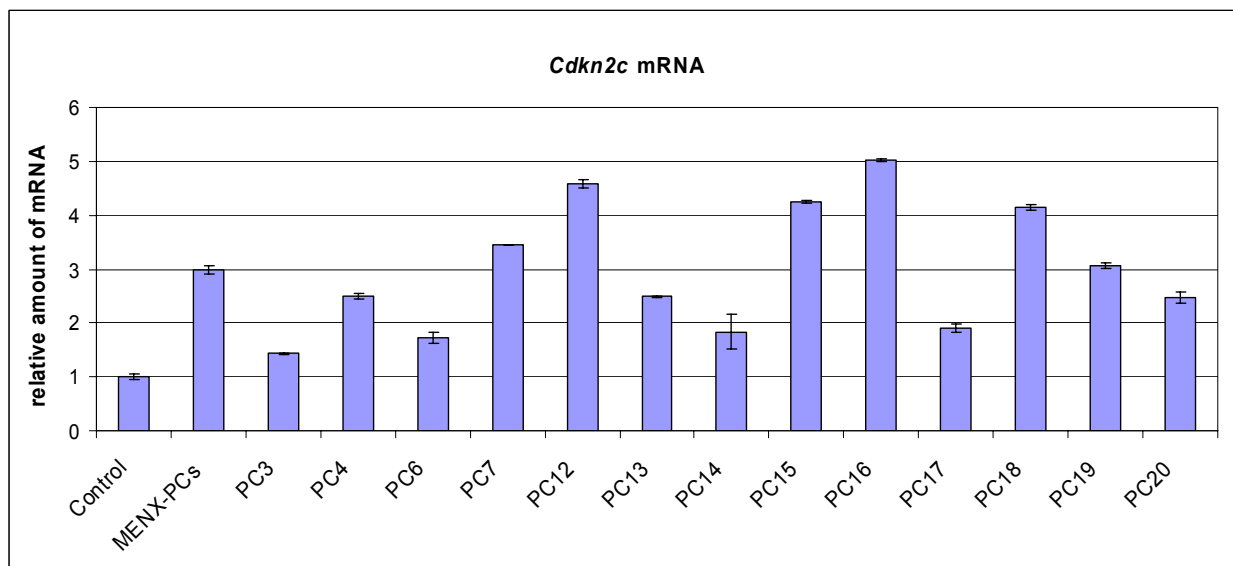


**Fig. 4.12** Real-time RT-PCR to determine the level of expression of *Cdkn2c* in adrenal glands of MENX-affected and control rats. The average level of *Cdkn2c* mRNA in normal medullary tissue of adrenal glands of wild-type animals (n = 3) is arbitrarily set at 1. The level of *Cdkn2c* mRNA in PC samples is normalized against the averaged value of relative amount of *Cdkn2c* mRNA in normal adrenal medulla samples. Values are the mean of two experiments  $\pm$  standard deviation. Standard deviation of PC7 is equal to 0. The value of MENX-PCs corresponds to the mean value of *Cdkn2c* mRNA level in all analysed PC samples. There is significantly more *Cdkn2c* mRNA in PCs than in normal adrenal medulla tissues (P = 0.01; P<0.05; two-sided t-test).

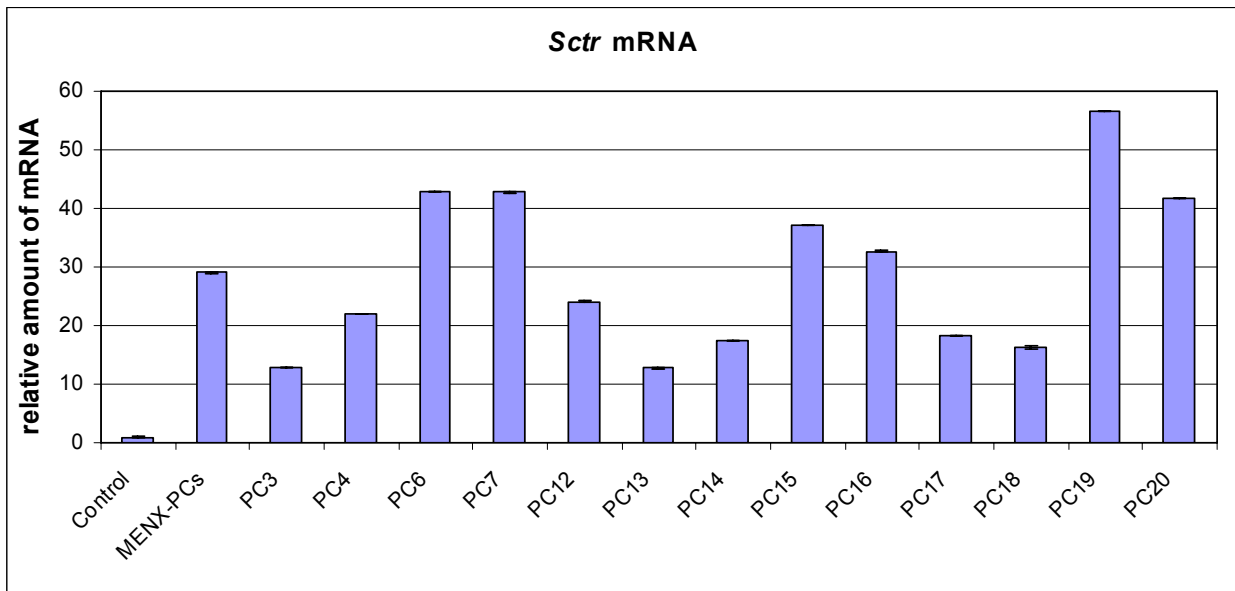


**Fig. 4.13** Real-time RT-PCR to determine the level of expression of *Sctr* in adrenal glands of MENX-affected and control rats. The average level of *Sctr* mRNA in normal medullary tissue of adrenal glands of wild-type animals (n = 3) is arbitrarily set at 1 (control). The level of *Sctr* mRNA in PC samples is normalized against the averaged value of relative amount of *Sctr* mRNA in normal adrenal medulla samples. Values are the mean of two experiments  $\pm$  standard deviation. Standard deviation of PC3, PC4, PC6, PC14, PC15, PC17, PC19, PC20 samples is  $\leq 0.035$  and not visible. The value of MENX-PCs corresponds to the mean value of *Sctr* mRNA level in all analysed PC samples There is significantly more *Sctr* mRNA in PCs than in normal adrenal medulla tissues (P = 0.006; P<0.05; two-sided t-test).

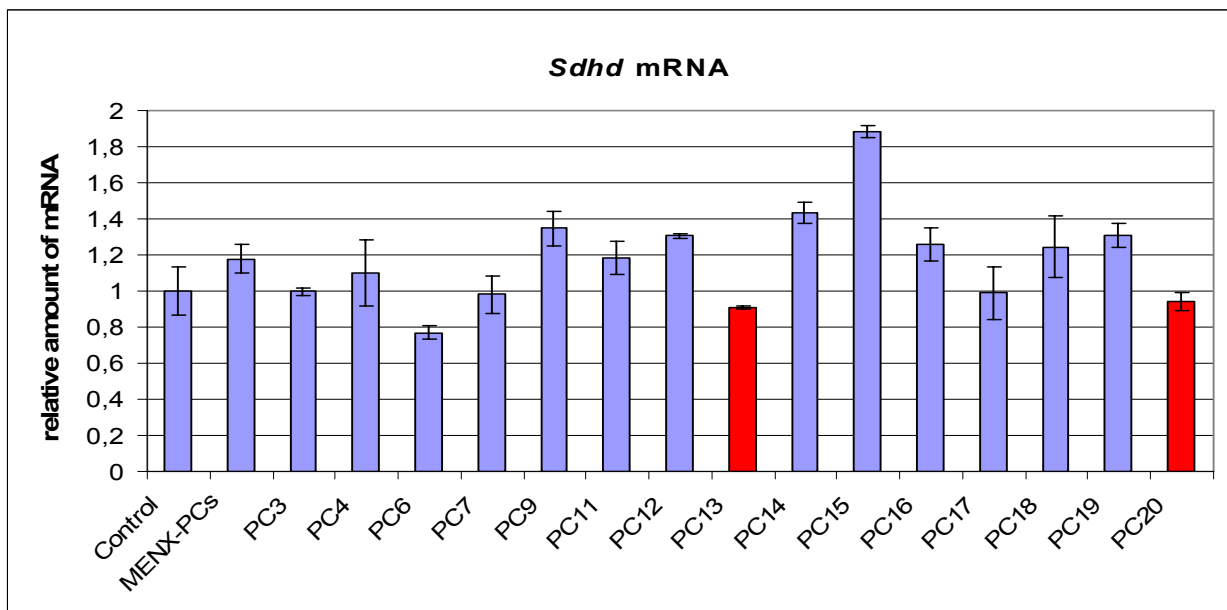


**Fig. 4.14** Real-time RT-PCR to determine the level of expression of *Sdhd* in adrenal glands of MENX-affected and control rats. The average level of *Sdhd* mRNA in normal medullary tissue of adrenal glands of wild-type animals (n = 4) is arbitrarily set at 1 (control). The level of *Sdhd* mRNA in PC samples is normalized against the averaged value of relative amount of *Sdhd* mRNA in normal adrenal medulla samples. Values are the mean of two experiments  $\pm$  standard deviation. The value of MENX-PCs corresponds to the mean value of *Sdhd* mRNA level in all analysed PC samples There is no significant difference in relative amount of mRNA between the analysed PC cases and the control group (P = 0.33; P>0.05; two-sided t-test). Cases PC13 and PC20 marked in red have both an allelic imbalance on chromosomes 8 (where *Sdhd* maps to 8q23) and 19.

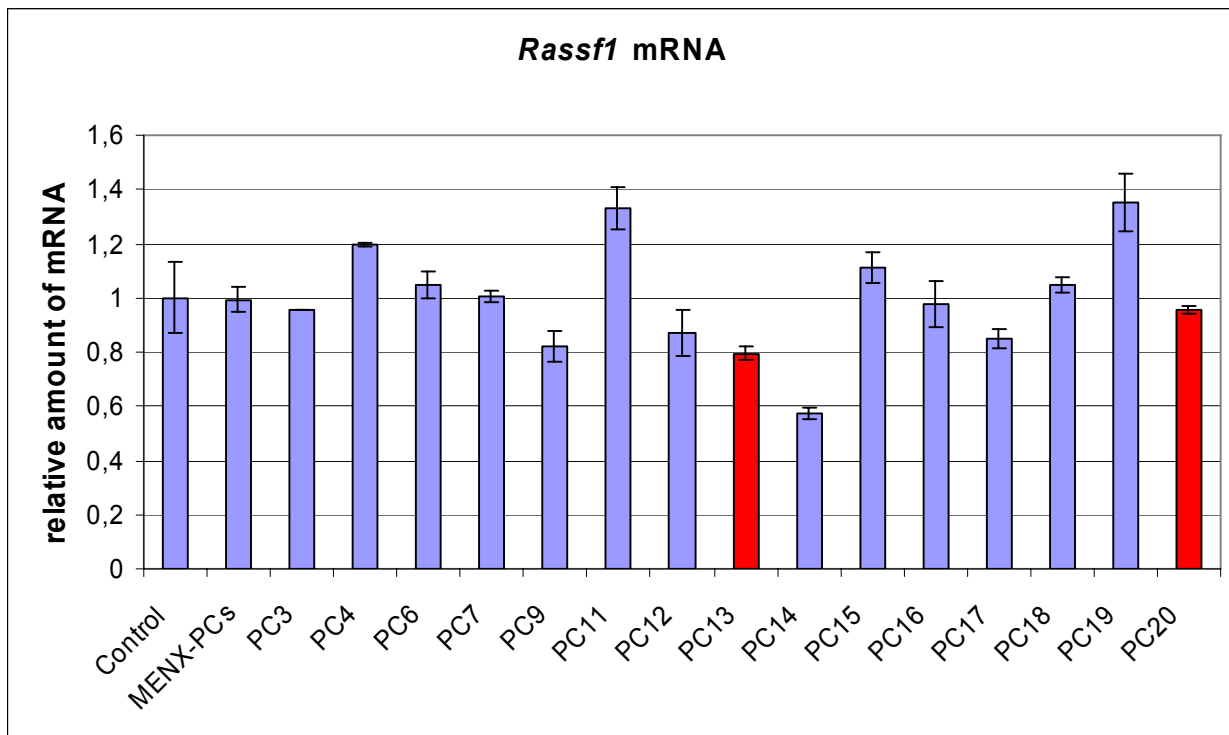


**Fig. 4.15** Real-time RT-PCR to determine the level of expression of *Rassf1* in adrenal glands of MENX-affected and control rats. The average level of *Rassf1* mRNA in normal medullary tissue of adrenal glands of wild-type animals (n = 4) is arbitrarily set at 1. The level of *Rassf1* mRNA in PC samples is normalized against the averaged value of relative amount of *Rassf1* mRNA in normal adrenal medulla samples. Values are the mean of two experiments  $\pm$  standard deviation. The value of MENX-PCs corresponds to the mean value of *Rassf1* mRNA level in all analysed PC samples. There is no significant difference in relative amount of mRNA between the analysed PC cases and the control group ( $P = 0.79$ ;  $P > 0.05$ ; two-sided t-test). Standard deviation of the PC3 case is equal to 0. Cases PC13 and PC20 marked in red have both an allelic imbalance on chromosomes 8 (where *Rassf1* maps to 8q32) and 19.

#### 4.4. *Sdhd* and *Rassf1* sequence analysis

As previously shown, we did not observe differences in mRNA levels for *Sdhd* and *Rassf1* in PCs compared to normal adrenal tissue. However, LOH/AI screening of the rat genome has revealed AI regions distributed over the whole chromosome 8 for 2 out of 20 MENX PCs (PC13 and PC20) (Fig. 4.6). Both genes *Sdhd* and *Rassf1* are in the regions of AI (Fig.4.9). In humans *SDHD* and *RASSF1* genes have been showed involved in PC development by different mechanisms (Introduction, 1.2.4, and 1.4.2). Hypermethylation of the CpG island in the promoter region of *RASSF1A* (isoform A of the *RASSF1* gene) is often detected in sporadic (Astuti *et al.*, 2001c; Dammann *et al.*, 2005) and MEN2-associated PCs (Dammann *et al.*, 2005) in humans. Germline heterozygous mutations (truncating and missense mutations) in the *SDHD* gene have been found in PCs (Gimenez-Roqueplo *et al.*, 2001; Cascon *et al.*, 2002; Eng *et al.*, 2003; Novosel *et al.*, 2004). Somatic mutations of the *SDHD* gene have been identified in

**Table 4.28** Summary of primers sequences, annealing temperatures, and PCR product sizes used for sequencing of *Sdhd* and *Rassf1* genes

Gene	Exon number (Ensembl, NCBI) 5' upstream region	Name of primers (Fw, Rev)	Sequence of primers (5' - 3')	Product size (bp)	Ta (°C)
<i>Sdhd</i>	ENSRNOE00000249089	Sdhd1ex Fw Sdhd1ex Rev	AGCCCTCACTCCTTCCTTTC CTTCGCCGTTCTTTACTCG	204	56
	ENSRNOE00000249067	Sdhd2ex Fw Sdhd2ex Rev	AGGAATGCAAAGGCACAGAC CACGTGGTGCACAGACATAC	355	56
	ENSRNOE00000249056	Sdhd3ex Fw Sdhd3ex Rev	CCAGATTTATTTGGCCACTG CTACCGTTCTGATGGTTCTGG	371	54
	ENSRNOE00000305758	Sdhd4ex Fw Sdhd4ex Rev	AAGACATTCTGCCACCAAC GGGGTGTGAGTGGGTACTTAAC	350	56
	<i>Rassf1</i>	ENSRNOE00000258785	Rassf1ex Fw Rassf1ex Rev	CTCGCCCCGTACGAACTC CTATGGTGCTGCCTTTGACC	369
ENSRNOE00000339240		Rassf2ex Fw Rassf2ex Rev	GTGTCCAGAGGTGCCTAACC GCCGAGAAATCGATAATTGG	381	55
ENSRNOE00000258766		Rassf3ex Fw Rassf3ex Rev	GCGTACTGACACGCTCACAC TGCCCACTCAACTACTCTCC	333	59
ENSRNOE00000258760		Rassf4ex Fw* Rassf4ex Rev	CAAGTTCCAAGCCAGACCAC AATACGTGGCTCGGACTCTC	294	59
ENSRNOE00000258750		Rassf_5a Fw Rassf_5a Rev Rassf_5b Fw Rassf_5b Rev	CAGCCTACCTCAGCCATCTC AGGGCCTCAATGACCTCAC AGCAAGAAACCGCCTTCC CTCAGCCCCTTAGTGACAG	290 297	58 55
ENSRNOE00000258738		Rassf6ex Fw Rassf6ex Rev	CTGTGCACTAAGGGGCTGAG GCCTCTAGGCCAGTTTCTCC	293	62
ENSRNOE00000258727		Rassf7ex Fw Rassf7ex Rev	GGAGGCCCTATCCTGCTTAC ATCAGAGGAGGACCTTCACG	371	59

Primers for sequencing *Sdhd* and *Rassf1* genes were designed using [www.frodo.wi.mit.edu](http://www.frodo.wi.mit.edu).

\*Rassf4exFw primer can not be used for sequencing of ENSRNOE00000258760 exon of *Rassf1* gene although with the pair of primers Rassf4exFw/Rev this exon can be easily amplified. The sequence of this exon was analysed only using Rassf4exRev primer.

For sequence analysis Ensembl Genome Browser was used ([www.ensembl.org/Rattus\\_norvegicus/exon-view](http://www.ensembl.org/Rattus_norvegicus/exon-view)).

Abbreviations: Fw, forward primer; Rev, reverse primer; Ta, annealing temperature

sporadic PCs (Gimm *et al.*, 2000). Therefore, *Sdhd* and *Rassfl* genes were screened for the presence of mutations in 20 PC samples (PC1 - PC20) of MENX affected animals. The control group included 4 DNA samples: 1) one sample of parental DNA from the inbred Wistar Kyoto (Wky) rat strain; 2) one DNA sample extracted from the ear take (normal tissue) of MENX-affected animal: case PC13 for sequencing of the *Sdhd* gene and case PC1 for the *Rassfl* gene; 3) DNA sample from Brown Norway rat strain; 4) DNA sample from Spontaneously Hypertensive rat strain. Primers were designed to cover the entire coding region of *Sdhd* and *Rassfl* genes (Table 4.28). After sequence analysis no mutations were detected for exons of *Sdhd* and *Rassfl* genes.

## 4.5. FISH analysis of AI regions on chromosomes 8 and 19

### 4.5.1. Verification and validation of the BAC clones as FISH probes, metaphase FISH analysis

To analyze regions of AI on chromosomes 8 and 19 in adrenal tissue sections fluorescence in situ hybridization (FISH) analysis was performed using BAC clones as probes.

BAC clones were selected that map to the area of AI on those two chromosomes (Table 4.29).

**Table 4.29** The probe set of BAC clones for chromosomes 8 and 19

Chromosome	Bac clone ID	Probe label	Specificity of the probe	Cytogenetic location
8	CH230-385B22	Dig	specific	8q22
	CH230-406J14	Bio	unspecific	-
19	CH230-398H16	Dig	specific	19q11
	CH230-110L11	Dig	specific	19q11
	CH230-89I12	Bio	specific	19q12
	CH230-388N4	Bio	specific	19q12

BAC clones were chosen using BES clone map of NCBI database ([www.ncbi.nlm.nih.gov/mapview/maps.cgi](http://www.ncbi.nlm.nih.gov/mapview/maps.cgi)).

Abbreviations: Dig, digoxigenin; Bio, biotin.

BAC clones were obtained from the CHORI center (BACPAC Resources) and grown in LB medium at recommended conditions (Materials and Methods, 3.8.1). To verify the BAC clones, primers specific for introns of genes predicted to map to the DNA insert of the BAC clones were designed (Table 4.30). PCR was performed at standard conditions used for amplification of

**Table 4.30** Summary of primer sequences, annealing temperatures, and PCR product sizes used for verification of BAC clones

Bac clone	Gene	Intron number (Ensembl, NCBI) 5' upstream sequence	Name of primers (Fw, Rev)	Sequence of primers (5'→ 3')	Product size (bp)	Ta (°C)
CH230-385B22	<i>Ttc12</i>	Intron 1-2	Ttc12 Fw Ttc 12 Rev	GGAGAACATTTCCTTCACATCC TTCAGGTCCTTCTGGCTTTTAG	500	56
CH230-406J14	<i>Impg1</i>	Intron 15-16	Impg1 Fw Impg1Rev	GCCACCATACCTGGTTCTAAAG TGGCTTCTGTAAGATAGCAAAAC	244	56
CH230-398H16	<i>Man2b1</i>	Intron 1-2	Man2b1Fw Man2b1Rev	CCTCCCTGTGACTCCAAGTG GACAGGTTTTCCAGCAGAGC	181	58
CH230-110L11	<i>DNase2</i>	Intron 5-6	DNase2Fw DNase2Rev	GGGGAGGCTCTCAAACAAG GGATCTCAGGTGGAGTCGAG	179	57
CH230-89I12	<i>Hsbp1</i>	Intron 2-3	Hsbp1Fw Hsbp1Rev	GACACAGCTGACTACCCAAGC CCAGTTTCATCCGGCTACAG	248	58
CH230-388N4	<i>Dpep1</i>	Intron 1-2	Dpep1Fw Dpep1Rev	AGGATGGACTGGAGGTGATG GGATGTCCTGGGTCACAGG	226	58

Introns of the genes were named according to the Ensembl database ([www.ensembl.org/Rattus\\_norvegicus/exonview](http://www.ensembl.org/Rattus_norvegicus/exonview)). Genes of DNA insert of above mentioned BAC clones were chosen randomly using Genes\_seq map of NCBI database ([www.ncbi.nlm.nih.gov/mapview/maps.cgi](http://www.ncbi.nlm.nih.gov/mapview/maps.cgi))

Abbreviations: Fw, forward primer; Rev, reverse primer; Ta, annealing temperature

microsatellite markers (Methods, 3.4.2) at 35 cycles using a single E.coli colony. Annealing temperature was adjusted for each set of primers. 10 µl of PCR product was resolved on 2% agarose gel. 10 different E.coli clones containing a DNA insert of interest were tested for each gene mentioned into the Table 4.30 (Fig. 4.16). The length of the PCR product corresponded to the predicted product size of DNA amplified with specific primers for introns of genes of different DNA inserts of BAC clones.

To validate the BAC probes we hybridized them to rat metaphase chromosomes. The appearance of two pairs of doublet signals at the same chromosomal location in a metaphase spread is the hallmark of a specific probe localization. Of the 2 probes tested for rat chromosome 8 only one of them, CH230-385B22, labelled with digoxigenin, was specific and mapped to 8q22 on both copies of chromosome 8 (Fig. 4.17). Biotinylated probe CH230-406J14 chosen for the locus 8q31 of chromosome 8 was unspecific and could not be used for interphase FISH analysis (data not shown) (Table 4.29). For chromosome 19 all 4 probes were specific (Table 4.29): both probes labelled with digoxigenin (CH230-110H16 and CH230-110L11) were localized to 19q11 and both biotinylated probes (CH230-89I12 and CH230-388N4) mapped to 19q12 (Fig. 4.18). DAPI counterstaining was used to identify chromosomal bands in FISH- labelled metaphases. The counterstain is taken up preferentially by double- stranded AT-rich sequences, producing characteristic light and dark banding patterns specific for each chromosome. Cytogenetic analysis of the FISH- labelled rat metaphases spreads was performed by Dr. Guilly (CEA, France).

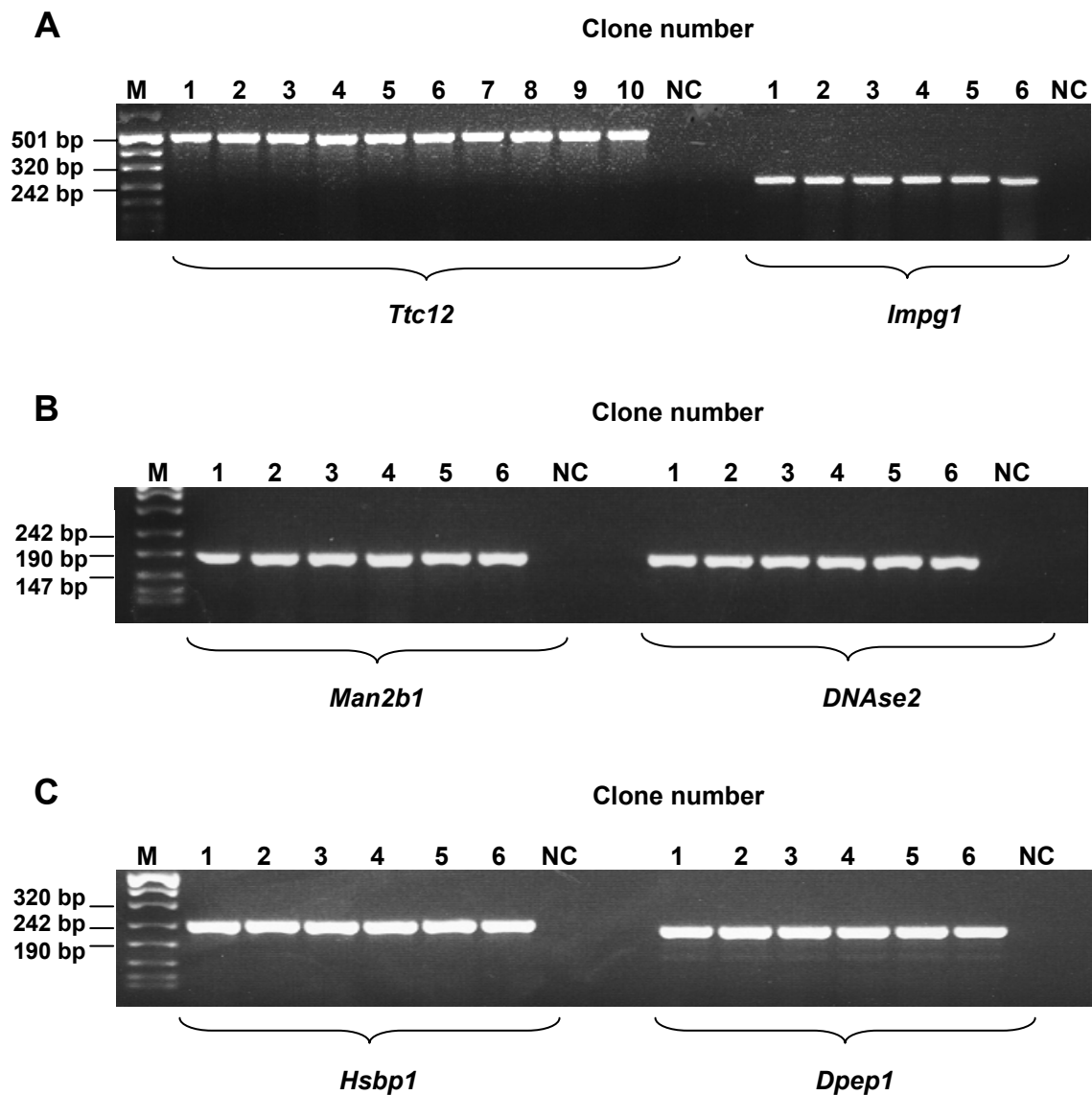


**Fig. 4.16** Verification of BAC clones by PCR. Clone number corresponds to *E. coli* single colony containing DNA insert which was verified by amplification of intron sequences of different genes predicted to map to the DNA insert. (A) PCR amplification of *Ttc12* gene (intron 1-2) of CH230-385B22 BAC clone and *Impg1* gene (intron 15-16) of CH230-406J14 BAC clone. (B) PCR amplification of *Man2b1* gene (intron 1-2) of CH230-398H16 BAC clone and *DNase2* gene (intron 5-6) of CH230-110L11 BAC clone. (C) PCR amplification of *Hsbp1* gene (intron 2-3) of CH230-89I12 BAC clone and *Dpep1* gene (intron 1-2) of CH230-388N4 BAC clone. Abbreviations: M, molecular weight marker VIII; NC, negative control.

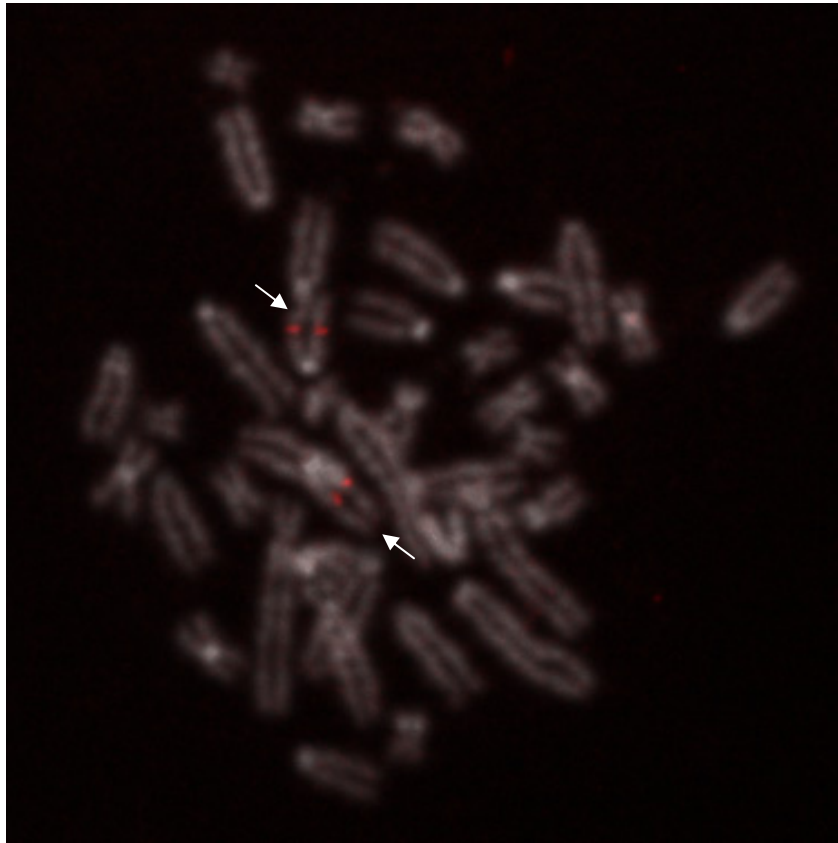
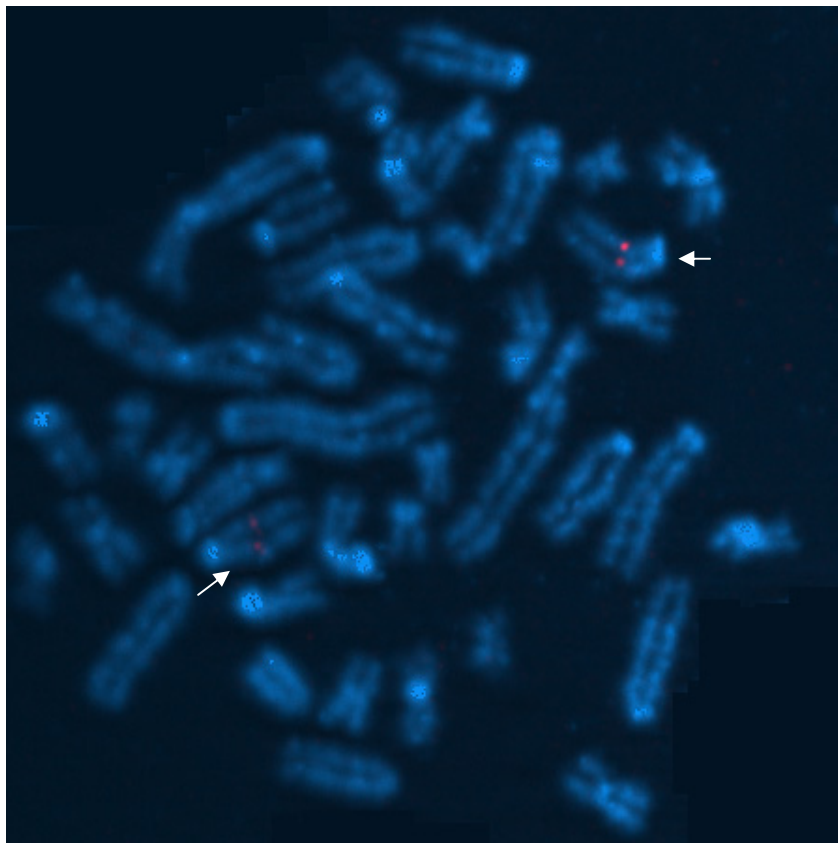


#### 4.5.2. Interphase FISH analysis

To analyze PC cases having AI previously identified with microsatellite analysis we performed interphase FISH on tissue sections of 10  $\mu\text{m}$  thickness of paraffin-embedded tissue derived from adrenal glands with PC. Interphase FISH was performed for PC13, PC20 having AI on chromosome 8 (Table 4.32) and for the group of PC cases having AI on chromosome 19, including samples PC12, PC13, PC14, PC16, PC18, PC20 (Table 4.33). One hundred interphase nuclei with strong hybridization signals were scored for each medullary part of the adrenal glands with PC (tumor area), for adjacent non-tumor cells from the adrenal cortex and for the medulla of normal adrenal gland from control animals. The procedure of FISH analysis is described in detail (Methods, 3.8).

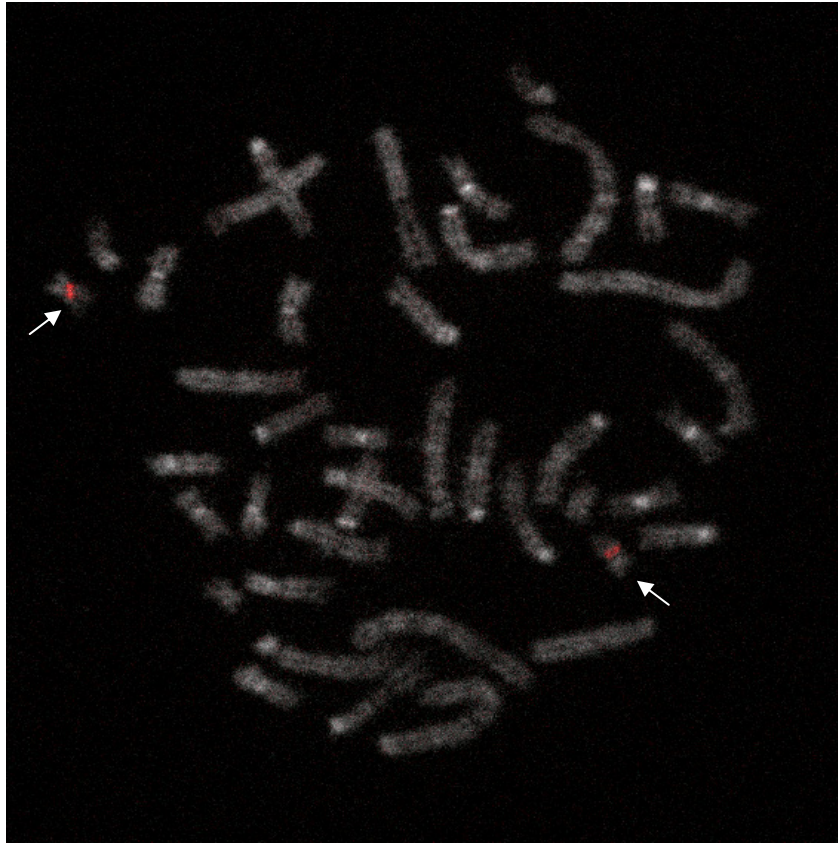
For PC13 and PC20 the presence of a deletion of rat chromosome 8 was confirmed by the FISH analysis. The results of interphase FISH analysis performed on paraffin-embedded tissue sections of PC13 using locus specific probe CH230-385B22 (8q22) are illustrated in the Fig.4.19. The cortical part of the same adrenal gland with PC was used as a control for FISH hybridization and FISH data analysis (Fig. 4.20). As only one locus-specific probe CH230-385B22 was used for FISH analysis on chromosome 8 it is not possible to say whether there is an interstitial deletion of chromosome 8 or the complete loss of one copy of the chromosome.

Among samples with AI on chromosome 19 the presence of a deletion was corroborated for PC13, PC16 and PC18 cases; for PC12, PC14, PC20 deletion of chromosome 19 was not seen with FISH. Dual color FISH with differently labelled locus specific probes CH230-398H16 (19q11) and CH230-89I12 (19q12) for PC13 is shown in Fig. 4.21 and 4.22.

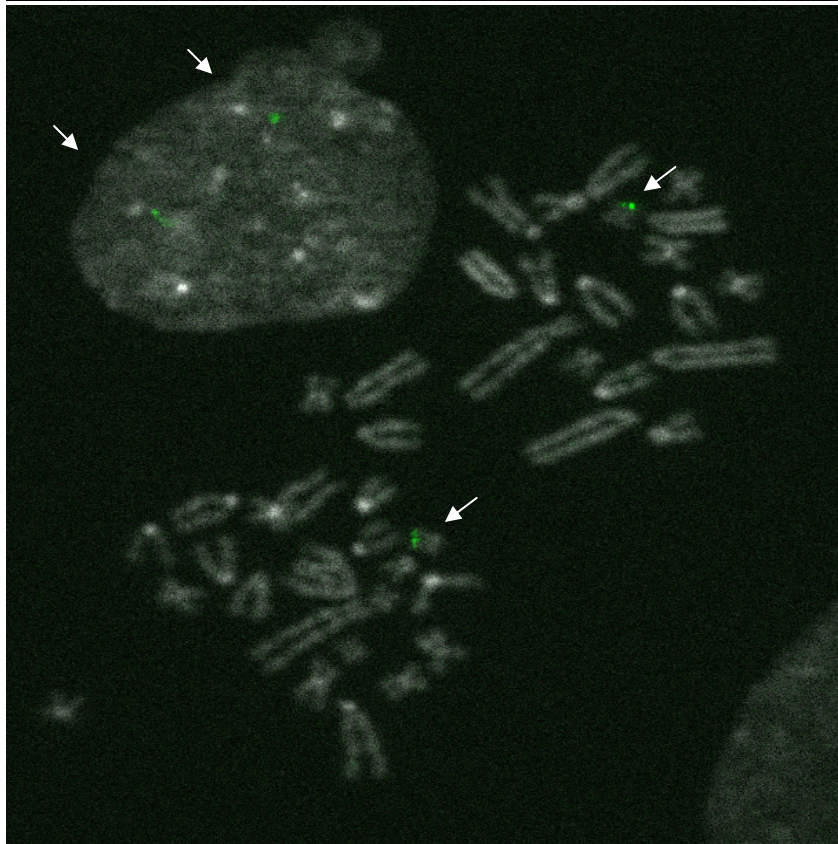
**A****B**

**Fig. 4.17** Rat lymphocyte metaphases. FISH mapping of single copy probes. CH230-385B22 BAC clone. The chromosomes are counterstained with Hoechst (A), DAPI (B). Doublet signals of a genomic BAC probe are mapped to 8q22 on both homologues of rat chromosome 8 (indicated by the arrows).

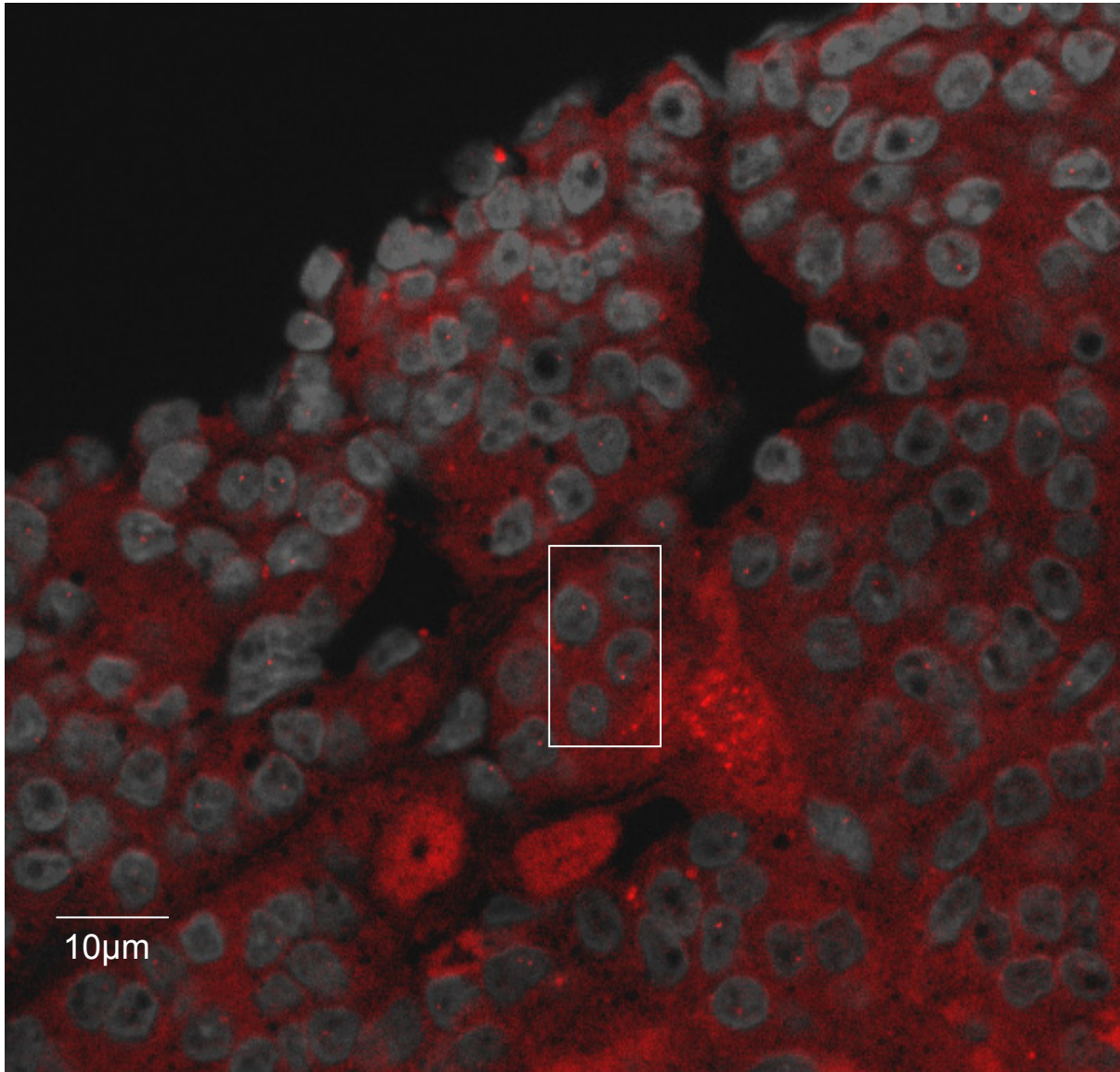
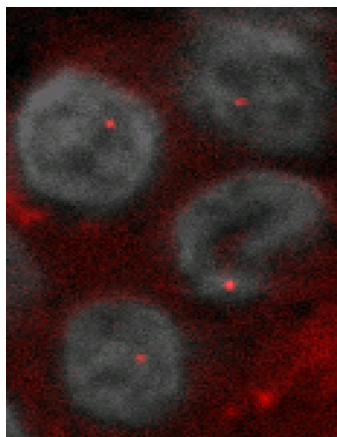
A



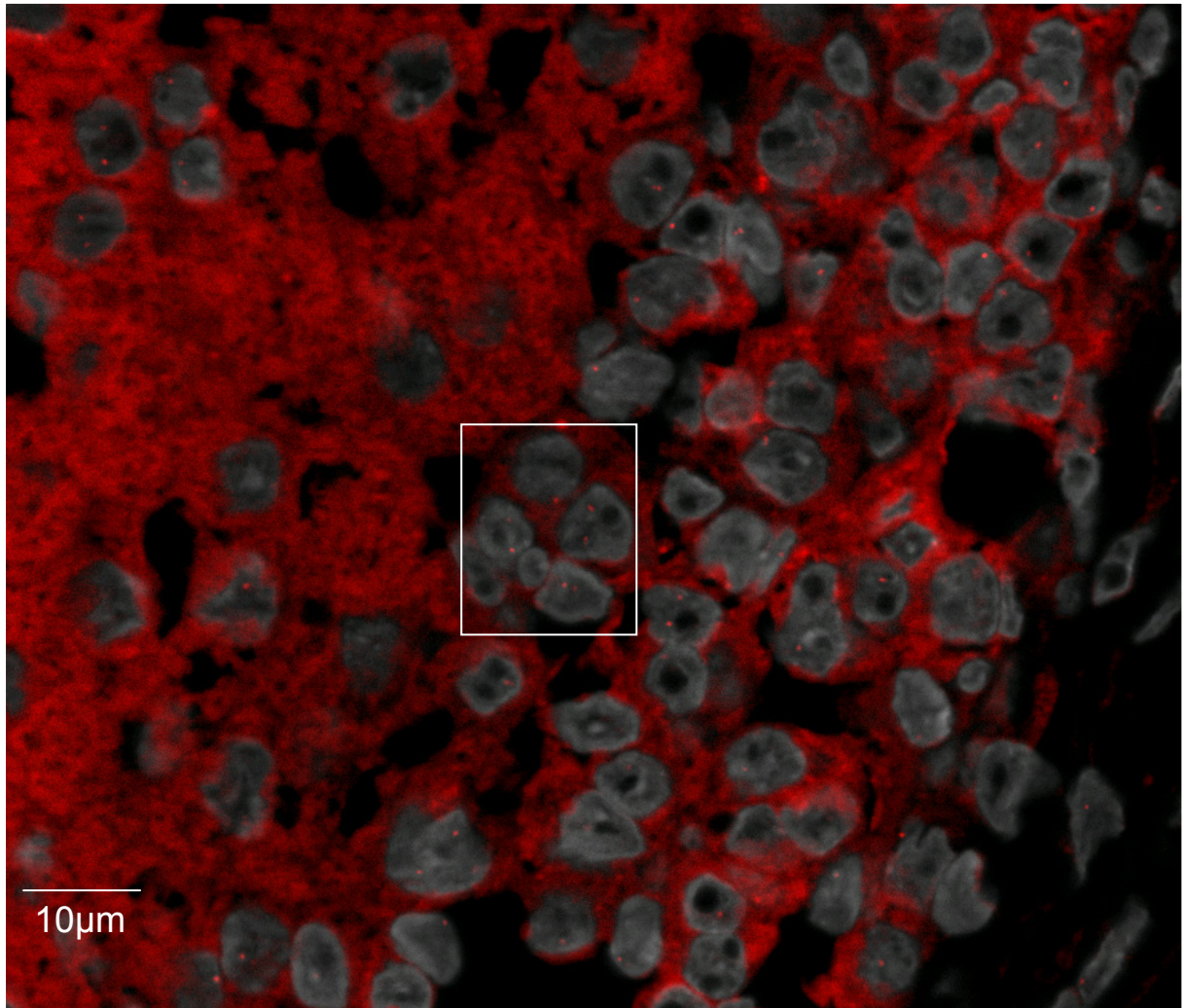
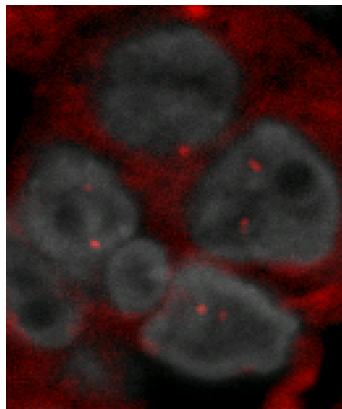
B



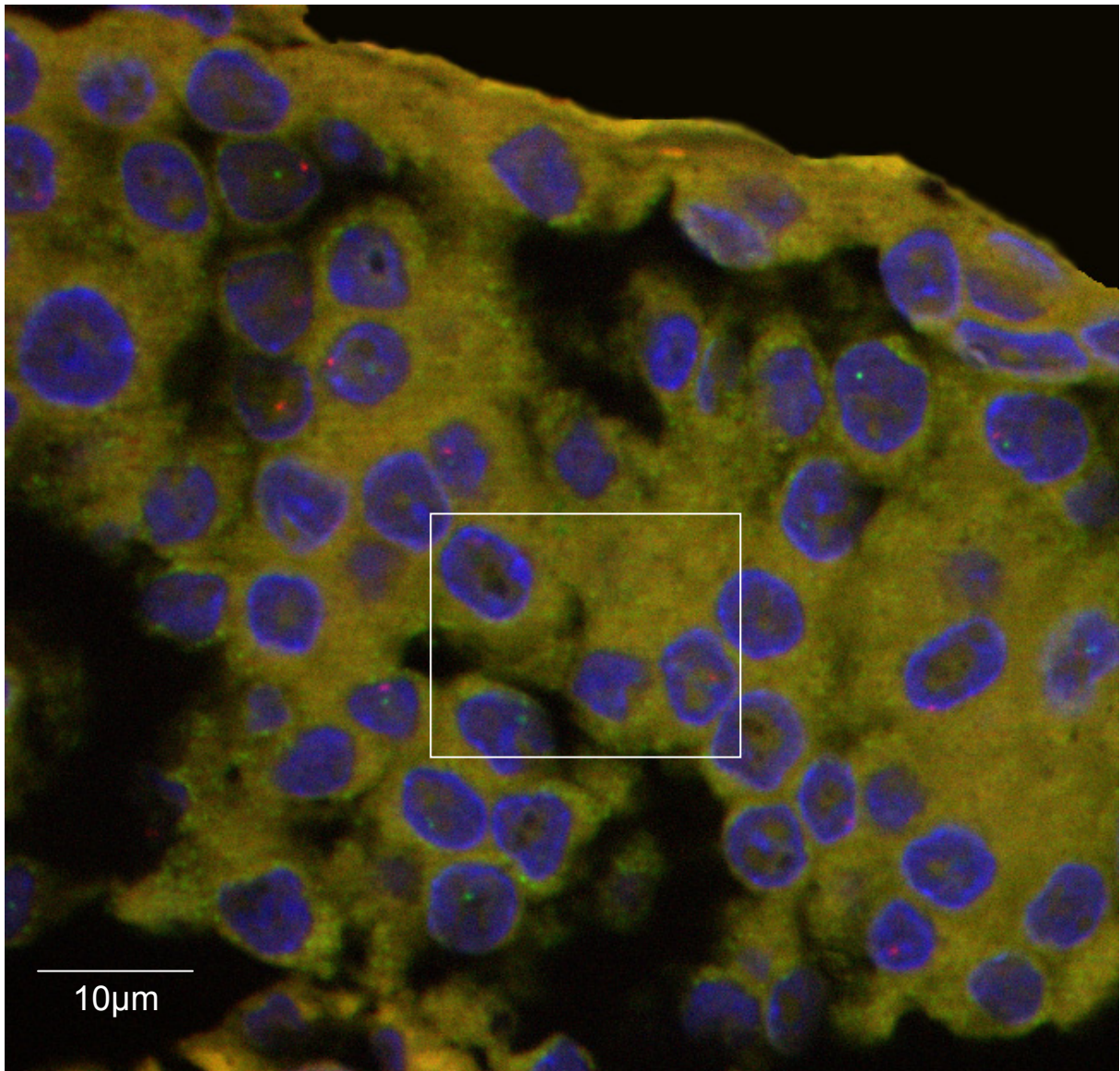
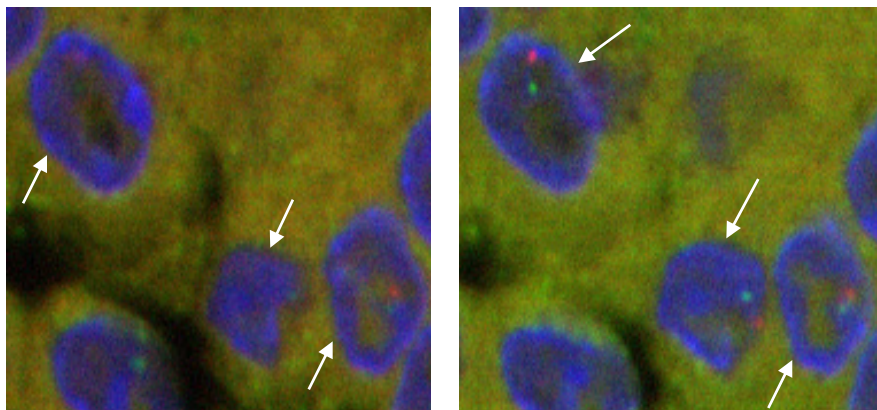
**Fig. 4.18** Rat lymphocyte metaphases. FISH mapping of single copy probes. The chromosomes are counterstained with DAPI. Doublet signals of BAC probes are mapped to 19q11 (A, CH230-398H16 BAC probe) and to 19q12 (B, CH230-89I12 BAC probe) on both homologues of rat chromosome 19. An interphase nucleus with two biotin signals is shown (B, indicated by two arrows).

**A****B**

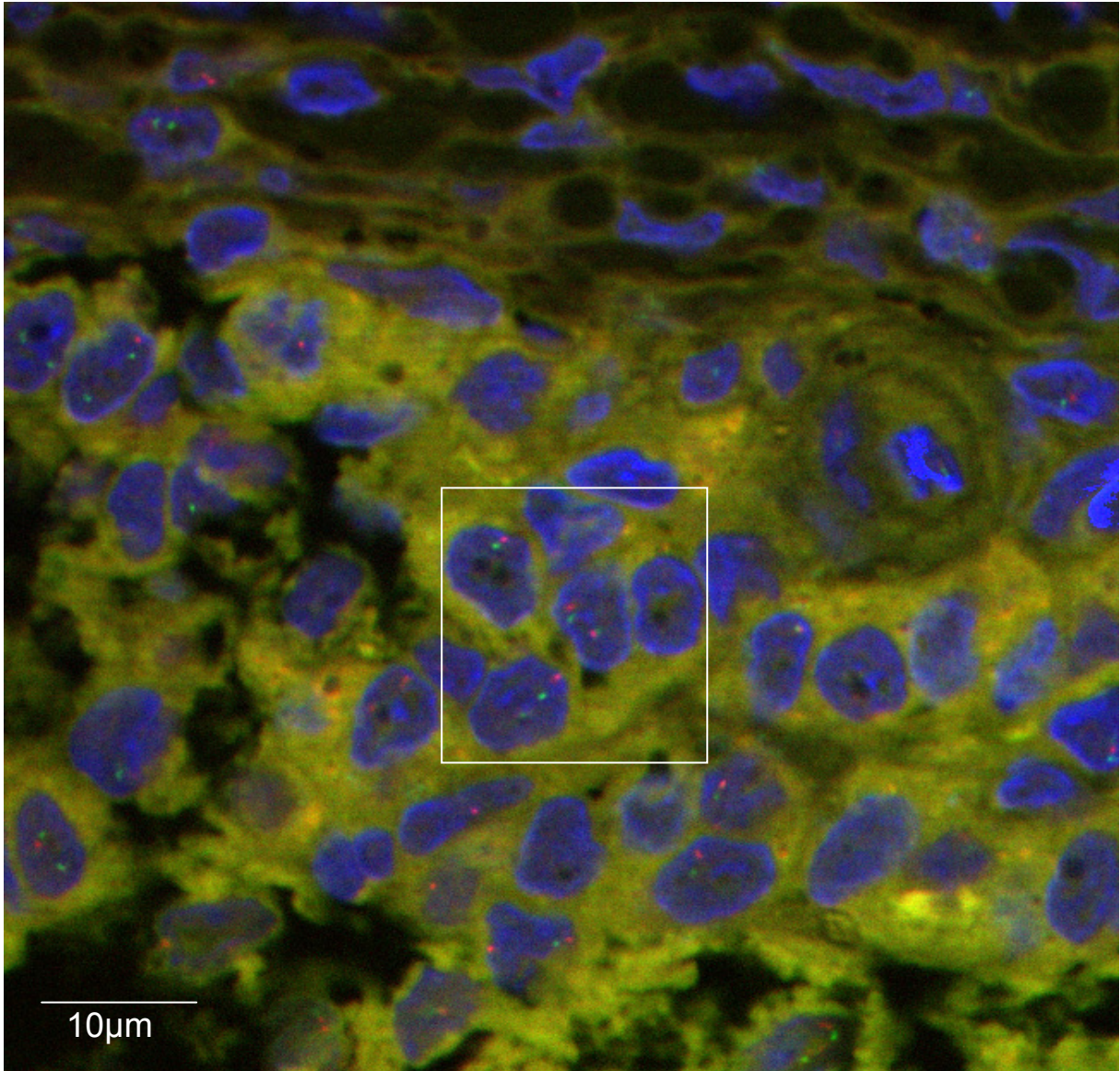
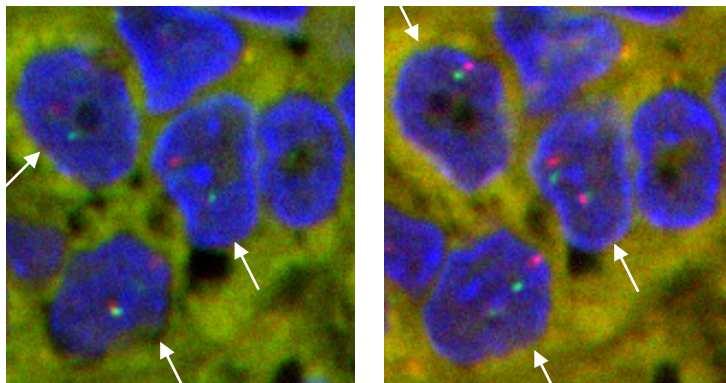
**Fig. 4.19** (A) FISH analysis of the adrenal gland with PC (case PC13) using CH230-385B22 BAC probe specific for the locus 8q22 of rat chromosome 8. BAC probe was labelled with digoxigenin and detected with rhodamin (red signals). A fragment of medullary part of adrenal gland with PC. Tumor cells of adrenal medulla show only one signal for the probe indicating chromosome 8q22 deletion. (B) Enlargement.

**A****B**

**Fig. 4.20** (A) FISH analysis of the adrenal gland with PC (case PC13) using CH230-385B22 BAC probe specific for the locus 8q22 of rat chromosome 8. BAC probe was labelled with digoxigenin and detected with rhodamin (red signals). A fragment of cortical part of adrenal gland with PC. Non-tumor cells from the adrenal cortex show the normal 2 signals for this probe. (B) Enlargement.

**A****B**

**Fig. 4.21** (A) Two-color FISH with differently labelled probes for the locus 19q12 (biotinylated CH230-89112 BAC probe, green signals) and the locus 19q11 (CH230-398H16 BAC probe labelled with digoxigenin, red signals) of rat chromosome 19. A fragment of medullary part of the adrenal gland with PC (case PC13). Tumor cells show only one signal for each probe indicating loss of one copy of chr 19. FISH was performed on the section of paraffin-embedded tissue. One optical section is shown. (B) Two consecutive optical sections (enlargement) showing a total of 2 signals in the tumor cell (arrows).

**A****B**

**Fig. 4.22** (A) Two-color FISH with differently labelled probes for the locus 19q12 (biotinylated CH230-89112 BAC probe, green signals) and the locus 19q11 (CH230-398H16 BAC probe labelled with digoxigenin, red signals) of rat chromosome 19. A fragment of cortical part of the adrenal gland with PC (case PC13). Normal cortical cells show 2 signals for each probe (control). FISH is performed on the section of paraffin-embedded tissue. One optical section is shown. (B) Two consecutive optical sections (enlargement) showing a total of 4 signals in the cell (arrows).

**Table 4.32** Signal distribution of FISH with the locus-specific probe CH230-385B22 (8q22) on cells from tumor medullary and normal cortical part of adrenal glands with PC and on cells from normal adrenal medulla.

Percent of cells with different number of signals (%)	1 signal	2 signals	3 signals	4 signals	Number of analyzed nuclei per case
<b>PC cases</b>					
PC13 (medulla)	82.3	17.3	0.4	0	100
PC13 (cortex)*	14.0	85.0	0.6	0.4	100
PC20 (medulla)	98.0	2.0	0	0	100
PC20 (cortex)*	9.0	91.0	0	0	100
Normal adrenal gland (medulla)*	12.0	88.0	0	0	100

A cut off value was obtained by screening 100 cells from each control area. To determine the cut off value, the mean percentage of cells of control areas showing 1 signal from digoxigenin-labelled probe was calculated plus/minus three standard deviations:  $10.1 \pm 12.1$ . The percentage of tumor cells of PC13 (medulla) and PC20 (medulla) samples with 1 signal is 4 times higher than the cut-off value determined: 82.3% of tumor medullary cells of PC13 and 98% medullary cells of PC20 show 1 signal while only 10.1% of cells of control tissues have 1 signal. It indicates the presence of deletion for both PC13 and PC20 cases. Cells of control areas (85-90% of nuclei) exhibit two copies of 8q22 signals (CH230-385B22 probe).

\*Control areas comprise cortical part of PC samples, medulla of normal adrenal gland from control animals (n=2).

**Table 4.33** Signal distribution of FISH with locus-specific probes CH230-398H16 (19q11) and CH230-89I12 (19q12) on cells from tumor medullary and normal cortical part of adrenal glands with PC and on cells from normal adrenal gland

Percent of cells with different ratio of signals (%)	1:1 ratio of signals	2:2 ratio of signals	2:1 ratio of signals	1:2 ratio of signals	2:3 ratio of signals	3:3 ratio of signals	Number of analyzed nuclei per case
<b>PC cases</b>							
PC12 (medulla)	3.8	88.6	2.9	2.9	0.9	0.9	100
PC12 (cortex)*	0.9	96.5	1.7	0.9	0	0	100
<b>PC13 (medulla)</b>	94.7	4.5	0.8	0	0	0	100
PC13 (cortex)*	0.9	93.9	1.7	2.6	0.9	0	100
PC14 (medulla)	2.9	89.3	2.9	3.9	0	1.0	100
PC14 (cortex)*	1.0	95.2	3.8	0	0	0	100
<b>PC16 (medulla)</b>	89.3	7.8	1.9	0	1.0	0	100
PC16 (cortex)*	1.0	98.0	0	1.0	0	0	100
<b>PC18 (medulla)</b>	93.1	5.9	1.0	0	0	0	100
PC18 (cortex)*	0	96.0	1.0	2.0	0	1.0	100
PC20 (medulla)	4.0	90.0	1.0	5.0	0	0	100
PC20 (cortex)*	2	93.0	1.0	4.0	0	0	100
Normal adrenal gland (medulla)*	3.4	93.2	0.9	2.5	0	0	100

A cut off value was obtained by screening 100 cells from each control area. To determine the cut off value, the mean percentage of cells of control areas showing 1 signal from digoxigenin-labelled CH230-398H16 probe and 1 signal from biotinylated CH230-89I12 probe (1:1 ratio of signals) was calculated plus/minus three standard deviations:  $1.4 \pm 3.8$ . Almost 90% of tumor cells of PC13 (medulla), PC16 (medulla), PC18 (medulla) samples show 1:1 ratio of signals while only 1.4 % of cells of control tissue have 1:1 ratio of signals. These results demonstrate the presence of deletion for PC13, PC16 and PC18 cases, they are labelled in bold. PC12, PC14, PC20 samples have a percent of tumor cells with 1:1 ratio of signals comparable with a percent of cells of control areas having the same signal distribution. 90-100% of cells of control areas of adrenal gland tissue sections have normal distribution of FISH signals: 2:2 ratio of signals. Almost 90 % of medullary tumor cells of PC12, PC14, PC20 samples show normal 2:2 ratio of signals (2 signals from digoxigenated and 2 signals from biotinylated probes).

\*Control areas comprise cortical part of PC samples, medulla of normal adrenal gland from control animals (n=2).



FISH data for chromosomes 8 and 19 are summarized in the Table 4.34.

**Table 4.34** Summary of interphase FISH data for rat chromosomes 8 and 19

Chromosome	PC sample	MA analysis	FISH
8	PC13	AI	deletion
	PC20	AI	deletion
19	PC12	AI	no changes
	PC13	AI	deletion
	PC14	AI	no changes
	PC16	AI	deletion
	PC18	AI	deletion
	PC20	AI	no changes

Abbreviations: PC, pheochromocytoma; MA analysis, microsatellite analysis; AI, allelic imbalance

For PC13 and PC20 the FISH and microsatellite analysis results are consistent and show chromosome 8q22 deletion.

Interphase FISH with locus-specific probes for chromosome 19 confirmed the presence of deletion of one copy of chromosome for PC13, PC16, PC18 that was seen in microsatellite assays.

PC20 case showed retention of heterozygosity at all informative microsatellite loci on chromosome 19 except for one marker located on 19q12 (Fig. 4.7). Two microsatellite markers were tested for this locus: *D19Rat64* and *D19Rat4*. PC20 was noninformative for the marker *D19Rat64* and showed an AI at the marker *D19Rat4*. BAC probe CH230-89I12 (19q12) used for dual interphase FISH analysis on chromosome 19 does not cover the area of AI at *D19Rat4* identified with microsatellite analysis. This suggests that a potential deletion of the terminal part of chromosome 19 may exist, but this is invisible to the FISH assay.

Both probes CH230-398H16 (19q11) and CH230-89I12 (19q12) are in the region of AI determined with microsatellite analysis for PC12 and PC14. No copy changes were identified for these samples with FISH analysis. A possible explanation for this observation may be the local heterogeneity of PCs, with some regions of tumor showing LOH while the others do not. It is known that neuroendocrine tumors represent a group of neoplasias characterized by significant histopathologic and biological heterogeneity (Blanes *et al.*, 2006). Our own studies show quite complex focal growth patterns during development of PC in MENX-affected rats (Pellegata *et al.*, 2006).

#### **4.6. CGH array studies to identify genomic losses or gains in PC of MENX rats**

The resolution (average distance between markers) of the genome-wide screening for LOH/AI by microsatellite markers (Results, 4.2) was 20-30 Mb, therefore smaller intra-chromosomal deletions were likely to be missed. In addition, the tumors available for the study were from F2 hybrid MENX rats which means that the animals are not informative for 50% of the microsatellite markers in the genome. To get a complete picture of copy number changes (losses but also gains) in the genome of MENX-affected rats comparative genomic hybridization (CGH) analysis was carried out using a whole genome oligonucleotide microarray with a median probe spacing of 5.3 kb (NimbleGen).

In order to perform CGH array, high quality, RNA-free genomic DNA was extracted from a panel of 7 fresh frozen cases of PC: PC1, PC3, PC7, PC10, PC16, PC19, and PC20. Among the analysed PC samples 4 were derived from males (PC1, PC3, PC7 and PC19) and 3 from female rats (PC10, PC16, PC20). As the internal control pooled DNA from 7 female rats was used. The DNA of the control group (reference sample) was extracted from ear takes (normal tissue) of 7 MENX-affected females: PC10, PC11, PC12, PC13, PC16, PC17, and PC20.

The whole procedure of CGH analysis including isothermal oligo design, array fabrication, DNA labelling, hybridization of labeled DNAs to arrays, extraction data from the array was carried out by NimbleGen Systems, Inc., at their facility in Iceland (Methods, 3.9).

For CGH array data analysis NimbleGen uses Olshen's circular binary segmentation algorithm to segment the averaged  $\log_2$  ratio data ( $\log_2 (PM_{\text{test}}/PM_{\text{reference}})$ ). There are four kinds of output produced by the DNA segmentation analysis: genome-wide CGH profile (single panel plots in pdf format), chromosome specific CGH profile (multi panel plots in pdf format), a segmentation table, and a GFF file. Genome-wide CGH profile data for all of the chromosomes for each array were compiled into a single plot, with the chromosomes or regions differentiated by color and by vertical dashed lines (Fig.4.23A). Chromosome specific plots show predicted DNA copy number changes on a chromosome-by-chromosome (or region-by-region) basis (Fig. 4.23B). Both these types of representations contain plots of the  $\log_2$  ratio values and the predicted DNA segmentations (DNA copy number changes) drawn as lines on the data points. The data points are normalized  $\log_2$  ratio values of probes used for CGH array analysis and the horizontal lines are the mean values of  $\log_2$  ratios among data points in segments (segmentation mean values) obtained by segmentation approach. Data of CGH array analysis can be visualised by the SignalMap software (gff files) that allows the comparison of different window size averaging data and unaveraged data for all samples simultaneously (Fig.4.23 (C)). The segmentation tables shows the endpoints and segmentation mean values of each predicted segment (Fig. 4.23 (D)).

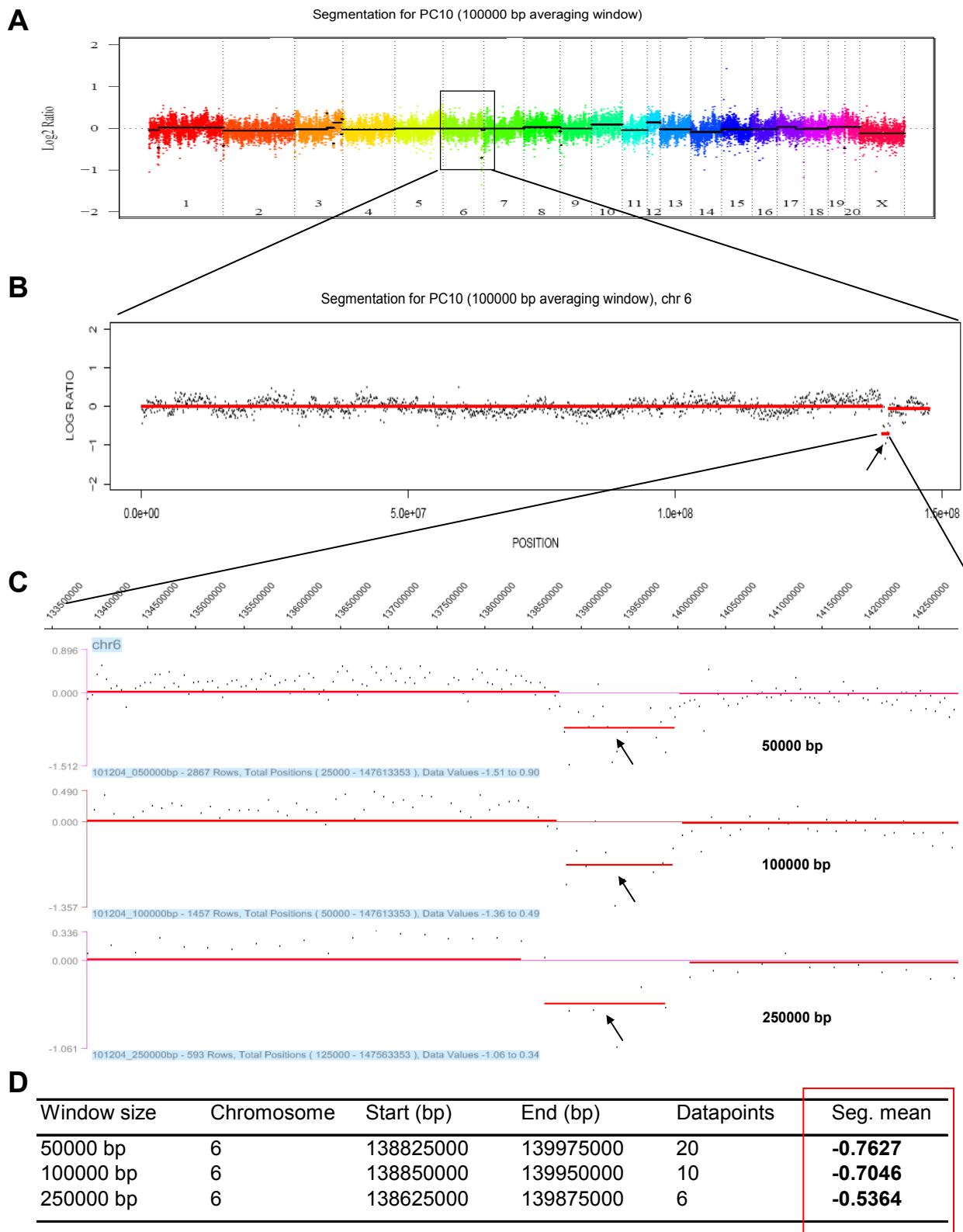


**Fig. 4.23** Array CGH analysis of genomic DNA of PC10 versus pooled genomic DNA. (A) Genome-wide profile for PC10 (the single panel PDF plot) showing copy number changes for the whole genome. Chromosome 6 with a copy number loss identified by CGH array is marked with a square. (B) Chromosome 6 profile (multi panel PDF plot). Deletion is indicated with an arrow. (C) GFF file with data for chromosome 6 in 3 windows with different averaging size (50000 bp, 100000 bp, 250000 bp). Areas of copy number loss are visible in all 3 windows (arrows). (D) A segmentation table of data averaged with 3 different averaging window size for a 138.6-140.0 Mb (6q32-q33) segment containing copy number loss, visible in plots (A, B, C). Values of segmentation mean (seg. mean) > 0.5 which indicates that the presence of deletion of 6q32-q33 region for PC10 is a high confident copy number variation call.

NimbleGen provided data for 20 rat autosomal chromosomes and for the X chromosome as well. There is no data for the Y chromosome.

CGH array was performed with sex-mismatched reference DNA to have an internal hybridization control for chromosome X copy number changes. All male samples PC1, PC3, PC7, and PC19 showed loss one copy of chromosome X (Fig. 4.24). These changes are visible in windows of three different sizes.

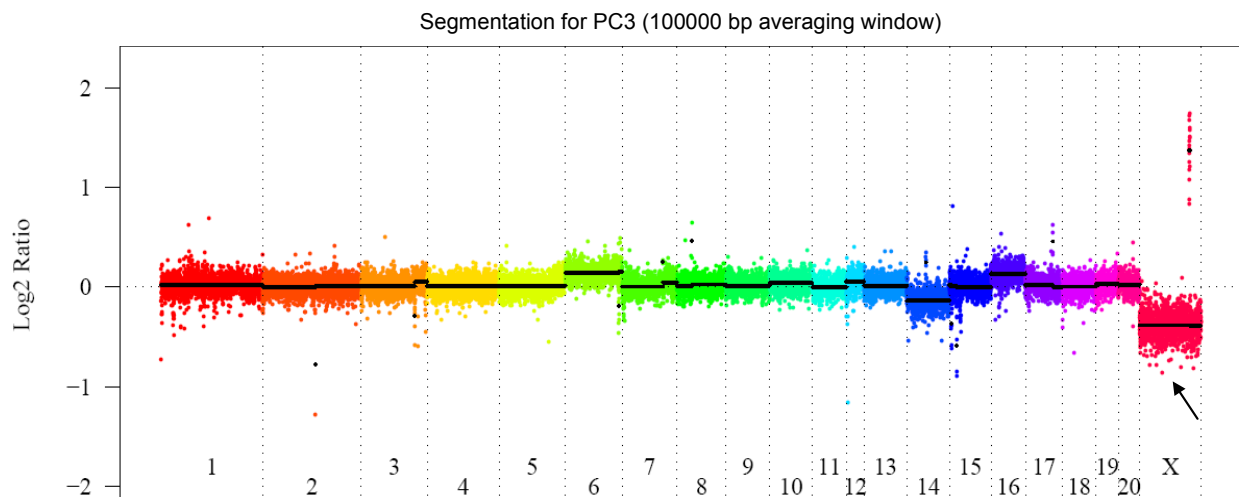


**Fig. 4.24** Genome-wide CGH profile for PC3. PC3 has a loss of one copy of chromosome X (deletion is indicated with an arrow). Seg.mean (averaged data) = -0.4.

#### 4.6.1. CGH array data analysis

For CGH array data analysis with NimbleGen values of  $\log_2(\text{PM}_{\text{test}}/\text{PM}_{\text{reference}})$  ratios from oligonucleotide probes with unique matches in the genome are analysed. Theoretical  $\log_2$  ratio values for copy number variations in homogenous tissue are illustrated in the Fig. 4.25. Validation of copy number changes regarding theoretical  $\log_2$  ratio values is discussed by van den Ijssel *et al.*, (2005).

If the tumor sample is heterogeneous the  $\log_2$  ratio values for II-V cases (Fig.4.25) will be below and will depend on the purity of analyzed tumor samples. It is known that normal cells present in a tumor sample effectively dampen the shift in  $\log_2$  signal ratio associated with genetic alterations in cancer cells (Lockwood *et al.*, 2006). A set of criteria has been proposed by the company imaGenes, that used NimbleGen CGH arrays for CGH array data analysis in heterogeneous tumor samples (Dr. Schad, imaGenes, personal communication): a) mean amplitude of  $\log_2$  shift across segment (segmentation mean value) =  $\pm 0.5$ , b) 5 or more probes

$$\log_2 \frac{PM_{\text{test}}}{PM_{\text{reference}}}$$

I. Normal tissue

$$\frac{PM_{\text{test}}}{PM_{\text{reference}}} = 1 \rightarrow \log_2 1 = 0$$

II. Tumor sample with homozygous amplification

$$\frac{PM_{\text{test}}}{PM_{\text{reference}}} = 2 \rightarrow \log_2 2 = 1$$

III. Tumor sample with heterozygous amplification

$$\frac{PM_{\text{test}}}{PM_{\text{reference}}} = 1.5 \rightarrow \log_2 1.5 = 0.58$$

IV. Tumor sample with homozygous deletion

$$\frac{PM_{\text{test}}}{PM_{\text{reference}}} < 0.5 \rightarrow \log_2(PM_{\text{test}}/PM_{\text{reference}}) < -1$$

V. Tumor sample with heterozygous deletion

$$\frac{PM_{\text{test}}}{PM_{\text{reference}}} = 0.5 \rightarrow \log_2 0.5 = -1$$

**Fig. 4.25** Theoretical log<sub>2</sub> ratio values corresponded to different copy number changes in homogenous tissue.

Abbreviations:  $PM_{\text{test}}$ , the perfect match signal intensity for the test sample, labelled with Cy3;  $PM_{\text{reference}}$ , the perfect match signal intensity for the reference sample, labelled with Cy5.

into the segment should have values of segmentation mean  $\geq 0.5$  in case of amplification or  $\leq -0.5$  in case of the presence of deletion. The same set of criteria has been used by Graubert *et al* (2007) to define the set of high confidence copy number variation calls in the mouse genome (C57BL76J mouse strain).

In the current study we have analysed segmentation mean values of averaged data of predicted segments corresponded to windows of three different size (segmentation mean tables). Raw averaged and unaveraged data have been analysed as well. For comparison between different samples the SignalMap software was used.

When performing CGH array the main challenge is to define a threshold value above which no false positives are retained without eliminating true positives (i.e. avoiding false negatives). Since the  $\log_2$  transformed normalized intensity ratios fluctuate in a Gaussian fashion around 0, the standard deviation can be used to define thresholds (Vermeesch *et al*, 2005).

To determine the threshold value for analysed tumor samples raw averaged data were used. For each tumor sample standard deviation of  $\log_2(\text{PM}_{\text{test}}/\text{PM}_{\text{reference}})$  intensity ratio of raw averaged data was calculated. The threshold was defined as  $\pm 1.5\text{SD}$ , where SD – standard deviation. For all tumor samples the defined threshold was equal to  $\pm 0.2$  of  $\log_2(\text{PM}_{\text{test}}/\text{PM}_{\text{reference}})$  ratio.

Fiegler *et al.*, (2006) has suggested that significant gains and losses can be defined as regions of at least three consecutive data points all above or all below 1.5 SD. van den Ijssel *et al.*, (2005) showed that three consecutive oligonucleotides are sufficient to call a single copy number change.

To identify high confidence regions of copy number variations for analysed tumor samples with PC we followed recommendations for CGH array analysis of heterogenous tumor samples (see above).

Taking into account all the above criteria we identified a set of copy number variation (gains and losses) and sorted them into 3 groups: 1) the first group includes chromosomal regions with segmentation mean  $\geq 0.5$  ( for gain) and  $\leq -0.5$  (for loss); 2) the second one includes copy number variations of chromosomes with range of the segmentation mean values  $0.4 \leq \text{segmentation mean} \leq 0.5$  ( for gains ) and  $-0.4 \leq \text{segmentation mean} \leq -0.5$  (for loss); 3) the third group contains chromosomal regions with DNA copy number alterations with segmentation mean values in a range  $0.2 \leq \text{segmentation mean} \leq 0.4$  ( for copy number gain) and  $-0.2 \leq \text{segmentation mean} \leq -0.4$  ( for copy number loss) (Fig. 4.26). For selection of the second group we took into account the fact that values of the segmentation mean of the X chromosome where the deletion of the whole copy of X chromosome was identified for male rats vary from -0.38 to -0.47. The probability that copy number changes included in the second group reflect a real biological event is still very high. Cardoso *et al.*, (2004) performed BAC array CGH to analyse

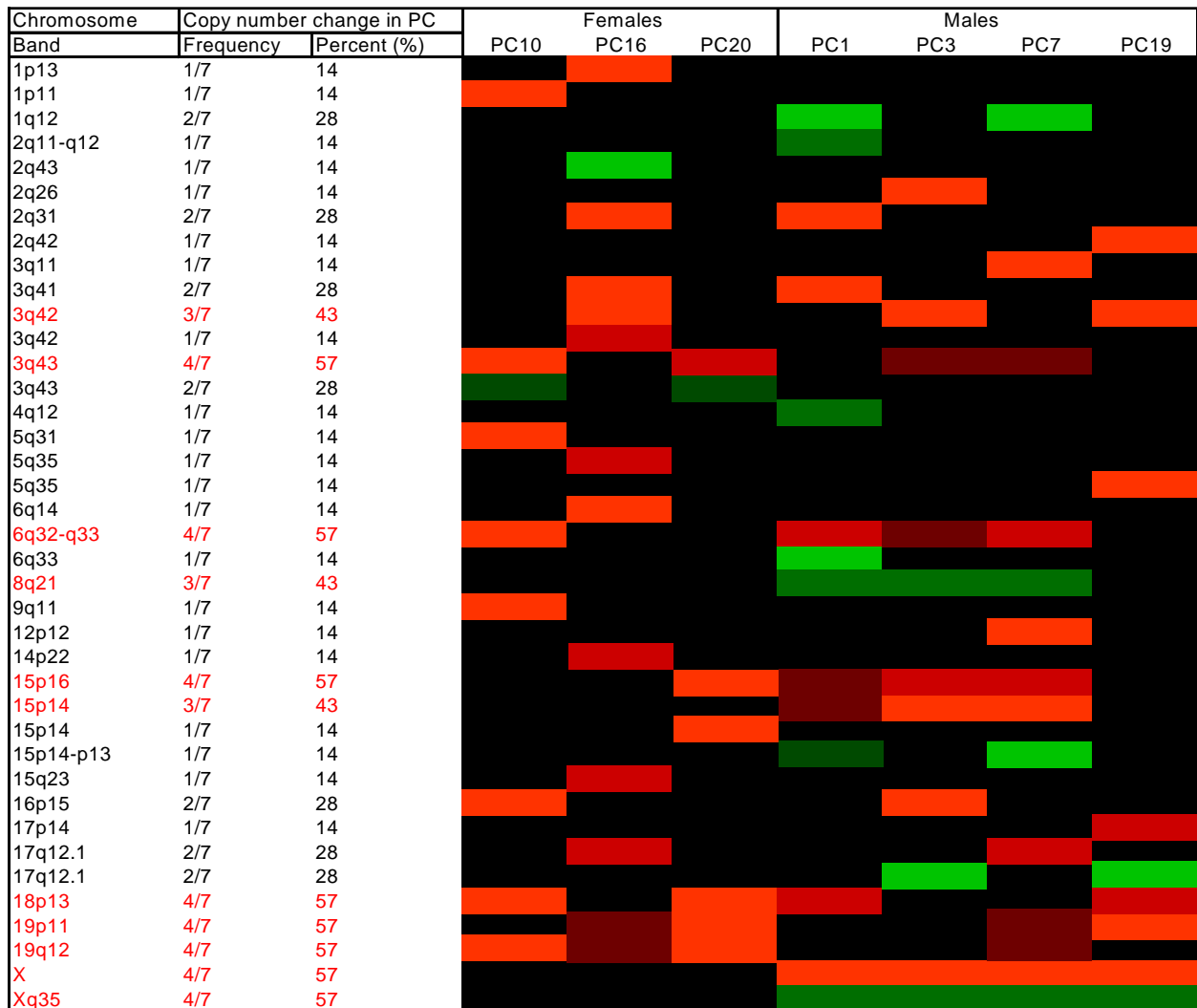
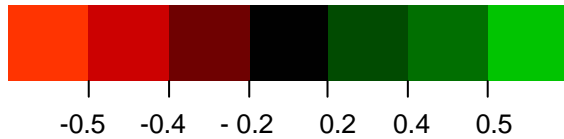


**Fig. 4.26** Heatmap representation of copy number changes in MENX-affected rats with PC. Common chromosomal regions of overlap for gains (green) and losses (red) are shown in the picture. Copy number variable regions visible either in three or two segmentation windows of different size are illustrated as well. To select regions of segmental gains and losses three types of thresholds was used. Chromosomal region was classified as amplified or deleted when the segmentation mean value fall outside “arbitrary” threshold (+ 0.5 and - 0.5 in  $\log_2$  scale) for copy number gain or loss respectively. Another threshold based on values of segmentation mean of  $\log_2$  ratios of probes on the X chromosome in male rats versus female control allowed to select a group of chromosomal loci with segmentation mean which vary in following range:  $0.4 \leq \text{segmentation mean} \leq 0.5$  ( for gains ) and  $-0.4 \leq \text{segmentation mean} \leq -0.5$  (for loss). Threshold, defined as  $\pm 1.5$  SD, was applied as well to the third group of copy number variations with segmentation mean values in a range  $0.2 \leq \text{segmentation mean} \leq 0.4$  ( for copy number gain) and  $-0.2 \leq \text{segmentation mean} \leq -0.4$  ( for copy number loss). Chromosomal loci shown in black are regarded as areas without copy number changes. Chromosomal bands were named using Ensembl Genome Browser. In red, PC loci names of chromosomal regions with the highest frequency of copy number variations (gains or losses) among analysed PC samples.

\*In all PC samples from male rats the loss of one copy of chromosome X was detected.

genomic profiling of colorectal adenomatous polyps and demonstrated variability prone areas to be dependent on the chosen threshold. The authors of this paper emphasize the importance of using different thresholds for the evaluation of probe-specific effects.

Identifying the minimum region of gain or loss that is shared by several tumors is of great interest because it might shed light on the mechanism of tumor progression. Among the 7 PC samples investigated chromosomal losses were more frequent than gains (Fig.4.26). The most frequent copy number losses (4/7, 57%) were observed in 3q43 (166.8 -167.1 Mb), 6q32-q33 (138.7- 140.0 Mb), 15p16 (5.0-6.0 Mb), 18p13 (525.0-675.0 kb), 19p11 (14.7-14.8 Mb), 19q12 (58.9 - 59.2 Mb). The highest percent of amplifications was determined in Xq35 (128.9- 130.5 Mb). But only male rats demonstrated the presence of copy number gain at this region, which suggests that it can be a sex-related copy number change. Other frequently deleted regions are 3q42 (147.3-147.5 Mb), 15p14 (19.4-20.0 Mb) with 43% of PC samples showing alterations. Region 8q21 (39.8-40.1 Mb) was amplified in 43% of PC samples. No copy number changes were observed for chromosomes 7, 10, 11, 13 and 20.

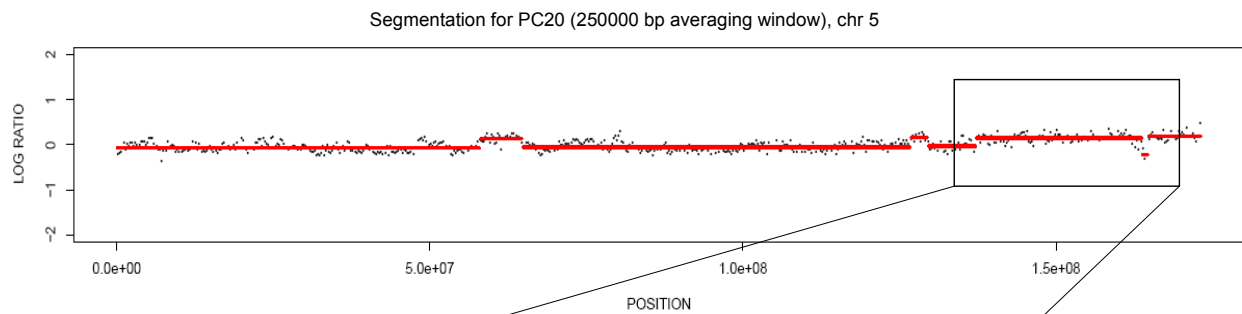
Rat homologs of genes predisposing to PC development, candidate tumor suppressor genes (Table 4.27) and genes showing overexpression in PCs (Results, 4.3) were analysed for the presence of copy number changes. For analysis of copy number changes for individual genes of interest the data of segmentation tables corresponding to 50000 bp, 100000 bp and 250000 bp window sizes could not be used because the segment size masks changes at the gene level. In other words, the segmentation approach can smooth possible copy number variations of genes being within the predicted segments because the number of intragenic probes for a gene is much smaller than the overall number of probes of the segment. Therefore, for this analysis raw averaged and unaveraged data was used. First of all data about intragenic probes for the genes of interest was collected using a special program facilitating the process of data sorting for different chromosomes. This program was written in IDL 6.1 by Dr. Tischenko (Institute of Radiation Protection, GSF). To be sure that selected probes belong to the analysed genes the gene annotation file provided by NimbleGen was used. This file can be visualized with SignalMap software and has a link to Ensembl Genome Browser. For almost all analysed genes no copy number changes were detected except for the *Ptprf*, and *Nfl* genes.

Copy number gain was found for PC10 and PC20 in the area of the *Ptprf* gene (Fig. 4.27). Seven intragenic probes have values of  $\log_2$  ratio  $\geq 0.2$ :  $\log_2$  ratio values vary in the range 0.3-0.4 (PC10) and in the range from 0.3 to 0.7 (PC20), which suggests the presence of amplification (Fig. 4.27 C). Copy number gains for both PC cases are visible only in 250000 bp window (Fig. 4.27A and B).

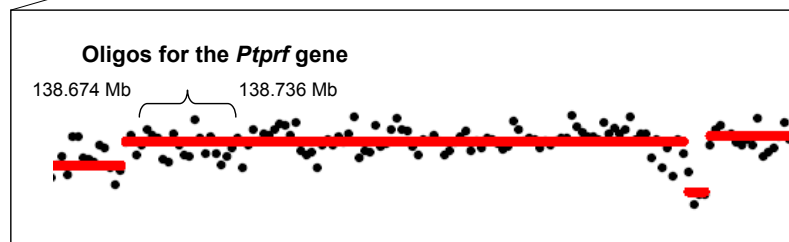


Copy number gain was detected also for the *Nfl* gene (Fig. 4.28). Only 1 animal out of 7 (PC1 case) showed amplification of the *Nfl* gene. Thirteen intragenic probes for the *Nfl* gene probes have  $\log_2$  ratio values  $\geq 0.2$  ( $\log_2$  ratio values vary from 0.2 to 0.6) (Fig.4.28C). Possible amplification of *Nfl* gene is visible only in the 250000 bp window (Fig. 4.28A and B).

**A**



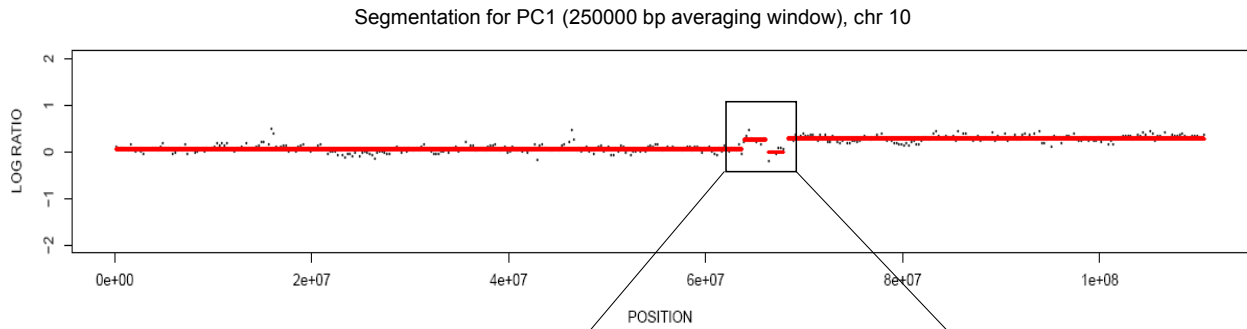
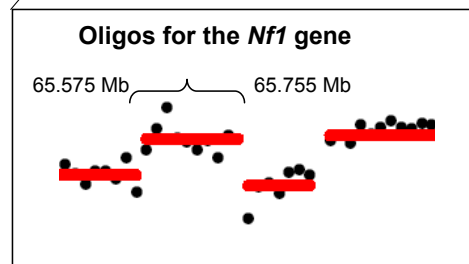
**B**



**C**

Chromosome	Probe position (bp)	Probe number	$\log_2$ (Cy3/Cy5)
chr05	138674457	1	0.2760
chr05	138679182	1	0.3270
chr05	138688808	1	0.6760
chr05	138703090	1	0.6710
chr05	138712643	1	0.4450
chr05	138731696	1	0.3360
chr05	138736221	1	0.4530

**Fig. 4.27** Detection of copy number gain for the *Ptpvf* gene in sample PC20. Data are processed with a 250000 bp averaging window and displayed as a  $\log_2$ -ratio plot. (A) Detailed chromosome 5 CGH profile of genomic DNA of PC20 (a segment). The chromosomal region (137.4 - 163.6 Mb) containing the *Ptpvf* gene is marked with a square. The segmentation mean value of the selected segment of the chromosome 5 is equal to 0.15 (B) Enlargement of (A). Position of oligonucleotide probes (oligos) for the *Ptpvf* gene is indicated with a brace. (C) Table containing unaveraged data of  $\log_2$  Cy3/Cy5 for intragenic probes of the *Ptpvf* gene. Seven intragenic probes for this gene have  $\log_2$  ratio values  $> 0.2$ , indicating gene amplification.

**A****B****C**

Chromosome	Probe position (bp)	Probe number	$\log_2(\text{Cy3/Cy5})$
chr10	65574873	1	0.3050
chr10	65614009	1	0.2680
chr10	65625794	1	0.2310
chr10	65664816	1	0.2020
chr10	65670005	1	0.3090
chr10	65675936	1	0.3450
chr10	65680436	1	0.5920
chr10	65691630	1	0.2550
chr10	65723049	1	0.2080
chr10	65727867	1	0.2440
chr10	65745197	1	0.3190
chr10	65750019	1	0.2200
chr10	65755335	1	0.4060

**Fig. 4.28** Detection of copy number gains for the *Nf1* gene in sample PC1. Data are processed with a 250000 bp averaging window and displayed as a  $\log_2$ -ratio plot. (A) Detailed chromosome 10 CGH profile of genomic DNA of PC1 (a segment). The chromosomal region (63.9 - 66.1 Mb) containing *Nf1* gene is marked with a square. The segmentation mean value of the selected segment of the chromosome 5 is equal to 0.3 (B) Enlargement of (A). Position of oligonucleotide probes (oligos) for the *Nf1* gene is indicated with a brace. (C) Table containing unaveraged data of  $\log_2$  Cy3/Cy5 for intragenic probes of the *Nf1* gene. 13 intragenic probes for this gene have  $\log_2$  ratio values  $\geq 0.2$ , indicating gene amplification.

The difficulty during the analysis of copy number changes for the genes of the interest was that for many analysed genes only a few intragenic probes were available: *Men1* (2 probes), *Vhl* (1 probe), *Cdkn1b* (1 probe), *Cdkn2b* (1 probe), *Cdkn2a* (2 probes), *Cdkn2c* (1 probe), *Sdhd* (2 probes), *Rassf1* (3 probes) and *Tp53* (2 probes).

To estimate biological relevance of copy number changes (gains and losses) identified using three-level threshold approach other techniques should be used. Chromosomal deletions can be confirmed by PCR amplification of informative microsatellite markers and/or of single nucleotide polymorphisms located in these regions, and using FISH with gene-specific and locus-specific probes. Copy number gains can be validated using quantitative Real Time RT-PCR and FISH analysis as well.

#### 4.6.2. Comparative analysis of data received after microsatellite analysis, FISH and CGH array analysis for rat chromosomes 8 and 19

Among the PC samples used for CGH array analysis there were samples (PC16 and PC20) with chromosomal aberrations of chromosomes 8 and 19 detected with other methods (LOH/AI analysis, FISH analysis). Comparative analysis of data from these three methods for PC16 and PC20 was done (Table 4.35).

**Table 4.35** Summary of MA analysis data, FISH data and CGH array data for 8 and 19 rat chromosomes

Chromosome	PC cases	MA analysis	FISH analysis	CGH array
8	PC13	AI	deletion (locus specific probe )	ND
	PC20	AI	deletion (locus specific probe )	The presence of the deletion is not obvious in all 3 windows ( 50000 bp, 100000 bp, 250000 bp)
19	PC16	AI	deletion (dual FISH)	Copy number loss. Copy number changes are visible into the three segmentation windows (50000 bp, 100000 bp and 250000 bp)
	PC20	AI ( <i>D19Rat4</i> )	no deletion (dual FISH)	Copy number loss. Copy number change is visible only in one window (50000 bp)

Abbreviations: PC, pheochromocytoma; MA, microsatellite analysis; ND, not determined

For PC20 AI was detected at all informative loci of chromosome 8. The presence of a deletion at the locus 8q22 was confirmed by FISH analysis (CH230-385B22 FISH BAC probe). But CGH array analysis did not reveal the presence of copy number losses of chromosome 8. For the analysis two group of data were used: a) segmentation mean values corresponded to different segmentation windows (50000 bp, 100000 bp and 250000 bp), b) log<sub>2</sub> ratio values of probes spanning the 8q22 locus. Segmentation mean values of three averaging windows is > -0.2 and

equal to -0.12. Analysis of the  $\log_2$  ratio values of probes for the 8q22 locus showed that 4 probes out of 28 (total number of probes for 8q22 chromosomal region) have  $\log_2$  ratio values  $\leq -0.2$  which vary in the range from -0.3 to -0.8. But only 2 out of these 4 probes are consecutive probes. Contradictions among data received for PC20 after CGH array analysis can be explained either by nontumor DNA contamination of the tumor or by genetic heterogeneity of the different areas of adrenal medulla of PC sample. Blanes *et al.*, (2006) demonstrated topographic genetic intratumor heterogeneity in the group of MEN2-related and sporadic PCs.

Data obtained for PC16 after microsatellite analysis, FISH analysis and CGH array are consistent: deletion of one copy of the chromosome 19 was confirmed by all three methods. Segmentation mean values of  $\log_2$  ratios of probes for chromosome 19 are  $< -0.2$  and range from -0.2 to -0.4, which suggests copy number loss. Segmentation mean values of three averaging windows were analysed.

For PC20 copy number loss of the distal part of 19q12 (58.9 - 59.2 Mb) was detected. Deletion is visible only in the one segmentation window (50000 bp) and the segmentation mean value of the segment with copy number loss is  $< -0.2$  and equal to -0.5. There is no microsatellite analysis data and FISH data for this region. PC20 showed retention of the heterozygosity at all informative markers dispersed over the whole chromosome 19 except for *DI9Rat4* (19q12) (Fig. 4.7). Deletion of chromosome 19 was not identified by dual FISH using CH230-398H16 (19q11) and CH230-89I12 (19q12) BAC clones as FISH probes. CH230-89I12 BAC probe does not overlap with microsatellite marker *DI9Rat4*.

## 5. DISCUSSION

MENX-affected rats have a homozygous frameshift mutation of the *Cdkn1b* gene which encodes for a non-functional p27(KIP1) protein thereby predisposing them to PC and PGL development (Pellegata *et al.*, 2006). Heterozygous germline mutations in the human *Cdkn1b* gene were also identified in suspected MEN1 patients (Pellegata *et al.*, 2006; Georgitsi *et al.*, 2007). These findings demonstrate that mutations in *Cdkn1b* may be “initiating” events, predisposing to PC formation in rat and humans. It was also found that p27(KIP1) expression is frequently reduced or lost somatically in human PCs but less in PGLs (Pellegata *et al.*, 2007), demonstrating that *Cdkn1b* also plays a role in PC development and progression.

In general, accumulation of genetic alterations has been associated with the development and progression of the tumor. It appears that the relative order in which such events occur is less important in tumor progression than the additive effect of the genetic changes (Mulligan *et al.*, 1993a).

Using a set of different methods, genome-wide microsatellite analysis, CGH array, FISH and Real Time TaqMan RT-PCR analysis, we identified the somatic genetic lesions that need to accumulate for the development of PC. We then compared our findings to those known to be involved in human PC initiation and progression. Comparative mapping studies have determined that there are evolutionarily conserved regions in human and rat that are linked to the same phenotype in both species (Stoll *et al.*, 2000). This means that the genes found to be important in tumor formation in the rat are likely to contribute to similar disease processes in humans. Moreover, it is known that the rat genomic sequence is ~90% identical to that of man in coding regions (Lazar *et al.*, 2005). Available data indicates that there are similarities in the genes involved in carcinogenesis in humans and rodents. For instance, many proto-oncogenes and tumor suppressors are the same or homologous in humans and rodents. Examples include the *TP53* and *RBI* tumor suppressors, as well as *MYC*, *RAS* and tyrosine-kinase-receptor proto-oncogenes (Anisimov *et al.*, 2005). These observations facilitate comparative genetic mapping between rats and humans.

### 5.1. Candidate LOH/AI loci in MENX-PCs

The genome-wide scan for LOH/AI of 20 advanced MENX-related PCs allowed us to determine candidate AI regions that were mostly localised on the rat chromosomes 8 and 19.

Two animals out of 20 (PC13 and PC20) showed AI at all informative loci of chromosome 8, which indicates that they have a complete loss of one copy of the chromosome (Fig.4.6). To confirm these findings FISH analysis was done. FISH proved the presence of the deletion in both tumor samples in the 8q22 chromosomal locus (Table 4.32). As only one BAC probe was used for FISH analysis it is not possible to estimate the size of the deletion by FISH.

The allelotyping revealed AI at informative loci of chromosome 19 in 6 of 20 tumors (PC12, PC13, PC14, PC16, PC18, PC20) (Fig. 4.7). These results allowed us to assume that there is a loss of one copy of chromosome 19 in all 6 tumors. Using FISH analysis with two BAC probes, specific for the 19q11 and 19q12 chromosomal loci, respectively, we confirmed deletions in these two regions for 3 out of the 6 analysed tumors (Table 4.33). These results allowed us to conclude, that, indeed, PC13, PC16 and PC18 have a loss of one copy of chromosome 19. For PC12, PC14 and PC20 no chromosomal aberrations were found with FISH analysis. It can be explained by possible tumor heterogeneity of PC samples (Diaz-Cano *et al.*, (2000); Blanes *et al.*, 2006), which makes the tissue used for DNA extraction may be of a different cellular composition from that analysed by FISH.

AI was also detected at chromosomes 1q55 (13%) and 3p13 (13%) in PC14, chromosome 3q23 (13%) in PC5 and chromosome 11q23 (8%) in PC14. Additional microsatellite markers need to be tested to determine the minimal AI region and to exclude the probability of a random occurrence of AI at these regions.

The overall frequency of LOH/AI determined is  $\leq 30\%$ . This modest frequency of the AI can be explained by the fact that the twenty analysed PCs came from a cohort of F2 hybrid MENX-affected rats. F2 hybrid MENX-affected animals were generated by backcrossing F1 ( $SD^{we}/Wky$ )  $\times$   $SD^{we}/SD^{we}$  rats (Dr. Pellegata, personal communication). These animals are expected to be not informative for 50% of the microsatellite markers in the genome. In fact, for LOH/AI study in total 158 microsatellite markers have been used, of which only 85 turned out to be informative (heterozygous) in at least half of the cases.

Only AI but not complete LOH was detected in our LOH/AI study of MENX-related PCs. It can indicate that PCs are heterogeneous endocrine tumors. Similar topographic intratumor genetic heterogeneity was demonstrated in 33 PCs, including 12 MEN2A-associated and 21 sporadic PCs, by Blanes *et al.* (2006). The authors revealed lower cell turnover and apoptosis down-regulation, resulting in accumulation of genetic alterations and segregation of tumor cells with differential genetic background, in the deep/peripheral compartments of adrenal medulla of PCs compare to the adrenal medulla internal compartments of the same tumor samples. Genes, such as *TP53*, *RBI*, and *NFI* were shown to have different microsatellite pattern (LOH/AI) in the peripheral and internal compartments of adrenal medulla of PCs (Blanes *et al.*, 2006). Blanes *et*

*al.* (2006) also showed the accumulation of tumor suppressor genes microsatellite abnormalities in the medullary peripheral compartment of adrenal gland of PCs. Using clonality analysis and immunohistochemistry a polyclonal pattern was also revealed in 6 out of 29 sporadic PCs (five locally invasive and one benign ) by Diaz-Cano *et al.* (2000).

Rat chromosomes 8 and 19 have a complex homology to the human genome (Fig. 5.1). Data about LOH/AI loci of rat chromosomes 8 and 19 and their syntenic regions in the human genome are summarized in the Table 5.1.

**Table 5.1** LOH/AI loci in rat MENX-associated PCs and their respective syntenic regions in the human genome

Rat chromosome number	Genomic location	Mb (Ensembl)	LOH/AI locus (microsat. marker)	LOH/AI frequency, %	Syntenic region in human genome
8	8q11-q12	0-15.9	<i>D8Rat170</i>	11%	11q14.3-q22.3
	8q22-q24	43.2-57.5	<i>D8Rat46</i>	12%	11q22.3-q24.1
	8q22-q24	43.2-57.5	<i>D8Rat44</i>	18%	11q22.3-q24.1
	8q22-q24	43.2-57.5	<i>D8Rat113</i>	9%	11q22.3-q24.1
	8q24	58.0-80.5	<i>D8Rat185</i>	15%	15q21.3-24.3
	8q24	58.0-80.5	<i>D8Rat33</i>	7%	15q21.3-24.3
	8q31-q32	95.3-111.2	<i>D8Rat167GSF1</i>	9%	3q21.3-q24
	<b>8q31-q32</b>	<b>95.3-111.2</b>	<b><i>D8Rat76</i></b>	<b>29%</b>	<b>3q21.3-q24</b>
19	<b>19p14-p12</b>	<b>0.3-11.9</b>	<b><i>D19Rat97</i></b>	<b>30%</b>	<b>16q21</b>
	<b>19q11</b>	<b>24.7-26.3</b>	<b><i>D19Rat13</i></b>	<b>28%</b>	<b>19p13.13-p13.12</b>
	19q11	26.3-34.4	<i>D19Rat25</i>	15%	4q31.21-q31.23
	19q12	37.6-53.9	<i>D19Rat64</i>	20%	16q22.2-q24.3
	19q12	53.9-56.9	<i>D19Rat4</i>	23%	1q42.13-q42.3

Human syntenic regions were found by using [http://www.ensembl.org/Rattus\\_norvegicus/synteniview](http://www.ensembl.org/Rattus_norvegicus/synteniview). Only loci of rat chromosomes 8 and 19, having an AI are regarded. Regions highlighted in bold font show the highest frequency of AI.

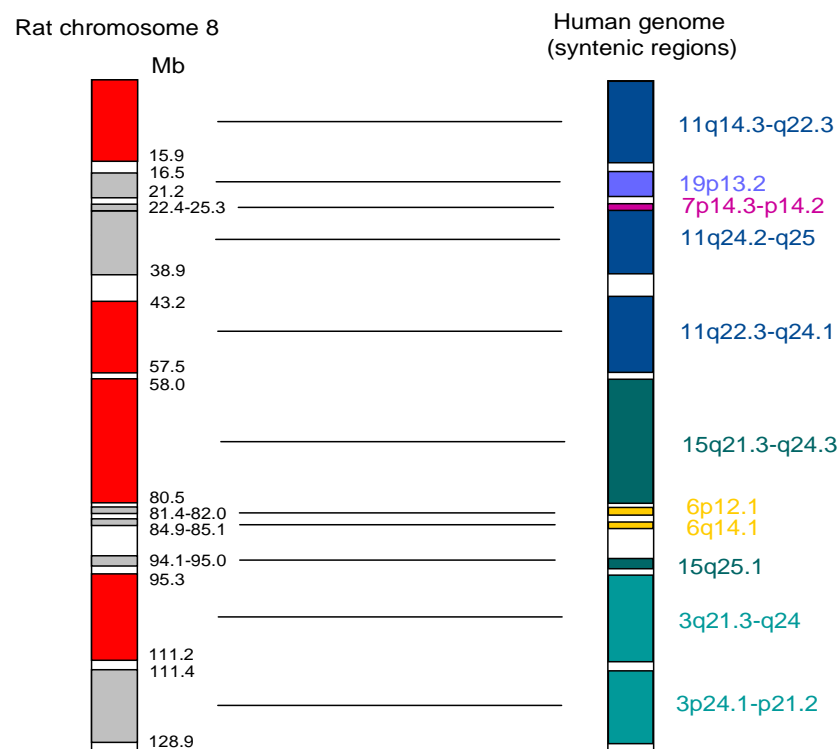
### 5.1.1. LOH/AI loci on rat chromosome 8 and their syntenic regions in the human genome

All loci affected by LOH/AI on rat chromosome 8 have synteny with regions of the human genome previously reported to be involved in human PC development (Table 5.2).

#### 5.1.1.1. Rat chromosomal locus 8q31-q32

The highest percent of AI (29%) on rat chromosome 8 was observed at the 8q31-q32 chromosomal locus, which has synteny to the 3q21.3-q24 human chromosomal locus (Table 5.1, 5.2). Dannenberg *et al.* (2000) found frequent loss of chromosome 3q in the series of sporadic PCs. Loss of chromosome 3q was more often encountered in benign than in malignant tumors (Dannenberg *et al.*, 2000). This might point to diverging pathways in the development of benign and malignant PCs.

A



B

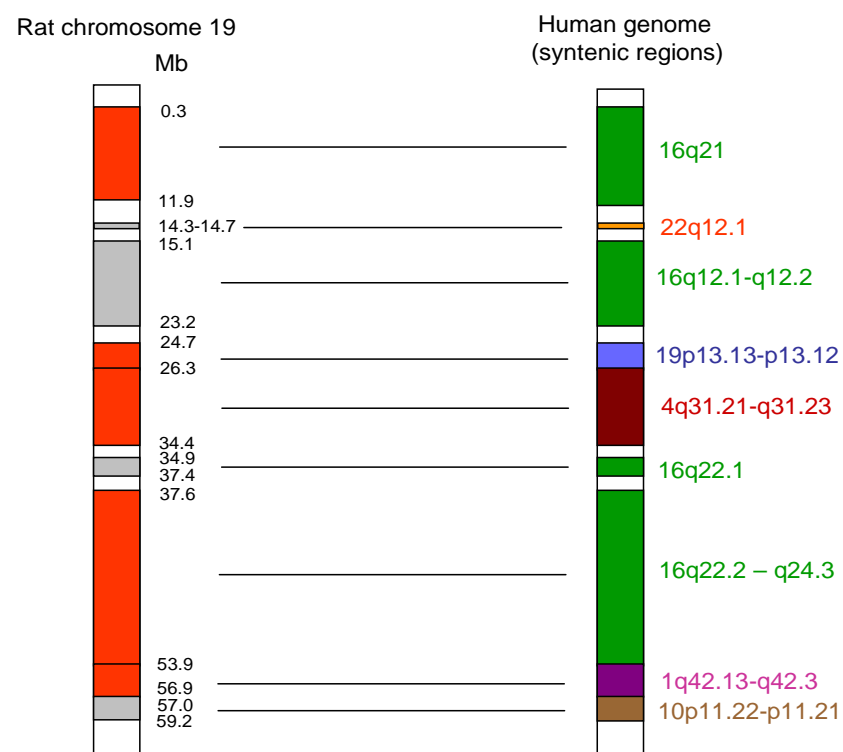


**Fig. 5.1** Rat chromosomes 8 and 19 and their syntenic regions on the human genome. Genetic loci of rat chromosomes 8 and 19, having an AI, are marked in red. Syntenic regions on the human genome which are corresponded to the AI regions of rat chromosomes 8 and 19 are labelled in different colors. Human syntenic regions were found by using [http://www.ensembl.org/Rattus\\_norvegicus/sytenyview](http://www.ensembl.org/Rattus_norvegicus/sytenyview). Rat chromosomal regions (in gray) are excluded from the syntenic analysis between rat chromosomal loci, showing an AI, and human genome as there are no data about possible chromosomal aberrations in these regions. (A) Rat chromosome 8 has syntenic regions with human chromosomes 3p, 3q, 6p, 6q, 7p, 11q, 15q, 19p. (B) Rat chromosome 19 has syntenic regions with human chromosomes 1q, 4q, 10p, 16q, 19p, 22q. Abbreviations: AI, allelic imbalance.



**Table 5.2** Syntenic regions of rat chromosomal loci, showing AI, and human genome. LOH and/or CGH data of human chromosomal regions syntenic to LOH/AI loci identified in MENX-related PCs and known to be involved in human PC development

LOH/AI loci in rat MENX-PC	Syntenic region in human genome	LOH and/or CGH data available for human PC	Chromosomal change		Copy number changes		Type of PC and/or PGL
			losses	gains	frequency,% PC	PGL	
8q11-q12 8q22-q24	11q14.3-q22.3 11q22.3-q24.1	Lui <i>et al.</i> , 2002 Dannenberg <i>et al.</i> , 2000  Edström <i>et al.</i> , 2000	11q13-qter 11q  11q14-qter, 11q13-q23, 11q13-qter, 11q22-qter		21/41(51%) 29 (28%)*  3/23 (13%)	2/11(18%)	VHL- associated PCs sporadic PCs, extra-adrenal PCs sporadic PCs, abdominal PGLs sporadic PC
8q24	15q21.3-24.3	Lui <i>et al.</i> , 2002 Edström <i>et al.</i> , 2000  Edström <i>et al.</i> , 2000	15q15-qter 15q, 15cen-q21, 15q22-qter, 15q23-qter	11q  15q, 15q21-q24, 15cen-q21	1/23 (4%) 1/41(2%) 2/23 (9%)  3/23 (13%)	2/11 (18%)	VHL- associated PCs sporadic PCs, abdominal PGLs MEN2-associated PCs, sporadic PCs
8q31-q32	3q21.3-q24	Mulligan <i>et al.</i> , 1993  Lui <i>et al.</i> , 2002 Dannenberg <i>et al.</i> , 2000  Edström <i>et al.</i> , 2000	3q 3q12-qter  3q 3q  3q22-q25		9/15 (60%)  1/41 (2%) 29 (52%)*  8/23 (39%)	5/11 (45%)	MEN2-associated PCs sporadic PCs, extra-adrenal PCs MEN2A-associated PCs, Nf1-associated PCs, sporadic PCs, abdominal PGLs PCs
19p14-p12 19q11 <sup>1</sup>	16q21 19p13.13-p13.12	Cascón <i>et al.</i> , 2005 Edström <i>et al.</i> , 2000 Lui <i>et al.</i> , 2002 Edström <i>et al.</i> , 2000	3q   3q	16q 19p 19p	21/29 (72%)  1/41(2%) 6/23 (26%)	1/11 (9%) 2/11 (18%)	abdominal PGLs VHL- associated PCs, MEN2A-associated PCs, sporadic PCs
19q11 <sup>2</sup>	4q31.21-q31.23	Cascón <i>et al.</i> , 2005 Lui <i>et al.</i> , 2002 Edström <i>et al.</i> , 2000	4q 4q, 4q21-qter, 4q28-qter	19p	17/29 (59%) <sup>†</sup> 1/41 (2%) 4/23 (17%)	13/24(54%) <sup>†</sup> 3/11 (27%)	PCs, head and neck PGLs MEN2-associated PCs sporadic PCs, MEN2A- associated PCs, abdominal PGLs
19q12 <sup>1</sup>	16q22.2-q24.3	Edström <i>et al.</i> , 2000		16q		1/11 (9%)	abdominal PGLs
19q12 <sup>2</sup>	1q42.13-q42.3	Edström <i>et al.</i> , 2000		1q	1/23 (4%)	2/11 (18%)	NF1-associated PC, abdominal PGL

\*The percent of copy number changes was identified in the group of adrenal and extra-adrenal PCs.

<sup>†</sup>The percent of PCs and PGLs showing 19p gain in the study by Cascón *et al.*, (2005) includes PCs and PGLs with gain of the whole chromosome or the short arm of chromosome 19.

19q11<sup>1</sup> and 19q11<sup>2</sup> loci correspond to 24.7-26.3 Mb and 26.3-34.4 Mb rat chromosomal regions of chromosome 19, respectively. 19q12<sup>1</sup> and 19q12<sup>2</sup> loci correspond to 37.6-53.9 Mb and 53.9-56.9 Mb rat chromosomal regions of chromosome 19, respectively.

Abbreviations: PC, pheochromocytoma; PGL, paraganglioma; MEN2, multiple endocrine neoplasia type 2; VHL, von Hippel-Lindau disease; NF1, neurofibromatosis type 1; LOH, loss of heterozygosity; AI, allelic imbalance.

In the study by Lui *et al.* (2002) only one of five MEN2 - related PCs showed 3q chromosome loss. The percent of MEN2-related PCs having loss of 3q is higher in the studies of Mulligan *et al.* (1993) and Edström *et al.* (2000). In the CGH array study of Edström *et al.* (2000) loss of 3q22-25 was frequently detected in both PCs (39%) and PGLs (45%). Mulligan *et al.* (1993) determined that 3qter-q12 is the shortest region of overlap for allelic loss, which can be involved in tumorigenesis of sporadic and MEN2-associated PCs. The highest percent of 3q loss (72%) in PCs was observed in the study by Cascón *et al.* (2005). The authors showed that loss of 3q was more frequent in PCs than in PGLs.

All these observations suggest that the 3q chromosome region may contain specific genes related to the development of both PCs and PGLs.

#### **5.1.1.2. Rat chromosomal loci 8q11-q12 and 8q22-q24**

The average percent of AI for the 8q11-q12 and the 8q22-q24 regions was 11% and 13%, respectively (Table 5.1). Deletion of the 8q22 locus found in two PCs samples, PC13 and PC20, and confirmed by FISH analysis using a BAC specific probe for this locus. The rat genomic region 8q11-q12 has synteny to the 11q14.3-q22.3 chromosomal region. 8q22-q24 region has a syntenic region 11q22.3-q24.1 in human. Earlier results of CGH array studies showed that losses of different loci of human 11q chromosome are involved in the development of VHL- related and sporadic PCs as well as in PGLs (Lui *et al.*, 2002; Dannenberg *et al.*, 2000, Edström *et al.*, 2000) (Table 5.2).

Loss of 11q13-qter was found in 51% of VHL-related PCs (Lui *et al.*, 2002). It was the second most common genetic imbalance detected in VHL-associated PCs after loss of chromosome 3p or the whole chromosome 3. Liu *et al.* (2002) showed that partial or complete loss of chromosome 11 was PC-specific since it was not present in any of the central nervous system haemangioblastomas studied. The authors suggest that partial or complete loss of chromosome 11 is an important hit in PC progression which can confer a further growth advantage to the tumor cells. Loss of chromosome 11 (loss of 11p and/or 11q or complete loss of the chromosome) in VHL-related PCs is significantly more common than in sporadic PCs (Lui *et al.*, 2002). A lower percent of 11q loss was found in series of sporadic PCs and PGLs (Dannenberg *et al.*, 2000, Edström *et al.*, 2000) (Table 5.2). Edström *et al.* (2000) showed that the major difference between benign and malignant PCs was involvement of chromosome 11, which was partly lost and /or gained in the majority of malignant cases. Loss of 11q22-23 (including the *PGL1* locus) was particularly common in malignant PCs (Edström *et al.*, 2000).

### 5.1.1.3. Rat chromosomal locus 8q24

An average AI frequency of 11 % was detected on the rat locus 8q24, syntenic to the human 15q21.3-24.3 locus (Table 5.1). Loss of different loci on chromosome 15q in the group of VHL-related and sporadic PCs and abdominal PGLs in CGH array studies were detected by Edsröm *et al.* (2000), and Lui *et al.* (2002) (Table 5.2). In addition to the losses gains of 15q loci were also found in the MEN2-associated and sporadic PCs (Edsröm *et al.*, 2000).

### 5.1.2. LOH/AI loci on rat chromosome 19 and their syntenic regions in the human genome

#### 5.1.2.1. Chromosomal loci 19p14-p12 and 19q12 (37.6-53.9 Mb)

Chromosomal loci 19p14-p12 and 19q12 are affected in 30% and 20% of MENX-PCs, respectively. In 3 PCs (PC13, PC16, PC18), the deletion of 19q12 was corroborated by FISH analysis. Both of these regions are syntenic to human chromosome 16q: 19p14-p12 has synteny to 16q21, and 19q12 region has synteny to 16q22.2-q24.3 (Table 5.1). The high percent of AI detected in these regions indicate a strong probability that tumor suppressor genes related to PC development are present. No data showing 16q LOH/AI in human PCs has been reported to date. Edström *et al.* (2000) found that 9% of human abdominal PGLs have a gain of 16q (Table 5.2).

The long arm of chromosome 16 is a target for LOH in a wide variety of different tumor types, suggesting that 16q harbors multiple tumor suppressor genes (Rakha *et al.*, 2006) (Table 5.3). Based on breast cancer LOH/AI studies two predominant regions of LOH have been determined: 16q22.1 and 16q24.3 (Cleton-Jansen *et al.*, 2001; Callen *et al.*, 2002; Miller *et al.*, 2003).

Results of LOH/AI study at chromosome arm 16q in a set of 712 breast tumors showed that 16q24.3 LOH even is more frequent than LOH at 16q22 (Cleton-Jansen *et al.*, 2001), suggesting that AI at 16q24.3 may be an early event in the progression of breast cancer (Reddy *et al.*, 1999). *FBX031* is a candidate breast tumor suppressor gene, located on the 16q24.3 chromosomal region (Kumar *et al.*, 2005). The authors showed that *FBX031* can induce cellular senescence in the breast cancer cell line MCF-7. Cell cycle analysis showed that inhibition of growth of breast cancer cell lines by ectopic *FBX031* expression seems to be caused by cells not progressing normally past G1 phase of the cell cycle. *FBX031* expression is cell cycle regulated in the breast cell lines MCF-10A and SKBR3 with maximal expression from late G2 to early G1 phase. A functional similarity between *FBX031* and the Skp2 protein present in the SCF<sup>Skp2-Cks1</sup> ubiquitin ligase complex (Bashir *et al.*, 2004) is suggested (Kumar *et al.*, 2005). Therefore, it was proposed that *FBX031* can form a functional SCF<sup>FBX031</sup> complex that would recruit and ubiquitinate critical cell cycle proteins for subsequent degradation (Kumar *et al.*, 2005).

It is interesting to note that Skp2 is required for ubiquitin-mediated degradation of phosphorylated p27(KIP1) thereby playing a critical role in the control of S phase entry of the cell cycle (Carrano *et al.*, 1999; Viglietto *et al.*, 2002).

Another cell senescence gene, *SEN16*, has been mapped within a 3-7 cM genetic interval at 16q24.3 (Reddy *et al.*, 1999; Reddy *et al.*, 2000). Firstly, it was shown that *SEN16* can restore senescence in different human and rat mammary tumor cells (Reddy *et al.*, 1999; Reddy *et al.*, 2000). Later it was demonstrated that introduction of chromosome 16q23-qter, containing the *SEN16* gene, can also restore senescence in immortal cell lines derived from hepatoma, prostate, ovarian tumors (Reddy *et al.*, 2000). All these findings suggest that a defect in *SEN16* may be common to many different tumors. Taking into account the fact that five PC tumors, PC12, PC13, PC14, PC16 and PC20, showed AI in a rat chromosomal region 19q12, syntenic to the human chromosomal locus 16q22.2-q24.3, and deletion of 19q12 locus was observed by FISH in three PC tumors, PC13, PC16 and PC18, one can speculate that *SEN16* may play a role in the tumorigenesis of PC.

Eight members of the cadherin gene family have been mapped to a region on the long arm of chromosome 16 (Kremmidiotis *et al.*, 1998; Chalmers *et al.*, 2001).

The cadherins are a family of a transmembrane glycoproteins mediating cell adhesion, communication and intercellular signalling, and playing an important role during embryogenesis and morphogenesis (Gumbiner *et al.*, 1996). They are implicated in tumor metastasis and progression (Chalmers *et al.*, 2001) and are considered as prime candidates for tumor suppressor genes (Kremmidiotis *et al.*, 1998; Braungart *et al.*, 1999).

Downregulation and mutation of E-cadherin, or *CDH1*, mapped at 16q22.1 chromosomal region, are associated with breast cancer (Chalmers *et al.*, 2001), gastric carcinomas (Braungart *et al.*, 1999; Becker *et al.*, 1994; Becker *et al.*, 1995); colonic cancer (Braungart *et al.*, 1999); prostate cancer (Abate-Shen and Shen, 2000) and ovarian carcinoma (Rizinger *et al.*, 1994). In the study by Gupta *et al.* (2000) it was shown that the majority of benign and malignant PCs do not express E-cadherin. E-cadherin can also be silenced by epigenetic mechanisms as well (Tamura *et al.*, 2000).

Shaffer *et al.* (2005) in the model of *Cdkn1b*-deficient transgenic mice, developing prostate carcinoma at a greatly accelerated rate, showed that *Cdkn1b* deficiency may contribute to earlier inactivation of a late-stage tumor suppressor, such as E-cadherin, which promotes tumor progression.

Cadherin-8 (*CDH8*) and OB-Cadherin (*CDH11*) were localized to 16q21 (Kremmidiotis *et al.*, 1998; Chalmers *et al.*, 2001). Loss of a cadherin-11 allele was seen in 5 of 23 colonic cancers

**Table 5.3** Loss of 16q in different types of human cancer

Region	Authors	Tumor type
16q21-23.2	Horwitz <i>et al.</i> , 1997	acute myeloid leukemia
16q11.2-q22.1	Mason <i>et al.</i> , 2000	Wilms' tumor
16q21-22	Suzuki <i>et al.</i> , 1996	prostate cancer
16q22.1-q22.3	Godfrey <i>et al.</i> , 1997	
16q23.2- q24.2		
16q23.2-q24.1		
16q24.3-qter		
16q22.1	Lee <i>et al.</i> , 1996	breast cancer
16q24.3	Chalmers <i>et al.</i> , 2001 Cleton-Jansen <i>et al.</i> , 2001 Callen <i>et al.</i> , 2002 Miller <i>et al.</i> , 2003	
16q22	Braungart <i>et al.</i> , 1999  Becker <i>et al.</i> , 1994; 1995	gastric cancer, colonic cancer gastric carcinoma
16q24.1-24.2	Bando <i>et al.</i> , 2000  Sato <i>et al.</i> , 1998	hepatocellular carcinoma lung cancer
16q23-qter	Visser <i>et al.</i> , 1997	rhabdomyosarcoma
16q21-23.2	Marchong <i>et al.</i> , 2004	retinoblastoma
16q24	Gratias <i>et al.</i> , 2007	
16q24	Kawakami <i>et al.</i> , 1999	ovarian cancer
16q24	Kitamura <i>et al.</i> , 2000a  Kitamura <i>et al.</i> , 2000b	anaplastic thyroid carcinoma papillary thyroid carcinoma
16q	Snijders <i>et al.</i> , 2003	fallopian tubes carcinoma

(Braungart *et al.*, 1999). Chalmers *et al.* (2001) showed involvement of *CDH11* in invasive ductal carcinoma tumorigenesis. Allelic loss and decreased expression at the RNA level of *CDH11* cadherin was shown in retinoblastomas (Marchong *et al.*, 2004; Gratias *et al.*, 2007).

H-Cadherin (*CDH13*) and M-Cadherin (*CDH15*) were mapped to chromosome 16q24.2 and 16q24.3, respectively (Kremmidiotis *et al.*, 1998; Chalmers *et al.*, 2001). Studies with *CDH13* suggest that this gene is associated with the 16q24 LOH in breast cancer (Lee *et al.*, 1996) and ovarian cancer (Kawakami *et al.*, 1999).

All these data show that multiple cadherin loci may be affected by losses of chromosome 16q.

In summary, *FBX031*, *SEN16*, the cadherin family genes (*CDH1*, *CDH8*, *CDH11*, *CDH13*, and *CDH15*) are candidate genes which can play role in PC initiation and progression.

### **5.1.2.2. Rat chromosomal locus 19q11 (24.7-26.3 Mb)**

Another frequently observed (28%) chromosomal aberration on rat chromosome 19 is an AI of the 19q11 region, which is syntenic to human 19p13.13-p13.12 chromosomal loci (Tables 5.1, 5.2).

Chromosome 19p gain, but not loss, was identified in 1/36 (2%) VHL-associated PCs by Lui *et al.* (2002). The higher percent of 19p gain was detected in the CGH array study by Edström *et al.* (2000) in the group of PCs and abdominal PGLs. Six out of 23 (26%) MEN2A-related and apparently sporadic PCs and 2/11 (18%) abdominal PGLs showed a gain of 19p chromosome (Edström *et al.*, 2000). Cascon *et al.* (2005) also reported frequent gain of 19q in the series of PC (59%) and PGL (54%).

It is interesting to note that 5 PC tumors, PC12, PC13, PC14, PC16 and 18, showed AI on the 19q locus, but the presence of the deletion was confirmed by FISH analysis only for PC13, PC16 and PC18. For PC12 and PC14 no copy number changes of chromosome 19 were revealed. Negative results after FISH analysis for these 2 tumors can be explained by possible heterogeneity of the PC tissue samples (Diaz-Cano *et al.* 2000; Blanes *et al.*, 2006).

Deletion of chromosome 19p has been found in many kinds of human cancers, including thyroid carcinoma (Kitamura *et al.*, 2000a; Stankov *et al.*, 2004; Kimmel *et al.*, 2006), lung cancer (Virmani *et al.*, 1998), ovarian cancer (Amfo *et al.*, 1995; Tsui *et al.*, 2005), hepatocellular carcinoma (Li *et al.*, 2001; Wang *et al.*, 2001).

In the study by Zhang *et al.*, (2003) high levels of AI at 19p13.1 in hepatocellular carcinoma (HCC) were identified. Moreover, the authors demonstrated that these high levels of AI are related to metastasis of HCC (Zhang *et al.*, 2003).

### **5.1.2.3. Rat chromosomal locus 19q12 (53.9-56.9 Mb)**

Three PCs, PC13, PC16 and PC20, showed AI (23%) on the rat 19q12 (53.9-56.9 Mb) chromosomal region (Fig. 4.7), syntenic to human chromosome 1q42.13-42.3 (Tables 5.1, 5.2). As mentioned above, FISH analysis confirmed the deletion of 19q12 locus for PC13 and PC16, but not for PC20 (Table 4.33). With the CGH array we identified a copy number loss in PC20 on chromosome 19q12 in 58.9-59.2 Mb region, proximal to the region of AI, identified with the microsatellite analysis. Basing on microsatellite analysis, CGH array and FISH data, one can suggest that PC20 has a deletion of the terminal part of the long arm of chromosome 19 but no deletion of the whole copy of chromosome 19.

Gain of 1q was found in 1 NF1-related PC and 2 abdominal PGLs in the study by Edström *et al.* (2000).

Loss of 1q42-qter is the most frequent rearrangement found in the PGLs (Cascon *et al.*, 2005). It is interesting to note that Cascon *et al.* (2005) found loss of 1q only in PGLs but not in PCs. Studies on anaplastic and papillary thyroid carcinomas showed a frequency of 40% LOH at 1q31-42 (Kitamura *et al.*, 2000a) and 37% LOH at 1q32-43 (Kitamura *et al.*, 2000b). KISS1, a novel human malignant melanoma metastasis-suppressor gene on 1q32-41, is the one putative tumor suppressor gene known in this chromosomal locus (Lee *et al.*, 1996). There are no other known candidate tumor suppressor genes on 1q (Kitamura *et al.*, 2000a).

#### **5.1.2.4. Rat chromosomal locus 19q11 (26.3-34.4 Mb)**

19q11 locus showing 15 % LOH/AI is syntenic to 4q31.21-q31.23 human chromosome (Tables 5.1, 5.2). Losses of 4q chromosome were identified in the MEN2-associated and sporadic PCs and abdominal PGLs (Edsröm *et al.*, 2000; Lui *et al.*, 2002). But the link between changes on chromosomal region 4q and tumorigenesis of PC remains unknown.

## **5.2. Copy number changes of candidate regions in MENX-PCs**

Because of the limitations of LOH analysis, such as insufficient density of informative microsatellite markers (Dannenberg *et al.*, 2003), we have used CGH array analysis to get a more complete picture of genome-wide copy number changes (losses, but also gains) in MENX-associated PCs. We characterized the genetic profiles of 7 MENX-related PCs with CGH array (Fig.4.26). The most commonly encountered chromosomal aberrations in the MENX-associated PCs involve 3q, 6q, 8q, 15p, 18p, 19p, 19q, and the X chromosome (Table 5.4). Losses were more common than gains (Fig. 4.26), indicating that the inactivation of tumor suppressor genes can play a critical role in PC tumorigenesis.

CGH array did not confirm partial or complete deletion of one copy of chromosome 8 in the PC20. Results of microsatellite analysis point to the presence of complete loss of the copy of chromosome 8 in PC20. FISH analysis corroborated this observation at least for the locus 8q22 that was tested. There are some factors, which could affect the negative results of CGH array analysis:

- genetic heterogeneity of the tumor sample PC20 and, as a possible consequence, absence of chromosome aberrations in cell clones of tumor area used for CGH array;
- sample “contamination” from too high percentage of normal tissues in the tumor samples;
- the copy number changes were too small, lying below the detection threshold of the CGH.

There is a good correlation between CGH array data, FISH and microsatellite analysis data for PC16 (Table 4.35). The results of all these three methods show that PC16 has a deletion of one copy of chromosome 19.

The majority of chromosomal regions demonstrating copy number changes with a high frequency (43-57%), reported in the Table 5.4, to date have no syntenic regions in the human genome. Some of them have known synteny to the mouse genome (Table 5.4).

**Table 5.4** Copy number changes in rat MENX-associated PCs and their respective syntenic regions in the human and mouse genome.

Rat chromosome number	Genomic location	Mb (Ensembl)	Copy number changes	Frequency, (%)	Syntenic region in human genome	Syntenic region in mouse genome
3	3q42	147.3-147.5	loss	43%	20q11.21-q13.33	-
	3q43	166.8-167.1	loss	57%	20q11.21-q13.33	-
6	6q32-q33	138.7-140.0	loss	57%	-	12F1-F2
8	8q21	39.8-40.1	gain	43%	-	9A1-D
15	15p16	5.0-6.0	loss	57%	-	-
	15p14	19.4-20.0	loss	43%	-	-
18	18p13	0.5-0.7	loss	57%	-	1F3
19	19p11	14.7-14.8	loss	57%	-	8C2-D1
	19q12	58.9-59.2	loss	57%	10p11.22-p11.21	-
X	Xq35	128.9-130.5	gain	57%	-	-

Only data of copy number changes detected with the highest frequency (43-57%) are shown. Human and mouse syntenic regions were found by using [http://www.ensembl.org/Rattus\\_norvegicus/syntenyview](http://www.ensembl.org/Rattus_norvegicus/syntenyview) Abbreviations: -, denotes that the rat genomic region has no regions syntenic to human or mouse chromosomes.

A few copy number changes involve regions, such as 15p16, 15p14, Xq35, which have no clear synteny to human or mouse genomes. It seems that alterations in the regions 15p16, 15p14, Xq35 can be rat-specific. For example, Iwamoto *et al.* (2005) mapped a novel gene family, *Spetex2* (spermatid expressing gene-2), which contains multicopied genes in a cluster, on rat chromosome 15p16. *Spetex2* genes are rat specific (Iwamoto *et al.*, 2005). The authors hypothesize that *Spetex2* might be correlated with cell differentiation of spermatids in rat testis.

There are three regions which are frequently affected in MENX-PCs and have clear syntenic regions to the human genome: 3q42, 3q43 and 19q12 (58.9-59.2 Mb) (Table 5.4).

The 19q12 (58.9-59.2 Mb) rat genomic region, affected in 57% of PC samples (Table 5.4), is syntenic to 10p11.22-p11.21 chromosome in the human genome. There are no literature data about the involvement of 10p11.22-p11.21 locus in PC development in humans. In the paper by Pack *et al.* (2005) it was reported about losses of 10p chromosome in 25% of hereditary and sporadic pituitary adenomas. The hereditary group of pituitary adenomas included adenomas associated with MEN1 syndrome and Carney complex. Loss of 10p was one of the most frequently detected losses of chromosomal material in pituitary adenomas (Pack *et al.*, 2005).



Mutations of *Cdkn1b* gene were reported in patients with suspected MEN1 phenotype, developing in one case pituitary adenoma and acromegaly (Pellegata *et al.*, 2006) and in other case pituitary adenoma in combination with carcinoid tumor and hyperparathyroidism (Georgitsi *et al.*, 2007). It is interesting to note that approximately 77% of MENX-affected rats carrying homozygous mutation in *Cdkn1b* gene develop pituitary adenoma and 65% of affected rats develop parathyroid adenoma (Fritz *et al.*, 2002). Probably, genes, containing in 10p locus, may play a critical role in the progression of endocrine tumors, including PC.

Copy number losses were detected on the rat chromosomal loci 3q43 and 3q42 with high frequency: 57% and 43%, respectively (Table 5.4). Both loci have synteny to 20q11.21-q13.33 region in humans. In the CGH study by Edström *et al.*, (2002) gain of 20q was detected in 2 out of 23 sporadic PCs. Gain of chromosome 20q was observed in 2 out of 6 VHL-associated haemangioblastomas (Lui *et al.*, 2002). Copy number gains and losses of 20q were reported in pituitary adenomas (Fan *et al.*, 2001; Pack *et al.*, 2005).

The small number of tumor samples (n=7), used for CGH array is a big limitation into the interpretation of our CGH array data. Increase of the number of analysed tumors would allow us to reevaluate CGH array data and, possibly, find new regions of copy number changes which are frequently involved in MENX-PC development.

### **5.3. Analysis of rat homologs of genes predisposing to or involved in PC development**

With microsatellite analysis we searched for LOH/AI for the rat homologs of genes known to predispose to PC development such as *Ret*, *Vhl*, *Nf1*, *Sdhd*, *Sdhb\_predicted* and candidate tumor suppressor genes, such as *Men1*, *Cdkn2b*, *Cdkn2a*, *Cdkn2c*, *Tp53*, *Rb1* (Table 4.27). *Ptprf* and *Rassf1* genes also were analysed, because they are known to be involved in PC development (Introduction, 1.4.2.).

Neither AI nor LOH was found for the *Pten* gene using intragenic microsatellite marker *RND1Lev1*. For genes *Men1*, *Cdkn2b*, *Cdkn2a*, *Cdkn2c*, *Ptprf*, *Sdhb\_predicted*, *Sdhd*, *Rassf1*, *Tp53*, *Nf1* and *Rb1* flanking microsatellite markers were used and LOH/AI can be excluded in upstream and downstream regions of all of these genes (Fig. 4.9). For *Vhl*, *Ret* and *Cdkn1b* genes we could not receive any information about LOH/AI with microsatellite analysis because all tested microsatellite markers for these genes were not suitable for the analysis due to homozygosity of the gene region in MENX rats (Table 4.27).

All above mentioned genes were analysed for the presence of copy number changes with CGH array analysis (Results, 4.6.1.). The small number of intragenic probes available for the genes of

our interest was a limitation for this analysis. For the majority of analysed genes, except for the *Ptprf* and *Nf1* gene, we detected no copy number changes. In two tumors, PC10 and PC20, a copy number gain of the *Ptprf* gene was found. Only PC1 showed copy number gain of the *Nf1* gene (Results, 4.6.1). More animals should be analysed to estimate the frequency of chromosomal aberrations of *Ptprf* and *Nf1* gene chromosomal regions.

Both genes, *Sdhd* and *Rassf1*, known to be involved in PC development in humans (Introduction 1.2.4., 1.4.2), reside on rat chromosomal loci 8q23 and 8q32, respectively. LOH/AI and FISH data analysis point to the presence of partial or complete deletion of one copy of the chromosome 8 in 2 PC tumors, PC13 and PC20. In view of the presence of AI on chromosome 8, including the 8q23 and 8q32 loci, we analysed expression level of *Sdhd* and *Rassf1* genes in 15 MENX-related PC, including PC13 and PC20. No changes in the mRNA level of *SDHD* and *Rassf1* were detected in PC samples (Results, 4.3.3., Fig. 4.14, 4.15). AI found in PC13 and PC20 did not affect gene expression. No mutations were found in the *Sdhd* and *Rassf1* genes as well (Results, 4.4). The absence of mutations in the *Rassf1* gene is consistent with the data of Astuti *et al.* (2001c) for a set of sporadic PCs.

To date, there is no literature data about increased expression of *Cdkn2a*, *Cdkn2c* and *Sctr* genes in PC tumors. Upregulation of *Cdkn2a*, *Cdkn2c* and the *Sctr* was found in expression array analysis of samples with adrenal gland medullary hyperplasia (Dr. Pellegata, unpublished observation). The expression of *Cdkn2a*, *Cdkn2c*, and *Sctr* genes was analysed in 13 PC samples (Results, 4.3.2.). We detected overexpression of *Cdkn2a*, *Cdkn2c*, and *Sctr* genes in mature PCs (Fig. 4.11, 4.12, 4.13). These findings indicate that dysregulation of *Cdkn2a*, *Cdkn2c*, and *Sctr* occurs already at the stage of adrenal medulla hyperplasia, early stage of PC tumorigenesis. Both *Cdkn2a*, *Cdkn2c* are members of Ink4 family of cyclin kinase inhibitors. The INK4 family members function only at G1 and serve as effectors of the G1 checkpoint. They bind to monomeric Cdk4 and Cdk6 but not to Cdk2, thereby precluding the association of these Cdks with cyclins D (Sherr and Roberts, 1999; Viglietto *et al.*, 2002a; Tessema *et al.*, 2004).

There are models which are generally consistent with the idea that CDK4 partitions between INK4 (p15(INK4B), p16(INK4A), p18(INK4C), p19(INK4D)) and Cip/Kip (p21(CIP1), p27(KIP1), and p57(KIP2))-bound states (McConnell *et al.*, 1999; Parry *et al.*, 1999; Sherr and Roberts, 1999). Increased amounts of INK4A proteins would alter the distribution of CDK4 in favour of INK4-CDK4 complexes and thereby reverse the normal sequestration of Cip/Kip proteins that occur during G<sub>1</sub> phase. The release of the Cip/Kip proteins from the latent pool can lead to cyclin E-CDK2 inhibition and to G<sub>1</sub>-phase arrest (Sherr and Roberts, 1999). Taking into account this model, one can assume that upregulation of *Cdkn2a*, and *Cdkn2c* is a compensatory reaction of PC cells in response to downregulation of *Cdkn1b*, a member of Cip/Kip family. It is

interesting to note that the increase of *Cdkn2a* expression observed in MENX-PCs was more prominent compared to that of *Cdkn2c* (Results, 4.3.2., Fig. 4.11, 4.12).

PC is a highly vascularized tumor (Hes *et al.*, 2003; Favier *et al.*, 2005; Dahia *et al.*, 2005a). The high expression of genes encoding angiogenic factors, such as vascular endothelial growth factor (VEGF) and its receptor VEGF-R1 are observed in PCs with VHL and SDH mutations (mutations of *SDHB* or *SDHD* genes) (Gimenez-Roqueplo *et al.*, 2001; Gimenez-Roqueplo *et al.*, 2002; Dahia *et al.*, 2005a). In this context it is interesting to note the role of *CDKN2A* in the regulation of glioma angiogenesis (Harada *et al.*, 1999). The authors found that reexpression of *CDKN2A* using the recombinant adenoviral vector Ad5CMVK- *CDKN2A* in *CDKN2A*-deleted glioma cells significantly reduce the expression of VEGF, which is thought to be a pivotal mediator of tumor angiogenesis. The study also showed *in vivo* that restoring wild-type *CDKN2A* expression into *CDKN2A*-deleted glioma cells markedly inhibit tumor neovascularization as compared with the effect of wild-type *TP53* (Harada *et al.*, 1999).

Another study demonstrated that *CDKN2A* overexpression suppress tumor cell invasion by an inhibition of matrix metalloproteinase 2 in glioma cells (Chintala *et al.*, 1997).

All these findings suggest that the anti-cancer effect of the tumor suppressor gene *CDKN2A* may be modulated by different factors, such as cell cycle arrest, growth inhibition, suppression of invasiveness, and inhibition of angiogenesis.

The levels of mRNA of *Sctr* in PC samples were also highly elevated: mRNA level was 13-57 times higher in tumor samples compared to normal medullary tissue of adrenal glands (Results, 4.3.2., Fig. 4.13). Secretin, the ligand for the secretin receptor (SCTR), exhibits pleiotropic functions in many different tissues, such as the gastrointestinal tract, heart, lung, kidney, adrenal gland, reproductive system. Secretin acts as a gastrointestinal hormone regulating exocrine secretion from the pancreas, gall bladder, and stomach, its role as a neuropeptide also was shown (Chu *et al.*, 2006). As a neuropeptide in the central nervous system secretin participates in neuronal signalling, behavioural modulation, as well as central-peripheral interactions (Chu *et al.*, 2006; Siu *et al.*, 2006). To carry out its functions secretin interacts specifically with SCTR, cell surface receptor (Siu *et al.*, 2006). SCTR is a member of guanine nucleotide-binding protein (G protein)-coupled receptor in the secretin/VIP/glucagons subfamily. The binding of secretin to its receptor triggers the activation of several signal transduction pathways, such as GTP- $G\alpha_s$  mediated cAMP/PKA signalling pathway and GTP- $G\alpha_q$  mediated DAG/IP<sub>3</sub> pathway which yields two signals including protein kinase C and inositol-1,4,5-triphosphate (IP<sub>3</sub>) (Sui *et al.*, 2006). In the PC12 cells, a rat catecholamine-secreting PC cell line derived from adrenal medulla, secretin was found to stimulate the catecholamine biosynthetic pathway by increasing the tyrosine hydroxylase activity via a PKA-dependent pathway (Wessels-Reiker *et al.*, 1993). Consistent

with this, Mahapatra *et al.* (2003) demonstrated an induction of up to 26% of the total catecholamine release from PC12 cells upon secretin administration. Secretin activates transcription of the major vesicular core protein chromogranin A (CgA) (Mahapatra *et al.*, 2003). CgA is now established to be a crucial regulatory switch, controlling dense-core secretory granule biogenesis and hormone secretion in endocrine cells. Its presence and absence can turn on and off, respectively, secretory granule formation in chromaffin and other endocrine cells (Kim *et al.*, 2001). The CgA is co-stored and co-released by exocytosis together with catecholamines from chromaffin granules of normal adrenal medulla (Takiyyuddin *et al.*, 1990a; Takiyyuddin *et al.*, 1990b) and PC (Hsiao *et al.*, 1990; Hsiao *et al.*, 1991; Ahlman, 2006). The measurement of plasma CgA is useful in the diagnosis of PC, and a markedly elevated CgA may suggest the diagnosis of malignant PC (Rao *et al.*, 2000). Moreover, Rao *et al.* (2000) showed that during chemotherapy of malignant PC, CgA can be used to gauge tumor response and relapse. Plasma concentration of CgA correlates with the secretory activity and tumor burden of PC (Hsiao *et al.*, 1990; Hsiao *et al.*, 1991; Rao *et al.*, 2000; Baudin *et al.*, 2001). Taking in account all of these findings one can assume that SCTR with its role in regulation of CgA transcription can be a useful and valuable marker in the diagnosis and treatment of PC.

In conclusion, most of the identified rat candidate regions localised on chromosomes 8 and 19 have synteny to human genome regions known to be involved in PC development. Candidate regions on rat chromosomes 3q42, 3q43, 19p14-p12, 19q12 are syntenic to human genomic loci which were shown to be highly affected in other endocrine tumors, such as thyroid carcinoma and pituitary adenoma. Overexpression of *Cdkn2a*, *Cdkn2c*, and *Sctr* also was shown in MENX-related PCs, confirming findings in adrenal medullary hyperplasia tissues. Validation of the role of these genes in the genesis and progression of PC will be performed in future. Identification of new genes in the candidate regions of MENX PCs also can shed light on mechanisms of molecular pathogenesis of neuroendocrine tumors, in particular PC.

## 6. SUMMARY

- PCs are rare tumors of the adrenal gland that arise from the chromaffin cells in the adrenal medulla. PCs are usually indolent tumors but have the potential to become malignant (10-20% of cases) and thereby difficult to treat. Currently it is not possible to identify patients at higher risk of progression toward a metastatic phenotype. Both familial (up to 30%) and sporadic forms of PC are recognized. At present the susceptibility genes known to predispose to PC development are *VHL*, *RET*, *NF1*, *SDHB* and *SDHD* genes. However, mutations of these genes can explain only a fraction of PCs, suggesting that other, still unknown, genes might be involved in the pathogenesis of PC. Elucidating the molecular mechanisms of PC development may help in both early diagnosis and predicting disease outcome.
- A rat model of the MEN-like syndrome (MENX syndrome), showing phenotypic overlap with both MEN1 and MEN2 human syndromes, was used in this study. MENX-affected rats carry a homozygous frameshift mutation in *Cdkn1b*, encoding the cyclin-dependent kinase inhibitor p27(KIP1), which was shown to be responsible for the development of the MENX syndrome. Advanced MENX-associated PCs arising in F2 hybrid MENX rats were analysed in the study. PC shows complete penetrance in MENX rats: adrenal medullary hyperplasia is already evident at 2 months of age and progresses to PC within six-twelve months.
- A set of methods, including genome-wide screen for LOH/AI in rat PC, CGH array, FISH analysis, Real Time TaqMan PCR, sequencing analysis of genes of the interest, was used to search for additional genetic lesions involved in the initiation and progression of MENX-related PCs. Genetic alterations identified in the rat tumors were compared *in silico* with literature data about chromosomal aberrations known to be involved in human PC pathogenesis.
- Genome-wide scan for LOH/AI of the MENX-PCs revealed candidate AI regions, mostly localised on the rat chromosomes 8 and 19: 8q11-q12, 8q22-q24, 8q24, 8q31-q32, 19p14-p12, 19q11, 19q12. In 2 out of 20 analysed PCs (10%), AI was observed at all informative loci of chromosome 8, suggesting the loss of one copy of chromosome 8. Partial deletion of chromosome 8 (8q22 locus) was confirmed in all LOH/AI cases with FISH analysis. The LOH/AI study revealed AI at informative loci of chromosome 19 in 30% of tumors (6 out of 20). The complete loss of one copy of chromosome 19 was found with FISH analysis in 3 out of 6 analysed tumors having an AI. The combined data of LOH/AI study and CGH array data analysis indicates the presence of deletion of the terminal part of 19q12 in 1 out of these 6 tumors.
- Additional candidate loci were determined with the CGH array. Copy number losses were more common than copy number gains, indicating that the inactivation of tumor suppressor

genes can play a critical role in PC tumorigenesis. The most frequent copy number losses were observed in 3q42, 3q43, 6q32-33, 15p14, 15p16, 18p13, 19p11 and 19q12 chromosomal regions. The highest percentage of copy number gains was detected at the 8q21 and Xq35 loci.

– Using rat-human synteny mapping the human loci corresponding to rat candidate chromosomal regions, found with the LOH/AI study and CGH array, were identified and their role in PC development considered. It was shown that in most cases rat candidate regions linked to the PC have a synteny to human chromosomal regions known to be involved in PC development:

- The highest percent of AI on rat chromosome 8 was observed at the locus 8q31-32, which is syntenic to 3q21.3-q24. The losses 3q12-qter, 3q22-q25 and 3q were reported frequently in human MEN2-associated, NF1-associated and sporadic PCs and paragangliomas (extra-adrenal PCs).
- Rat chromosomal regions 8q11-q12, 8q22-q24 are syntenic to 11q14.3-q22.3 and 11q22.3-q24.1 in the human genome, respectively. Losses of different loci of human 11q are reported in VHL-associated, sporadic adrenal and extra-adrenal PCs in humans.
- Human MEN2-related, VHL-related, sporadic PCs and extra-adrenal PCs are all recorded to have copy number losses and gains of different loci on chromosome 15, including locus 15q21.3-24.3, which has a synteny to the 8q24 rat chromosomal region we show to be affected by AI.
- Rat chromosomal region 19q11 (24.7-26.3 Mb), syntenic to the 19p13.13-p13.12 chromosomal region in the human genome, is one of the highly affected regions on the rat chromosome 19. AI was observed in 28% of analysed PCs. There are literature data showing 19p copy number gains in human MEN2A- and VHL-associated, sporadic PCs and head and neck paragangliomas.
- Rat chromosomal region 19q12 (53.9-56.9 Mb region) has a synteny to the human chromosome 1q42.13-42.3. Gain of 1q has been shown in human Nf1-related adrenal and extra-adrenal PCs. Losses of different loci of 1q, including 1q43.13-42.3 loci, were reported in abdominal paragangliomas and thyroid carcinomas in humans.
- Losses of 4q human chromosome corresponded to 19q11 (26.3-34.4 Mb) rat chromosome have been described in MEN2-associated and sporadic adrenal and extra-adrenal PCs.

Rat chromosomal loci 19p14-p12 and 19q12 (37.6-53.9 Mb) are highly affected in MENX-PCs and have a synteny to human 16q21 and 16q22.2-q24.3 loci, respectively. There is no direct evidence in the literature data showing involvement of 16q21 and 16q22.2-q24.3 chromosomal loci in PC tumorigenesis in humans, besides gain of 16q shown in abdominal paragangliomas in

one study. But there are genes mapped to the long arm of human chromosome 16, *FBX031*, *CDH1*, which can play a role in the regulation of p27(KIP1) level in the cell, or interact with p27(KIP1) through the different signal transduction mechanisms. Other genes, such as *SEN16*, the cadherin family genes (cadherins *CDH8*, *CDH11*, *CDH13*, and *CDH15*) which also reside on human 16q chromosome may play role in the initiation and progression of PC.

– The majority of chromosomal regions identified with the CGH array and demonstrating copy number changes with a high frequency (43-57%) have no clear syntenic regions in the human genome. But rat chromosomal regions, 3q42-q43 and 19q12 (58.9-59.2 Mb region), demonstrating copy number losses with high frequency, have a synteny to 20q11.21-q13.33 and 10p11.22-p11.21 in humans, respectively. Both chromosomes 10p11.22-p11.21 and 20q11.21-q13.33 are shown to be frequently affected in pituitary adenomas in humans. Interestingly, approximately 77% of MENX-affected rats also develop pituitary adenoma. Therefore, genes containing in the loci 10p11.22-p11.21 and 20q11.21-q13.33 may be involved in the development of neuroendocrine tumors.

– With microsatellite analysis we searched for LOH/AI for the rat homologs of genes known to predispose to PC development such as *Ret*, *Vhl*, *Nf1*, *Sdhd*, *Sdhb\_predicted* and candidate tumor suppressor genes, such as *Men1*, *Cdkn2b*, *Cdkn2a*, *Cdkn2c*, *Tp53*, *Rb1*, *Pten*. *Ptprf* and *Rassf1* genes also were analysed, because they are known to be involved in PC development. LOH/AI can be excluded in upstream and downstream regions of following genes *Men1*, *Cdkn2b*, *Cdkn2a*, *Cdkn2c*, *Ptprf*, *Sdhb\_predicted*, *Sdhd*, *Rassf1*, *Tp53*, *Nf1* and *Rb1*. Neither AI nor LOH were found for the *Pten* gene using intragenic microsatellite marker *RND1Lev1*.

– Copy number gains were revealed into the genes *Nf1* and *Ptprf* with the CGH array analysis in 14% (1 out of 7 analysed tumors) and 29% (2 out of 7 analysed tumors) PCs, respectively.

– Sequence analysis of two PC-related genes on chromosome 8, *Sdhd* and *Rassf1*, did not show any mutations. At the mRNA level the *Sdhd* and *Rassf1* genes were expressed at comparable levels in tumor and normal adrenal tissues.

– Overexpression of *Cdkn2a*, *Cdkn2c* and *Sctr* genes was detected with the Real Time TaqMan PCR. Taking into the account that both *Cdkn2a* and *Cdkn2c* are members of Ink4 family of cyclin kinase inhibitors and serve as effectors of the G1 checkpoint, one can assume that upregulation of *Cdkn2a* and *Cdkn2c* can be a compensatory reaction of PC cells in response to downregulation of *Cdkn1b*, a member of Cip/Kip family of cyclin kinase inhibitors.

Secretin, the ligand of SCTR, activates transcription of the major vesicular core protein CgA, which is known as one of the tumor marker in plasma for PC. There are data indicating that markedly elevated CgA may suggest the diagnosis of malignant PC and plasma concentration of CgA correlates with the secretory activity and tumor burden of PC. SCTR, with its role in

regulation of CgA transcription, may prove to be a useful and valuable marker in the diagnosis and treatment of PC.

– The high concordance between loci affected in rat and human PCs demonstrates that the MENX rat model is the unique genetic system for investigation of mechanisms of PC tumorigenesis.



## 6. ZUSAMMENFASSUNG

– PCs sind selten auftretende Tumore der Nebennierenrinde, welche sich aus den chromaffinen Zellen des Nebennierenmarks entwickeln. Etwa 10 – 20% der PCs sind maligne und dadurch schwer therapierbar. Gegenwärtig ist es nicht möglich, Patienten mit einem erhöhten Risiko im Hinblick auf die Entwicklung von Metastasen zu identifizieren. Für das PC existieren sowohl sporadische wie auch familiäre Formen, wobei letztere etwa 30% ausmachen. Zurzeit sind die Gene *VHL*, *RET*, *NF1*, *SDHB* und *SDHD* für die erbliche Prädisposition von PCs bekannt. Jedoch erklären Mutationen in diesen Genen nur teilweise das Auftreten von PCs, so dass die Existenz weiterer noch zu identifizierender Gene, die in deren Pathogenese involviert sind, impliziert. Durch die weitere Aufklärung der molekularen Mechanismen der Pathogenese von PC erhofft man sich damit, eine bessere diagnostische wie auch prognostische Charakterisierung der klinischen Fälle zu erreichen.

– In der hier vorgelegten Arbeit wurde das Rattenmodell mit dem MEN-ähnlichen Syndrom (MENX-Syndrom) verwendet. Der Phänotyp überlappt hierbei mit beiden im Menschen auftretenden Syndromen, MEN1 und MEN2. MENX-Ratten tragen eine homozygote Leserasterverschiebung im *Cdkn1b* Gen, welches für den cyclin-abhängigen Kinaseinhibitor p27(KIP1) codiert. Es konnte bereits gezeigt werden, dass diese Mutation für die Entstehung des MENX-Syndroms verantwortlich ist. Fortgeschrittene MENX-assoziierte PCs, welche in der F2 Rückkreuzungs-Generation von MENX Ratten entstehen, wurden in dieser Arbeit analysiert. PC zeigt dabei eine vollständige Penetranz in MENX Ratten: die Hyperplasie des Nebennierenmarks ist bereits in Zweimonatstieren evident und entwickelt sich zu einem PC innerhalb von 6 bis 12 Monaten.

– Genetische Veränderungen, die bei der Entstehung und im Verlauf von MENX-assoziiierter PCs involviert sind, wurden durch einen Genom-weitern Screen nach LOH/AI, CGH-Array, FISH Analyse, Real Time TaqMan PCR sowie die Sequenzierung von interessanten Genen bestimmt. Anschließend wurden die in dieser Arbeit identifizierten genetischen Veränderungen in Rattentumoren *in silico* mit in der Literatur beschriebenen Chromosomenaberrationen bei humanen PCs verglichen.

– Der Genom-weite Screen nach LOH/AI in MENX-Tumoren resultierte in potentiellen Abschnitten allelischen Ungleichgewichtes, welche vor allem auf den Rattenchromosomen 8 und 19 lokalisiert sind: 8q11-q12, 8q22-q24, 8q24, 8q31-q32 und 19p14-p12, 19q11, 19q12. In 2 von 20 analysierten PCs (10%) wurde das AI in allen informativen Loci auf Chromosom 8 gefunden. Dies legt den Verlust einer Kopie des gesamten Chromosoms 8 nahe. Verlust von Teilen des Chromosoms 8 konnte in allen LOH/AI positiven Fällen durch FISH Analyse am Locus 8q22

bestätigt werden. Weiterhin zeigte der Screen das Auftreten von AI in informativen Loci des Chromosoms 19 in 30% der Tumore (6 von 20 Fällen). Der vollständige Verlust einer Kopie des Chromosoms 19 konnte ebenfalls durch die Anwendung der FISH Analyse in 3 von diesen 6 Fällen bestätigt werden. Die Kombination der Daten der LOH/AI Studie mit denen des CGH-Array weist auf den Verlust des terminalen Teils von 19q12 in einem von diesen 6 Fällen hin.

– Die Anwendung des CGH-Arrays führte zur Identifizierung weiterer potentieller Loci. Dabei waren Verluste der Kopienzahl häufiger als deren Zunahme, welche auf eine Inaktivierung von Tumorsuppressorgenen in der Tumorgenese von PCs hindeuteten. Die häufigsten Kopienzahlverluste traten in den chromosomalen Regionen 3q42, 3q43, 6q32-33, 15p14, 15p16, 18p13, 19p11 und 19q12 auf. Der höchste Anteil in der Zunahme der Kopienzahl wurde in den Loci 8q21 und Xq35 detektiert.

– Durch das Mapping der Syntänie zwischen den Genomen der Ratte und des Menschen wurden die korrespondierenden humanen Loci der im Rattenmodell veränderten Loci identifiziert und deren mögliche Rolle in der Entwicklung von PCs näher untersucht. Das Resultat der Literaturrecherche zeigte, dass in den meisten Fällen die Kandidatenregionen der Ratte eine syntäne Region im humanen Genom aufweisen, welche ebenfalls in die Entwicklung von PCs involviert ist.

- Der höchste Anteil des AI des Chromosoms 8 der Ratte wurde für den Lokus 8q31-32 gefunden, welcher syntänisch zu 3q21.3-q24 ist. Die Verluste von 3q12-qter, 3q22-q25 und 3q wurden häufig bei humanen MEN 2-Syndrom-assoziierten, NF1-assoziierten und sporadischen PCs als auch in Paragangliomen (extra-adrenale PCs) gefunden.
- Die chromosomalen Regionen 8q11-q12 und 8q22-q24 der Ratte sind syntän zu 11q14.3-q22.3 und 11q22.3-q24.1 des Menschen. Verluste von verschiedenen Loci im humanen 11q sind in VHL-assoziierten, sporadischen PCs und extra adrenalen PCs beschrieben.
- Für humane MEN2-assoziierte, VHL-assoziierte, sporadische PCs und extra adrenale PCs wurden Verluste als auch Zunahmen der Kopienzahl für verschiedene Loci auf Chromosom 15 beschrieben. Einer dieser Loci 15q21.3-24.3 ist syntänisch zu 8q24 der Ratte, für welchen in dieser Arbeit ein AI gefunden wurde.
- Als am stärksten betroffener Bereich des Chromosoms 19 der Ratte wurde die Region 19q11 (24.7-26.3 Mb) identifiziert. Diese ist syntän zu den humanen Abschnitten 19p13.13-p13.12. AI wurde für 28% der analysierten PCs gefunden. In der Literatur wurden für humane MEN 2A-Syndrom-assoziierte, VHL-assoziierte, sporadischen PCs und auch in verschiedenen Paragangliomen (Kopf und Hals) eine Zunahme der Kopienzahl für 19p beschrieben.

- Die chromosomale Region 19q12 (53.9-56.9 Mb) der Ratte weist eine Syntänie zur humanen Region 1q42.13-42.3 auf. Zunahmen der Kopienzahl in 1q wurden für humane NF1-assoziierte adrenale und extra adrenale PCs gefunden. Verluste in der Kopienzahl in verschiedenen Loci von 1q, welche auch die Loci 1q43.13-42.3 beinhalten, wurden in abdominalen Paragangliomen und in Schilddrüsentumoren beschrieben.
- Verluste in der Kopienzahl des humanen Chromosoms 4q, welche eine Syntänie zur 19q11 (26.3-34.4 Mb) Region des Chromosoms der Ratte aufweisen, konnten in MEN2-assoziierten, sporadischen adrenalen und extra adrenalen PCs nachgewiesen werden.

Die chromosomalen Loci 19p14-p12 und 19q12 (37.6-53.9 Mb) der Ratte zeigen starke Veränderungen in MENX-PCs. Veränderungen der im humanen Genom syntänischen Loci 16q21 und 16q22.2-q24.3 wurden, neben einer Studie, die eine Zunahme der Kopienzahl in 16q in abdominalen Paragangliomen zeigte, bis jetzt nicht in der Tumorgenese von PCs in der Literatur beschrieben. Jedoch wurden die Gene *FBX031* und *CDH1* auf dem langen Arm des Chromosoms 16 kartiert, deren Proteinprodukte das zelluläre Level von p27(KIP1) regulieren können oder durch verschiedene Signaltransduktionswege mit p27(KIP1) interagieren können. Weitere Gene, wie *SEN16* und Mitglieder der Cadherin Familie (cadherins *CDH8*, *CDH11*, *CDH13*, und *CDH15*), welche ebenfalls auf dem Chromosom 16q lokalisiert, sind könnten eine Rolle bei der Entstehung und im Verlauf von PCs spielen.

– Die Mehrheit der durch CGH-Array identifizierten chromosomalen Regionen, welche eine Kopienzahlveränderung mit einer hohen Häufigkeit von 43-57% zeigten, weisen keine offensichtliche Syntänie mit dem humanen Genom auf. Allerdings weisen die chromosomalen Regionen 3q42-q43 und 19q12 (58.9-59.2 Mb) der Ratte, die eine hohe Häufigkeit für den Verlust der Kopienzahl zeigten, eine Syntänie zu 10p11.22-p11.21 und 20q11.21-q13.33 des Menschen auf. Beide Chromosomen 10p11.22-p11.21 und 20q11.21-q13.33 zeigen häufig eine Veränderung bei Hypophysenadenomen. Interessant hierbei ist die Tatsache, dass ca. 77% alle MENX-Ratten ebenfalls Hypophysen-adenome entwickeln. Demzufolge könnten Gene, welche in diesen Loci lokalisiert sind, an der Entwicklung von neuroendokrinen Tumoren beteiligt sein.

– Mit Hilfe der Mikrosatellitenanalyse wurden die in der Ratte homologen Gene auf LOH/AI untersucht, welche als prädisponierend für PCs bekannt sind (*Ret*, *Vhl*, *Nf1*, *Sdhd*, *Sdhd\_predicted*), als auch potentielle Tumorsuppressorgene, wie *Men1*, *Cdkn2b*, *Cdkn2a*, *Cdkn2c*, *Tp53*, *Rb1*, *Pten*. Weiterhin wurden *Ptprf* und *Rassf1* analysiert, da diese in der Entwicklung von PCs beteiligt sind. Für folgende Gene kann in den *upstream* und *downstream* gelegenen Bereichen ein LOH/AI ausgeschlossen werden: *Men1*, *Cdkn2b*, *Cdkn2a*, *Cdkn2c*, *Ptprf*, *Sdhd\_predicted*, *Sdhd*, *Rassf1*, *Tp53*, *Nf1* und *Rb1*. Ebenfalls wurde keine LOH/AI innerhalb des Gens *Pten* mit dem Mikrosatellitenmarker *RND1Lev1* gefunden.

- Eine Zunahme in der Kopienzahl wurde mit Hilfe des CGH-Arrays für das Gen *Nf1* mit 14% (1 von 7 Fällen) und für *Ptprf* mit 29% (2 von 7 Fällen) nach-gewiesen.
- Die Sequenzanalyse von zwei PC-assozierten Genen auf Chromosom 8, *Sdhd* und *Rassf1*, wies keine Mutationen auf. Ebenfalls auf der mRNA Ebene war die Menge an mRNAs für beide Gene in Tumorgewebe mit der im gesunden Nebennierengewebe vergleichbar.
- Durch Anwendung der Real Time TaqMan PCR wurde die Überexpression von *Cdkn2a*, *Cdkn2c* und *Sctr* detektiert. Unter Berücksichtigung, dass beide *Cdkn2a* und *Cdkn2c* Mitglieder der Ink4 Familie der Cyclinkinase-Inhibitoren sind und als Effektoren im G1 Kontrollpunkt fungieren, kann man annehmen, dass die Hochregulation dieser beiden Proteine eine kompensatorische Reaktion auf die Herunterregulation von *Cdkn1b*, als Mitglied der Cip/Kip Familie der Cyclinkinase-Inhibitoren, darstellt.

Sekretin (der Ligand für SCTR) aktiviert die Transkription von CgA, welches als einer der Tumormarker im Blutplasma von PCs bekannt ist. Ein merklich erhöhter Spiegel an CgA deutet auf eine positive Diagnose für maligne PCs hin. Ebenfalls korreliert die Blutplasmakonzentration von CgA mit der sekretorischen Aktivität und der Tumorgröße von PCs. Deswegen könnte sich SCTR in seiner Funktion als Regulator der CgA Transkription als wertvoller und nützlicher Marker in der Diagnostik und der Therapie von PCs erweisen.

- Zusammenfassend lässt sich sagen, dass die hohe Übereinstimmung der veränderten Loci in PCs von Menschen und Ratten klar die Anwendbarkeit des MENX Rattenmodells als einzigartiges genetisches System für die Untersuchung der zugrunde liegenden Mechanismen der PC Tumorgenese demonstriert.

## 7. REFERENCES

- Aarts M, Dannenberg H, deLeeuw RJ, van Nederveen FH, Verhofstad AA, Lenders JW *et al* (2006). Microarray-based CGH of sporadic and syndrome-related pheochromocytomas using a 0.1-0.2 Mb bacterial artificial chromosome array spanning chromosome arm 1p. *Genes Chromosomes Cancer* **45**: 83-93.
- Abate-Shen C, Shen MM (2000). Molecular genetics of prostate cancer. *Genes Dev* **14**: 2410-34.
- Aguiar RC, Dahia PL, Sill H, Toledo SP, Goldman JM, Cross NC (1996). Deletion analysis of the p16 tumour suppressor gene in phaeochromocytomas. *Clin Endocrinol (Oxf)* **45**: 93-6.
- Aguiar RC, Cox G, Pomeroy SL, Dahia PL (2001). Analysis of the SDHD gene, the susceptibility gene for familial paraganglioma syndrome (PGL1), in pheochromocytomas. *J Clin Endocrinol Metab* **86**: 2890-4.
- Ahlman H (2006). Malignant pheochromocytoma: state of the field with future projections. *Ann N Y Acad Sci* **1073**: 449-64.
- Amar L, Bertherat J, Baudin E, Ajzenberg C, Bressac-de Paillerets B, Chabre O *et al* (2005). Genetic testing in pheochromocytoma or functional paraganglioma. *J Clin Oncol* **23**: 8812-8.
- Amfo K, Neyns B, Teugels E, Lissens W, Bourgain C, De Sutter P *et al* (1995). Frequent deletion of chromosome 19 and a rare rearrangement of 19p13.3 involving the insulin receptor gene in human ovarian cancer. *Oncogene* **11**: 351-8.
- Anisimov VN, Ukraintseva SV, Yashin AI (2005). Cancer in rodents: does it tell us about cancer in humans? *Nat Rev Cancer* **5**: 807-19.
- Astuti D, Latif F, Dallol A, Dahia PL, Douglas F, George E *et al* (2001a). Gene mutations in the succinate dehydrogenase subunit SDHB cause susceptibility to familial pheochromocytoma and to familial paraganglioma. *Am J Hum Genet* **69**: 49-54.
- Astuti D, Douglas F, Lennard TW, Aligianis IA, Woodward ER, Evans DG *et al* (2001b). Germline SDHD mutation in familial phaeochromocytoma. *Lancet* **357**: 1181-2.
- Astuti D, Agathangelou A, Honorio S, Dallol A, Martinsson T, Kogner P *et al* (2001c). RASSF1A promoter region CpG island hypermethylation in phaeochromocytomas and neuroblastoma tumours. *Oncogene* **20**: 7573-7.
- Badenhop RF, Cherian S, Lord RS, Baysal BE, Taschner PE, Schofield PR (2001). Novel mutations in the SDHD gene in pedigrees with familial carotid body paraganglioma and sensorineural hearing loss. *Genes Chromosomes Cancer* **31**: 255-63.
- Baldassarre G, Belletti B, Bruni P, Boccia A, Trapasso F, Pentimalli F *et al* (1999). Overexpressed cyclin D3 contributes to retaining the growth inhibitor p27 in the cytoplasm of thyroid tumor cells. *J Clin Invest* **104**: 865-74.
- Bando K, Nagai H, Matsumoto S, Koyama M, Kawamura N, Tajiri T *et al* (2000). Identification of a 1-Mb common region at 16q24.1-24.2 deleted in hepatocellular carcinoma. *Genes Chromosomes Cancer* **28**: 38-44.
- Bashir T, Dorrello NV, Amador V, Guardavaccaro D, Pagano M (2004). Control of the SCF(Skp2-Cks1) ubiquitin ligase by the APC/C(Cdh1) ubiquitin ligase. *Nature* **428**: 190-3.
- Baudin E, Bidart JM, Bachelot A, Ducreux M, Elias D, Ruffie P *et al* (2001). Impact of chromogranin A measurement in the work-up of neuroendocrine tumors. *Ann Oncol* **12 Suppl 2**: S79-82.

- Bausch B, Neumann H, The European-American Paranglioma Study Group (2006a). OR4-21: molecular genetic analysis of the NF1 gene in neurofibromatosis associated-pheochromocytoma. *J Exp Clin Endocrinol Diabetes* **114**: 7
- Bausch B, Borozdin W, Neumann HP (2006b). Clinical and genetic characteristics of patients with neurofibromatosis type 1 and pheochromocytoma. *N Engl J Med* **354**: 2729-31.
- Bausch B, Koschker AC, Fassnacht M, Stoevesandt J, Hoffmann MM, Eng C *et al* (2006c). Comprehensive mutation scanning of NF1 in apparently sporadic cases of pheochromocytoma. *J Clin Endocrinol Metab* **91**: 3478-81.
- Bausch B, Borozdin W, Mautner VF, Hoffmann MM, Boehm D, Robledo M *et al* (2007). Germline NF1 mutational spectra and loss-of-heterozygosity analyses in patients with pheochromocytoma and neurofibromatosis type 1. *J Clin Endocrinol Metab* **92**: 2784-92.
- Baysal BE, Ferrell RE, Willett-Brozick JE, Lawrence EC, Myssiorek D, Bosch A *et al* (2000). Mutations in SDHD, a mitochondrial complex II gene, in hereditary paraganglioma. *Science* **287**: 848-51.
- Baysal BE, Willett-Brozick JE, Lawrence EC, Drovdic CM, Savul SA, McLeod DR *et al* (2002). Prevalence of SDHB, SDHC, and SDHD germline mutations in clinic patients with head and neck paragangliomas. *J Med Genet* **39**: 178-83.
- Baysal BE, Willett-Brozick JE, Filho PA, Lawrence EC, Myers EN, Ferrell RE (2004). An Alu-mediated partial SDHC deletion causes familial and sporadic paraganglioma. *J Med Genet* **41**: 703-9.
- Beatty B., Mai S. & Squire, J., eds. (2002) FISH: A Practical Approach Oxford Univ. Press, Oxford.
- Becker KF, Atkinson MJ, Reich U, Becker I, Nekarda H, Siewert JR *et al* (1994). E-cadherin gene mutations provide clues to diffuse type gastric carcinomas. *Cancer Res* **54**: 3845-52.
- Becker KF, Hofler H (1995). Frequent somatic allelic inactivation of the E-cadherin gene in gastric carcinomas. *J Natl Cancer Inst* **87**: 1082-4.
- Bender BU, Gutsche M, Glasker S, Muller B, Kirste G, Eng C *et al* (2000). Differential genetic alterations in von Hippel-Lindau syndrome-associated and sporadic pheochromocytomas. *J Clin Endocrinol Metab* **85**: 4568-74.
- Benn DE, Dwight T, Richardson AL, Delbridge L, Bambach CP, Stowasser M *et al* (2000). Sporadic and familial pheochromocytomas are associated with loss of at least two discrete intervals on chromosome 1p. *Cancer Res* **60**: 7048-51.
- Benn DE, Crosson MS, Tucker K, Bambach CP, Richardson AL, Delbridge L *et al* (2003). Novel succinate dehydrogenase subunit B (SDHB) mutations in familial phaeochromocytomas and paragangliomas, but an absence of somatic SDHB mutations in sporadic phaeochromocytomas. *Oncogene* **22**: 1358-64.
- Benn DE, Gimenez-Roqueplo AP, Reilly JR, Bertherat J, Burgess J, Byth K *et al* (2006). Clinical presentation and penetrance of pheochromocytoma/paraganglioma syndromes. *J Clin Endocrinol Metab* **91**: 827-36.
- Besson A, Gurian-West M, Schmidt A, Hall A, Roberts JM (2004). p27Kip1 modulates cell migration through the regulation of RhoA activation. *Genes Dev* **18**: 862-76.
- Blagosklonny MV (2002). Are p27 and p21 cytoplasmic oncoproteins? *Cell Cycle* **1**: 391-3.

- Blanes A, Sanchez-Carrillo JJ, Diaz-Cano SJ (2006). Topographic molecular profile of pheochromocytomas: role of somatic down-regulation of mismatch repair. *J Clin Endocrinol Metab* **91**: 1150-8.
- Boehm M, Yoshimoto T, Crook MF, Nallamshetty S, True A, Nabel GJ *et al* (2002). A growth factor-dependent nuclear kinase phosphorylates p27(Kip1) and regulates cell cycle progression. *EMBO J* **21**: 3390-401.
- Brauch H, Hoepfner W, Jahnig H, Wohl T, Engelhardt D, Spelsberg F *et al* (1997). Sporadic pheochromocytomas are rarely associated with germline mutations in the vhl tumor suppressor gene or the ret protooncogene. *J Clin Endocrinol Metab* **82**: 4101-4.
- Braungart E, Schumacher C, Hartmann E, Nekarda H, Becker KF, Hofler H *et al* (1999). Functional loss of E-cadherin and cadherin-11 alleles on chromosome 16q22 in colonic cancer. *J Pathol* **187**: 530-4.
- Bryant J, Farmer J, Kessler LJ, Townsend RR, Nathanson KL (2003). Pheochromocytoma: the expanding genetic differential diagnosis. *J Natl Cancer Inst* **95**: 1196-204.
- Carrano AC, Eytan E, Hershko A, Pagano M (1999). SKP2 is required for ubiquitin-mediated degradation of the CDK inhibitor p27. *Nat Cell Biol* **1**: 193-9.
- Callen DF, Crawford J, Derwas C, Cleton-Jansen AM, Cornelisse CJ, Baker E (2002). Defining regions of loss of heterozygosity of 16q in breast cancer cell lines. *Cancer Genet Cytogenet* **133**: 76-82.
- Cardoso J, Molenaar L, de Menezes RX, Rosenberg C, Morreau H, Moslein G *et al* (2004). Genomic profiling by DNA amplification of laser capture microdissected tissues and array CGH. *Nucleic Acids Res* **32**: e146.
- Cascón A, Ruiz-Llorente S, Cebrian A, Telleria D, Rivero JC, Diez JJ *et al* (2002). Identification of novel SDHD mutations in patients with pheochromocytoma and/or paraganglioma. *Eur J Hum Genet* **10**: 457-61.
- Cascón A, Ruiz-Llorente S, Rodriguez-Perales S, Honrado E, Martinez-Ramirez A, Leton R *et al* (2005). A novel candidate region linked to development of both pheochromocytoma and head/neck paraganglioma. *Genes Chromosomes Cancer* **42**: 260-8.
- Castilla-Guerra L, Moreno AM, Fernandez-Moreno MC, Utrilla JC, Fernandez E, Galera-Davison H (1997). Expression and prognostic value of c-erbB-2 oncogene product in human pheochromocytomas. *Histopathology* **31**: 144-9.
- Ciaparrone M, Yamamoto H, Yao Y, Sgambato A, Cattoretti G, Tomita N *et al* (1998). Localization and expression of p27KIP1 in multistage colorectal carcinogenesis. *Cancer Res* **58**: 114-22.
- Chalmers IJ, Aubele M, Hartmann E, Braungart E, Werner M, Hofler H *et al* (2001). Mapping the chromosome 16 cadherin gene cluster to a minimal deleted region in ductal breast cancer. *Cancer Genet Cytogenet* **126**: 39-44.
- Chandel NS, McClintock DS, Feliciano CE, Wood TM, Melendez JA, Rodriguez AM *et al* (2000). Reactive oxygen species generated at mitochondrial complex III stabilize hypoxia-inducible factor-1 $\alpha$  during hypoxia: a mechanism of O<sub>2</sub> sensing. *J Biol Chem* **275**: 25130-8.
- Chandrasekharappa SC, Guru SC, Manickam P, Olufemi SE, Collins FS, Emmert-Buck MR *et al* (1997). Positional cloning of the gene for multiple endocrine neoplasia-type 1. *Science* **276**: 404-7.
- Chetty R, Pillay P, Jaichand V (1998). Cytokeratin expression in adrenal pheochromocytomas and extra-adrenal paragangliomas. *J Clin Pathol* **51**: 477-8.

- Chu JY, Yung WH, Chow BK (2006). Secretin: a pleiotrophic hormone. *Ann N Y Acad Sci* **1070**: 27-50.
- Cleton-Jansen AM, Callen DF, Seshadri R, Goldup S, McCallum B, Crawford J *et al* (2001). Loss of heterozygosity mapping at chromosome arm 16q in 712 breast tumors reveals factors that influence delineation of candidate regions. *Cancer Res* **61**: 1171-7.
- Chintala SK, Fueyo J, Gomez-Manzano C, Venkaiah B, Bjerkvig R, Yung WK *et al* (1997). Adenovirus-mediated p16/CDKN2 gene transfer suppresses glioma invasion in vitro. *Oncogene* **15**: 2049-57.
- Clifford SC, Cockman ME, Smallwood AC, Mole DR, Woodward ER, Maxwell PH *et al* (2001). Contrasting effects on HIF-1alpha regulation by disease-causing pVHL mutations correlate with patterns of tumorigenesis in von Hippel-Lindau disease. *Hum Mol Genet* **10**: 1029-38.
- Collard JG (2004). Cancer: Kip moving. *Nature* **428**: 705-8.
- Crossey PA, Foster K, Richards FM, Phipps ME, Latif F, Tory K *et al* (1994). Molecular genetic investigations of the mechanism of tumorigenesis in von Hippel-Lindau disease: analysis of allele loss in VHL tumours. *Hum Genet* **93**: 53-8.
- Dammann R, Schagdarsurengin U, Seidel C, Trumpler C, Hoang-Vu C, Gimm O *et al* (2005). Frequent promoter methylation of tumor-related genes in sporadic and MEN2-associated pheochromocytomas. *Exp Clin Endocrinol Diabetes* **113**: 1-7.
- Dahia PL, Aguiar RC, Tsanaclis AM, Bendit I, Bydlowski SP, Abelin NM *et al* (1995). Molecular and immunohistochemical analysis of P53 in pheochromocytoma. *Br J Cancer* **72**: 1211-3.
- Dahia PL, Aguiar RC, Honegger J, Fahlbush R, Jordan S, Lowe DG *et al* (1998). Mutation and expression analysis of the p27/kip1 gene in corticotrophin-secreting tumours. *Oncogene* **16**: 69-76.
- Dahia PL, Ross KN, Wright ME, Hayashida CY, Santagata S, Barontini M *et al* (2005a). A HIF1alpha regulatory loop links hypoxia and mitochondrial signals in pheochromocytomas. *PLoS Genet* **1**: 72-80.
- Dahia PL, Hao K, Rogus J, Colin C, Pujana MA, Ross K *et al* (2005b). Novel pheochromocytoma susceptibility loci identified by integrative genomics. *Cancer Res* **65**: 9651-8.
- Dannenberg H, Speel EJ, Zhao J, Saremaslani P, van Der Harst E, Roth J *et al* (2000). Losses of chromosomes 1p and 3q are early genetic events in the development of sporadic pheochromocytomas. *Am J Pathol* **157**: 353-9.
- Dannenberg H, Komminoth P, Dinjens WN, Speel EJ, de Krijger RR (2003). Molecular genetic alterations in adrenal and extra-adrenal pheochromocytomas and paragangliomas. *Endocr Pathol* **14**: 329-50.
- De Krijger RR, van der Harst E, van der Ham F, Stijnen T, Dinjens WN, Koper JW *et al* (1999). Prognostic value of p53, bcl-2, and c-erbB-2 protein expression in pheochromocytomas. *J Pathol* **188**: 51-5.
- De Krijger RR, van der Harst E, Muletta-Feurer S, Bruining HA, Lamberts SW, Dinjens WN *et al* (2000). RET is expressed but not mutated in extra-adrenal paragangliomas. *J Pathol* **191**: 264-8.
- Diaz-Cano SJ, de Miguel M, Blanes A, Tashjian R, Galera H, Wolfe HJ (2000). Clonal patterns in pheochromocytomas and MEN-2A adrenal medullary hyperplasias: histological and kinetic correlates. *J Pathol* **192**: 221-8.
- Dluhy RG (2002). Pheochromocytoma - death of an axiom. *N Engl J Med* **346**: 1486-8.



- Edström E, Frisk T, Farnebo F, Hoog A, Backdahl M, Larsson C (2000a). Expression analysis of RET and the GDNF/GFRalpha-1 and NTN/GFRalpha-2 ligand complexes in pheochromocytomas and paragangliomas. *Int J Mol Med* **6**: 469-74.
- Edström E, Mahlamaki E, Nord B, Kjellman M, Karhu R, Hoog A *et al* (2000b). Comparative genomic hybridization reveals frequent losses of chromosomes 1p and 3q in pheochromocytomas and abdominal paragangliomas, suggesting a common genetic etiology. *Am J Pathol* **156**: 651-9.
- Eisenhofer G, Huynh TT, Pacak K, Brouwers FM, Walther MM, Linehan WM *et al* (2004a). Distinct gene expression profiles in norepinephrine- and epinephrine-producing hereditary and sporadic pheochromocytomas: activation of hypoxia-driven angiogenic pathways in von Hippel-Lindau syndrome. *Endocr Relat Cancer* **11**: 897-911.
- Eisenhofer G, Bornstein SR, Brouwers FM, Cheung NK, Dahia PL, de Krijger RR *et al* (2004b). Malignant pheochromocytoma: current status and initiatives for future progress. *Endocr Relat Cancer* **11**: 423-36.
- Eng C, Crossey PA, Mulligan LM, Healey CS, Houghton C, Prowse A *et al* (1995). Mutations in the RET proto-oncogene and the von Hippel-Lindau disease tumour suppressor gene in sporadic and syndromic pheochromocytomas. *J Med Genet* **32**: 934-7.
- Eng C (1996). Seminars in medicine of the Beth Israel Hospital, Boston. The RET proto-oncogene in multiple endocrine neoplasia type 2 and Hirschsprung's disease. *N Engl J Med* **335**: 943-51.
- Eng C, Kiuru M, Fernandez MJ, Aaltonen LA (2003). A role for mitochondrial enzymes in inherited neoplasia and beyond. *Nat Rev Cancer* **3**: 193-202.
- Erlanson M, Portin C, Linderholm B, Lindh J, Roos G, Landberg G (1998). Expression of cyclin E and the cyclin-dependent kinase inhibitor p27 in malignant lymphomas-prognostic implications. *Blood* **92**: 770-7.
- Esposito V, Baldi A, De Luca A, Groger AM, Loda M, Giordano GG *et al* (1997). Prognostic role of the cyclin-dependent kinase inhibitor p27 in non-small cell lung cancer. *Cancer Res* **57**: 3381-5.
- Estus S, Zaks WJ, Freeman RS, Gruda M, Bravo R, Johnson EM, Jr. (1994). Altered gene expression in neurons during programmed cell death: identification of c-jun as necessary for neuronal apoptosis. *J Cell Biol* **127**: 1717-27.
- Fan X, Paetau A, Aalto Y, Valimaki M, Sane T, Poranen A *et al* (2001). Gain of chromosome 3 and loss of 13q are frequent alterations in pituitary adenomas. *Cancer Genet Cytogenet* **128**: 97-103.
- Favier J, Briere JJ, Stropf L, Amar L, Filali M, Jeunemaitre X *et al* (2005). Hereditary paraganglioma/pheochromocytoma and inherited succinate dehydrogenase deficiency. *Horm Res* **63**: 171-9.
- Feng L, Yunoue S, Tokuo H, Ozawa T, Zhang D, Patrakitkomjorn S *et al* (2004). PKA phosphorylation and 14-3-3 interaction regulate the function of neurofibromatosis type I tumor suppressor, neurofibromin. *FEBS Lett* **557**: 275-82.
- Fero ML, Randel E, Gurley KE, Roberts JM, Kemp CJ (1998). The murine gene p27Kip1 is haplo-insufficient for tumour suppression. *Nature* **396**: 177-80.
- Forsti A, Luo L, Vorechovsky I, Soderberg M, Lichtenstein P, Hemminki K (2001). Allelic imbalance on chromosomes 13 and 17 and mutation analysis of BRCA1 and BRCA2 genes in monozygotic twins concordant for breast cancer. *Carcinogenesis* **22**: 27-33.

- Franklin DS, Godfrey VL, O'Brien DA, Deng C, Xiong Y (2000). Functional collaboration between different cyclin-dependent kinase inhibitors suppresses tumor growth with distinct tissue specificity. *Mol Cell Biol* **20**: 6147-58.
- Fritz A, Walch A, Piotrowska K, Rosemann M, Schaffer E, Weber K *et al* (2002). Recessive transmission of a multiple endocrine neoplasia syndrome in the rat. *Cancer Res* **62**: 3048-51.
- Georgitsi M, Raitila A, Karhu A, van der Luijt RB, Aalfs CM, Sane T *et al* (2007). Germline CDKN1B/p27Kip1 mutation in multiple endocrine neoplasia. *J Clin Endocrinol Metab* **92**: 3321-5.
- Gerald D, Berra E, Frapart YM, Chan DA, Giaccia AJ, Mansuy D *et al* (2004). JunD reduces tumor angiogenesis by protecting cells from oxidative stress. *Cell* **118**: 781-94.
- Gimenez-Roqueplo AP, Favier J, Rustin P, Mourad JJ, Plouin PF, Corvol P *et al* (2001). The R22X mutation of the SDHD gene in hereditary paraganglioma abolishes the enzymatic activity of complex II in the mitochondrial respiratory chain and activates the hypoxia pathway. *Am J Hum Genet* **69**: 1186-97.
- Gimenez-Roqueplo AP, Favier J, Rustin P, Rieubland C, Kerlan V, Plouin PF *et al* (2002). Functional consequences of a SDHB gene mutation in an apparently sporadic pheochromocytoma. *J Clin Endocrinol Metab* **87**: 4771-4.
- Gimenez-Roqueplo AP, Favier J, Rustin P, Rieubland C, Crespin M, Nau V *et al* (2003). Mutations in the SDHB gene are associated with extra-adrenal and/or malignant pheochromocytomas. *Cancer Res* **63**: 5615-21.
- Gimenez-Roqueplo AP (2006). New advances in the genetics of pheochromocytoma and paraganglioma syndromes. *Ann N Y Acad Sci* **1073**: 112-21.
- Gimm O, Armanios M, Dziema H, Neumann HP, Eng C (2000). Somatic and occult germ-line mutations in SDHD, a mitochondrial complex II gene, in nonfamilial pheochromocytoma. *Cancer Res* **60**: 6822-5.
- Gumbiner BM (1996). Cell adhesion: the molecular basis of tissue architecture and morphogenesis. *Cell* **84**: 345-57.
- Callen DF, Crawford J, Derwas C, Cleton-Jansen AM, Cornelisse CJ, Baker E (2002). Defining regions of loss of heterozygosity of 16q in breast cancer cell lines. *Cancer Genet Cytogenet* **133**: 76-82.
- Clifford SC, Prowse AH, Affara NA, Buys CH, Maher ER (1998). Inactivation of the von Hippel-Lindau (VHL) tumour suppressor gene and allelic losses at chromosome arm 3p in primary renal cell carcinoma: evidence for a VHL-independent pathway in clear cell renal tumourigenesis. *Genes Chromosomes Cancer* **22**: 200-9.
- Godfrey TE, Cher ML, Chhabra V, Jensen RH (1997). Allelic imbalance mapping of chromosome 16 shows two regions of common deletion in prostate adenocarcinoma. *Cancer Genet Cytogenet* **98**: 36-42.
- Gottlieb E, Tomlinson IP (2005). Mitochondrial tumour suppressors: a genetic and biochemical update. *Nat Rev Cancer* **5**: 857-66.
- Gratias S, Rieder H, Ullmann R, Klein-Hitpass L, Schneider S, Boloni R *et al* (2007). Allelic loss in a minimal region on chromosome 16q24 is associated with vitreous seeding of retinoblastoma. *Cancer Res* **67**: 408-16.
- Gupta D, Shidham V, Holden J, Layfield L (2000). Prognostic value of immunohistochemical expression of topoisomerase alpha II, MIB-1, p53, E-cadherin, retinoblastoma gene protein product, and HER-2/neu in adrenal and extra-adrenal pheochromocytomas. *Appl Immunohistochem Mol Morphol* **8**: 267-74.

- Gutmann DH, Cole JL, Stone WJ, Ponder BA, Collins FS (1994). Loss of neurofibromin in adrenal gland tumors from patients with neurofibromatosis type I. *Genes Chromosomes Cancer* **10**: 55-8.
- Gutmann DH, Geist RT, Rose K, Wallin G, Moley JF (1995). Loss of neurofibromatosis type I (NF1) gene expression in pheochromocytomas from patients without NF1. *Genes Chromosomes Cancer* **13**: 104-9.
- Gutmann DH (2001). The neurofibromatoses: when less is more. *Hum Mol Genet* **10**: 747-55.
- Ham J, Babij C, Whitfield J, Pfarr CM, Lallemand D, Yaniv M *et al* (1995). A c-Jun dominant negative mutant protects sympathetic neurons against programmed cell death. *Neuron* **14**: 927-39.
- Hansford JR, Mulligan LM (2000). Multiple endocrine neoplasia type 2 and RET: from neoplasia to neurogenesis. *J Med Genet* **37**: 817-27.
- Harada H, Nakagawa K, Iwata S, Saito M, Kumon Y, Sakaki S *et al* (1999). Restoration of wild-type p16 down-regulates vascular endothelial growth factor expression and inhibits angiogenesis in human gliomas. *Cancer Res* **59**: 3783-9.
- Hatta Y, Takeuchi S, Yokota J, Koeffler HP (1997). Ovarian cancer has frequent loss of heterozygosity at chromosome 12p12.3-13.1 (region of TEL and Kip1 loci) and chromosome 12q23-ter: evidence for two new tumour-suppressor genes. *Br J Cancer* **75**: 1256-62.
- Hergovich A, Lisztwan J, Barry R, Ballschmieter P, Krek W (2003). Regulation of microtubule stability by the von Hippel-Lindau tumour suppressor protein pVHL. *Nat Cell Biol* **5**: 64-70.
- Herman JG, Latif F, Weng Y, Lerman MI, Zbar B, Liu S *et al* (1994). Silencing of the VHL tumour-suppressor gene by DNA methylation in renal carcinoma. *Proc Natl Acad Sci U S A* **91**: 9700-4.
- Herfarth KK, Wick MR, Marshall HN, Gartner E, Lum S, Moley JF (1997). Absence of TP53 alterations in pheochromocytomas and medullary thyroid carcinomas. *Genes Chromosomes Cancer* **20**: 24-9.
- Hes FJ, Hoppener JW, Lips CJ (2003). Clinical review 155: Pheochromocytoma in Von Hippel-Lindau disease. *J Clin Endocrinol Metab* **88**: 969-74.
- Heutink P, van der Mey AG, Sandkuijl LA, van Gils AP, Bardoel A, Breedveld GJ *et al* (1992). A gene subject to genomic imprinting and responsible for hereditary paragangliomas maps to chromosome 11q23-qter. *Hum Mol Genet* **1**: 7-10.
- Heutink P, van Schothorst EM, van der Mey AG, Bardoel A, Breedveld G, Pertijs J *et al* (1994). Further localization of the gene for hereditary paragangliomas and evidence for linkage in unrelated families. *Eur J Hum Genet* **2**: 148-58.
- Hoffman MA, Ohh M, Yang H, Klco JM, Ivan M, Kaelin WG, Jr. (2001). von Hippel-Lindau protein mutants linked to type 2C VHL disease preserve the ability to downregulate HIF. *Hum Mol Genet* **10**: 1019-27.
- Hofstra RM, Stelwagen T, Stulp RP, de Jong D, Hulsbeek M, Kamsteeg EJ *et al* (1996). Extensive mutation scanning of RET in sporadic medullary thyroid carcinoma and of RET and VHL in sporadic pheochromocytoma reveals involvement of these genes in only a minority of cases. *J Clin Endocrinol Metab* **81**: 2881-4.
- Horwitz M, Benson KF, Li FQ, Wolff J, Leppert MF, Hobson L *et al* (1997). Genetic heterogeneity in familial acute myelogenous leukemia: evidence for a second locus at chromosome 16q21-23.2. *Am J Hum Genet* **61**: 873-81.

- Hsiao RJ, Neumann HP, Parmer RJ, Barbosa JA, O'Connor DT (1990). Chromogranin A in familial pheochromocytoma: diagnostic screening value, prediction of tumor mass, and post-resection kinetics indicating two-compartment distribution. *Am J Med* **88**: 607-13.
- Hsiao RJ, Parmer RJ, Takiyyuddin MA, O'Connor DT (1991). Chromogranin A storage and secretion: sensitivity and specificity for the diagnosis of pheochromocytoma. *Medicine (Baltimore)* **70**: 33-45.
- Hsueh Y (2007). Neurofibromin signalling and synapses. *J of Biomedical Science* **14**: 461-66.
- Huang SC, Koch CA, Vortmeyer AO, Pack SD, Lichtenauer UD, Mannan P *et al* (2000). Duplication of the mutant RET allele in trisomy 10 or loss of the wild-type allele in multiple endocrine neoplasia type 2-associated pheochromocytomas. *Cancer Res* **60**: 6223-6.
- Huber K, Combs S, Ernsberger U, Kalcheim C, Unsicker K (2002). Generation of neuroendocrine chromaffin cells from sympathoadrenal progenitors: beyond the glucocorticoid hypothesis. *Ann N Y Acad Sci* **971**: 554-9.
- Inoki K, Corradetti MN, Guan KL (2005). Dysregulation of the TSC-mTOR pathway in human disease. *Nat Genet* **37**: 19-24.
- Iwamoto Y, Kaneko T, Ichinose J, Mori T, Shibata Y, Toshimori K *et al* (2005). Molecular cloning of rat Spetex2 family genes mapped on chromosome 15p16, encoding a 23-kilodalton protein associated with the plasma membranes of haploid spermatids. *Biol Reprod* **72**: 284-92.
- Jacks T, Shih TS, Schmitt EM, Bronson RT, Bernards A, Weinberg RA (1994). Tumour predisposition in mice heterozygous for a targeted mutation in Nf1. *Nat Genet* **7**: 353-61.
- Jiménez C, Cote G, Arnold A, Gagel RF (2006). REVIEW: Should patients with apparently sporadic pheochromocytomas or paragangliomas be screened for hereditary syndromes? *J Clinical endocrinology and metabolism* **9**: 2851-2858.
- Johannessen CM, Reczek EE, James MF, Brems H, Legius E, Cichowski K (2005). The NF1 tumor suppressor critically regulates TSC2 and mTOR. *Proc Natl Acad Sci U S A* **102**: 8573-8.
- Kawakami M, Staub J, Cliby W, Hartmann L, Smith DI, Shridhar V (1999). Involvement of H-cadherin (CDH13) on 16q in the region of frequent deletion in ovarian cancer. *Int J Oncol* **15**: 715-20.
- Khosla S, Patel VM, Hay ID, Schaid DJ, Grant CS, van Heerden JA *et al* (1991). Loss of heterozygosity suggests multiple genetic alterations in pheochromocytomas and medullary thyroid carcinomas. *J Clin Invest* **87**: 1691-9.
- Kibel AS, Freije D, Isaacs WB, Bova GS (1999). Deletion mapping at 12p12-13 in metastatic prostate cancer. *Genes Chromosomes Cancer* **25**: 270-6.
- Kim T, Tao-Cheng JH, Eiden LE, Loh YP (2001). Chromogranin A, an "on/off" switch controlling dense-core secretory granule biogenesis. *Cell* **106**: 499-509.
- Kim WY, Kaelin WG (2004). Role of VHL gene mutation in human cancer. *J Clin Oncol* **22**: 4991-5004.
- Kimmel RR, Zhao LP, Nguyen D, Lee S, Aronszajn M, Cheng C *et al* (2006). Microarray comparative genomic hybridization reveals genome-wide patterns of DNA gains and losses in post-Chernobyl thyroid cancer. *Radiat Res* **166**: 519-31.
- King A, Selak MA, Gottlieb E (2006). Succinate dehydrogenase and fumarate hydratase: linking mitochondrial dysfunction and cancer. *Oncogene* **25**: 4675-82.

- Kitamura Y, Shimizu K, Tanaka S, Ito K, Emi M (2000a). Allelotyping of anaplastic thyroid carcinoma: frequent allelic losses on 1q, 9p, 11, 17, 19p, and 22q. *Genes Chromosomes Cancer* **27**: 244-51.
- Kitamura Y, Shimizu K, Tanaka S, Ito K, Emi M (2000b). Association of allelic loss on 1q, 4p, 7q, 9p, 9q, and 16q with postoperative death in papillary thyroid carcinoma. *Clin Cancer Res* **6**: 1819-25.
- Knudson AG, Jr. (1986). Genetics of human cancer. *Annu Rev Genet* **20**: 231-51.
- Koch CA, Huang SC, Vortmeyer AO, Zhuang Z, Chrousos GP, Pacak K (2000). A patient with MEN 2 and multiple mutations of RET in the germline. *Exp Clin Endocrinol Diabetes* **108**: 493.
- Koch CA, Vortmeyer AO, Zhuang Z, Brouwers FM, Pacak K (2002a). New insights into the genetics of familial chromaffin cell tumors. *Ann N Y Acad Sci* **970**: 11-28.
- Koch CA, Pacak K, Chrousos GP (2002b). The molecular pathogenesis of hereditary and sporadic adrenocortical and adrenomedullary tumors. *J Clin Endocrinol Metab* **87**: 5367-84.
- Koch CA, Huang SC, Zhuang Z, Stolle C, Azumi N, Chrousos GP *et al* (2002c). Somatic VHL gene deletion and point mutation in MEN 2A-associated pheochromocytoma. *Oncogene* **21**: 479-82.
- Koff A, Ohtsuki M, Polyak K, Roberts JM, Massague J (1993). Negative regulation of G1 in mammalian cells: inhibition of cyclin E-dependent kinase by TGF-beta. *Science* **260**: 536-9.
- Komuro H, Valentine MB, Rubnitz JE, Saito M, Raimondi SC, Carroll AJ *et al* (1999). p27KIP1 deletions in childhood acute lymphoblastic leukemia. *Neoplasia* **1**: 253-61.
- Korbonits M, Chahal HS, Kaltsas G, Jordan S, Urmanova Y, Khalimova Z *et al* (2002). Expression of phosphorylated p27(Kip1) protein and Jun activation domain-binding protein 1 in human pituitary tumors. *J Clin Endocrinol Metab* **87**: 2635-43.
- Korpershoek E, Van Nederveen FH, Dannenberg H, Petri BJ, Komminoth P, Perren A *et al* (2006). Genetic analyses of apparently sporadic pheochromocytomas: the Rotterdam experience. *Ann N Y Acad Sci* **1073**: 138-48.
- Kremmidiotis G, Baker E, Crawford J, Eyre HJ, Nahmias J, Callen DF (1998). Localization of human cadherin genes to chromosome regions exhibiting cancer-related loss of heterozygosity. *Genomics* **49**: 467-71.
- Kumar R, Neilsen PM, Crawford J, McKirdy R, Lee J, Powell JA *et al* (2005). FBXO31 is the chromosome 16q24.3 senescence gene, a candidate breast tumor suppressor, and a component of an SCF complex. *Cancer Res* **65**: 11304-13.
- Kuosaite V. (2001). Mapping of allelic imbalance in  $\alpha$ -particle-radiation-induced murine osteosarcoma. Dissertation.
- Lam KY, Lo CY, Wat NM, Luk JM, Lam KS (2001). The clinicopathological features and importance of p53, Rb, and mdm2 expression in pheochromocytomas and paragangliomas. *J Clin Pathol* **54**: 443-8.
- Lasko D, Cavenee W, Nordenskjold M (1991). Loss of constitutional heterozygosity in human cancer. *Annu Rev Genet* **25**: 281-314.
- Latif F, Tory K, Gnarr J, Yao M, Duh FM, Orcutt ML *et al* (1993). Identification of the von Hippel-Lindau disease tumor suppressor gene. *Science* **260**: 1317-20.
- Lazar J, Moreno C, Jacob HJ, Kwitek AE (2005). Impact of genomics on research in the rat. *Genome Res* **15**: 1717-28.

- Le Hir H, Colucci-D'Amato LG, Charlet-Berguerand N, Plouin PF, Bertagna X, de Franciscis V *et al* (2000). High levels of tyrosine phosphorylated proto-ret in sporadic pheochromocytomas. *Cancer Res* **60**: 1365-70.
- Lee SW (1996). H-cadherin, a novel cadherin with growth inhibitory functions and diminished expression in human breast cancer. *Nat Med* **2**: 776-82.
- Lee S, Nakamura E, Yang H, Wei W, Linggi MS, Sajan MP *et al* (2005). Neuronal apoptosis linked to EglN3 prolyl hydroxylase and familial pheochromocytoma genes: developmental culling and cancer. *Cancer Cell* **8**: 155-67.
- Lei PP, Zhang ZJ, Shen LJ, Li JY, Zou Q, Zhang HX (2005). Expression and hypermethylation of p27 kip1 in hepatocarcinogenesis. *World J Gastroenterol* **11**: 4587-91.
- Liang J, Zubovitz J, Petrocelli T, Kotchetkov R, Connor MK, Han K *et al* (2002). PKB/Akt phosphorylates p27, impairs nuclear import of p27 and opposes p27-mediated G1 arrest. *Nat Med* **8**: 1153-60.
- Li SP, Wang HY, Li JQ, Zhang CQ, Feng QS, Huang P *et al* (2001). Genome-wide analyses on loss of heterozygosity in hepatocellular carcinoma in Southern China. *J Hepatol* **34**: 840-9.
- Lin SR, Lee YJ, Tsai JH (1994). Mutations of the p53 gene in human functional adrenal neoplasms. *J Clin Endocrinol Metab* **78**: 483-91.
- Lloyd RV, Erickson LA, Jin L, Kulig E, Qian X, Cheville JC *et al* (1999). p27kip1: a multifunctional cyclin-dependent kinase inhibitor with prognostic significance in human cancers. *Am J Pathol* **154**: 313-23.
- Loda M, Cukor B, Tam SW, Lavin P, Fiorentino M, Draetta GF *et al* (1997). Increased proteasome-dependent degradation of the cyclin-dependent kinase inhibitor p27 in aggressive colorectal carcinomas. *Nat Med* **3**: 231-4.
- Lockwood WW, Chari R, Chi B, Lam WL (2006). Recent advances in array comparative genomic hybridization technologies and their applications in human genetics. *Eur J Hum Genet* **14**: 139-48.
- Longo MC, Berninger MS, Hartley JL (1990). Use of uracil DNA glycosylase to control carry-over contamination in polymerase chain reactions. *Gene* **93**: 125-8.
- Liu J, Zabarovska VI, Braga E, Alimov A, Klein G, Zabarovsky ER (1999). Loss of heterozygosity in tumor cells requires re-evaluation: the data are biased by the size-dependent differential sensitivity of allele detection. *FEBS Lett* **462**: 121-8.
- Lui WO, Chen J, Glasker S, Bender BU, Madura C, Khoo SK *et al* (2002). Selective loss of chromosome 11 in pheochromocytomas associated with the VHL syndrome. *Oncogene* **21**: 1117-22.
- Mahapatra NR, Mahata M, O'Connor DT, Mahata SK (2003). Secretin activation of chromogranin A gene transcription. Identification of the signaling pathways in cis and in trans. *J Biol Chem* **278**: 19986-94.
- Maher ER, Eng C (2002). The pressure rises: update on the genetics of pheochromocytoma. *Hum Mol Genet* **11**: 2347-54.
- Maher ER (2006). Genetics of pheochromocytoma. *Br Med Bull* **79-80**: 141-51.
- Manger WM (2006). An overview of pheochromocytoma: history, current concepts, vagaries, and diagnostic challenges. *Ann N Y Acad Sci* **1073**: 1-20.

- Mangoura D, Sun Y, Li C, Singh D, Gutmann DH, Flores A *et al* (2006). Phosphorylation of neurofibromin by PKC is a possible molecular switch in EGF receptor signaling in neural cells. *Oncogene* **25**: 735-45.
- Manie S, Santoro M, Fusco A, Billaud M (2001). The RET receptor: function in development and dysfunction in congenital malformation. *Trends Genet* **17**: 580-9.
- Mannelli M, Ianni L, Cilotti A, Conti A (1999). Pheochromocytoma in Italy: a multicentric retrospective study. *Eur J Endocrinol* **141**: 619-24.
- Marchong MN, Chen D, Corson TW, Lee C, Harmandayan M, Bowles E *et al* (2004). Minimal 16q genomic loss implicates cadherin-11 in retinoblastoma. *Mol Cancer Res* **2**: 495-503.
- Martin GA, Viskochil D, Bollag G, McCabe PC, Crosier WJ, Haubruck H *et al* (1990). The GAP-related domain of the neurofibromatosis type 1 gene product interacts with ras p21. *Cell* **63**: 843-9.
- Mariman EC, van Beersum SE, Cremers CW, Struycken PM, Ropers HH (1995). Fine mapping of a putatively imprinted gene for familial non-chromaffin paragangliomas to chromosome 11q13.1: evidence for genetic heterogeneity. *Hum Genet* **95**: 56-62.
- Masciullo V, Sgambato A, Pacilio C, Pucci B, Ferrandina G, Palazzo J *et al* (1999). Frequent loss of expression of the cyclin-dependent kinase inhibitor p27 in epithelial ovarian cancer. *Cancer Res* **59**: 3790-4.
- Mason JE, Goodfellow PJ, Grundy PE, Skinner MA (2000). 16q loss of heterozygosity and microsatellite instability in Wilms' tumor. *J Pediatr Surg* **35**: 891-6; discussion 896-7.
- Matias-Guiu X, Colomer A, Mato E, Cuatrecasas M, Komminoth P, Prat J *et al* (1995). Expression of the ret proto-oncogene in pheochromocytoma. An in situ hybridization and northern blot study. *J Pathol* **176**: 63-8.
- McConnell BB, Gregory FJ, Stott FJ, Hara E, Peters G (1999). Induced expression of p16(INK4a) inhibits both CDK4- and CDK2-associated kinase activity by reassembly of cyclin-CDK-inhibitor complexes. *Mol Cell Biol* **19**: 1981-9.
- McNicol AM. (2001). Differential diagnosis of pheochromocytomas and paragangliomas *J Endocr Pathol* **12**: 407-415
- McNicol AM. (2006). Pheochromocytoma and extra-adrenal paragangliomas. *J Pathology Case Reviews* **11**: 292-297
- Menko FH, van der Luijt RB, de Valk IA, Toorians AW, Sepers JM, van Diest PJ *et al* (2002). Atypical MEN type 2B associated with two germline RET mutations on the same allele not involving codon 918. *J Clin Endocrinol Metab* **87**: 393-7.
- Miller BJ, Wang D, Krahe R, Wright FA (2003). Pooled analysis of loss of heterozygosity in breast cancer: a genome scan provides comparative evidence for multiple tumor suppressors and identifies novel candidate regions. *Am J Hum Genet* **73**: 748-67.
- Miše N, Drosten M, Racek T, Tannapfel A, Putzer BM (2006). Evaluation of potential mechanisms underlying genotype-phenotype correlations in multiple endocrine neoplasia type 2. *Oncogene* **25**: 6637-47.
- Mizumatsu S, Tamiya T, Ono Y, Abe T, Matsumoto K, Furuta T *et al* (1999). Expression of cell cycle regulator p27Kip1 is correlated with survival of patients with astrocytoma. *Clin Cancer Res* **5**: 551-7.

- Modigliani E, Vasen HM, Raue K, Dralle H, Frilling A, Gheri RG *et al* (1995). Pheochromocytoma in multiple endocrine neoplasia type 2: European study. The Euromen Study Group. *J Intern Med* **238**: 363-7.
- Moley JF, Brother MB, Fong CT, White PS, Baylin SB, Nelkin B *et al* (1992). Consistent association of 1p loss of heterozygosity with pheochromocytomas from patients with multiple endocrine neoplasia type 2 syndromes. *Cancer Res* **52**: 770-4.
- Moeller BJ, Cao Y, Li CY, Dewhirst MW (2004). Radiation activates HIF-1 to regulate vascular radiosensitivity in tumors: role of reoxygenation, free radicals, and stress granules. *Cancer Cell* **5**: 429-41.
- Mulligan LM, Gardner E, Smith BA, Mathew CG, Ponder BA (1993a). Genetic events in tumour initiation and progression in multiple endocrine neoplasia type 2. *Genes Chromosomes Cancer* **6**: 166-77.
- Mulligan LM, Kwok JB, Healey CS, Elsdon MJ, Eng C, Gardner E *et al* (1993b). Germ-line mutations of the RET proto-oncogene in multiple endocrine neoplasia type 2A. *Nature* **363**: 458-60.
- Mulligan LM, Eng C, Healey CS, Clayton D, Kwok JB, Gardner E *et al* (1994). Specific mutations of the RET proto-oncogene are related to disease phenotype in MEN 2A and FMTC. *Nat Genet* **6**: 70-4.
- Nakatsuka S, Liu A, Yao M, Takakuwa T, Tomita Y, Hoshida Y *et al* (2003). Methylation of promoter region in p27 gene plays a role in the development of lymphoid malignancies. *Int J Oncol* **22**: 561-8.
- Nakayama K, Ishida N, Shirane M, Inomata A, Inoue T, Shishido N *et al* (1996). Mice lacking p27(Kip1) display increased body size, multiple organ hyperplasia, retinal dysplasia, and pituitary tumors. *Cell* **85**: 707-20.
- Neumann HP, Wiestler OD (1991). Clustering of features and genetics of von Hippel-Lindau syndrome. *Lancet* **338**: 258.
- Neumann HP, Reincke M, Eng C (2001). Case 13-2001: genetic testing in pheochromocytoma. *N Engl J Med* **345**: 547-8.
- Neumann HP, Bausch B, McWhinney SR, Bender BU, Gimm O, Franke G *et al* (2002). Germ-line mutations in nonsyndromic pheochromocytoma. *N Engl J Med* **346**: 1459-66.
- Neumann HP, Pawlu C, Peczkowska M, Bausch B, McWhinney SR, Muresan M *et al* (2004). Distinct clinical features of paraganglioma syndromes associated with SDHB and SDHD gene mutations. *JAMA* **292**: 943-51.
- Niemann S, Steinberger D, Muller U (1999). PGL3, a third, not maternally imprinted locus in autosomal dominant paraganglioma. *Neurogenetics* **2**: 167-70.
- Niemann S, Muller U (2000). Mutations in SDHC cause autosomal dominant paraganglioma, type 3. *Nat Genet* **26**: 268-70.
- Niemann S, Muller U, Engelhardt D, Lohse P (2003). Autosomal dominant malignant and catecholamine-producing paraganglioma caused by a splice donor site mutation in SDHC. *Hum Genet* **113**: 92-4.
- Nikitin AY, Juarez-Perez MI, Li S, Huang L, Lee WH (1999). RB-mediated suppression of spontaneous multiple neuroendocrine neoplasia and lung metastases in Rb<sup>+/-</sup> mice. *Proc Natl Acad Sci U S A* **96**: 3916-21.
- Novosel A, Heger A, Lohse P, Schmidt H (2004). Multiple pheochromocytomas and paragangliomas in a young patient carrying a SDHD gene mutation. *Eur J Pediatr* **163**: 701-3.



- Opocher G, Schiavi F, Iacobone M, Toniato A, Sattarova S, Erlic Z *et al* (2006). Familial nonsyndromic pheochromocytoma. *Ann N Y Acad Sci* **1073**: 149-55.
- Pack SD, Qin LX, Pak E, Wang Y, Ault DO, Mannan P *et al* (2005). Common genetic changes in hereditary and sporadic pituitary adenomas detected by comparative genomic hybridization. *Genes Chromosomes Cancer* **43**: 72-82.
- Pagano M, Tam SW, Theodoras AM, Beer-Romero P, Del Sal G, Chau V *et al* (1995). Role of the ubiquitin-proteasome pathway in regulating abundance of the cyclin-dependent kinase inhibitor p27. *Science* **269**: 682-5.
- Parry D, Bates S, Mann DJ, Peters G (1995). Lack of cyclin D-Cdk complexes in Rb-negative cells correlates with high levels of p16INK4/MTS1 tumour suppressor gene product. *EMBO J* **14**: 503-11.
- Pellegata NS, Quintanilla-Martinez L, Siggelkow H, Samson E, Bink K, Hofler H *et al* (2006). Germ-line mutations in p27Kip1 cause a multiple endocrine neoplasia syndrome in rats and humans. *Proc Natl Acad Sci U S A* **103**: 15558-63.
- Pellegata NS, Quintanilla-Martinez L, Keller G, Liyanarachchi S, Hofler H, Atkinson MJ *et al* (2007). Human pheochromocytomas show reduced p27Kip1 expression that is not associated with somatic gene mutations and rarely with deletions. *Virchows Arch* **451**: 37-46.
- Pietenpol JA, Bohlander SK, Sato Y, Papadopoulos N, Liu B, Friedman C *et al* (1995). Assignment of the human p27Kip1 gene to 12p13 and its analysis in leukemias. *Cancer Res* **55**: 1206-10.
- Piotrowska K, Pellegata NS, Rosemann M, Fritz A, Graw J, Atkinson MJ (2004). Mapping of a novel MEN-like syndrome locus to rat chromosome 4. *Mamm Genome* **15**: 135-41.
- Piva R, Cancelli I, Cavalla P, Bortolotto S, Dominguez J, Draetta GF *et al* (1999). Proteasome-dependent degradation of p27/kip1 in gliomas. *J Neuropathol Exp Neurol* **58**: 691-6.
- Philipp-Staheli J, Payne SR, Kemp CJ (2001). p27(Kip1): regulation and function of a haploinsufficient tumor suppressor and its misregulation in cancer. *Exp Cell Res* **264**: 148-68.
- Plas DR, Thompson CB (2005). Akt-dependent transformation: there is more to growth than just surviving. *Oncogene* **24**: 7435-42.
- Podsypanina K, Ellenson LH, Nemes A, Gu J, Tamura M, Yamada KM *et al* (1999). Mutation of Pten/Mmac1 in mice causes neoplasia in multiple organ systems. *Proc Natl Acad Sci U S A* **96**: 1563-8.
- Podsypanina K, Lee RT, Politis C, Hennessy I, Crane A, Puc J *et al* (2001). An inhibitor of mTOR reduces neoplasia and normalizes p70/S6 kinase activity in Pten<sup>+/-</sup> mice. *Proc Natl Acad Sci U S A* **98**: 10320-5.
- Pollard PJ, Briere JJ, Alam NA, Barwell J, Barclay E, Wortham NC *et al* (2005). Accumulation of Krebs cycle intermediates and over-expression of HIF1alpha in tumours which result from germline FH and SDH mutations. *Hum Mol Genet* **14**: 2231-9.
- Polyak K, Kato JY, Solomon MJ, Sherr CJ, Massague J, Roberts JM *et al* (1994). p27Kip1, a cyclin-Cdk inhibitor, links transforming growth factor-beta and contact inhibition to cell cycle arrest. *Genes Dev* **8**: 9-22.
- Pomares FJ, Canas R, Rodriguez JM, Hernandez AM, Parrilla P, Tebar FJ (1998). Differences between sporadic and multiple endocrine neoplasia type 2A pheochromocytoma. *Clin Endocrinol (Oxf)* **48**: 195-200.

- Ponder BA (1999). The phenotypes associated with ret mutations in the multiple endocrine neoplasia type 2 syndrome. *Cancer Res* **59**: 1736s-1741s; discussion 1742s.
- Powers JF, Evinger MJ, Tsokas P, Bedri S, Alroy J, Shahsavari M *et al* (2000). Pheochromocytoma cell lines from heterozygous neurofibromatosis knockout mice. *Cell Tissue Res* **302**: 309-20.
- Powers JF, Schelling KH, Tischler AS (2001). Chromaffin cell mitogenesis by neurturin and glial cell line-derived neurotrophic factor. *Neuroscience* **108**: 341-9.
- Powers JF, Brachold JM, Ehsani SA, Tischler AS (2005). Up-regulation of ret by reserpine in the adult rat adrenal medulla. *Neuroscience* **132**: 605-12.
- Prowse AH, Webster AR, Richards FM, Richard S, Olschwang S, Resche F *et al* (1997). Somatic inactivation of the VHL gene in Von Hippel-Lindau disease tumors. *Am J Hum Genet* **60**: 765-71.
- Puc J, Placha G, Wocial B, Podsypanina K, Parsons R, Gaciong Z (2006). Analysis of PTEN mutation in non-familial pheochromocytoma. *Ann N Y Acad Sci* **1073**: 317-31.
- Qian X, Jin L, Kulig E, Lloyd RV (1998). DNA methylation regulates p27kip1 expression in rodent pituitary cell lines. *Am J Pathol* **153**: 1475-82.
- Qiao S, Iwashita T, Furukawa T, Yamamoto M, Sobue G, Takahashi M (2001). Differential effects of leukocyte common antigen-related protein on biochemical and biological activities of RET-MEN2A and RET-MEN2B mutant proteins. *J Biol Chem* **276**: 9460-7.
- Rao AB, Koeller KK, Adair CF (1999). From the archives of the AFIP. Paragangliomas of the head and neck: radiologic-pathologic correlation. Armed Forces Institute of Pathology. *Radiographics* **19**: 1605-32.
- Rao F, Keiser HR, O'Connor DT (2000). Malignant pheochromocytoma. Chromaffin granule transmitters and response to treatment. *Hypertension* **36**: 1045-52.
- Rakha EA, Green AR, Powe DG, Roylance R, Ellis IO (2006). Chromosome 16 tumor-suppressor genes in breast cancer. *Genes Chromosomes Cancer* **45**: 527-35.
- Rautenstrauß B. and Liehr T. (2002) FISH Technology: Lab Manual (Springer Lab Manual) Springer-Verlag, Berlin-Heidelberg
- Reddy DE, Sandhu AK, DeRiel JK, Athwal RS, Kaur GP (1999). Identification of a gene at 16q24.3 that restores cellular senescence in immortal mammary tumor cells. *Oncogene* **18**: 5100-017.
- Reddy DE, Keck CL, Popescu N, Athwal RS, Kaur GP (2000). Identification of a YAC from 16q24 carrying a senescence gene for breast cancer cells. *Oncogene* **19**: 217-22.
- Reed SI (2002). Keeping p27(Kip1) in the cytoplasm: a second front in cancer's war on p27. *Cell Cycle* **1**: 389-90.
- Reynolds RM, Browning GG, Nawroz I, Campbell IW (2003). Von Recklinghausen's neurofibromatosis: neurofibromatosis type 1. *Lancet* **361**: 1552-4.
- Richards FM (2001). Molecular pathology of von HippelLindau disease and the VHL tumour suppressor gene. *Expert Rev Mol Med* **2001**: 1-27.
- Ritland SR, Rowse GJ, Chang Y, Gendler SJ (1997). Loss of heterozygosity analysis in primary mammary tumors and lung metastases of MMTV-MTAG and MMTV-neu transgenic mice. *Cancer Res* **57**: 3520-5.

- Risinger JI, Berchuck A, Kohler MF, Boyd J (1994). Mutations of the E-cadherin gene in human gynecologic cancers. *Nat Genet* **7**: 98-102.
- Rodier G, Montagnoli A, Di Marcotullio L, Coulombe P, Draetta GF, Pagano M *et al* (2001). p27 cytoplasmic localization is regulated by phosphorylation on Ser10 and is not a prerequisite for its proteolysis. *EMBO J* **20**: 6672-82.
- Rodriguez-Cuevas S, Lopez-Garza J, Labastida-Almendaro S (1998). Carotid body tumors in inhabitants of altitudes higher than 2000 meters above sea level. *Head Neck* **20**: 374-8.
- Rocco JW, Sidransky D (2001). p16(MTS-1/CDKN2/INK4a) in cancer progression. *Exp Cell Res* **264**: 42-55.
- Santoro M, Carlomagno F, Romano A, Bottaro DP, Dathan NA, Grieco M *et al* (1995). Activation of RET as a dominant transforming gene by germline mutations of MEN2A and MEN2B. *Science* **267**: 381-3.
- Santoro M, Carlomagno F, Melillo RM, Fusco A (2004). Dysfunction of the RET receptor in human cancer. *Cell Mol Life Sci* **61**: 2954-64.
- Sato Y, Suto Y, Pietenpol J, Golub TR, Gilliland DG, Davis EM *et al* (1995). TEL and KIP1 define the smallest region of deletions on 12p13 in hematopoietic malignancies. *Blood* **86**: 1525-33.
- Sato M, Mori Y, Sakurada A, Fukushige S, Ishikawa Y, Tsuchiya E *et al* (1998). Identification of a 910-kb region of common allelic loss in chromosome bands 16q24.1-q24.2 in human lung cancer. *Genes Chromosomes Cancer* **22**: 1-8.
- Schulz N, Propst F, Rosenberg MP, Linnoila RI, Paules RS, Kovatch R *et al* (1992). Pheochromocytomas and C-cell thyroid neoplasms in transgenic c-mos mice: a model for the human multiple endocrine neoplasia type 2 syndrome. *Cancer Res* **52**: 450-5.
- Selak MA, Armour SM, MacKenzie ED, Boulahbel H, Watson DG, Mansfield KD *et al* (2005). Succinate links TCA cycle dysfunction to oncogenesis by inhibiting HIF-alpha prolyl hydroxylase. *Cancer Cell* **7**: 77-85.
- Shaffer DR, Viale A, Ishiwata R, Leversha M, Olgac S, Manova K *et al* (2005). Evidence for a p27 tumor suppressive function independent of its role regulating cell proliferation in the prostate. *Proc Natl Acad Sci U S A* **102**: 210-5.
- Sherr CJ, Roberts JM (1999). CDK inhibitors: positive and negative regulators of G1-phase progression. *Genes Dev* **13**: 1501-12.
- Shin E, Fujita S, Takami K, Kurahashi H, Kurita Y, Kobayashi T *et al* (1993). Deletion mapping of chromosome 1p and 22q in pheochromocytoma. *Jpn J Cancer Res* **84**: 402-8.
- Shin I, Yakes FM, Rojo F, Shin NY, Bakin AV, Baselga J *et al* (2002). PKB/Akt mediates cell-cycle progression by phosphorylation of p27(Kip1) at threonine 157 and modulation of its cellular localization. *Nat Med* **8**: 1145-52.
- Singh SP, Lipman J, Goldman H, Ellis FH, Jr., Aizenman L, Cangi MG *et al* (1998). Loss or altered subcellular localization of p27 in Barrett's associated adenocarcinoma. *Cancer Res* **58**: 1730-5.
- Siu FK, Lam IP, Chu JY, Chow BK (2006). Signaling mechanisms of secretin receptor. *Regul Pept* **137**: 95-104.
- Slingerland J, Pagano M (2000). Regulation of the cdk inhibitor p27 and its deregulation in cancer. *J Cell Physiol* **183**: 10-7.

- Smith-Hicks CL, Sizer KC, Powers JF, Tischler AS, Costantini F (2000). C-cell hyperplasia, pheochromocytoma and sympathoadrenal malformation in a mouse model of multiple endocrine neoplasia type 2B. *EMBO J* **19**: 612-22.
- Snijders AM, Nowee ME, Fridlyand J, Piek JM, Dorsman JC, Jain AN *et al* (2003). Genome-wide-array-based comparative genomic hybridization reveals genetic homogeneity and frequent copy number increases encompassing CCNE1 in fallopian tube carcinoma. *Oncogene* **22**: 4281-6.
- Stern MC, Benavides F, Klingelberger EA, Conti CJ (2000). Allelotype analysis of chemically induced squamous cell carcinomas in F(1) hybrids of two inbred mouse strains with different susceptibility to tumor progression. *Carcinogenesis* **21**: 1297-301.
- Stankov K, Pastore A, Toschi L, McKay J, Lesueur F, Kraimps JL *et al* (2004). Allelic loss on chromosomes 2q21 and 19p 13.2 in oxyphilic thyroid tumors. *Int J Cancer* **111**: 463-7.
- Strachan T, Read, AP (2004). Human Molecular Genetics (3rd edition). Garland Publishing, New York
- Straub JA, Lipscomb EA, Yoshida ES, Freeman RS (2003). Induction of SM-20 in PC12 cells leads to increased cytochrome c levels, accumulation of cytochrome c in the cytosol, and caspase-dependent cell death. *J Neurochem* **85**: 318-28.
- Stoll M, Kwitek-Black AE, Cowley AW, Jr., Harris EL, Harrap SB, Krieger JE *et al* (2000). New target regions for human hypertension via comparative genomics. *Genome Res* **10**: 473-82.
- Suzuki H, Komiya A, Emi M, Kuramochi H, Shiraishi T, Yatani R *et al* (1996). Three distinct commonly deleted regions of chromosome arm 16q in human primary and metastatic prostate cancers. *Genes Chromosomes Cancer* **17**: 225-33.
- Takaya K, Yoshimasa T, Arai H, Tamura N, Miyamoto Y, Itoh H *et al* (1996). Expression of the RET proto-oncogene in normal human tissues, pheochromocytomas, and other tumors of neural crest origin. *J Mol Med* **74**: 617-21.
- Takeuchi S, Bartram CR, Wada M, Reiter A, Hatta Y, Seriu T *et al* (1995). Allelotype analysis of childhood acute lymphoblastic leukemia. *Cancer Res* **55**: 5377-82.
- Takeuchi S, Koeffler HP, Hinton DR, Miyoshi I, Melmed S, Shimon I (1998). Mutation and expression analysis of the cyclin-dependent kinase inhibitor gene p27/Kip1 in pituitary tumors. *J Endocrinol* **157**: 337-41.
- Takiyuddin MA, Cervenka JH, Hsiao RJ, Barbosa JA, Parmer RJ, O'Connor DT (1990a). Chromogranin A. Storage and release in hypertension. *Hypertension* **15**: 237-46.
- Takiyuddin MA, Cervenka JH, Sullivan PA, Pandian MR, Parmer RJ, Barbosa JA *et al* (1990b). Is physiologic sympathoadrenal catecholamine release exocytotic in humans? *Circulation* **81**: 185-95.
- Tamura G, Yin J, Wang S, Fleisher AS, Zou T, Abraham JM *et al* (2000). E-Cadherin gene promoter hypermethylation in primary human gastric carcinomas. *J Natl Cancer Inst* **92**: 569-73.
- Tanaka N, Nishisho I, Yamamoto M, Miya A, Shin E, Karakawa K *et al* (1992). Loss of heterozygosity on the long arm of chromosome 22 in pheochromocytoma. *Genes Chromosomes Cancer* **5**: 399-403.
- Tessema M, Lehmann U, Kreipe H (2004). Cell cycle and no end. *Virchows Arch* **444**: 313-23.
- Tisi MA, Xie Y, Yeo TT, Longo FM (2000). Downregulation of LAR tyrosine phosphatase prevents apoptosis and augments NGF-induced neurite outgrowth. *J Neurobiol* **42**: 477-86.

- Tischler AS, Ruzicka LA, Donahue SR, DeLellis RA (1989). Chromaffin cell proliferation in the adult rat adrenal medulla. *Int J Dev Neurosci* **7**: 439-48.
- Tischler AS, McClain RM, Childers H, Downing J (1991). Neurogenic signals regulate chromaffin cell proliferation and mediate the mitogenic effect of reserpine in the adult rat adrenal medulla. *Lab Invest* **65**: 374-6.
- Tischler AS, Riseberg JC, Hardenbrook MA, Cherington V (1993). Nerve growth factor is a potent inducer of proliferation and neuronal differentiation for adult rat chromaffin cells in vitro. *J Neurosci* **13**: 1533-42.
- Tischler AS, Riseberg JC, Cherington V (1994). Multiple mitogenic signalling pathways in chromaffin cells: a model for cell cycle regulation in the nervous system. *Neurosci Lett* **168**: 181-4.
- Tischler AS, Ziar J, Downing JC, McClain RM (1995). Sustained stimulation of rat adrenal chromaffin cell proliferation by reserpine. *Toxicol Appl Pharmacol* **135**: 254-7.
- Tischler AS, Powers JF, Pignatello M, Tsokas P, Downing JC, McClain RM (1999). Vitamin D3-induced proliferative lesions in the rat adrenal medulla. *Toxicol Sci* **51**: 9-18.
- Trovó-Marqui AB, Tajara EH (2006). Neurofibromin: a general outlook. *Clin Genet* **70**: 1-13.
- Tsihlias J, Kapusta LR, DeBoer G, Morava-Protzner I, Zbieranowski I, Bhattacharya N *et al* (1998). Loss of cyclin-dependent kinase inhibitor p27Kip1 is a novel prognostic factor in localized human prostate adenocarcinoma. *Cancer Res* **58**: 542-8.
- Tsutsumi M, Yokota J, Kakizoe T, Koiso K, Sugimura T, Terada M (1989). Loss of heterozygosity on chromosomes 1p and 11p in sporadic pheochromocytoma. *J Natl Cancer Inst* **81**: 367-70.
- Tsuji T, Catusus L, Prat J (2005). Is loss of heterozygosity at 9q22.3 (PTCH gene) and 19p13.3 (STK11 gene) involved in the pathogenesis of ovarian stromal tumors? *Hum Pathol* **36**: 792-6.
- Upadhyaya M, Han S, Consoli C, Majounie E, Horan M, Thomas NS *et al* (2004). Characterization of the somatic mutational spectrum of the neurofibromatosis type 1 (NF1) gene in neurofibromatosis patients with benign and malignant tumors. *Hum Mutat* **23**: 134-46.
- van den Ijssel P, Tijssen M, Chin SF, Eijk P, Carvalho B, Hopmans E *et al* (2005). Human and mouse oligonucleotide-based array CGH. *Nucleic Acids Res* **33**: e192.
- Vargas MP, Zhuang Z, Wang C, Vortmeyer A, Linehan WM, Merino MJ (1997). Loss of heterozygosity on the short arm of chromosomes 1 and 3 in sporadic pheochromocytoma and extra-adrenal paraganglioma. *Hum Pathol* **28**: 411-5.
- Vermeesch JR, Melotte C, Froyen G, Van Vooren S, Dutta B, Maas N *et al* (2005). Molecular karyotyping: array CGH quality criteria for constitutional genetic diagnosis. *J Histochem Cytochem* **53**: 413-22.
- Viglietto G, Motti ML, Fusco A (2002a). Understanding p27(kip1) deregulation in cancer: down-regulation or mislocalization. *Cell Cycle* **1**: 394-400.
- Viglietto G, Motti ML, Bruni P, Melillo RM, D'Alessio A, Califano D *et al* (2002b). Cytoplasmic relocalization and inhibition of the cyclin-dependent kinase inhibitor p27(Kip1) by PKB/Akt-mediated phosphorylation in breast cancer. *Nat Med* **8**: 1136-44.
- Virmani AK, Fong KM, Kodagoda D, McIntire D, Hung J, Tonk V *et al* (1998). Allelotyping demonstrates common and distinct patterns of chromosomal loss in human lung cancer types. *Genes Chromosomes Cancer* **21**: 308-19.

- Visser M, Sijmons C, Bras J, Arceci RJ, Godfried M, Valentijn LJ *et al* (1997). Allelotype of pediatric rhabdomyosarcoma. *Oncogene* **15**: 1309-14.
- Vogel KS, Brannan CI, Jenkins NA, Copeland NG, Parada LF (1995). Loss of neurofibromin results in neurotrophin-independent survival of embryonic sensory and sympathetic neurons. *Cell* **82**: 733-42.
- Walther MM, Herring J, Enquist E, Keiser HR, Linehan WM (1999). von Recklinghausen's disease and pheochromocytomas. *J Urol* **162**: 1582-6.
- Wang G, Zhao Y, Liu X, Wang L, Wu C, Zhang W *et al* (2001). Allelic loss and gain, but not genomic instability, as the major somatic mutation in primary hepatocellular carcinoma. *Genes Chromosomes Cancer* **31**: 221-7.
- Wessels-Reiker M, Basiboina R, Howlett AC, Strong R (1993). Vasoactive intestinal polypeptide-related peptides modulate tyrosine hydroxylase gene expression in PC12 cells through multiple adenylate cyclase-coupled receptors. *J Neurochem* **60**: 1018-29.
- White R, O'Connell P (1991). Identification and characterization of the gene for neurofibromatosis type 1. *Curr Opin Genet Dev* **1**: 15-9.
- Williams BO, Schmitt EM, Remington L, Bronson RT, Albert DM, Weinberg RA *et al* (1994a). Extensive contribution of Rb-deficient cells to adult chimeric mice with limited histopathological consequences. *EMBO J* **13**: 4251-9.
- Williams BO, Remington L, Albert DM, Mukai S, Bronson RT, Jacks T (1994b). Cooperative tumorigenic effects of germline mutations in Rb and p53. *Nat Genet* **7**: 480-4.
- Woodward ER, Maher ER (2006). Von Hippel-Lindau disease and endocrine tumour susceptibility. *Endocr Relat Cancer* **13**: 415-25.
- Xia Z, Dickens M, Raingeaud J, Davis RJ, Greenberg ME (1995). Opposing effects of ERK and JNK-p38 MAP kinases on apoptosis. *Science* **270**: 1326-31.
- Xu W, Mulligan LM, Ponder MA, Liu L, Smith BA, Mathew CG *et al* (1992). Loss of NF1 alleles in phaeochromocytomas from patients with type I neurofibromatosis. *Genes Chromosomes Cancer* **4**: 337-42.
- Yang T, Martignetti JA, Massa SM, Longo FM (2000). Leukocyte common-antigen-related tyrosine phosphatase receptor: altered expression of mRNA and protein in the New England Deaconess Hospital rat line exhibiting spontaneous pheochromocytoma. *Carcinogenesis* **21**: 125-31.
- Yoshimoto T, Naruse M, Zeng Z, Nishikawa T, Kasajima T, Toma H *et al* (1998). The relatively high frequency of p53 gene mutations in multiple and malignant phaeochromocytomas. *J Endocrinol* **159**: 247-55.
- You MJ, Castrillon DH, Bastian BC, O'Hagan RC, Bosenberg MW, Parsons R *et al* (2002). Genetic analysis of Pten and Ink4a/Arf interactions in the suppression of tumorigenesis in mice. *Proc Natl Acad Sci U S A* **99**: 1455-60.
- Zarnegar R, Brunaud L, Clark OH (2002). Multiple endocrine neoplasia type I. *Curr Treat Options Oncol* **3**: 335-48.
- Zeiger MA, Zbar B, Keiser H, Linehan WM, Gnarr JR (1995). Loss of heterozygosity on the short arm of chromosome 3 in sporadic, von Hippel-Lindau disease-associated, and familial pheochromocytoma. *Genes Chromosomes Cancer* **13**: 151-6.

Zhang LH, Qin LX, Ma ZC, Ye SL, Liu YK, Ye QH *et al* (2003). Allelic imbalance regions on chromosomes 8p, 17p and 19p related to metastasis of hepatocellular carcinoma: comparison between matched primary and metastatic lesions in 22 patients by genome-wide microsatellite analysis. *J Cancer Res Clin Oncol* **129**: 279-86.

Zhang J, Fan Z, Gao Y, Xiao Z, Li C, An Q *et al* (2001). Detecting bladder cancer in the Chinese by microsatellite analysis: ethnic and etiologic considerations. *J Natl Cancer Inst* **93**: 45-50.

Zhu Y, Parada LF (2001). Neurofibromin, a tumor suppressor in the nervous system. *Exp Cell Res* **264**: 19-28.

## 8. APPENDIX

**Table 4.2** Panel of polymorphic microsatellite markers for genome-wide scan for LOH/AI in pheochromocytoma from SD<sup>we</sup> × Wky F2 hybrids

Name	Genetic map FHH×ACI v.7 cM	Genetic map SHRSP×BN v.7 cM	Radiation Hybrid map v.2.1 cR	Source of primer sequence	High molecular weight allele	Low molecular weight allele	Method	Notes			
<b>Chromosome 1</b>											
D1Rat20	30.3	27.2	355.9	NCBI, Ensembl.	SD <sup>we</sup>	Wky	Agarose				
D1Rat213	42.3	–	–	NCBI, Ensembl.	SD <sup>we</sup>	Wky/SD <sup>we</sup>	Agarose				
D1Rat30	–	51.4	605.1	NCBI, Ensembl.	SD <sup>we</sup>	Wky	Agarose				
D1Rat49	71.0	77.9	825.0	NCBI, Ensembl.	Wky	SD <sup>we</sup>	Agarose				
D1Rat112	96.6	–	1122.4	NCBI, Ensembl.	Wky	SD <sup>we</sup>	Agarose				
D1Rat74	109.0	117.6	–	NCBI, Ensembl.	SD <sup>we</sup>	Wky	Agarose				
RND1Lev1	intragenic marker for <i>Ret</i> gene				SD <sup>we</sup>	Wky	Agarose	Prof.Dr. Atkinson, personal communication			
D1Rat90	–	148.2	1313.2	NCBI, Ensembl.	SD <sup>we</sup>	Wky	Agarose				
<b>Chromosome 2</b>											
D2Rat273	–	32.0	403.2	NCBI, Ensembl.	SD <sup>we</sup>	Wky	Agarose				
D2Rat123	50.1	38.7	533.9	NCBI, Ensembl.	SD <sup>we</sup>	Wky	Agarose				
D2Arb20	–	73.6	–	NCBI, Ensembl.	Wky	SD <sup>we</sup>	Agarose				
<b>Chromosome 3</b>											
D3Rat56	2.5	2.5	–	NCBI, Ensembl.	SD <sup>we</sup>	Wky	Agarose				
D3Rat65	42.7	–	–	NCBI, Ensembl.	SD <sup>we</sup>	Wky	Agarose/PAGE				
D3Rat108	42.7	37.3	–	NCBI, Ensembl.	Wky	SD <sup>we</sup>	Agarose				
D3Rat27	–	47.3	440.8	NCBI, Ensembl.	SD <sup>we</sup>	Wky	Agarose				
<b>Chromosome 4</b>											
D4Rat136	–	0	65.7	NCBI, Ensembl.	SD <sup>we</sup>	Wky	Agarose				
D4Mgh4	46.9	37.4	551.7	NCBI, Ensembl.	Wky	SD <sup>we</sup>	Agarose/PAGE				
D4Rat53	–	55.5	803.2	NCBI, Ensembl.	SD <sup>we</sup>	Wky	Agarose				
<b>Chromosome 5</b>											
D5Rat82	27.0	26.0	263.1	NCBI, Ensembl.	SD <sup>we</sup>	Wky	Agarose				
D5Rat143	–	43.4	416.5	NCBI, Ensembl.	SD <sup>we</sup>	Wky	Agarose				
D5Rat152	–	58.2	–	NCBI, Ensembl.	SD <sup>we</sup>	Wky	Agarose				
D5Rat71	54.6	–	702.6	NCBI, Ensembl.	SD <sup>we</sup>	Wky/SD <sup>we</sup>	Agarose				
D5Rat95	–	64.9	759.3	NCBI, Ensembl.	Wky	SD <sup>we</sup>	Agarose				
D5Rat79	84.3	87.6	940.4	NCBI, Ensembl.	Wky	SD <sup>we</sup>	Agarose				
D5Rat47	92.0	94.3	1086.7	NCBI, Ensembl.	Wky	SD <sup>we</sup>	Agarose				
<b>Chromosome 6</b>											
D6Rat156	26.0	–	222.7	NCBI, Ensembl.	SD <sup>we</sup>	Wky/SD <sup>we</sup>	Agarose				
D6Rat64	46.0	40.9	–	NCBI, Ensembl.	Wky	SD <sup>we</sup>	Agarose/PAGE				
D6Arb20	–	55.6	859.3	NCBI, Ensembl.	SD <sup>we</sup>	Wky	Agarose				



D6Rat12	73.6	66.9	960.9	NCBI, Ensembl.	SD <sup>we</sup>	Wky	Agarose				
D6Rat79	90.5	80.5	–	NCBI, Ensembl.	Wky	SD <sup>we</sup>	Agarose				
<b>Chromosome 7</b>											
D7Rat163	36.7	–	–	NCBI, Ensembl.	Wky	SD <sup>we</sup>	Agarose				
D7Rat140	–	52.3	549.2	NCBI, Ensembl.	Wky	SD <sup>we</sup>	Agarose/PAGE				
<b>D7Rat16</b>	50.1	59.1	607.2	NCBI, Ensembl.	SD <sup>we</sup>	Wky/SD <sup>we</sup>	Agarose/PAGE/Frag.				
D7Rat78	53.4	65.8	678.9	NCBI, Ensembl.	Wky	SD <sup>we</sup>	Agarose/PAGE				
D7Rat5	–	76.0	750.8	NCBI, Ensembl.	SD <sup>we</sup>	Wky/SD <sup>we</sup>	Agarose				
<b>Chromosome 8</b>											
D8Rat170	4.9	–	–	NCBI, Ensembl.	Wky	SD <sup>we</sup>	Agarose				
<b>D8Rat46</b>	32.5	32.3	275.8	NCBI, Ensembl.	SD <sup>we</sup>	Wky/SD <sup>we</sup>	Agarose/PAGE/Frag.				
<b>D8Rat44</b>	47.0	38.1	402.4	NCBI, Ensembl.	SD <sup>we</sup>	Wky	Agarose				
D8Rat113	–	41.2	450	NCBI, Ensembl.	Wky	SD <sup>we</sup>	Agarose				
<b>D8Rat185</b>	–	43.6	–	NCBI, Ensembl.	SD <sup>we</sup>	Wky	Agarose/Frag.				
D8Rat33	51.3	44.8	646.7	NCBI, Ensembl.	SD <sup>we</sup>	Wky	Agarose				
D8Rat167GSF1	72.37	–	–	NCBI, Ensembl.	Wky/SD <sup>we</sup>	SD <sup>we</sup>	Agarose/PAGE/Frag.	primers are designed with www.frodo. wi.mit.edu			
<b>D8Rat76</b>	79.0	–	–	NCBI, Ensembl.	SD <sup>we</sup>	Wky	Agarose/PAGE/Frag.				
<b>Chromosome 9</b>											
D9Rat38	11.2	12.9	80.3	NCBI, Ensembl.	Wky	SD <sup>we</sup>	Agarose				
D9Rat60	32.4	41.1	–	NCBI, Ensembl.	Wky	SD <sup>we</sup>	Agarose				
D9Rat110	–	64.7	–	NCBI, Ensembl.	Wky	SD <sup>we</sup>	Agarose				
<b>Chromosome 10</b>											
D10Rat47	10.1	8.1	130.9	NCBI, Ensembl.	Wky	SD <sup>we</sup>	Agarose				
D10Rat116	–	45.4	–	NCBI, Ensembl.	SD <sup>we</sup>	Wky/SD <sup>we</sup>	Agarose				
D10Mit2	–	46.6	637.5	NCBI, Ensembl.	SD <sup>we</sup>	Wky/SD <sup>we</sup>	Agarose				
D10Arb27	53.7	47.6	–	NCBI, Ensembl.	Wky	SD <sup>we</sup>	Agarose				
<b>Chromosome 11</b>											
<b>D11Rat40</b>	7.8	2.6	628.9	NCBI, Ensembl.	SD <sup>we</sup>	Wky/SD <sup>we</sup>	PAGE/Frag.				
D11Rat13	12.2	–	–	NCBI, Ensembl.	Wky/SD <sup>we</sup>	SD <sup>we</sup>	PAGE	primers are designed with www.frodo. wi.mit.edu			
D11Rat64	–	28.5	–	NCBI, Ensembl.	SD <sup>we</sup>	Wky	PAGE	primers are designed with www.frodo. wi.mit.edu			
D11Rat46GSF1	–	35.8	60.2	NCBI, Ensembl.	SD <sup>we</sup>	Wky	Agarose, PAGE	primers are designed with www.frodo. wi.mit.edu			
<b>Chromosome 12</b>											
D12Rat60	–	12.7	–	NCBI, Ensembl.	Wky	SD <sup>we</sup>	Agarose				
D12Rat48GSF1	34.9	–	511.5	NCBI, Ensembl.	SD <sup>we</sup>	Wky	Agarose	primers are designed with www.frodo. wi.mit.edu			
<b>Chromosome 13</b>											
D13Arb5	9.0	7.9	–	NCBI, Ensembl.	Wky/SD <sup>we</sup>	SD <sup>we</sup>	Agarose/ PAGE	primers are designed with www.frodo. wi.mit.edu			
D13Rat132	–	33.9	–	NCBI, Ensembl.	SD <sup>we</sup>	Wky	Agarose	primers are designed with www.frodo. wi.mit.edu			
<b>Chromosome 14</b>											
D14Rat6	–	6.9	196.2	NCBI, Ensembl.	Wky/SD <sup>we</sup>	SD <sup>we</sup>	Agarose	primers are designed with www.frodo. wi.mit.edu			
<b>D14Rat92</b>	–	42.8	–	NCBI, Ensembl.	SD <sup>we</sup>	Wky	PAGE/Frag.	primers are designed with www.frodo. wi.mit.edu			

Chromosome 15									
<i>D15Rat16</i>	46.4	33.5	–	NCBI, Ensembl.	Wky	SD <sup>we</sup>	Agarose		
<i>D15Rat133</i>	46.4	–	–	NCBI, Ensembl.	SD <sup>we</sup>	Wky	Agarose		
<i>D15Mgh9</i>	–	52.8	–	NCBI, Ensembl.	Wky	SD <sup>we</sup>	Agarose		
Chromosome 16									
<i>D16Rat31</i>	–	3.4	31.4	NCBI, Ensembl.	SD <sup>we</sup>	Wky	Agarose	primers are designed with www.frodo.wi.mit.edu	
<i>D16Rat9</i>	12.2	7.9	268.7	NCBI, Ensembl.	Wky	SD <sup>we</sup>	Agarose/PAGE	primers are designed with www.frodo.wi.mit.edu	
<i>D16Rat72</i>	–	12.4	–	NCBI, Ensembl.	SD <sup>we</sup>	Wky	Agarose	primers are designed with www.frodo.wi.mit.edu	
<i>D16Rat17</i>	25.5	–	592.6	NCBI, Ensembl.	SD <sup>we</sup>	Wky	Agarose/ PAGE	primers are designed with www.frodo.wi.mit.edu	
<i>D16Rat55</i>	–	38.6	815	NCBI, Ensembl.	SD <sup>we</sup>	Wky	Agarose	primers are designed with www.frodo.wi.mit.edu	
Chromosome 17									
<i>D17Rat6</i>	4.5	27.0	57.0	NCBI, Ensembl.	Wky	SD <sup>we</sup>	Agarose	primers are designed with www.frodo.wi.mit.edu	
<i>D17Arb4</i>	–	27.0	–	NCBI, Ensembl.	SD <sup>we</sup>	Wky	Agarose	primers are designed with www.frodo.wi.mit.edu	
<i>D17Rat64</i>	40.0	–	–	NCBI, Ensembl.	Wky	SD <sup>we</sup>	Agarose	primers are designed with www.frodo.wi.mit.edu	
<i>D17Rat45</i>	–	40.9	600.6	NCBI, Ensembl.	Wky	SD <sup>we</sup>	Agarose	primers are designed with www.frodo.wi.mit.edu	
Chromosome 18									
<i>D18Rat108</i>	–	5.9	795.2	NCBI, Ensembl.	Wky	SD <sup>we</sup>	PAGE.	primers are designed with www.frodo.wi.mit.edu	
<i>D18Mgh3</i>	48.5	38.7	224.7	NCBI, Ensembl.	Wky	SD <sup>we</sup>	Agarose/ PAGE	primers are designed with www.frodo.wi.mit.edu	
<b><i>D18Rat1</i></b>	64.5	–	–	NCBI, Ensembl.	Wky	SD <sup>we</sup>	PAGE/ Frag.	primers are designed with www.frodo.wi.mit.edu	
Chromosome 19									
<b><i>D19Rat97</i></b>	–	4.5	92.7	NCBI, Ensembl.	Wky	SD <sup>we</sup>	PAGE/Frag.	primers are designed with www.frodo.wi.mit.edu	
<b><i>D19Rat13</i></b>	21.7	–	–	NCBI, Ensembl.	Wky	SD <sup>we</sup>	PAGE/Frag.	primers are designed with www.frodo.wi.mit.edu	
<b><i>D19Rat25</i></b>	22.2	20.3	313.9	NCBI, Ensembl.	Wky	SD <sup>we</sup>	PAGE/Frag.	primers are designed with www.frodo.wi.mit.edu	
<b><i>D19Rat64</i></b>	–	38.0	612.7	NCBI, Ensembl.	SD <sup>we</sup>	Wky/SD <sup>we</sup>	PAGE/Frag.	primers are designed with www.frodo.wi.mit.edu	
<b><i>D19Rat4</i></b>	–	43.8	722.0	NCBI, Ensembl.	Wky	SD <sup>we</sup>	PAGE/Frag.	primers are designed with www.frodo.wi.mit.edu	
Chromosome 20									
<i>D20Rat59</i>	4.7	–	152.3	NCBI, Ensembl.	SD <sup>we</sup>	Wky	Agarose	primers are designed with www.frodo.wi.mit.edu	
<i>D20Mit4</i>	15.7	22.4	–	NCBI, Ensembl.	SD <sup>we</sup>	Wky/SD <sup>we</sup>	Agarose/ PAGE	primers are designed with www.frodo.wi.mit.edu	
Chromosome X									
<i>DXRat36</i>	7.9	6.9	212.7	NCBI, Ensembl.	Wky	SD <sup>we</sup>	PAGE	primers are designed with www.frodo.wi.mit.edu	
<i>DXRat67</i>	16.7	14.9	471.6	NCBI, Ensembl.	SD <sup>we</sup>	Wky	PAGE	primers are designed with www.frodo.wi.mit.edu	

Position of markers shown from genetic maps FHH × ACI v.7, SHRSP × BN v.7 and radiation hybrid map v.2.1. The source of primer sequences for microsatellite markers, the size ratio between the parental alleles and electrophoretical separation method are indicated. In bold microsatellite markers for which microsatellite fragment analysis was performed.

Abbreviations: Ensembl, Ensembl Genome Browser; NCBI, the National Center for Biotechnology ; SD<sup>we</sup>, Sprague-Dawley white eye rat strain; Wky, Wistar Kyoto rat strain; Agarose, 3% agarose gel; PAGE, 10% polyacrilamide gel; Frag., microsatellite fragment analysis with using fluorescently labelled primers.

**Table 4.3** Other microsatellite markers tested in SD<sup>we</sup> × Wky F2 rats

Name	Genetic map FHH×ACI v.7 cM	Genomic map SHRSP×BN v.7 cM	Radiation Hybrid map v.2.1 cR	Source of primer sequence	Polymorphism	Method	Comments			
<b>Chromosome 1</b>										
D1Rat5	-	-	29.3	NCBI, Ensembl	NP	Agarose				
D1Rat7	-	-	166.1	NCBI, Ensembl	NP	Agarose	marker from the Radiation hybrid Map v.3.4			
D1Rat131	67.7	74.5	728.9	NCBI, Ensembl	NP	Agarose				
D1Rat113	100		1147.5	NCBI, Ensembl	NP	Agarose				
<b>Chromosome 2</b>										
D2Rat94	18.6	10.5	117.7	NCBI, Ensembl	NP	Agarose				
D2Rat179	67.8	60.5	-	NCBI, Ensembl	No product	Agarose				
D2Rat165	-	93.1	1102.1	NCBI, Ensembl	NP	Agarose				
<b>Chromosome 3</b>										
D3Rat82	-	15.1	-	NCBI, Ensembl	Polym/ Weak product	Agarose				
D3Rat45	-	25.7	281.2	NCBI, Ensembl	Polym/ Wky weak product	Agarose				
<b>D3Mgh21</b>	29.4	28.2	290.4	NCBI, Ensembl	P, Low informativeness (3 out of 20)	Agarose/PAGE				
D3Rat123	-	32.8	-	NCBI, Ensembl	No product	Agarose				
D3Rat223	-	42.8	-	NCBI, Ensembl	NP	Agarose				
<b>D3Rat200</b>	73.5	-	-	NCBI, Ensembl	P, Low informativeness (4 out of 20)	Agarose/PAGE				
D3Rat4	90.2	75.5	927.4	NCBI, Ensembl	NP	Agarose				
<b>Chromosome 4</b>										
D4Rat151	-	17.1	215.3	NCBI, Ensembl	NP	Agarose				
<b>D4Rat23</b>	-	32.8	381.6	NCBI, Ensembl	P, Low informativeness (1out of 20)	Agarose				
<b>D4Rat195</b>	-	65.7	897.9	NCBI, Ensembl	P, Low informativeness (2 out of 20)	Agarose				
D4VHL1	intragenic marker for <i>Vhl</i> gene				NP	Agarose	primers are designed with www.frodo. wi.mit.edu			
D4Rat61	88.0	73.6	951.2	NCBI, Ensembl	Polym/F2 progeny not informative	Agarose				
D4Ret13	intragenic marker for <i>Ret</i> gene				Polym/Weak product	Agarose	Dr. Pellegata, personal communication			
<b>D4Ret23</b>	intragenic marker for <i>Ret</i> gene				P, Low informativeness (1out of 20)		Dr. Pellegata, personal communication			
<b>D4Rat201</b>	-	76.0	-	NCBI, Ensembl	P, Low informativeness (1out of 20)					
D4Mgh11	107.9	87.2	1078.1	NCBI, Ensembl	NP	Agarose				
<b>D4Rat112</b>	112.4	98.8	1084.6	NCBI, Ensembl	P, Low informativeness (3 out of 20)	Agarose				
<b>Chromosome 5</b>										
D5Rat126	-	16.0	-	NCBI, Ensembl	NP	Agarose				
D5Rat95	-	64.9	759.3	NCBI, Ensembl	Polym	Agarose				
D5Rat29	-	68.3	831.7	NCBI, Ensembl	NP	Agarose				
D5Rat31	70.9	70.6	860.3	NCBI, Ensembl	NP	Agarose				
<b>Chromosome 6</b>										
D6Rat62	4.9	5.5	0	NCBI, Ensembl	NP					
D6Rat67	-	33.0	-	NCBI, Ensembl	NP	Agarose				
D6Rat129	-	48.9	-	NCBI, Ensembl	No product					

Chromosome 7									
D7Rat32	-	11.4	105.6	NCBI, Ensembl	NP	Agarose			
D7Rat107	24.6	28.1	337.8	NCBI, Ensembl	Polym/Weak product	Agarose			
Chromosome 8									
D8Mit9	-	-	95.7	NCBI, Ensembl	NP	Agarose, PAGE			
D8Mit5	-	-	167.4	NCBI, Ensembl	Polym/ Sd <sup>we</sup> weak product	Agarose			
<b>SDHD2</b>	intragenic marker for <i>Sdhd</i> gene				P, Low informativeness (2 out of 20)	PAGE	primers are designed with <a href="http://www.frodo.wi.mit.edu">www.frodo.wi.mit.edu</a>		
D8Rat30	51.3	44.8	665.3	NCBI, Ensembl	NP	Agarose, PAGE			
D8Rat16	66.9	57.2	815.3	NCBI, Ensembl	Polym/ weak PCR product	Agarose			
D8Rat167	72.37	-	-	NCBI, Ensembl	Polym/ weak PCR product	Agarose, PAGE			
D8Rat7	84.6	77.3	985.5	NCBI, Ensembl	Polym ? in PAGE	Agarose, PAGE			
D8Rat138	-	48.2	772.9	NCBI, Ensembl	Polym/ Sd <sup>we</sup> weak product	Agarose, PAGE			
D8Rat81	-	81.9	1005.4	NCBI, Ensembl	Polym/ Sd <sup>we</sup> weak product	Agarose, PAGE			
Chromosome 9									
D9Rat55	45.6	-	721.8	NCBI, Ensembl	No product	Agarose			
Chromosome 10									
D10Rat39	-	32.9	345.4	NCBI, Ensembl	NP	Agarose			
D10Rat62	40.4	-	568.7	NCBI, Ensembl	NP	Agarose			
D10Mgh20	-	-	567.8	NCBI, Ensembl	NP	Agarose			
Chromosome 11									
D11Rat15	12.2	8.2	469.5	NCBI, Ensembl	NP	PAGE			
D11Rat 6	49.7	19.5	-	NCBI, Ensembl	NP	Agarose / PAGE			
D11Rat93	48.5	29.8	-	NCBI, Ensembl	NP	PAGE			
D11Rat46	-	35.8	60.2	NCBI, Ensembl	Polym/ weak PCR product	PAGE			
Chromosome 12									
D12Rat38	9.0	23.8	225.6	NCBI, Ensembl	NP	Agarose			
D12Rat48	34.9	-	511.5	NCBI, Ensembl	Polym/ weak PCR product	Agarose			
Chromosome 13									
D13Rat93	2.6	1.2	-	NCBI, Ensembl	Polym/ Wky weak product	Agarose / PAGE	primers are designed with <a href="http://www.frodo.wi.mit.edu">www.frodo.wi.mit.edu</a>		
D13Rat27	22.7	22.6	-	NCBI, Ensembl	No product	Agarose	primers are designed with <a href="http://www.frodo.wi.mit.edu">www.frodo.wi.mit.edu</a>		
D13Rat153	-	44.2	682.1	NCBI, Ensembl	NP	Agarose			
Chromosome 14									
D14Rat11	-	27.2	498.2	NCBI, Ensembl	NP	Agarose	primers are designed with <a href="http://www.frodo.wi.mit.edu">www.frodo.wi.mit.edu</a>		
D14Rat12	-	27.2	500.7	NCBI, Ensembl	NP	PAGE	primers are designed with <a href="http://www.frodo.wi.mit.edu">www.frodo.wi.mit.edu</a>		
D14Rat88	-	30.5	-	NCBI, Ensembl	NP	Agarose	primers are designed with <a href="http://www.frodo.wi.mit.edu">www.frodo.wi.mit.edu</a>		
D14Rat22	76.0	66.2	823.7	NCBI, Ensembl	Polym ? in PAGE	Agarose / PAGE	primers are designed with <a href="http://www.frodo.wi.mit.edu">www.frodo.wi.mit.edu</a>		
Chromosome 15									
D15Rat80	-	21.1	141.8	NCBI, Ensembl	NP	Agarose			
Chromosome 16									
Chromosome 17									
D17Rat12	27.8	21.8	254.9	NCBI, Ensembl	Polym ? in PAGE	Agarose/PAGE	primers are designed with <a href="http://www.frodo.wi.mit.edu">www.frodo.wi.mit.edu</a>		
Chromosome 18									
D18Rat48	2.5	2.5	815.3	NCBI, Ensembl	Polym ? in PAGE	Agarose/PAGE	primers are designed with <a href="http://www.frodo.wi.mit.edu">www.frodo.wi.mit.edu</a>		
D18Rat70	12.2	9.3	694.5	NCBI, Ensembl	NP	Agarose	primers are designed with <a href="http://www.frodo.wi.mit.edu">www.frodo.wi.mit.edu</a>		
D18Rat92	-	20.5	-	NCBI, Ensembl	NP	PAGE	primers are designed with <a href="http://www.frodo.wi.mit.edu">www.frodo.wi.mit.edu</a>		
D18Rat57	30.4	21.7	409.0	NCBI, Ensembl	NP	Agarose	primers are designed with <a href="http://www.frodo.wi.mit.edu">www.frodo.wi.mit.edu</a>		
D18Rat44	65.8	52.4	0	NCBI, Ensembl	Polym ? in PAGE	Agarose/ PAGE	primers are designed with <a href="http://www.frodo.wi.mit.edu">www.frodo.wi.mit.edu</a>		

Chromosome 19							
<i>D19Rat84</i>	-	4.5	-	NCBI, Ensembl	NP	Agarose/ PAGE	primers are designed with www.frodo.wi.mit.edu
<i>D19Rat101</i>	19.0	-	-	NCBI, Ensembl	Polym/ Sd <sup>we</sup> weak product	Agarose/ PAGE	primers are designed with www.frodo.wi.mit.edu
<i>D19Rat46</i>	29.1	23.6	421.3	NCBI, Ensembl	Polym/ Sd <sup>we</sup> weak product	Agarose/ PAGE	primers are designed with www.frodo.wi.mit.edu
<i>D19Rat33</i>	29.2	-	433.1	NCBI, Ensembl	NP	PAGE	primers are designed with www.frodo.wi.mit.edu
Chromosome 20							
<i>D20Mit1</i>	31.8	44.6	603.7	NCBI, Ensembl	NP	Agarose	primers are designed with www.frodo.wi.mit.edu
Chromosome X							
<b><i>DXRat79</i></b>	-	0.1	0	NCBI, Ensembl	P, Low informativeness (2 out of 20)	PAGE	primers are designed with www.frodo.wi.mit.edu
<i>DXRat65</i>	-	17.2	-	NCBI, Ensembl	NP	PAGE	primers are designed with www.frodo.wi.mit.edu
<i>DXRat105</i>	-	44.6	749.3	NCBI, Ensembl	NP	PAGE	primers are designed with www.frodo.wi.mit.edu

In bold polymorphic informative microsatellite markers which can not be used for genome-wide scan for LOH/AI because of the low heterogenous rate (the number of informative heterogenous samples is too small to be used for LOH/AI analysis).

Abbreviations: NP, nonpolymorphic microsatellite markers; No product, PCR did not work; Polym/Weak product, polymorphic microsatellite markers with low efficiency of PCR reaction; Polym ? in PAGE, polymorphism of the marker is not clear on 10% polyacrilamide gel.

**Table 4.4** Allelic imbalance (in %) on chromosome 1 in twenty pheochromocytomas in comparison to normal tissue at each microsatellite locus analysed

NCBI, Ensembl map position (Mb)	48.78	81.6	106.0	157.6	206.7	227.2	236.9	267.3	Allelic imbalance
Marker name	<i>D1Rat20</i>	<i>D1Rat213</i>	<i>D1Rat30</i>	<i>D1Rat49</i>	<i>D1Rat112</i>	<i>D1Rat74</i>	<i>RND1Lev1</i>	<i>D1Rat90</i>	
Pheochromocytoma cases (PC)									
PC1	Non inform.	2	Non inform.	0	Non inform.	Non inform.	Non inform..	Non inform.	
PC2	Non inform.	Non inform.	Non inform.	Non inform.	Non inform.	Non inform.	10	6	
PC3	Non inform.	5	6	5	11	Non inform.	2	Non inform.	
PC4	6	14	28	Non inform.	Non inform.	Non inform.	Non inform.	Non inform.	
PC5	5	Non inform.	Non inform.	6	Non inform.	Non inform.	Non inform.	Non inform.	
PC6	Non inform.	Non inform.	Non inform.	5	Non inform.	Non inform.	Non inform.	Non inform.	
PC7	Non inform.	Non inform.	Non inform.	17	13	13	7	Non inform.	
PC8	16	7	8	17	Non inform.	Non inform.	Non inform.	Non inform.	
PC9	15	1	8	3	8	1	5	3	
PC10	Non inform..	6	3	6	3	Non inform.	Non inform.	Non inform.	
PC11	Weak product	15	Non inform.	26	20	Weak product	3	Weak product	
PC12	Non inform.	Non inform.	Non inform.	8	8	4	7	18	
PC13	Non inform.	Non inform.	Non inform.	6	3	1	6	13	
PC14	Non inform.	7	13	1	10	0	7	<b>68</b>	Sd <sup>we</sup> ↓ Wky ↑
PC15	4	6	3	1	2	10	3	8	
PC16	5	4	2	2	16	Non inform.	17	28	
PC17	Non inform.	Non inform.	Non inform.	18	4	Non inform.	22	28	
PC18	Non inform.	2	Non inform.	Non inform.	Non inform.	1	19	Non inform.	
PC19	Non inform.	6	Non inform.	1	5	Non inform.	Non inform.	Non inform.	
PC20	Non inform.	9	Non inform.	Non inform.	Non inform.	Non inform.	Non inform.	Non inform.	

Allelic imbalance at certain marker above 50% is taken as LOH/AI and marked in grey. Allelic imbalance is indicated.

Abbreviations: Weak product, evaluation of LOH/AI was impossible because the efficiency of PCR reaction of either tumor sample or corresponding to it sample from normal tissue was low.

**Table 4.5** Allelic imbalance (in %) on chromosome 2 in twenty pheochromocytomas in comparison to normal tissue at each microsatellite locus analysed

NCBI, Ensembl map position (Mb)	75,3	112,3	193,2	Allelic imbalance
Marker name	<i>D2Rat273</i>	<i>D2Rat123</i>	<i>D2Arb20</i>	
Pheochromocytoma cases (PC)				
PC1	Non inform.	Non inform.	2	
PC2	27	19	6	
PC3	9	13	Non inform.	
PC4	Non inform.	Non inform.	Non inform.	
PC5	Non inform.	Non inform.	25	
PC6	Non inform.	Non inform.	Non inform.	
PC7	Non inform.	Non inform.	Non inform.	
PC8	Non inform.	Non inform.	Non inform.	
PC9	28	10	6	
PC10	Non inform.	Non inform.	13	
PC11	Non inform.	4	3	
PC12	21	10	2	
PC13	Non inform.	Non inform.	15	
PC14	Non inform.	Non inform.	Non inform.	
PC15	Non inform.	Non inform.	5	
PC16	2	8	Non inform.	
PC17	3	7	Non inform.	
PC18	Non inform.	Non inform.	12	
PC19	No product	4	11	
PC20	21	18	Non inform.	

Abbreviations: No product, PCR reaction for either tumor or matched normal sample does not work.

**Table 4.6** Allelic imbalance (in %) on chromosome 3 in twenty pheochromocytomas in comparison to normal tissue at each microsatellite locus analysed

NCBI, Ensembl map position (Mb)	3,6	58,5	59,7	88	Allelic imbalance
Marker name	<i>D3Rat56</i>	<i>D3Rat65</i>	<i>D3Rat108</i>	<i>D3Rat27</i>	
Pheochromocytoma cases (PC)					
PC1	16	Non inform.	Non inform.	Non inform.	
PC2	Non inform.	Non inform.	Non inform.	Non inform.	
PC3	3	Non inform.	Non inform.	Non inform.	
PC4	21	10	23	Non inform.	
PC5	Non inform.	31	<b>58</b>	30	Sd <sup>we</sup> ↑ Wky ↓
PC6	Non inform.	Non inform.	Non inform.	Non inform.	
PC7	14	Non inform.	Non inform.	Non inform.	
PC8	Non inform.	Non inform.	Non inform.	Non inform.	
PC9	Non inform.	Non inform.	Non inform.	Non inform.	
PC10	Non inform.	31	12	0	
PC11	8	Non inform.	Non inform.	Non inform.	
PC12	Non inform.	Non inform.	Non inform.	5	
PC13	Non inform.	10	12	26	
PC14	<b>67</b>	12	8	Non inform.	Sd <sup>we</sup> ↑ Wky ↓
PC15	Non inform.	17	16	10	
PC16	Non inform.	Non inform.	Non inform.	Non inform.	
PC17	Non inform.	9	13	16	
PC18	12	Non inform.	Non inform.	Non inform.	
PC19	10	Non inform.	Non inform.	Non inform.	
PC20	Non inform.	12	15	4	

Allelic imbalance at certain marker above 50% is taken as LOH/AI and marked in grey. Allelic imbalance is indicated.



**Table 4.7** Allelic imbalance (in %) on chromosome 4 in twenty pheochromocytomas in comparison to normal tissue at each microsatellite locus analysed

NCBI, Ensembl map position (Mb)	8.0	78.3	126.3	Allelic imbalance
Marker name	<i>D4Rat136</i>	<i>D4Mgh4</i>	<i>D4Rat53</i>	
Pheochromocytoma cases (PC)				
PC1	2	Non inform.	Non inform.	
PC2	2	Non inform.	Non inform.	
PC3	Non inform.	3	16	
PC4	Non inform.	Non inform.	Non inform.	
PC5	11	13	19	
PC6	Non inform.	9	13	
PC7	Non inform.	Non inform.	Non inform.	
PC8	Non inform.	Non inform.	Non inform.	
PC9	12	3	6	
PC10	5	Non inform.	Non inform.	
PC11	0	Non inform.	Non inform.	
PC12	16	Non inform.	Non inform.	
PC13	Non inform.	Non inform.	Non inform.	
PC14	Non inform.	Non inform.	Non inform.	
PC15	Non inform.	Non inform.	Non inform.	
PC16	Non inform.	Mutation ?	Non inform.	
PC17	Non inform.	6	4	
PC18	Non inform.	19	5	
PC19	3	4	Non inform.	
PC20	4	13	10	

Abbreviations: Mutation?, the size of alleles of paired normal-tumor amplified DNA is different compare to those of other amplified matched normal-tumor DNA samples.

**Table 4.8** Allelic imbalance (in %) on chromosome 5 in twenty pheochromocytomas in comparison to normal tissue at each microsatellite locus analysed

NCBI, Ensembl map position (Mb)	45.8	78.1	107.6	115.4	130.6	156.5	163.3	Allelic imbalance
Marker name	<i>D5Rat82</i>	<i>D5Rat143</i>	<i>D5Rat152</i>	<i>D5Rat71</i>	<i>D5Rat95</i>	<i>D5Rat79</i>	<i>D5Rat47</i>	
Pheochromocytoma cases (PC)								
PC1	10	17	0	weak product	2	no product	29	
PC2	49*	13	10	8	8	Non inform.	Non inform.	
PC3	35	7	15	1	10	Non inform.	Non inform.	
PC4	6	9	25	15	13	10	15	
PC5	0	Non inform.	Non inform.	10	3	12	7	
PC6	Non inform.	Non inform.	Non inform.	Non inform.	Non inform.	Non inform.	Non inform.	
PC7	16	0	No product	33	10	4	6	
PC8	Non inform.	Non inform.	Non inform.	44	Non inform.	Non inform.	Non inform.	
PC9	Non inform.	Non inform.	Non inform.	6	0	35	8	
PC10	Non inform.	17	19	9	4	23	7	
PC11	Non inform.	2	12	31	1	18	6	
PC12	Non inform.	Non inform.	0	5	7	6	1	
PC13	Non inform.	Non inform.	Non inform.	Non inform.	Non inform.	Non inform.	Non inform.	
PC14	8	2	15	5	7	20	6	
PC15	2	6	Non inform.	9	Non inform.	Non inform.	Non inform.	
PC16	8	4	6	5	1	16	7	
PC17	10	7	25	33	5	20	Non inform.	
PC18	Non inform.	Non inform.	Non inform.	Non inform.	15	3	0	
PC19	Non inform.	Non inform.	Non inform.	24	Non inform.	Non inform.	6	
PC20	4	10	3	11	16	6	3	

\*The value of allelic imbalance for PC2 (marker *D5Rat82*) is equal to 49% because of the unequal intensity of allele amplification of DNA from ear take (normal tissue for LOH/AI study). The amplification of alleles of tumor DNA is approximately the same. This phenomenon is related to the feature of PCR amplification of normal sample but not to the presence of the real allelic imbalance.

Abbreviations: Weak product, evaluation of LOH/AI was impossible because the efficiency of PCR reaction of either tumor sample or corresponding to it sample from normal tissue was low; No product, PCR reaction for either tumor or corresponding normal sample did not work.

**Table 4.9** Allelic imbalance (in %) on chromosome 6 in twenty pheochromocytomas in comparison to normal tissue at each microsatellite locus analysed

NCBI, Ensembl map position (Mb)	26.9	54.6	97.5	114.0	131.0	Allelic imbalance
Marker name	<i>D6Rat156</i>	<i>D6Rat64</i>	<i>D6Arb20</i>	<i>D6Rat12</i>	<i>D6Rat79</i>	
Pheochromocytoma cases (PC)						
PC1	6	Non inform.	Weak product	Non inform.	Non inform.	
PC2	Non inform.	6	Non inform.	1	14	
PC3	18	Non inform.	Non inform.	Non inform.	Non inform.	
PC4	8	Non inform.	31	23	8	
PC5	7	9	Non inform.	Non inform.	Non inform.	
PC6	Non inform.	Non inform.	Non inform.	2	5	
PC7	1	16	22	Non inform.	Non inform.	
PC8	26	Non inform.	27	21	Non inform.	
PC9	3	11	0	12	3	
PC10	Non inform.	Non inform.	Weak product	16	26	
PC11	No product	Mutation ?	Non inform.	Non inform.	Weak product	
PC12	Non inform.	Non inform.	27	23	Weak product	
PC13	9	4	41	0	26	
PC14	5	18	Non inform.	Non inform.	Non inform.	
PC15	21	11	24	10	10	
PC16	Non inform.	Non inform.	4	Non inform.	5	
PC17	5	Non inform.	Non inform.	Non inform.	Non inform.	
PC18	2	Non inform.	6	Non inform.	Non inform.	
PC19	18	Non inform.	Non inform.	Non inform.	6	
PC20	0	Non inform.	Non inform.	Non inform.	41	

Abbreviations: Mutation?, the size of alleles of paired normal-tumor amplified DNA is different compare to those of other amplified matched normal-tumor DNA samples; Weak product, evaluation of LOH/AI was impossible because the efficiency of PCR reaction of either tumor sample or corresponding to it sample from normal tissue was low; No product, PCR reaction for either tumor or corresponding normal sample did not work.

**Table 4.10** Allelic imbalance (in %) on chromosome 7 in twenty pheochromocytomas in comparison to normal tissue at each microsatellite locus analysed

NCBI, Ensembl map position (Mb)	69.2	95.1	108.6	120.5	131.4	Allelic imbalance
Marker name	<i>D7Rat163</i>	<i>D7Rat140</i>	<i>D7Rat16*</i>	<i>D7Rat78</i>	<i>D7Rat5</i>	
Pheochromocytoma cases (PC)						
PC1	Non inform.	Non inform.	3	7	Non inform.	
PC2	9	Non inform.	9	5	Non inform.	
PC3	Non inform.	Non inform.	2	Non inform.	Non inform.	
PC4	24	16	10	7	Non inform.	
PC5	4	10	7	5	Non inform.	
PC6	Non inform.	6	7	5	Non inform.	
PC7	Non inform.	Non inform.	11	13	Non inform.	
PC8	Non inform.	8	12	Non inform.	Non inform.	
PC9	Non inform.	10	1	3	10	
PC10	6	Non inform.	0	Non inform.	15	
PC11	Non inform.	Non inform.	12	Non inform.	7	
PC12	1	Non inform.	12	6	39	
PC13	Non inform.	12	1	1	2	
PC14	Non inform.	3	8	11	Non inform.	
PC15	26	Non inform.	4	9	Non inform.	
PC16	Non inform.	5	4	0	Non inform.	
PC17	14	15	3	9	Non inform.	
PC18	6	Non inform.	Non inform.	4	10	
PC19	Non inform.	Non inform.	3	Non inform.	Non inform.	
PC20	Non inform.	Non inform.	0	10	Non inform.	

\*For the marker *D7Rat16* microsatellite fragment analysis was performed using 5'-FAM labelled primers.

**Table 4.11** Allelic imbalance (in %) on chromosome 8 in twenty pheochromocytomas in comparison to normal tissue at each microsatellite locus analysed

NCBI, Ensembl map position (Mb)	13.0	43.3	53.1	56.9	64.6	73.7	107.0	111.0	Allelic imbalance
Marker name	<i>D8Rat170</i>	<i>D8Rat46*</i>	<i>D8Rat44*</i>	<i>D8Rat113</i>	<i>D8Rat185*</i>	<i>D8Rat33</i>	<i>D8Rat167GSF1</i>	<i>D8Rat76*</i>	
Pheochromocytoma cases (PC)									
PC1	7	10	Non inform.	Non inform.	Non inform.	1	Non inform.	Non inform.	
PC2	Non inform.	18	Non inform.	Non inform.	Non inform.	15	4	Non inform.	
PC3	33	23	6	1	0	8	Non inform.	10	
PC4	Non inform.	Non inform.	11	9	17	7	1	Non inform.	
PC5	Non inform.	Non inform.	Non inform.	Non inform.	Non inform.	Non inform.	9	2	
PC6	Non inform.	14	5	3	6	1	Non inform.	Non inform.	
PC7	8	25	16	34	10	Non inform.	29	Non inform.	
PC8	Non inform.	4	Non inform.	Non inform.	Non inform.	34	17	Non inform.	
PC9	Non inform.	Non inform.	Non inform.	Non inform.	18	5	Non inform.	2	
PC10	24	6	16	2	4	3	Non inform.	Non inform.	
PC11	9	5	Non inform.	Non inform.	Non inform.	Non inform.	Non inform.	Non inform.	
PC12	1	11	12	0	1	11	Non inform.	Non inform.	
PC13	<b>63</b>	<b>52</b>	<b>61</b>	<b>66</b>	<b>50</b>	<b>46**</b>	Non inform.	<b>53</b>	Sd <sup>we</sup> ↑ Wky ↓
PC14	Non inform.	1	Non inform.	Non inform.	Non inform.	24	19	Non inform.	
PC15	15	2	12	11	14	10	2	Non inform.	
PC16	Non inform.	13	Non inform.	Non inform.	Non inform.	12	7	3	
PC17	19	2	10	7	23	Non inform.	7	5	
PC18	Non inform.	1	7	8	20	Non inform.	Non inform.	Non inform.	
PC19	Non inform.	13	Non inform.	39	24	5	10	Non inform.	
PC20	Non inform.	<b>64</b>	<b>49**</b>	Non inform.	<b>54</b>	Non inform.	<b>56</b>	<b>58</b>	Sd <sup>we</sup> ↓ Wky ↑

Allelic imbalance at certain marker above 50% is taken as LOH/AI and marked in grey. Allelic imbalance is indicated.

\*For the microsatellite markers *D8Rat46*, *D8Rat44*, *D8Rat185*, *D8Rat76* microsatellite fragment analysis was performed using 5'-FAM labelled primers only for samples having allelic imbalance and few samples without allelic imbalance (Table 4.26).

\*\*Allelic imbalance values of PC20 (marker *D8Rat44*) and PC13 (marker *D8Rat33*) are borderline values (49% and 46%, respectively) and regarded as allelic imbalance cases (Table 4.26).

PC13 and PC20 have allelic imbalance for all tested informative microsatellite markers on chromosome 8.

**Table 4.12** Allelic imbalance (in %) on chromosome 9 in twenty pheochromocytomas in comparison to normal tissue at each microsatellite locus analysed

NCBI, Ensembl map position (Mb)	11.5	45.0	94.2	Allelic imbalance
Marker name	<i>D9Rat38</i>	<i>D9Rat60</i>	<i>D9Rat110</i>	
Pheochromocytoma cases (PC)				
PC1	16	12	22	
PC2	12	21	8	
PC3	No product	12	6	
PC4	3	21	18	
PC5	Non inform.	10	31	
PC6	Non inform.	No product	6	
PC7	17	18	3	
PC8	Non inform.	Non inform.	4	
PC9	Non inform.	Non inform.	Non inform.	
PC10	3	10	7	
PC11	Non inform.	Non inform.	3	
PC12	Non inform.	Non inform.	Non inform.	
PC13	7	10	16	
PC14	Non inform.	Non inform.	11	
PC15	2	20	27	
PC16	7	Non inform.	No product	
PC17	17	10	19	
PC18	Non inform.	Non inform.	Non inform.	
PC19	Non inform.	14	Non inform.	
PC20	3	10	31	

Abbreviations: No product, PCR reaction for either tumor or corresponding normal sample did not work.

**Table 4.13** Allelic imbalance (in %) on chromosome 10 in twenty pheochromocytomas in comparison to normal tissue at each microsatellite locus analysed

NCBI, Ensembl map position (Mb)	16.1	54.2	64.9	69.2	Allelic imbalance
Marker name	<i>D10Rat47</i>	<i>D10Rat116</i>	<i>D10Mit2</i>	<i>D10Arb27</i>	
Pheochromocytoma cases (PC)					
PC1	Non inform.	9	Non inform.	16	
PC2	Non inform.	3	10	2	
PC3	Non inform.	11	6	Non inform.	
PC4	Non inform.	Non inform.	Non inform.	Non inform.	
PC5	15	2	15	3	
PC6	25	4	8	23	
PC7	Non inform.	3	8	No product	
PC8	Non inform.	15	Non inform.	8	
PC9	22	Non inform.	Non inform.	Non inform.	
PC10	Non inform.	0	Non inform.	7	
PC11	5	Non inform.	Non inform.	Non inform.	
PC12	Non inform.	Non inform.	Non inform.	Non inform.	
PC13	Non inform.	15	Non inform.	1	
PC14	11	4	16	6	
PC15	3	14	5	10	
PC16	Non inform.	11	11	14	
PC17	33	Non inform.	Non inform.	Non inform.	
PC18	20	9	10	Non inform.	
PC19	Weak product	22	0	Non inform.	
PC20	Non inform.	Non inform.	Non inform.	Non inform.	

Abbreviations: Weak product, evaluation of LOH/AI was impossible because the efficiency of PCR reaction of either tumor sample or corresponding to it sample from normal tissue was low; No product, PCR reaction for either tumor or corresponding normal sample did not work.

**Table 4.14** Allelic imbalance (in %) on chromosome 11 in twenty pheochromocytomas in comparison to normal tissue at each microsatellite locus analysed

NCBI, Ensembl map position (Mb)	16.0	31.8	64.6	81.1	Allelic imbalance
Marker name	<i>D11Rat40*</i>	<i>D11Rat13</i>	<i>D11Rat64</i>	<i>D11Rat46GSF1</i>	
Pheochromocytoma cases (PC)					
PC1	6	13	11	5	
PC2	30	Non inform.	Non inform.	12	
PC3	7	2	4	Non inform.	
PC4	2	Non inform.	Non inform.	Non inform.	
PC5	6	Non inform.	Non inform.	Non inform.	
PC6	4	9	No product	7	
PC7	Non inform.	Non inform.	Non inform.	Non inform.	
PC8	Non inform.	3	Non inform.	Non inform.	
PC9	Non inform.	12	5	13	
PC10	3	6	6	12	
PC11	No product	Non inform.	Non inform.	4	
PC12	No product	15	14	18	
PC13	Non inform.	1	3	1	
PC14	6	Non inform.	Non inform.	13	
PC15	7	Non inform.	Non inform.	Non inform.	
PC16	Non inform.	Non inform.	Non inform.	<b>52</b>	Sd <sup>we</sup> ↑ Wky ↓
PC17	0	Non inform.	Non inform.	Non inform.	
PC18	0	Non inform.	Non inform.	3	
PC19	Non inform.	0	4	5	
PC20	3	Non inform.	Non inform.	15	

Allelic imbalance at certain marker above 50% is taken as LOH/AI and marked in grey. Allelic imbalance is indicated.

\*For the marker *D11Rat40* microsatellite fragment analysis was performed.

Abbreviations: No product, PCR reaction for either tumor or corresponding normal sample did not work.



**Table 4.15** Allelic imbalance (in %) on chromosome 12 in twenty pheochromocytomas in comparison to normal tissue at each microsatellite locus analysed

NCBI, Ensembl map position (Mb)	10.4	37.3	Allelic imbalance
Marker name	<i>D12Rat60</i>	<i>D12Rat48GSF1</i>	
Pheochromocytoma cases (PC)			
PC1	3	Non inform.	
PC2	16	Non inform.	
PC3	6	Non inform.	
PC4	4	8	
PC5	Non inform.	3	
PC6	4	5	
PC7	Non inform.	15	
PC8	18	Non inform.	
PC9	8	Non inform.	
PC10	29	Non inform.	
PC11	Non inform.	Non inform.	
PC12	0	6	
PC13	Non inform.	4	
PC14	Non inform.	8	
PC15	Non inform.	6	
PC16	Non inform.	Non inform.	
PC17	Non inform.	11	
PC18	Non inform.	Non inform.	
PC19	Non inform.	Non inform.	
PC20	7	2	

**Table 4.16** Allelic imbalance (in %) on chromosome 13 in twenty pheochromocytomas in comparison to normal tissue at each microsatellite locus analysed

NCBI, Ensembl map position (Mb)	39.0	81.8	Allelic imbalance
Marker name	<i>D13Arb5</i>	<i>D13Rat132</i>	
Pheochromocytoma cases (PC)			
PC1	4	Non inform.	
PC2	18	28	
PC3	13	Non inform.	
PC4	5	22	
PC5	5	Non inform.	
PC6	Non inform.	8	
PC7	31	22	
PC8	Non inform.	Non inform.	
PC9	Non inform.	17	
PC10	16	Non inform.	
PC11	10	2	
PC12	Non inform.	7	
PC13	Non inform.	Non inform.	
PC14	Non inform.	11	
PC15	Non inform.	12	
PC16	11	5	
PC17	Non inform.	6	
PC18	10	Non inform.	
PC19	2	20	
PC20	Non inform.	3	

**Table 4.17** Allelic imbalance (in %) on chromosome 14 in twenty pheochromocytomas in comparison to normal tissue at each microsatellite locus analysed

NCBI, Ensembl map position (Mb)	16.4	84.9	Allelic imbalance
Marker name	<i>D14Rat6</i>	<i>D14Rat92*</i>	
Pheochromocytoma cases (PC)			
PC1	Non inform.	Non inform.	
PC2	Non inform.	3	
PC3	23	Non inform.	
PC4	Non inform.	Non inform.	
PC5	Non inform.	3	
PC6	Non inform.	1	
PC7	Non inform.	Non inform.	
PC8	23	10	
PC9	16	8	
PC10	Non inform.	11	
PC11	40	Non inform.	
PC12	11	15	
PC13	Non inform.	5	
PC14	Non inform.	3	
PC15	Non inform.	Non inform.	
PC16	Non inform.	0	
PC17	Non inform.	Non inform.	
PC18	Non inform.	1	
PC19	8	Non inform.	
PC20	Non inform.	9	

\*For the marker *D14Rat92* microsatellite fragment analysis was performed using 5'-FAM labelled primers.

**Table 4.18** Allelic imbalance (in %) on chromosome 15 in twenty pheochromocytomas in comparison to normal tissue at each microsatellite locus analysed

NCBI, Ensembl map position (Mb)	53.2	55.3	89.6	Allelic imbalance
Marker name	<i>D15Rat16</i>	<i>D15Rat133</i>	<i>D15Mgh9</i>	
Pheochromocytoma cases (PC)				
PC1	Non inform.	Non inform.	Non inform.	
PC2	3	11	35	
PC3	Non inform.	Non inform.	Non inform.	
PC4	17	6	13	
PC5	13	1	14	
PC6	Non inform.	Non inform.	6	
PC7	Non inform.	Non inform.	7	
PC8	10	3	16	
PC9	Non inform.	Non inform.	Non inform.	
PC10	4	3	11	
PC11	Non inform.	Non inform.	Non inform.	
PC12	19	17	Non inform.	
PC13	3	2	10	
PC14	6	7	7	
PC15	Non inform.	Non inform.	6	
PC16	7	8	7	
PC17	Non inform.	Non inform.	Non inform.	
PC18	Non inform.	Non inform.	Non inform.	
PC19	1	18	Non inform.	
PC20	Non inform.	Non inform.	19	

**Table 4.19** Allelic imbalance (in %) on chromosome 16 in twenty pheochromocytomas in comparison to normal tissue at each microsatellite locus analysed

NCBI, Ensembl map position (Mb)	8.3	22.6	42.5	53.5	76.6	Allelic imbalance
Marker name	<i>D16Rat31</i>	<i>D16Rat9</i>	<i>D16Rat72</i>	<i>D16Rat17</i>	<i>D16Rat55</i>	
Pheochromocytoma cases (PC)						
PC1	Non inform.	Non inform.	Non inform.	Non inform.	Non inform.	
PC2	Non inform.	10	Non inform.	10	Non inform.	
PC3	Non inform.	Non inform.	Non inform.	Non inform.	5	
PC4	21	1	2	10	Non inform.	
PC5	Non inform.	Non inform.	Non inform.	Non inform.	15	
PC6	Non inform.	Non inform.	Non inform.	Non inform.	Non inform.	
PC7	19	2	13	29	3	
PC8	Non inform.	Non inform.	Non inform.	18	Non inform.	
PC9	Non inform.	7	Non inform.	Non inform.	18	
PC10	Non inform.	6	11	10	1	
PC11	30	4	25	4	Non inform.	
PC12	17	4	20	8	Non inform.	
PC13	17	15	15	19	1	
PC14	Non inform.	20	Non inform.	11	6	
PC15	Non inform.	7	Non inform.	27	Non inform.	
PC16	Non inform.	4	Non inform.	2	1	
PC17	5	28	20	9	Non inform.	
PC18	16	6	7	3	14	
PC19	8	7	Non inform.	16	Non inform.	
PC20	21	12	Non inform.	7	Non inform.	

**Table 4.20** Allelic imbalance (in %) on chromosome 17 in twenty pheochromocytomas in comparison to normal tissue at each microsatellite locus analysed

NCBI, Ensembl map position (Mb)	16.1	40.7	64.2	82.3	Allelic imbalance
Marker name	<i>D17Rat6</i>	<i>D17Arb4</i>	<i>D17Rat64</i>	<i>D17Rat45</i>	
Pheochromocytoma cases (PC)					
PC1	Non inform.	16	Non inform.	Non inform.	
PC2	5	Non inform.	25	20	
PC3	14	Non inform.	9	Non inform.	
PC4	Non inform.	28	42	<b>55*</b>	
PC5	Non inform.	1	Non inform.	7	
PC6	Non inform.	6	8	14	
PC7	Non inform.	0	Non inform.	Non inform.	
PC8	0	1	17	Non inform.	
PC9	Non inform.	18	Non inform.	28	
PC10	Non inform.	Non inform.	Non inform.	1	
PC11	Non inform.	3	Non inform.	22	
PC12	Non inform.	16	Non inform.	Non inform.	
PC13	Non inform.	5	Non inform.	Non inform.	
PC14	Non inform.	Non inform.	0	0	
PC15	15	Non inform.	21	Non inform.	
PC16	Non inform.	1	Non inform.	Non inform.	
PC17	4	Non inform.	11	28	
PC18	Non inform.	Non inform.	Non inform.	Non inform.	
PC19	3	Non inform.	8	4	
PC20	Non inform.	16	Non inform.	Non inform.	

\*The value of allelic imbalance for PC4 (marker *D17Rat45*) is equal to 55% because of the unequal intensity of allele amplification of DNA from ear take (normal tissue for LOH/AI study). The amplification of alleles of tumor DNA is approximately the same. This phenomenon is related to the feature of PCR amplification of normal sample but not to the presence of the real allelic imbalance.

**Table 4.21** Allelic imbalance (in %) on chromosome 18 in twenty pheochromocytomas in comparison to normal tissue at each microsatellite locus analysed

NCBI, Ensembl map position (Mb)	11.6	69.0	86.9	Allelic imbalance
Marker name	<i>D18Rat108</i>	<i>D18Mgh3</i>	<i>D18Rat81*</i>	
Pheochromocytoma cases (PC)				
PC1	4	8	10	
PC2	1	2	Non inform.	
PC3	Non inform.	4	19	
PC4	2	Non inform.	4	
PC5	Non inform.	Non inform.	22	
PC6	Non inform.	2	13	
PC7	35	34	Non inform.	
PC8	8	6	0	
PC9	Non inform.	13	2	
PC10	11	4	4	
PC11	Non inform.	5	Non inform.	
PC12	Non inform.	16	18	
PC13	Non inform.	Non inform.	5	
PC14	Non inform.	Non inform.	11	
PC15	4	6	Non inform.	
PC16	6	9	3	
PC17	2	14	Non inform.	
PC18	20	13	3	
PC19	10	12	Non inform.	
PC20	Non inform.	10	7	

\*For the marker *D18Rat81* microsatellite fragment analysis was performed using 5'-FAM labelled primers.

**Table 4.22** Allelic imbalance (in %) on chromosome 19 in twenty pheochromocytomas in comparison to normal tissue at each microsatellite locus analysed

NCBI, Ensembl map position (Mb)	9.9	24.7	30.6	46.4	56.2	Allelic imbalance
Marker name	<i>D19Rat97</i>	<i>D19Rat13</i>	<i>D19Rat25</i>	<i>D19Rat64</i>	<i>D19Rat4</i>	
Pheochromocytoma cases (PC)						
PC1	Non inform.	Non inform.	4	11	Non inform.	
PC2	Non inform.	4	Non inform.	11	20	
PC3	16	2	5	4	2	
PC4	Non inform.	13	10	22	4	
PC5	Non inform.	10	Non inform.	7	Non inform.	
PC6	13	20	19	23	Non inform.	
PC7	Non inform.	20	Non inform.	16	6	
PC8	2	13	9	26	0	
PC9	6	16	2	Non inform.	2	
PC10	Non inform.	Non inform.	Non inform.	15	37	
PC11	Non inform.	27	43	Non inform.	38	
PC12	<b>61</b>	<b>64</b>	<b>35**</b>	<b>54</b>	Non inform.	Wky↓ Sd <sup>we</sup> ↑
PC13	Non inform.	<b>54</b>	Non inform.	Non inform.	<b>60</b>	Wky↓ Sd <sup>we</sup> ↑
PC14	<b>50</b>	<b>75</b>	<b>57</b>	<b>51</b>	Non inform.	Wky↓ Sd <sup>we</sup> ↑
PC15	5	1	3	1	<b>3</b>	
PC16	Non inform.	51	Non inform.	<b>46**</b>	<b>50</b>	Wky↓ Sd <sup>we</sup> ↑
PC17	Non inform.	22	7	9	11	
PC18	<b>53</b>	<b>53</b>	Non inform.	Non inform.	Non inform.	Wky↓ Sd <sup>we</sup> ↑
PC19	12	4	4	3	Non inform.	
PC20	3	7	7	Non inform.	<b>56</b>	Wky↓ Sd <sup>we</sup> ↑

Allelic imbalance at certain marker above 50% is taken as LOH/AI and marked in grey. Allelic imbalance is indicated. For all informative microsatellite markers microsatellite fragment analysis was performed using 5'-FAM labeled primers only for samples having allelic imbalance and few samples without allelic imbalance (Table 4.26). Tumor cases PC12 and PC16 have allelic imbalance for all informative microsatellite markers on chromosome 19.

\*\*Allelic imbalance values of PC12 (marker *D19Rat25*) and PC16 (marker *D19Rat64*) are signed as allelic imbalance cases (Table 4.26).



**Table 4.23** Allelic imbalance (in %) on chromosome 20 in twenty pheochromocytomas in comparison to normal tissue at each microsatellite locus analysed

NCBI, Ensembl map position (Mb)	11.0	32.6	Allelic imbalance
Marker name	<i>D20Rat59</i>	<i>D20Mit4</i>	
Pheochromocytoma cases (PC)			
PC1	Non inform.	10	
PC2	Non inform.	Non inform.	
PC3	Non inform.	Non inform.	
PC4	Non inform.	Non inform.	
PC5	5	4	
PC6	6	Non inform.	
PC7	Non inform.	Non inform.	
PC8	2	1	
PC9	Non inform.	Non inform.	
PC10	12	Non inform.	
PC11	6	13	
PC12	11	8	
PC13	Non inform.	Non inform.	
PC14	3	13	
PC15	9	7	
PC16	Non inform.	2	
PC17	Non inform.	16	
PC18	Non inform.	1	
PC19	Non inform.	1	
PC20	7	Non inform.	

**Table 4.24** Allelic imbalance (in %) on chromosome X in twenty pheochromocytomas in comparison to normal tissue at each microsatellite locus analysed

NCBI, Ensembl map position (Mb)	41.6	63.0	Allelic imbalance
Marker name	<i>DXRat36</i>	<i>DXRat67</i>	
Pheochromocytoma cases (PC)			
PC1	Non inform.	Non inform.	
PC2	Non inform.	Non inform.	
PC3	Non inform.	Non inform.	
PC4	Non inform.	Non inform.	
PC5	5	6	
PC6	Non inform.	Non inform.	
PC7	Non inform.	Non inform.	
PC8	Non inform.	Non inform.	
PC9	Non inform.	Non inform.	
PC10	29	10	
PC11	32	5	
PC12	21	9	
PC13	11	Non inform.	
PC14	Non inform.	Non inform.	
PC15	Non inform.	Non inform.	
PC16	Non inform.	8	
PC17	Non inform.	Non inform.	
PC18	Non inform.	Non inform.	
PC19	Non inform.	Non inform.	
PC20	Non inform.	Non inform.	

## **PRESENTATIONS**

Shyla A., Pellegata N. S., Graw J., Atkinson M. J. (2005). Genetic alterations in MENX-associated pheochromocytoma (poster). 7<sup>th</sup> Course in Molecular Cytogenetics and DNA microarrays, Bertinoro di Romagna (Italy).

Shyla A., Pellegata N. S., Graw J., Atkinson M. J. (2007). Genetic alterations in MENX-associated pheochromocytoma (oral presentation). 4<sup>th</sup> Annual ENETS Conference for the Diagnosis and Treatment of Neuroendocrine Tumor Disease, Barcelona (Spain).

**The second place prize in the basic research category for the oral presentation.**

## ACKNOWLEDGEMENTS

*I would like to thank...*

**Prof. Dr. Mike J. Atkinson** for giving me the opportunity to carry out my doctoral dissertation under his valuable guidance and supervision, for his continuous encouragement during my work and for critical evaluation of this manuscript.

**Prof. Dr. Jochen Graw** for great support and encouragement during my study, and for critical reading this work. I express my deepest gratitude to him for the help in getting an acknowledgement of my diploma.

**Dr. Natalia S. Pellegata** for her continuous guidance, support and help during the entire course of this project. I am very thankful to her for all critical comments and notes concerning this thesis.

**Dr. Karin Bink, Ulrike Buchholz, and Dr. Axel Walch** for their sincere efforts in teaching me FISH technique and very helpful discussion about FISH data analysis.

**Dr. Marie N. Guilly, and Dr. Sylvia Chevillard** for providing me slides with rat metaphases and for cytogenetic analysis of the slides after metaphase FISH analysis

**Dr. Julia Calzada-Wack, and Dr. Gabriele Hölzlwimmer** for histopathological evaluation of adrenal gland tissues used in this study. I am very grateful to them for their constant cooperation, all suggestions, great moral help and encouragement that has made this work easier.

**Eleonore Samson, Elke Pulz, and Ulrike Reich** for the skilled technical support, all advises and suggestions.

**Dr. Oleg Tischenko** for writing programs for CGH data analysis and very helpful discussions concerning this method. I want to express my warmest thanks to him for strong support and help.

**Dr. Kristian Unger** for teaching me to use threshold approach in the CGH data analysis, and **Dr. Jan Smida** for discussions about CGH array data analysis.

**Dr. Michael Rosemann** for formulas for quantitative Real-Time (TaqMan) RT-PCR data analysis, helpful discussions and support.

**Dr. Nataša Anastasov** for strong encouragement, long discussions and help.

**Dr. Soile Tapio** for her warm attitude, and moral support which helped me a lot during the writing this work.

**Dr. Franka Pluder** for her help at some critical points of writing the thesis and great encouragement.

All colleagues from the Institute of Pathology for friendly atmosphere, helpful discussions and suggestions during my work

**My parents, and my sister** for love, patience, believe in me and great support during the whole my life. And all well wishes who stood beside me during the course of my work.

# LEBENS LAUF

Alena Shyla

Adolf-Kolping Strasse 1  
80336 München, Deutschland  
Telefon: ++49 176 24553838

## Persönliche Angaben:

Geburtsdatum: 27.07.1980  
Geburtsort: Bobruisk (Belarus)  
Staatsangehörigkeit: Belarussisch  
Familienstand: ledig

## Ausbildung:

- Sep.1986 – Juli 1997 Höhere Schule 28, Bobruisk, Belarus  
(summa cum laude)
- Okt.1997 – Juli 2002 Abschluss in Biologie (Magister Äquivalent) mit einer  
Spezialisierung in Radiobiologie und Strahlenmedizin,  
Internationale Staatliche Ökologische Sacharow-Universität  
(ISEU), Minsk, Belarus  
(summa cum laude)  
Zusatzqualifikation: Immunologe  
*Hauptfächer:* Molekularbiologie, Biochemie, Radiobiologie,  
Genetik, Biophysik, normale und pathologische Physiologie des  
Menschen, Immunologie, Immundiagnostik
- Sep. 2002 – Feb. 2004 Wissenschaftlicher Mitarbeiter, in der Gruppe von Dr. A. G.  
Lapko, Internationale Staatliche Ökologische Sacharow-  
Universität (ISEU), Minsk, Belarus
- Feb. 2004 – Dez. 2007 Doktorarbeit am Institut für Pathologie, Helmholtz Zentrum  
München – Deutsches Forschungszentrum für Gesundheit und  
Umwelt, GmbH, München, Deutschland  
*Thema:* “Genetic alterations in MENX pheochromocytoma”  
*Betreuer:* Prof. Dr. M. J. Atkinson